Specific enzymatic cleavage and payload release from peptide-based hybrid nanocapsules

Dissertation

zur Erlangung des Grades
"Doktor der Naturwissenschaften"
im Promotionsfach Chemie

am Fachbereich Chemie, Pharmazie und Geowissenschaften
der Johannes Gutenberg-Universität in Mainz

vorgelegt von

Julien Andrieu
geboren in Nantes (Frankreich)

Mainz, 2011

Diese Dissertation wurde in der Zeit von Oktober 2008 bis November 2011 im Arbeitskreis Physikalische Chemie der Polymere von Prof. Dr. Katharina Landfester am Max-Planck-Institut für Polymerforschung in Mainz erstellt.

Ich versichere hiermit, dass ich diese Arbeit selbstständig angefertigt habe und keine anderen als die angegeben Quellen und Hilfsmittel benutzt sowie die wörtlich oder inhaltlich übernommenen Stellen als solche kenntlich gemacht habe.

Max-Planck-Institut für Polymerforschung
Max Planck Institute for Polymer Research

JG|U
JOHANNES GUTENBERG
UNIVERSITÄT MAINZ

Amtierender Dekan:	Prof. W. Hofmeister
1. Berichterstatter:	Prof. K. Landfester
2. Berichterstatter:	Prof. H. Frey
Mitglied der Prüfungskommission:	Prof. C. Sönnichsen
Tag der mündliche Prüfung:	7. Dezember 2011

A mes quatre grands-parents,

Table of contents

I Introduction & Motivation………………………. 1

II Theoretical background…………………….…. 5

II.1 Responsive materials……………………………………………………. 6
II.1.1 Temperature-responsive materials………………………………………. 6
II.1.2 pH-responsive materials…………………………………………………… 7
II.1.3 Light-responsive materials………………………………………………. 8
II.1.4 Redox-responsive materials………………………………………………… 9
II.1.5 Enzyme-responsive materials……………………………………………… 10

II.2 Bioconjugates……………………………………………………………. 11
II.2.1 Presentation of bioconjugates…………………………………………... 11
II 2.2 Defined peptide-polymer conjugates……………………………………… 11

II.3 Triggered release via enzymatic cleavage………………………………… 14

II.4 Solid-phase peptide synthesis……………………………………………… 16
II.4.1 Principle of the method…………………………………………………… 16
II.4.2 Mechanistic approach………………………………………………………… 19

II.5 Miniemulsion……………………………………………………………….. 24
II.5.1 Polymerization in heterophase…………………………………………….. 24
II.5.2 Miniemulsion principle……………………………………………………... 25
II.5.3 Inverse miniemulsion……………………………………………………… 29
II.5.4 Preparation of capsules via miniemulsion………………………………. 30

II.6 Polyaddition………………………………………………………………… 36
II.6.1 Characteristics of polyaddition………………………………………… 36
II.6.2 Reactivity of the isocyanate group……………………………………… 38

III Relevant methods for characterization……….. 43

III.1 MALDI-TOF mass spectrometry………………………………………. 44

III.2 Size-exclusion chromatography……………………………………………… 45

III.3 DOSY-NMR spectroscopy………………………………………………… 46

III.4 Electron Microscopy ……………………………………………………. 48

III.5 Light scattering……………………………………………………………….. 50

III.6 Absorption and fluorescence………………………………………………… 51
III.6.1 Absorption and UV-Vis Spectroscopy ……………………………. 51
III.6.2 Fluorescence ……………………………………………………… 52

IV. Results & discussion………………………… 59

Strategy**…………………….………………………………………… 60**

IV.1 Synthesis, characterization and cleavage of linear peptide-polymer conjugates 62
IV.1.1 Peptide-polymer conjugates via coupling in solution ……………………. 62
IV.1.2 Triblock peptide-polymer conjugates via coupling on solid phase ……… 63
IV.1.3 Enzymatic cleavage of triblock peptide-polymer conjugates…………. 73

IV.2 Development of a method to prepare peptide based hybrids nanocapsules … 75
IV 2.1 Choice of the surfactant ………………………………………………… 76
IV 2.2 Optimization of synthetic parameters…………………………………… 76
IV 2.3 Characterization of the peptide-based structures by electron microscopy.. 81

IV.3 Synthesis, characterization, and cleavage of hybrid nanocapsules with FRET pair Mant/Y(NO_2)……………………………………………………… 84
IV.3.1 Peptide used for capsules preparation …………………………………. 84
IV.3.2 Preparation and characterization of cleavable capsules with FRET pair… 88
IV.3.3 Redispersion in water and enzymatic cleavage experiments……………. 94
IV.3.4 Change to the FRET pair Mca/Dnp ………………………………….. 97
IV.3.5 Redispersion in water and enzymatic cleavage experiments…………… 103
IV.3.6 On the solubility of the polymer and phase separation………………… 105

IV.4 Synthesis, characterization, and cleavage of peptide based hybrid nanocapsules loaded with fluorescing polymer……………………………… 107
IV.4.1 Synthesis of the capsules & possible influence of encapsulated polymer on the capsules…...............……………………………………………….. 107
IV.4.2 Investigation with electron microscopy………………………………… 109
IV.4.3 Redispersion into water and preconditioning…………………………… 110
IV.4.4 Cleavage of nanocapsules with encapsulated fluorescent polymer ……… 112

IV.5 Synthesis, characterization, and cleavage of peptide based hybrid nanocapsules with release of fluorophore…………………………………... 113
IV.5.1 Synthesis of the capsules – Size and morphology……………………… 113
IV.5.2 Improved redispersion into water with mild ultrasonication…………… 115
IV.5.3 Influence of TDI equivalent and functionality of the peptide after the encapsulation of sulforhodamine……………….…………………..………………… 118
IV.5.4 Release of payload via enzymatic cleavage of peptide-based nanocapsules 122
IV.5.5 Quantitative approach of cleavage and release………………………. 126

IV.6 Hepsin-cleavable nanocapsules…………………………………………… 129
IV.6.1 Identification of hepsin-cleavable sequence ………………………….. 129
IV.6.2 Preparation of the capsules ……………………………………….….. 131
IV.6.3 Cleavage of the capsules in cell culture ……………………………. 132

V Conclusion and perspectives…………………… 135

VI Experimental part……………………………… 139

VI.1 Materials………………………………………………………………………… 140
VI.1.1 Chemicals…………………….……………………………………... 140
VI.1.2 Synthesis of carboxylic acid end-functionalized polystyrene by anionic polymerization ……………………..…………………………….………………… 141
VI.1.3 Radical synthesis of poly(vinylpyrrolidone-*co*-bodipy)…………………... 142

VI.2 Synthesis and preparation of peptides………………………………………… 144
VI.2.1 Solid-Phase Peptide Synthesis (SPPS)…………………………………... 144
VI.2.2 Peptides………………………………………………………………. 145

VI.3 Peptide-polymer coupling reactions…………………………………………… 150
VI.3.1 Peptide-polymer coupling in solution…………………………………... 151
VI.3.2 Peptide-polymer coupling on solid phase……………………………… 151

VI.4 Preparation of peptide-based nanocapsules in miniemulsion……………….. 152

VI.5 Appendix………………………………………………………………………… 154
VI.5.1 Methods……………………………………………………………… 154
VI.5.2 Summary of FRET-peptide based hybrid nanocapsules………………… 158

Abbreviation & Symbols………………………………………………………… 159

Bibliographic references ………………………………………………………… 161

Acknowledgments …………………………………………………….………… 168

Curriculum Vitae ………………………………………….…………………… 170

Publications and presentations…………………………………………………… 171

I. Introduction

Introduction & Motivation

Prostate cancer is one of the most frequent forms of cancer diagnosed in men, especially in developed countries like in North America or Western Europe.[1] In the USA, prostate cancer is the second cause of cancer-related death after lung cancer. For a country of 308 million inhabitants (153 million males), 240 000 new prostate tumors should appear in 2011 and 33 000 persons are estimated to die of prostate cancer this year.[2] Over a life time, 1/6 of the American male citizens will develop a – at least benign – tumor in the prostate and 1/36 will die of prostate cancer.[3] The prostate is an exocrine gland of the male reproductive system, around 3 cm in diameter and located directly under the bladder and surrounding the urethra, as displayed in **Figure 1**. Prostate secretes a fluid that usually constitutes 20-30% of the semen, along with spermatozoa (coming from the testicles) and seminal vesicle fluid.

Prostate cancer principally affects older people and mostly, the tumor remains benign. The majority of prostate cancer carriers die from other diseases before the tumor becomes malignant. Although it is not the most lethal type of cancer, the number of persons with prostate cancer makes the detection of this cancer a priority. Early detection is particularly important in persons developing a tumor at a relative young age, because of the risk of development of metastasis. Indeed, local therapy, i.e. surgery and radiation therapy can be curative; the efficacy of therapeutic treatments depends on early detection. Usually, prostate cancer is diagnosed after biopsy (tissue samples from the prostate are obtained via the rectum), following a digital rectal examination. An elevated concentration of the prostate specific antigen (PSA) protein in the blood is another risk factor, though can often result in "false positive" and "false negative" patients.[3] Undoubtedly, there is a need for other non-invasive methods for early-detection of localized tumors. Transrectal ultrasounds, usually the imaging investigation method used, give too many false-positive results. Endorectal magnetic resonance imaging was also tested with promising results.

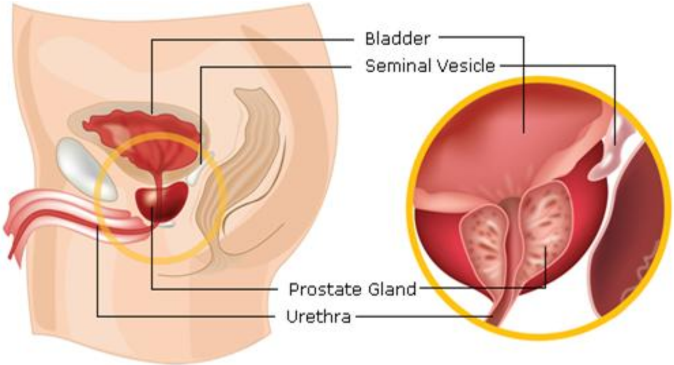

Figure 1: Localization of prostate in the human (male) body.
Source: http://www.roboticoncology.com

Another possibility to detect prostate cancer is the detection of hepsin, a transmembrane protease, which is highly upregulated by the prostate cancerous cells, and can be considered as a significant marker and target of prostate cancer.[4-6]

Searching for new drugs has always been a driving force of pharmaceutical research and will continue to be so because of the infinite possibilities available, e.g. with combinatorial chemistry for the synthesis, or proteomics for understanding the operation modus in a cell. Synthesizing complex (bio)molecules, which help to efficiently cure common diseases without side-effects or that help healing against others illnesses, will remain a big challenge. However, once a drug has been synthesized, it has to reach its target in the body in sufficient concentration and within a suitable time frame. The form of administration form also plays an important role here since it may be administered generally or locally. In the former case, the route of administration has to be chosen: direct parenteral injection, oral or inhalational, and in which dosage form: powder, pills, capsules, suppository, aerosol etc… The development of nanosciences has opened new perspectives for drug delivery, as nanoparticles e.g. nanocapsules, nanogels, vesicles, and micelles, are small enough to be directly taken up into the cells and pass vasculature without obstruction.[7] More interestingly, the preparation of materials responsive to different stimuli like temperature, pH, light, and enzymes to name a few, opens broad perspectives for the development of responsive nanoparticles, not only for drug delivery but also as chemical or biological sensors or for non-invasive treatments *in vivo*.[8, 9]

This work was performed in the frame of the project "Nanocapsule-based smart probes for Optical Imaging of Prostate Cancer" (Optimap), which proposes a new concept for optical detection and imaging of prostate cancer. This project was carried out in collaboration with the Institute for Laser Technologies in Medicine (ILM, University of Ulm, Germany) and the department of Urology and Pediatric Urology from the University of Ulm (Germany). The goal of the project is the preparation of nanoparticles or nanocapsules, with a polymer shell containing a peptide sequence, which is cleaved exclusively by the enzyme hepsin. The cleavage of the enzymatic sequence should be monitored optically by recovery of the fluorescence issued from the capsules, arising only in malignant tissues. One part of the project deals with the encapsulation of hydrophobic content in conjugated peptide-polymer particles,[10] whereas the work presented in this thesis is focused on the preparation of nanocapsules for the encapsulation of a hydrophilic payload.

The miniemulsion technique is a very efficient tool for the preparation of diverse nanomaterials. In particular, several routes (nanoprecipitation, phase separation, interfacial polymerization) can be employed to form nanocapsules with high encapsulation rates, and in the case of inverse miniemulsion, hydrophilic content.

In this work, the objective was the preparation of hepsin-cleavable peptide-based nanocapsules in miniemulsion, for the encapsulation and the release of hydrophilic content. A model peptide sequence for enzymatic degradation was chosen for the development of the preparation of the capsules. Two strategies were tested. Firstly, the synthesis of peptide-polymer conjugates, for further preparation of nanocapsules via nanoprecipitation is reported. Then, the preparation of peptide based nanocapsules via interfacial polyaddition is described. The enzymatic cleavage of the capsules and its monitoring via an optical system are presented. The encapsulation of a hydrophobic fluorescent dye and its release are also reported. Finally, a hepsin cleavable sequence was identified and the system was applied to this peptide sequence for the preparation of hepsin-cleavable capsules. The specific enzymatic degradation of these nanocapsules by cancerous cells is reported.

II. Theoretical background

II.1 Responsive materials

Nowadays, materials with high-performance properties (flexibility, lightness, insulation, chemical inertness…) can be prepared, in major part thanks to the polymers and their composites developed within the last 50 years. However, what would be if these materials could become “smart” and adapt or respond to some changes in their environment? The interest for these stimuli responsive materials has been growing strongly over the last years. In particular, stimuli responsive materials open a wide range of new possibilities in the case of the nanostructured materials. Numerous applications like sensors, and especially in the biomedical field for biotechnology and drug-delivery, are targeted. Organic as well as inorganic materials can be used for the preparation of nanostructured compounds, and several methods give access to nanostructured organic materials.[11] Among these methods, diverse heterophase polymerization mechanisms, such as emulsion or miniemulsion, allow the synthesis of nanoparticles, nanocapsules, or nanogels. Amphiphilic block copolymers aggregate in micellar structures or vesicles (polymersomes) and layer-by layer deposition of polyelectrolytes on template particles can also lead to capsules after removal of the sacrificial core. On the other side, a lot of potential triggers, that can interact or have an influence on the structure of some responsive materials, are considered: temperature, pH or ionic strength, light, redox and biomolecules like enzyme. To present briefly the achievements and perspectives opened by the (nanostructured) responsive materials, the main possible triggers are reviewed.

II.1.1 Temperature-responsive materials

Most of the temperature-responsive materials are based on water-soluble polymers having a lower critical solution temperature (LCST), above which they are not soluble in water anymore. This behavior is particularly interesting if the LCST is located in the physiological range, which is not the case for poly(ethylene oxide) (PEO, LCST ≈ 90 °C), for example. The most relevant polymers are poly(*N*-isopropylacrylamide) (PNIPAM) and the polymers based on oligo(ethlylene oxide) (meth)acrylate monomers (OEG(M)A). The LCST of PNIPAM is at 32 °C and this of poly(OEGMA) can be precisely adjusted with the length of the comonomers side-chains, typically oligo(ethylene glycol) methacrylate (OEGMA) and 2-(2-methoxyethoxy) ethyl methacrylate (MEO_2MA).[12] Both polymers have been comprehensively studied and were used for the preparation of numerous nanostructures, materials, and coatings.[13-16] Among them, thermoresponsive micelles consisting of block copolymers have been prepared.[17-20] The block copolymers were made with one hydrophobic and one responsive hydrophilic block, aggregating into micelles under the LCST of the hydrophilic block, and reversibly into larger aggregates when heated above LCST. Some micelles with drug release properties were also prepared, the payload being released more rapidly during LCST aggregation transition.[21-23] Hydrogels[24-26] and microgels[27, 28] were prepared with both types of polymers. All gels swelled well in water at low temperature and shrunk above LCST. In the case where a dye or a drug was encapsulated, the kinetic release was diffusional (pseudo zero order) below and above LCST. However, the release was faster for swollen gels (below LCST) than for shrunk gels (above LCST). Additionally, for the poly(NIPAM) based macrogels, two effects were reported: if the temperature increase is too quick, a burst effect is observed as water is quickly ejected out of the materials. On the other side, a slow transition creates a skin on the surface of the gel and no release at all is observed. Furthermore, “on-and-off” release properties were reported by cycling the system above and below the LCST.[26] The synthesis of thermoresponsive vesicles[29] and layer-by-layer capsules[30] was also reported. Thermosensitive cross-linked PNIPAM nanocapsules with encapsulated dye were also prepared, from a sacrificial silica core with dye entrapped in the inside. Like for the microgels, the dye was able to permeate the swollen shell easily under the LCST, while above the LCST, the release was inhibited.[31] Among the applications of this kind of polymer for materials, some are worth highlighting: in the case of surfaces covered with poly(OEGMA-*co*-MEO_2MA), the surfaces were bioadherent above LCST at 37 °C, but strongly bio-repellent at 25 °C. After cultivation of mouse fibroblasts at physiological temperature, this material allowed an enzyme-free cell detachment by simple buffer rinsing at room temperature.[32] Bioconjugates were also prepared, notably trypsin coupled to a poly(OEGMA-*co*-MEO_2MA) copolymer: the conjugates were found to be thermoresponsive, which help isolating the conjugated proteins. Interestingly, the enzymatic activity was higher than for unmodified trypsin.[33]

II.1.2 pH-responsive materials

pH-responsive materials have also been comprehensively studied, especially with drug-delivery perspective, as for example the pH value is more acidic in cancerous cells than in healthy cells. The incorporation of ionisable monomer units into a polymer backbone enables solubility changes and phase transitions dependent on the pH value. As a result, polymers bearing acidic or basic functions, like poly(propylacrylic acid) (PPAA)[34] and poly(methacrylic acid) (PMAA),[35] or poly(2-vinylpyridine) (P2VP)[36] were used to prepare pH-responsive nanostructures. Triblock copolymer poly[(ethylene oxide)-*b*-2 hydroxyethyl methacrylate-*b*-2-(diethylamino)ethyl methacrylate] (PEO-HEMA-DEA) prepared via ATRP from a PEO-based macro-initiator exhibited full solubility at low pH. Deprotonation of the DEA block above pH 8 led to micellization with DEA core, HEMA corona and PEO outer layer. Selective cross-linking of the HEMA corona was carried out, retaining DEA at the core. The resulting cross-linked micelles had a reversible pH-dependent swelling behavior.[37] The same group reported the preparation of "schizophrenic" micelles, made from the diblock copolymer poly(4-vinyl benzoic acid-*b*-2-(diethylamino) ethyl methacrylate). Inverted micelles were observed for pH < 2 (protonated basic block shell) and pH > 10 (deprotonated acid block shell).[38] Vesicles were prepared from P2VP-*b*-PEO copolymer. A decrease of the pH below 5 leads to protonation and dissolution of the PV2P blocks, inducing rupture of the membrane. The release of encapsulated hydrophilic dye was accelerated by dissolution of the vesicles.[36]

Hydrogels consisting of monomers with acidic or basic functionality are pH-responsive. In many cases, the pH-responsive character has been combined with the temperature sensitivity by copolymerization with NIPAM, to create double-responsive materials. In all cases, the swelling of the gel was studied by variation of pH and temperature.[39-41] Another approach combines hydrogel and layer-by-layer techniques: quantum dots were encapsulated in a PMAA hydrogel matrix, then covered by polyelectrolytes bilayers, which were cross-linked afterward. The system exhibited pH-responsive properties: the fluorescence intensity varied with the pH, which is of great interest for the development of pH or chemical sensors.[42]

Concerning the drug-delivery approach, the preparation of acid degradable microcapsules via interfacial polymerization was achieved via polycondensation of acid chloride and ketal-containing diamine. A significant release of encapsulated dye was observed at pH 5 (degradation of the ketal group) while the release was much lower at pH 7.5. It shows that a relatively sharp transition can also be obtained with pH as trigger.[43]

II.1.3 Light-responsive materials

While temperature and pH are parameters of the environment ("bulk" properties) varying continuously, light is a very promising trigger, because of its specificity (wavelength, intensity, polarization…), the precision of its localization (by lasers) but also because it can be switched on and off instantaneously. Hydrogels with reversible cross-linking via light-stimulated [2+2] cycloaddition of p-nitrocinnamate groups[44] or [4+4] dimerization of anthracene[45] were prepared. Recently, the reversible swelling induced by light on microgels was reported.[46] Moreover, the light-induced release of fluorophore entrapped in cross-linked microgels was investigated. It was found, that light irradiation accelerates the release of the dye, especially in the denser network.[47] Besides, light can also be responsible for the degradation of functional groups. The complete degradation of microgels by light-induced cleavage of its cross-linker was reported.[48] Dehybridization from double-stranded DNA attached to gold-nanoparticles used as plasmon resonant vectors was triggered by light, releasing single-stranded DNA inside the cells.[49] Finally, materials responsive to temperature, pH and light were prepared, via the incorporation of azo groups. Azo groups are instable and can be degraded by temperature increase, under acidic conditions as well as upon light radiation. Azo-containing diols were used for the preparation of polyurethane nanocapsules by interfacial polyaddition in miniemulsion. pH-, light- or temperature-induced irreversible degradation of the capsules was reported, with release of the encapsulated dye.[50]

II.1.4 Redox responsive materials

Redox active molecules are another type of trigger, which have been investigated, both oxidizing and reducing agents. In this case, the responsive character of the materials is due to the presence of oxidant- or reductant-sensitive groups in the polymer chains or as cross-linker. Several nanomaterials have already been prepared, based on different redox systems. The oxidation of hydrophobic poly(propylene sulfide) (PPS) in hydrophilic poly(propylene sulfoxide) and ultimately poly(propylene sulfone) was used to destabilize unilamellar vesicles consisting of ABA block copolymer with PPS as B block.[51] The same group prepared polysulfide particles by living emulsion polymerization, cross-linked with disulfide bridges for the encapsulation of a hydrophobic dye. The particles swelled and their content was released in oxidative conditions.[52] Capsules made of polyanions and polycations of poly(ferrocenyl silane) were prepared via the layer-by-layer technique. Fast capsules extension accompanied with a drastic permeability increase was observed via chemical oxidation.[53] Otherwise, nanoparticles functionalized with quenched dye were used as fluorogenic sensors for monitoring the peroxynitrite and hypochlorous acid production within cells. The quenched dyes were selectively released by the reaction with peroxynitrite and hypochlorous acid. The sensors were stable toward other oxidants like hydroxyl radical and hydrogen peroxide.[54]

The reduction of disulfide bridges from poly(methacrylic acid) functionalized with cysteamine was used to deconstruct of cross-linked polymer films and for the release of dye encapsulated in layer-by-layer colloids.[55]

Moreover, not only chemicals but also biomolecules, like enzymes, can be used as trigger. A polymer matrix containing immobilized glucose oxidase released insulin after addition and oxidation of glucose into gluconic acid, the consequent local pH variation increasing the insulin solubility.[56] Core-shell-corona micelles bearing disulfide cross-links released entrapped anti-cancer drugs via reduction of the disulfide groups in response to intracellular glutathione level (glutathione is an antioxidant tripeptide).[57] More recently, the release of a hydrophobic dye was achieved by the oxidation of PPS nanoparticles by oxidoreductase enzymes in hydrophilic polysulfones and polysulfoxydes.[58]

II.1.5 Enzyme responsive materials

In comparison to pH and temperature, enzymes are – like light – triggers for which it is reasonable to speak from presence/absence of the trigger and not only as the continuous variation of a parameter (like concentration in the case of enzymes). In biological systems, the apparition of some enzymes is often the consequence of a change or perturbation in the cells, e.g. inflammation. Cancerous cells are known to overexpress some enzymes. Hepsin, a cell surface protease, is widely reported to be over-expressed in prostate tumors.[4, 6] One can also mention cathepsin B or cathepsin D. Cathepsin B is overexpressed in lung, ovarian and colorectal tumor cells and is present extracellularly in tumor tissues. Cathepsin B levels in tumor cells and tissue of patient are significantly elevated and have been directly related to their prognosis.[59-61] Cathepsin D is highly overexpressed in breast cancer and has been related to its prognosis.[62] Moreover, the degradation of extracellular matrix components is an essential cascade event in tumor progression and cathepsin D was shown to be one of the proteinases involved in this process.[63] Similarly, matrix metalloproteinase (MMP) over-expression has been correlated with tumor metastasis and a host of inflammatory and vascular diseases.[64, 65] For these reasons, enzyme-responsive nanomaterials appear very suitable for the detection of certain diseases and selective drug delivery to heal them.

In the previous paragraph, materials responsive to enzyme with redox properties (oxidases and reductases) were presented. The materials where the enzymatic cleavage of peptide sequences is used to induce a response are reviewed later (see paragraph II.4). One should mention that all materials based on polysaccharides or synthetic biodegradable polymers such as poly(caprolactone) (PCL), polyhydroxyalkanoates (PHAS) and poly(lactic acid) (PLA) can also be considered as enzyme-responsive materials for the release of substances when confronted to their lysing enzyme (dextranase, amylase, esterase, etc.).

II.2 Bioconjugates

II.2.1 Presentation of bioconjugates

Building stimuli-responsive materials, in particular bio-responsive materials, can implicate the preparation of bio-conjugate (or bio-hybrid) macromolecules and materials. In general, the term “bio-conjugate” represents molecules or materials which are partly made of biomolecules and of synthetic moieties. The synthetic parts can be organic (polymer chain, polymeric network, or particles) or inorganic[66] (mesoporous silica, metal surface, or metal particles). Meanwhile, the term biomolecules should not be confused with natural molecules, as biomolecules can also be synthetized artificially. The interest of those materials is the numerous possibilities they offer by combining the properties of the two components,[67] e.g. bioactivity, recognition, cleavability, self-assembling properties for the biomolecular moiety and robustness, mechanical properties, (in)solubility in water or tunable solubility, stealth behavior or use as template for the artificial moiety. The term biomolecule designates a broad range of compounds, from small molecules such as metabolites to large macromolecules: polysaccharides, DNA[68], peptides and proteins. For example, surface functionalization of nanoparticles with peptides, proteins, or antibodies to increase cellular uptake or address the capsules to precise cells is a topic of huge interest, but it will not be discussed in this thesis. The next paragraph will present the state of the art concerning the synthesis of peptide-polymer (and protein-polymer) linear conjugates with organic synthetic polymers.

II.2.2 Defined peptide-polymer conjugates

There are several possibilities to classify peptide-polymer conjugates: the nature of the polymer, the synthetic strategy employed to prepare the conjugate, etc. Indeed, defined peptide-polymer conjugates can be prepared following different strategies.[69] The most frequently used methods are the following: the peptide and the already prepared polymer can be coupled together, or the monomer can be polymerized from the peptide.

Coupling reaction

In the case where a peptide is coupled to a polymer, different coupling reactions can be applied. The most straightforward is the peptide coupling reaction. This strategy takes advantage of the natural functionalities of all peptides: the presence of an amino group at the *N*-terminus and of a carboxylic group at the C-terminus, and in some other case on the side-chains. The polymer, suitably amino- or carboxy-functionalized at one of its extremity, reacts as a giant amino acid under similar conditions as for peptide synthesis.[70-74] Diverse polymers, such as poly(NIPAM), poly(n-butylacrylate) and PEO have been coupled successfully with this method. One interesting study reports the synthesis of a triblock polymer-peptide-polymer done entirely in solid phase, with relatively long polystyrene chains.[71] Another frequently used coupling reaction is the copper-catalyzed azide-alkyne Huisgen cycloaddition, which belongs to the so-called "click chemistry".[75] The main interest in this reaction for peptide coupling, in addition to the mild temperature necessary, is its specificity and consequent tolerance to the other functional groups of the peptide. In almost every case, the alkyne group is introduced at the *N*-terminus of the peptide via an artificial amino acid and is coupled afterwards to an azido-functionalized polymer. They are exceptions to this strategy: the cycloaddition coupling of α-alkyne- with α-azido-poly(amino acid), both previously prepared by ring-opening polymerization (ROP).[76] Another exception is the homopolymerization by cycloaddition of α-azido and ω-alkyne functionalized peptide (in solution).[77] In the case of click-chemistry as well, a variety of different polymers were successfully coupled: mainly hydrophilic e.g. poly(NIPAM)[78, 79] or poly(OEGA),[80] but coupling with polystyrene was also described[81, 82]. All the coupling reactions were achieved in solution, with rather long coupling times to insure satisfying yields. It is also worth mentioning that the cysteine residues of proteins can be used for the coupling reaction, whether to bound directly a water-soluble polymer via thiol-disulfide exchange chemistry after RAFT polymerization[78] or to introduce a functional group via thiol-ene reaction for a further alkyne-azide polymer cycloaddition on the modified biomolecule.[79] A lot of other coupling reactions, from natural or artificial amino acids, have been reported[83] as e.g. Michael´s addition or Staudinger ligation.

Polymerization from bioinitiator

A second strategy is the polymerization of the synthetic polymer directly from the peptide, which plays then the role of a macro-initiator. Free-radical polymerization can be employed,[84] but controlled radical polymerization (CRP) methods have been far more investigated, as they allow a better control of the length of the polymer chain. Atom transfer radical polymerization

(ATRP),[85-92] reversible addition-fragmentation chain transfer (RAFT) polymerization[78, 79, 93-97] and nitroxide meditated polymerization[87, 98] have been used over the past few years.

Concerning ATRP and NMP, the *N*-terminus of the peptide was suitably transformed, using an artificial amino acid in SPPS to introduce the initiator function. Then, the polymerization of various monomers was mainly carried out in solution, after cleavage of the peptide sequence from the resin. However, polymerization of the peptide initiator on solid phase was also achieved, with hydrophilic poly-(2-hydroxy ethyl methacrylate)[91] and hydrophobic poly(*tert*-butyl acrylate).[87] Interestingly, this solid-phase approach led to the highest degree of polymerization ($DP > 100$) as long as enough time is elapsed. Another strategy proposing the side-chain functionalization of serine, whether prior to[86] or after[88] SPPS allowed the synthesis of triblock and side-chain functionalized copolymer with a central peptide chain.

For the bio-conjugates synthesized by RAFT polymerization, a peptide chain transfer agent was prepared by addition of a chain transfer group at the extremity of the peptide in SPPS.[95-97] After cleavage of the peptide-RAFT agent from the resin, it was used in solution for the polymerization of hydrophilic and hydrophobic monomers. RAFT is also commonly used for direct polymerization from proteins after previous transformation into a giant macro-RAFT agent via functionalization of cysteine residues. In this case, hydrophilic poly(NIPAM) chains were grafted on bovine serum albumin protein.[93]

The synthesis of poly(γ-benzyl-L-glutamate-*block*-styrene) via NMP is emphasized, as the polystyrene was cross-linked afterwards yielding a very high molecular weight polymer forming core-shell nanocapsules with a pH-responsive poly(L-glutamic acid) shell.[98] In this case, the poly(benzyl-L-glutamate) block was polymerized via ring-opening polymerization of α-amino acid *N*-carboxyanhydrides. This technique has been widely used in the group of Lecommandoux for the preparation of responsive micelles,[99] polymersomes or vesicles,[100, 101] but will not be discussed in more details here, as the peptide blocks are homopolymers.

To summarize this part on the preparation of linear peptide-polymer conjugate, the following important facts are listed:

- The synthesis of peptide-polymer conjugate has been achieved with various methods and different synthetic strategies (coupling, grafting "from").
- Several polymers have been successfully conjugated. The most frequent of them are hydrophilic polymers: PEO, poly(NIPAM), poly(OEGA), poly(HEMA) even if the hydrophobic poly(n-butyl acrylate) is also mentioned regularly.

- The large majority of the conjugates prepared were diblock peptide-polymers and not tri- or multiblocks as it is intended to do in this thesis.

In addition to this, all publications cited are recent: this area of research is new and therefore the targeted function of the hybrid material prepared is not always specified. The few applications mentioned are listed here. The use of a thermoresponsive polymer with LCST causes aggregation in dependence of the temperature.[84] This can have an influence on the adhesion of cells on grafted surfaces.[32, 95] On the other side, more or less explained structures are described, depending on the amphiphilicity of the conjugate (micelles,[87, 96] vesicles[86]), or on the self-assembling properties of the peptide itself: from nanotubes[74] to helical superstructures[70] via β-sheet nanofibrils[77] and alternated polymer and β-sheet peptide domain[72]. The groups of Lecommandoux and Klok have been studying widely the self-assembling properties of peptide blocks in peptide-based compounds.[102-104]

Becker and coauthors used the a bioactive function of the peptide: enhanced anti-microbial activity was obtained with the anti-microbial peptide located at the surface of the micelles compared as in solution.[87] Concerning peptide/enzyme-polymer conjugates in general, other applications have also been reported. One can enhance the properties of the biomolecules: a higher activity of the enzyme has already been mentioned,[33] stealth behavior,[105] or improved solubility of small molecules in water.[106] One can also prepare bioactive hydrogels or materials for drug delivery; this will be discussed in the next paragraph.

II.3 Triggered release via enzymatic cleavage

It was reported in the previous paragraph that the cleavability of the peptide was not the most desired peptide property in the linear peptide-polymer conjugates. However the enzymatic degradability is a key property of the structures that are aimed at in the present work. Therefore, in this part, an overview on the peptide hybrid materials with enzymatically cleavable peptide sequences will be presented.

The interest for enzymatically triggered delivery has risen since the pioneering work of Duncan, Kopecek and coauthors,[107-110] who prepared a water-soluble *N*-(2-hydroxypropyl)methacrylamide copolymer with doxorubicin attached to the polymer backbone via a biodegradable peptidyl spacer. Later, it was shown that the enzymatic cleavage also proceeds in heterophase with water insoluble polymers.[111] Suzuki prepared a hydrogel with pending antibiotic attached via peptide linkers; the drug was released only in case of infection.[112] The same concept was applied to a system where the model chemotherapeutic agent was complexed to the pending cleavable peptide.[113] In a different but exciting approach, poly(ethylene oxide) hydrogels cross-linked with cleavable peptides were prepared via peptide coupling reactions and successfully degraded in the presence of enzyme.[114] Then this system was adapted to a cell culture with matrix-metalloproteinase (MMP)-specific degradable extracellular matrix, consisting of hydrogels cross-linked via Michael-type addition.[115, 116] The same concept was applied with success to cross-linked dextran hydrogel[117], and to thermoresponsive poly(NIPAM-*co*-AAC) hydrogels, where the peptide cross-linker with difunctional acrylate group was directly copolymerized as macromonomer.[118] Later, the release of encapsulated dextran (40 kDa) was achieved after swelling of hydrogels due to electrostatic repulsions of residual groups remaining after enzymatic cleavage of a pending peptide.[119]

More recently, several types of nanostructured materials, inorganic as well as organic, have been used to prepare enzyme-triggered release systems. See and al. showed the recovery of fluorescence after the release of a dye, connected to and quenched by gold nanoparticles via a peptide sequence.[120] Mesoporous silica, with pores covered by a grafted peptide, released their payload after cleavage of the surrounding peptide layer.[121-123] Concerning organic nanomaterials, a protein was encapsulated by adsorption and polymerization of monomers around it, including peptide cross-linkers. The protein recovered its activity after enzymatic cleavage of the cross-linking peptide.[124] Triggered release and activation of the drug were achieved inside cells after enzymatic cleavage of the outer layer, on nanoparticles covered with layer-by-layer assembly.[125] In his PhD thesis, Maier prepared hydrophobic peptide-polymer nanoparticles, where the peptide recognition sequence was selectively cleaved by a protease.[10] The cleavage was detected by fluorescence recovery of a FRET pair introduced around the recognition sequence.[126] Unstable liposomes, stabilized by a cross-linked polymer shell containing a peptide sequence cleaved by proteases, released their content when confronted to the enzyme.[127] Last but not least, nanoparticles made from polymerization of oligo(ethylene oxide) (meth)acrylate were prepared by a completely different method: step and flash imprint lithography. After UV photo-cross-linking with a cathepsin-B cleavable peptide macromonomer, the particles were able to release encapsulated antibodies and DNA in presence of the enzyme.[128]

Another work should also be mentioned, where a peptide based material, consisting of self-assembling β-sheet segments flanking a protease cleavable region, released a model therapeutic peptide when confronted to disease associated proteases.[129]

II.4 Solid-phase peptide synthesis[130-132]

II.4.1 Principle of the method

All peptides presented in this thesis were synthesized with solid-phase peptide synthesis (SPPS). This method was developed in the 1960s, mainly by Bruce Merrifield, who was awarded the Nobel Prize in 1984 for his work.[133, 134] The process is based on the stepwise growth of a peptide sequence on a cross-linked polymer resin. All amino acids are added through the same cycle consisting of deprotection, washing, coupling, and washing. When the whole sequence has been synthesized, cleavage from the resin and deprotection of the side chains of the functional amino acids are performed simultaneously in acidic solution. Such a method offers all the advantages from the solid-phase approach: work with excess reactant in solution to ensure very high coupling efficiency for each step, convenient washing between each step, and development of automated processes.

Compared to the biological process of protein and peptide biosynthesis, the chemical synthesis offers several advantages: the product is isolated very easily after cleavage from the resin, and no tedious purification from residues from organisms is required. Moreover, SPPS is a very versatile technique, as the desired peptide sequence can be easily changed (e.g., inversion of two amino acids or substitution of one amino acid by another). This versatility is also illustrated by the fact that non-natural (or artificial) amino acids can be used, like D-amino acids, spacers (e.g. PEO) or amino acids carrying specific physicochemical properties (fluorescence, orthogonal reactive group). Despite all these advantages, SPPS is only better adapted to relatively short peptide sequences (< 90 amino acids). Indeed, in contrary to biological synthesis, the chemical coupling step between each amino acid is not perfect with 100% yield. Therefore, longer peptides sequences become rapidly too impure, and give low yields after purification (typically by preparative HPLC). As a result, the synthesis of proteins (> 100 amino acids) remains the prerogative of biotechnology.

It was already stated that SPPS is a sequence of coupling and deprotection steps. More precisely, the peptide is synthesized from its C-terminal amino acid, which is anchored on porous “resin” beads. Typically, the porous resin beads consist of cross-linked polystyrene (1-2% divinylbenzene as crosslinking monomer) but other types of resins, made from poly(ethylene oxide) or polyacrylamide are on the market. In addition to their complete inertness to many solvents and reactants, the resins are designed (cross-linker amount, anchor group loading, mesh size) in such a way that a good swelling in the solvent leads to rapid diffusion of the reactants, activators and side products inside the polymeric network for efficient coupling and washing steps. The statistical distance between two growing peptides is chosen in such a manner that not too strong intermolecular interactions occur, which would lead to peptide aggregation and inefficient coupling. A schematic representation summarizing a solid-phase peptide synthesis can be found in **Figure 2,** with the example of the fluorenylmethyloxycarbonyl (Fmoc) as protective group.

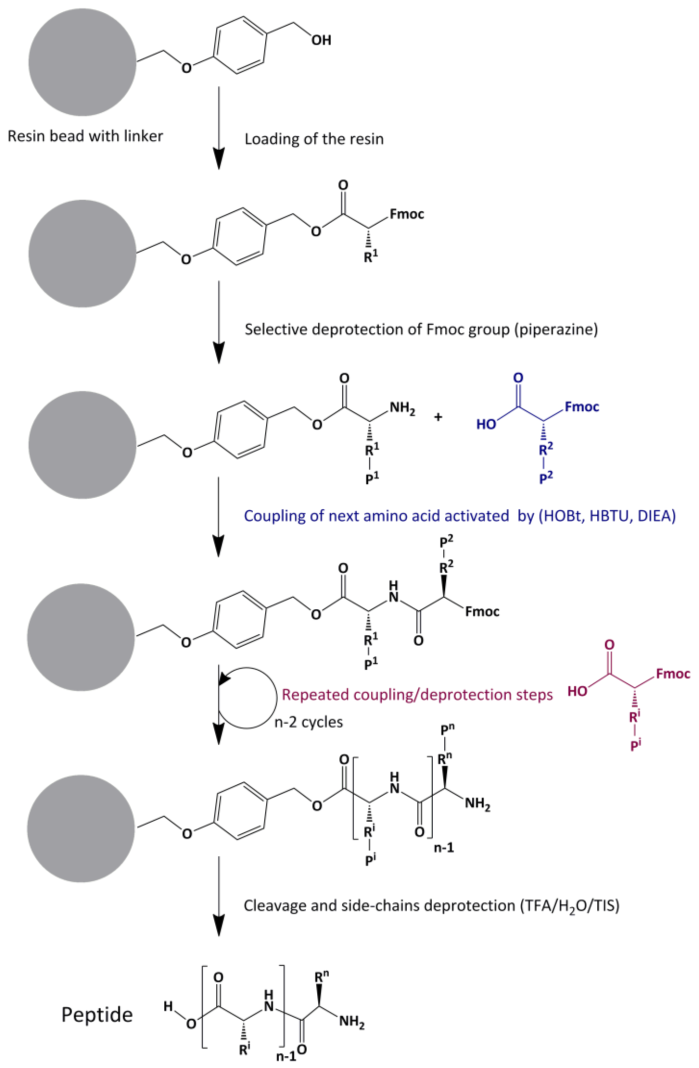
Resin bead with linker
OH
Loading of the resin
Fmoc
Selective deprotection of Fmoc group (piperazine)
NH2
HO
Coupling of next amino acid activated by (HOBt, HBTU, DIEA)
Repeated coupling/deprotection steps
n-2 cycles
n-1
Cleavage and side-chains deprotection (TFA/H2O/TIS)
Peptide

Figure 2: **Summary of solid-phase peptide synthesis by the Fmoc-strategy. R represents the side chain of an amino acid and P a protecting-group (if necessary) resisting to basic Fmoc deprotection.**

When a carboxylic acid group is desired in C-terminus (as it was the case in this thesis), a Wang resin, bearing *p*-benzyloxybenzyl alcohol, is used[135, 136] (see **Figure 2**). The first amino acid, typically provided on some commercial resins, is usually attached by esterification following the method of Sieber.[137] The growth of the peptide proceeds by successive coupling reactions between the carboxylic group of the *N*-protected amino acid, added in solution and the amino group of the peptide residue on the resin. This synthesis of a peptide (amide) bond is facilitated via the active ester method.

Two protecting groups can be used for the protection of the amino acids: fluorenylmethyloxycarbonyl (Fmoc) and *tert*-butyloxycarbonyl (Boc), which are both represented in **Figure 3**.

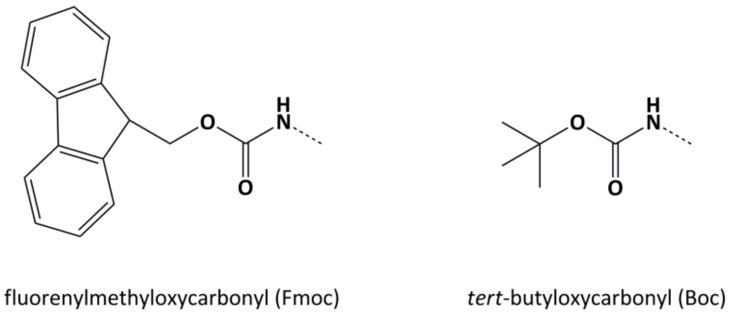
O
H
N
O
fluorenylmethyloxycarbonyl (Fmoc)
O
H
N
O
tert-butyloxycarbonyl (Boc)

Figure 3: Formula of Fmoc and Boc groups, two protecting groups of the amine function.

The Boc-group requires an acid deprotection step, while the Fmoc-group needs a basic deprotection. A consequence is that after deprotection, the Fmoc process leads to a neutral amine, whereas the Boc process results in an ammonium cation. As the coupling step is done in basic medium, this does not add a further step to the cycle, because the cation will be neutralized for coupling. The presence of the cation is even an advantage, as electrostatic repulsion limits the aggregation of the peptides. However, the Fmoc-procedure has become the standard technique, which can mainly be explained by the following reasons:

- the basic deprotection of the Fmoc groups allows an easier protection of the side chains, with various acid-sensitive protection groups, whereas the Boc-process requires acidic conditions for both deprotection and cleavage;
- for the same reason, an orthogonal synthesis is also made easier with basic-sensitive side groups;
- cleavage and final deprotection after Boc process requires hydrofluoric acid (HF), which means that special equipment is needed. HF is potentially more dangerous than trifluoroacetic acid (TFA), used in the Fmoc process.

Thus, the standard Fmoc procedure was preferred for the work in this thesis, as presented above in **Figure 2**.

II.4.2 Mechanistic approach

In the following paragraphs, the deprotection and coupling steps will be presented in further detail.

Cleavage of the Fmoc group

The deprotection of the amino acid (cleavage of the Fmoc group) after coupling proceeds under mild basic conditions (piperazine), as presented in **Figure 4**. It has the advantages that side chains of amino acid residues can be protected with acid-labile protecting groups.

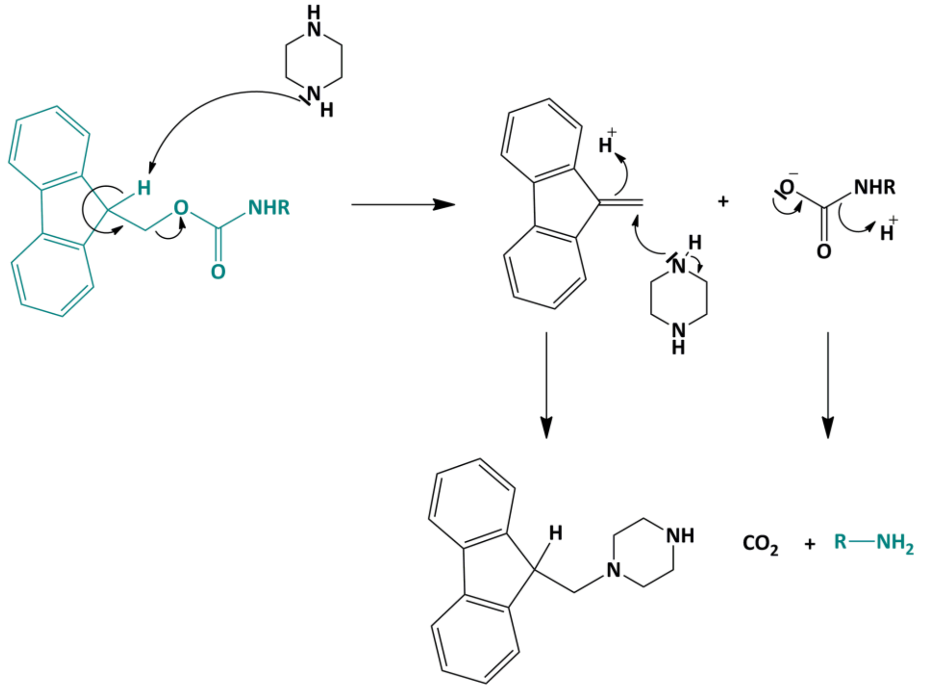

Figure 4: **Deprotection mechanism of the *N*-terminus via cleavage of the Fmoc group by piperazine (R= peptidyl group, attached to the resin in SPPS).**

Activation of the coupling reaction

The coupling reaction needs to be activated to reach high yields in a very short time. Therefore, the active ester method is used: to enhance the electrophilicity of the carboxylate group, the negatively charged oxygen must first be "activated" into a better leaving group. The negatively charged oxygen acts as a nucleophile, temporarily yields an ester with a very good leaving group, making the nucleophilic attack by the terminal amino group on the growing peptide more efficient. A broad range of activators can be found in the literature.[138] Among them, the family of the *O*-benzotriazol based compounds (HOBt[139], HBTU, HATU, BOP, PyBOP) is very frequently used. The esters formed with these compounds are so highly activated that their reactivity cannot only be explained by the good electron withdrawing properties of the ester moiety. The formation of a hydrogen bond between a pair of unshared electrons from the triaza group and a proton of the amine group promotes nucleophile attack at the carbonyl (see mechanism on **Figure 5** with the example of HOBt).[140] This neighboring group participation is referred to as anchimeric assistance, but can also be considered as an intramolecular base catalyzed reaction.

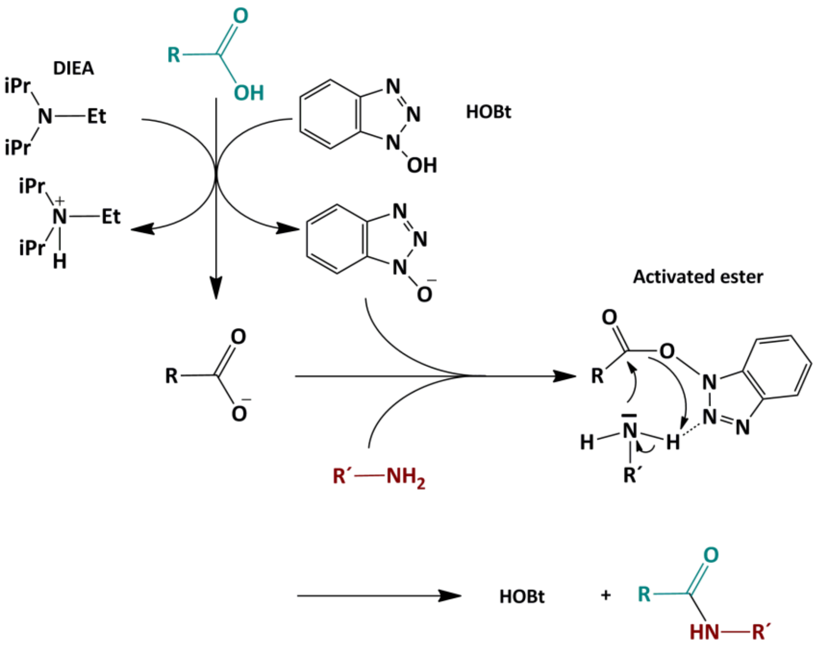

Figure 5: **Peptide coupling mechanism via the active ester method. Here the example of 1-hydroxybenzotriazole (HOBt) is shown. In the case of SPPS, R = Fmoc protected amino acid radical, R´= peptidyl group attached to the resin.**

Practically, one can observe that HOBt is almost always used in presence of phosphonium (BOP, PyBOP) or uronium (HATU, HBTU) derivates. The differences in the mechanism compared to HOBt with these activators are illustrated in **Figure 6**, with the example of HBTU. The carboxylate anion attacks more rapidly the coupling agent, giving an acyloxycarbenium intermediate, which can be aminolyzed (path in red) but is more likable to be converted in benzotriazolyl ester, and then into amine (path in blue). Even if the use of only phosphonium or uranium salt-based reagent leads to the peptide, HOBt is commonly used as excess additive (See "excess HOBt" annotation in **Figure 6**). It has been shown that additional HOBt in the form of the anion massively promotes the formation of the activated ester by equilibrium displacement.[141]

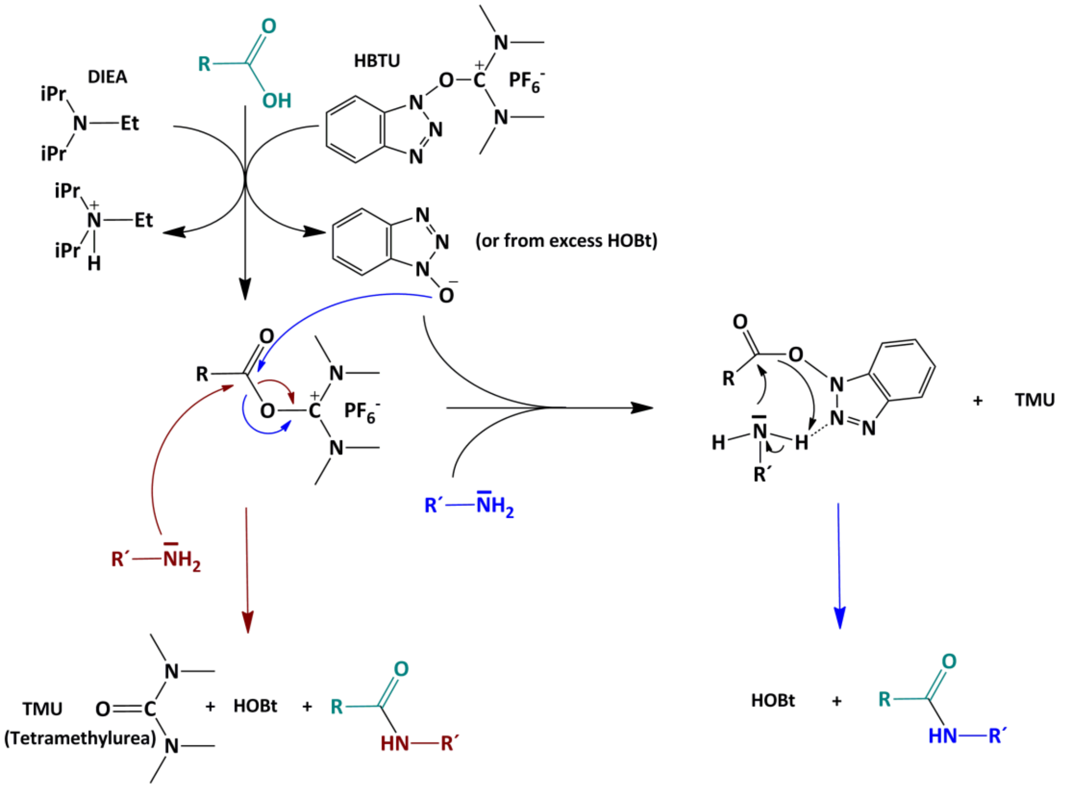

Figure 6: **Peptide coupling mechanism via the method of the activated ester. Here the example of HBTU is shown.**

Conservation of stereochemistry

Finally, HOBt plays a key role in an important desired property of the activated coupling reaction: the preservation of stereochemistry of the L-amino acid in C-terminus. This is a major problem in the synthesis of peptides, because of the consequent loss of tridimensional structure and biofunctionality. Indeed, with some activators like the carbodiimides, a possible intermediate on the way to the amide product is the formation of oxazolone from the activated species (*O*-acilyisourea when a carbodiimide is used as activator). Because of the possibility to form a conjugated system, the α-proton is in general very labile, with some variations due to the nature of the amino acid. In this case, the ketone-enol equilibrium leads to epimerization. As an acid, HOBt plays a double role to prevent the loss of chirality: it can protonate the *O*-acylisourea and therefore prevent the formation of oxazolone. If this happens, HOBt can still protonate the oxazolone, which hinders its enolization and favors the subsequent nucleophile attack of the amine group or of the oxybenzotriazole anion (see **Figure 7**). To sum up, HOBt is a key reactant of the coupling reaction, for both activation of the carboxylic group and conservation of the chirality of the amino acid.

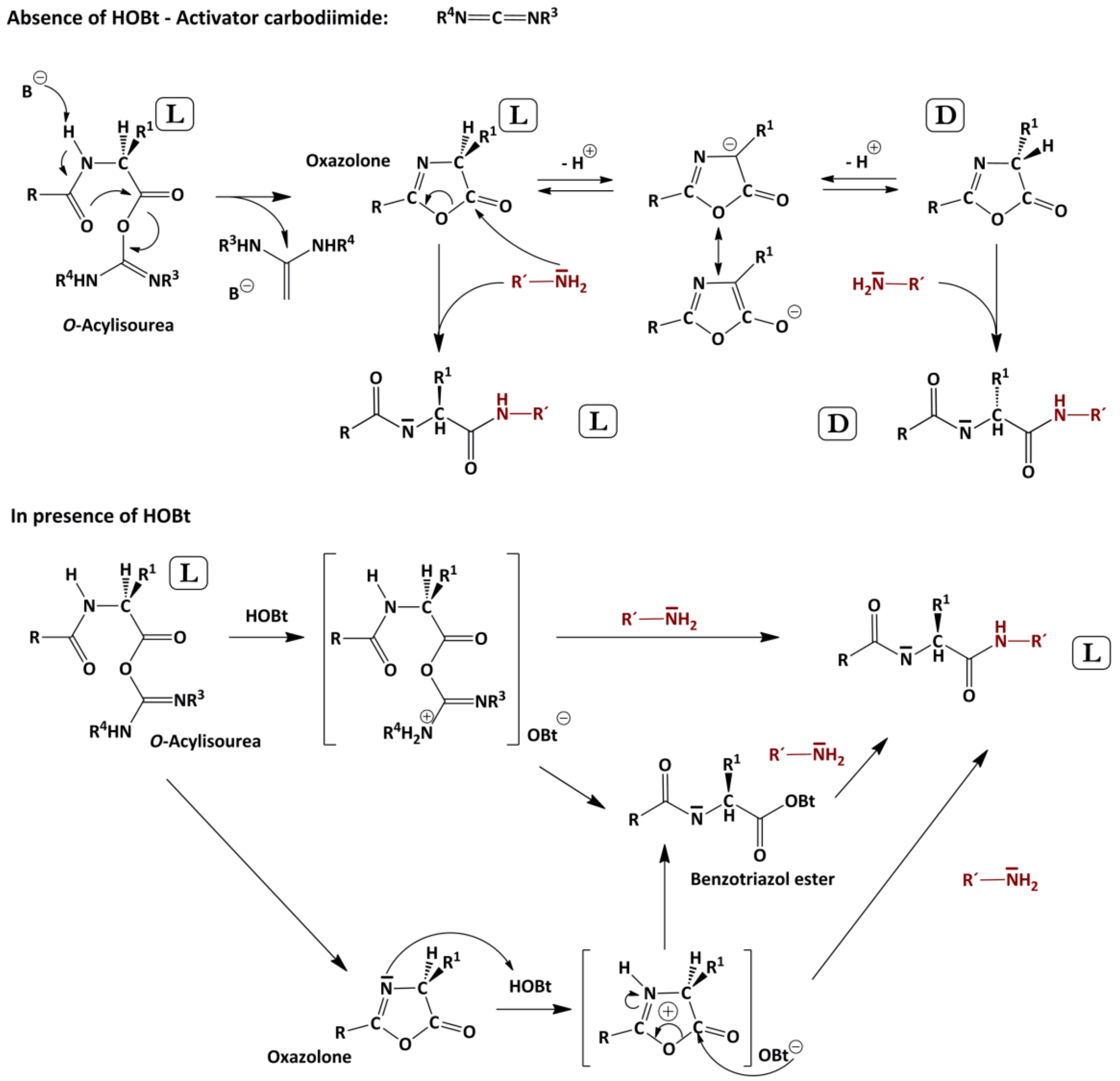
Absence of HOBt - Activator carbodiimide: $R^4N{=}C{=}NR^3$
O-Acylisourea
Oxazolone
L
D
- H
R´—NH₂
H₂N—R´
In presence of HOBt
HOBt
OBt
Benzotriazol ester

Figure 7: **Mechanism of the epimerization encountered with some activators (example of a carbodiimide) and mechanistic action of HOBt allowing the conservation of the chirality.**

Please note that recently, HOBt has been classified as explosive by the United Nations. Although almost always found as a hydrate, the product can no longer be shipped by air or sea. As a result, it has been removed from many chemical vendors. Within the last months of this thesis, HOBt was replaced by ethyl 2-cyano-2-(hydroxyimino)acetate (**Figure 8**, commercial name Oxyma Pure), which has recently been described as “as efficient as HOBt”.[142]

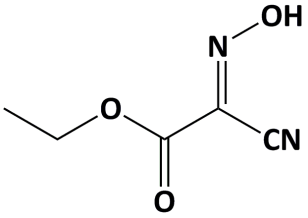

Figure 8: **Structure of 2-cyano-2-(hydroxyimino)acetate (Oxyma Pure).**

Choice of activating base

In every case, a base is necessary for the deprotonation of the carboxylic acid to form the nucleophilic carboxylate anion and neutralizing the acids liberated by aminolysis. However, this base should not be too strong, to avoid binding protons that were not intended to be removed. It has been found that tertiary amines are suitable bases, due to their strength and the steric hindrance around the basic non-nucleophilic nitrogen atom. Among certain tertiary amines, diisopropyethylamine (DIEA) was reported as the most efficient base for phosphonium and uranium salt-mediated coupling reactions.[143] However, tertiary amines promote the isomerization during phosphonium and uranium salt-mediated coupling reactions without any additive but again, the most hindered tertiary amine DIEA induced the lowest isomerization rate in DMF.[144]

Microwave-assisted peptide synthesis

Microwave irradiation was used in organic chemistry from the end of the 1980s, and became a very efficient way to accelerate reactions. A debate has started a few years ago concerning the idea that thanks to the electromagnetic radiations, microwaves could decrease the racemization and increase the yields of coupling thanks to lower aggregations.[145] In any case, microwave is a convenient method for rapid and homogenous heating of the peptidyl resin.

II.5 Miniemulsion

II.5.1 Polymerization in heterophase

Aqueous polymeric dispersions are used for numerous applications, such as synthetic rubber, adhesives, paints, additives in paper and textiles, binders for non-woven fabrics, etc. The rapid development of this industry can be explained by environmental regulations to limit solvent-based systems and substitute them by water borne products. In addition to these environmental aspects, polymeric dispersions also have properties that meet industrial demands such as lower viscosity, heat transfer, and convenient processability also for high solids content systems, making them interesting, also for high-tech applications. For example, they are used in biomedical and pharmaceutical areas for diagnostic tests and drug delivery systems.

Commonly, these products are prepared by free radical polymerization in suspension or emulsion polymerization. In suspension polymerization, large droplets are permanently agitated in the presence of protective colloids during polymerization. The addition of a small amount of surfactant (even far under the critical micellar concentration, CMC) results in the formation of smaller droplets. The monomer is polymerized from an oil-soluble initiator inside the droplets, and kinetically, each droplet acts as an independent reactor for bulk free radical polymerization. As a result, polymers beads with approximately the size of the droplets (from 0.1 to 10 mm) are formed.

In emulsion polymerization, the addition of surfactant in a concentration above the CMC generates micelles in addition to the stabilized monomer droplets (20-50 µm). The use of water-soluble initiators generates radicals in the continuous phase, where they oligomerize with monomer dissolved in water or diffusing between the monomer droplets. As growing oligomers become less soluble in water, they enter a micelle, where particle nucleation occurs and the polymerization continues. This is provided by diffusion of the monomer from the monomer droplets into the micelles. The particles produced by emulsion polymerization range from 50 to 500 nm.

II.5.2 Miniemulsion principle

In this paragraph, the principle of the miniemulsion is presented in general, taking the example of direct (oil-in-water) miniemulsion when necessary. The inverse miniemulsion is presented afterwards. Miniemulsion polymerization can be regarded as the adaptation of the suspension polymerization at a smaller scale, as the goal is that each nanodroplet behaves like an independent reactor. To achieve the formation and stabilization of the nanodroplets, several requirements have to be fulfilled:

Generating small nanodroplets requires high-energy input to overcome the increasing interfacial energy when the droplets become smaller. Indeed, the overall interfacial area increases when the size of the droplets decreases, and the interfacial energy required *dE* is proportional to the variation of the interfacial area *dA*, following Equation (1):

$$dE = \gamma_{LL} dA$$

Equation (1)

With: γ_{LL} the surface tension between the two liquid phases ($J \cdot m^{-2}$ or $N \cdot m^{-1}$)

High-pressure homogenizers (high shear forces) and ultrasonication tips (cavitation pressure) are the most frequently used devices. The presence of surfactant lowers the surface tension between continuous and disperse phase and helps considerably the emulsification process. The droplets need to be stabilized with surfactant to prevent fusion by collision, via steric or electrostatic repulsive forces. In miniemulsion, the concentration of surfactant is chosen such that after homogenization, the concentration in the continuous phase is below the CMC.

If the droplets do not all have exactly the same size after homogenization, Ostwald ripening occurs over time: diffusion of monomer from the smaller to the bigger droplets progressively removes the smaller droplets and the average size of the droplets increases continuously. The driving process of the Ostwald ripening is the Laplace pressure inside the droplets, or more exactly the difference of Laplace pressures between the smaller and bigger droplets (thermodynamically more stable). Laplace pressure P_L ($N \cdot m^{-2}$) expresses as following:

$$P_L = \frac{2\,\gamma_{LL}}{r}$$

Equation (2)

With: γ_{LL} the surface tension between the two liquid phases ($N \cdot m^{-1}$)

r the radius of the droplets (m)

Smaller droplets, with a higher Laplace pressure, are less stable than the bigger droplets, and tend to disappear slowly via monomer diffusion from the smaller to the bigger droplets, which become more stable as their size increases, etc. Moreover, the speed of Ostwald ripening increases with the solubility of the monomer in the continuous phase, as the monomer can diffuse faster to the bigger droplets.

To counteract and minimize Ostwald ripening, an osmotic agent is added to the disperse phase. The osmotic agent has a very low solubility in the continuous phase and cannot diffuse between the droplets (e.g. hexadecane in direct miniemulsion). Thus, the osmotic agent creates an osmotic pressure inside the droplets (see Laplace equation below and Equation (3)), which suppresses the Ostwald ripening if the osmotic agent is homogenously distributed. Its presence within the droplets creates an osmotic pressure, described by:

$$\Pi_{osm} = c \cdot R \cdot T$$

Equation (3)

With: c the concentration of the osmotic agent (mol·L^{-1})

R the ideal gas constant (8.314 J·K^{-1}·mol^{-1})

T the temperature (K)

As a result, the homogenous distribution of the osmotic agent increases the stability of the smaller droplets. Diffusion of monomer between the droplets can still occur but is compensated. The roles of the surfactant and of the osmotic agent are illustrated in **Figure 9**.

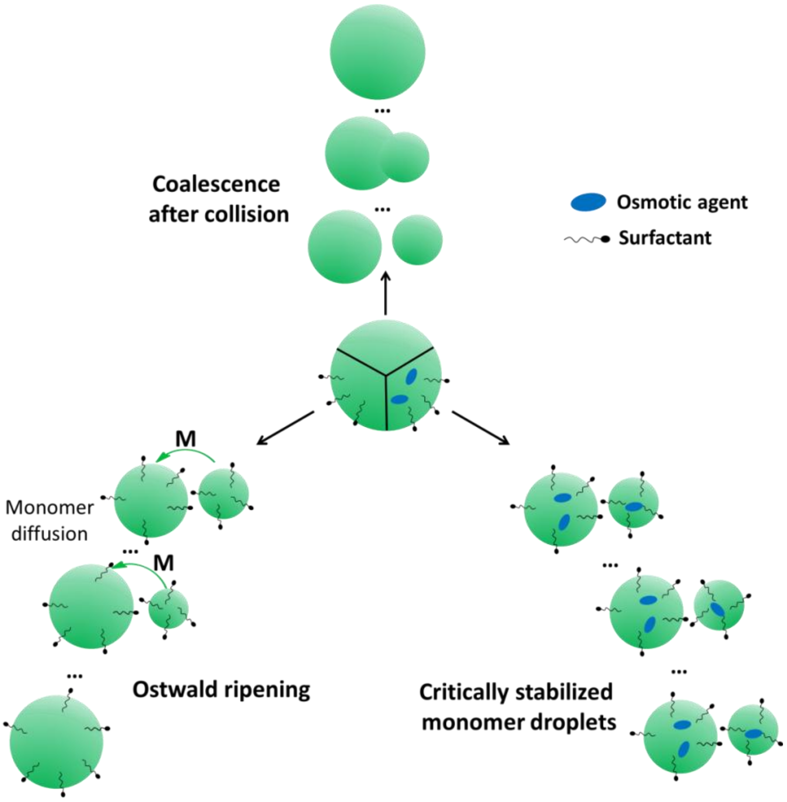

Figure 9 : **From non-stabilized to critically stabilized nanodroplets. Surfactant and osmotic agent act against fusion and Ostwald ripening.**

It is important to precise that under standard conditions and after ultra-homogenization, the osmotic pressure does not necessarily fully compensate the Laplace pressure. However the droplets are highly stable, thanks to the different stabilization mechanisms. The miniemulsion is not a thermodynamically stable state, but a critically stabilized steady-state. The surface of the droplets is not fully covered with surfactant molecules and no micelles formation occurs in the continuous phase. Since nearly no surfactant is present in the form of micelles, free radical polymerization of nanoparticles nucleated via entry of radical into monomer nanodroplets is possible. Initiator directly incorporated in the droplets can also be used, as long as it not disrupted by the high energetic homogenization process. But most of all, each nanodroplet can be considered as an independent nanoreactor[146] with one-to-one copy from the monomer droplet to the polymeric particle (**Figure 10**).

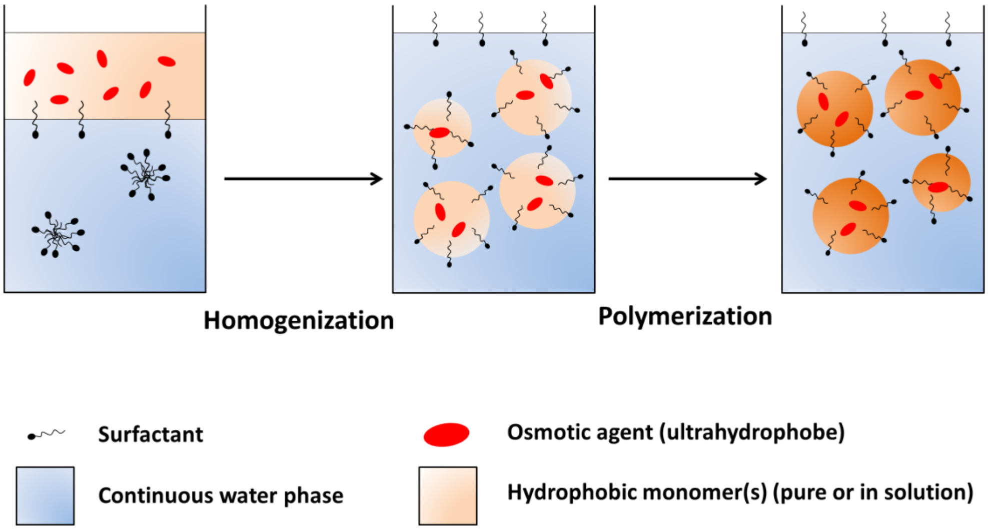
Homogenization
Polymerization
Surfactant
Osmotic agent (ultrahydrophobe)
Continuous water phase
Hydrophobic monomer(s) (pure or in solution)

Figure 10: **General principle of direct miniemulsion polymerization. After being subjected to high shear, the two immiscible phases result in narrowly distributed hydrophobic nanodroplets (containing the osmotic pressure agent) in water. Ideally, no change of the droplets is observed during the consecutive reaction process.**

This decisive property allows other types of polymerization than free radical polymerization in heterophase, like polycondensation, polyaddition or anionic polymerization[147, 148] and gives access to various structures at the nanoscale,[148, 149] especially capsules as explained below in paragraph II.5.4. It also permits the highly efficient encapsulation of compounds soluble or dispersible in the disperse phase, such as dyes, biomolecules, or inorganic nanoparticles.[150, 151]

II.5.3 Inverse miniemulsion

The principle of miniemulsion can also be applied to inverse systems (**Figure 11**). In inverse (or water-in-oil) miniemulsion, the hydrophilic phase is dispersed in a hydrophobic continuous phase. In this case, the water (or polar) droplets are stabilized with surfactants with low hydrophilic-lipophilic balance (HLB <7), e.g. of certain non-ionic block copolymers with suitable block-lengths ratio. Hydrophilic osmotic agents are used to balance diffusion between the droplets, e.g. inorganic salts, sugars, or alcohols. The main interest in inverse miniemulsion is the possibility to prepare particles or capsules with a hydrophilic payload.[152] Moreover, regarding the process employed and the non-solubility of the hydrophilic payload in the dispersed phase, very high encapsulation yields are achieved.[153] It makes these materials highly interesting for bio-applications after redispersion in water, as they carry then the hydrophilic payload at high concentrations in water-based system.

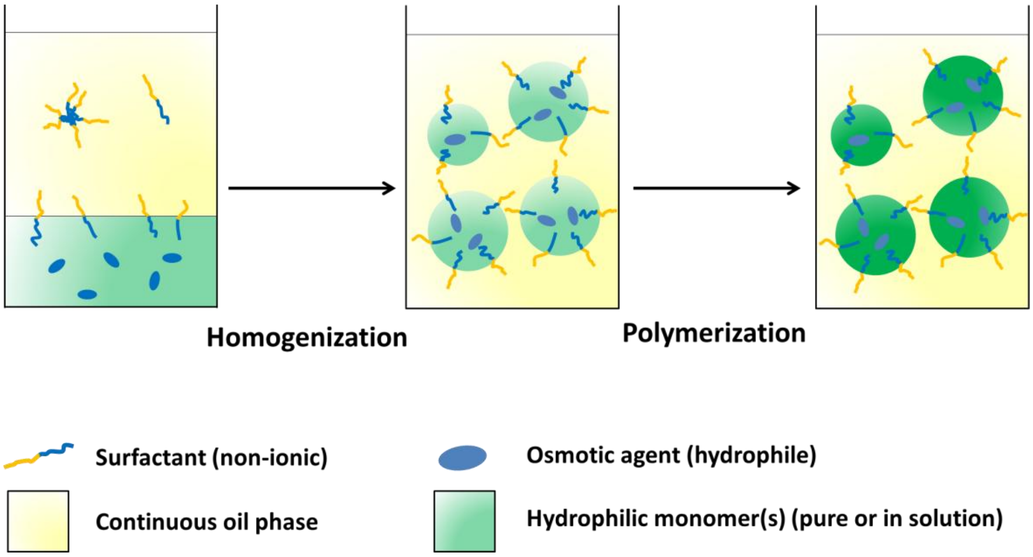
Homogenization
Polymerization
Surfactant (non-ionic)
Osmotic agent (hydrophile)
Continuous oil phase
Hydrophilic monomer(s) (pure or in solution)

Figure 11: **General principle of inverse miniemulsion polymerization. Here, the dispersed phase is made of hydrophilic droplets. Ideally, thanks to the osmotic pressure agent and the surfactant, no change of the droplets is observed during the consecutive reaction process. Hydrophilic content can be encapsulated by prior dispersion or dissolution in the dispersed phase.**

II.5.4 Preparation of capsules via miniemulsion

Capsules are generally particles with a liquid core. It has been explained in the previous paragraph why the mechanism of miniemulsion makes this technique very suitable for the synthesis of nanocapsules with hydrophobic content (direct miniemulsion) or hydrophilic content (inverse miniemulsion). Other methods allow the preparation of nanocapsules, like the layer-by-layer approach,[154, 155] which is also suitable for the encapsulation of larger biomolecules.[156] The available possibilities to prepare nanocapsules via the miniemulsion process are: 1) phase separation by polymerization, 2) nanoprecipitation of polymers, and 3) interfacial polymerization. This three processes will be presented in the following paragraphs are schematically represented in **Figure 12**.

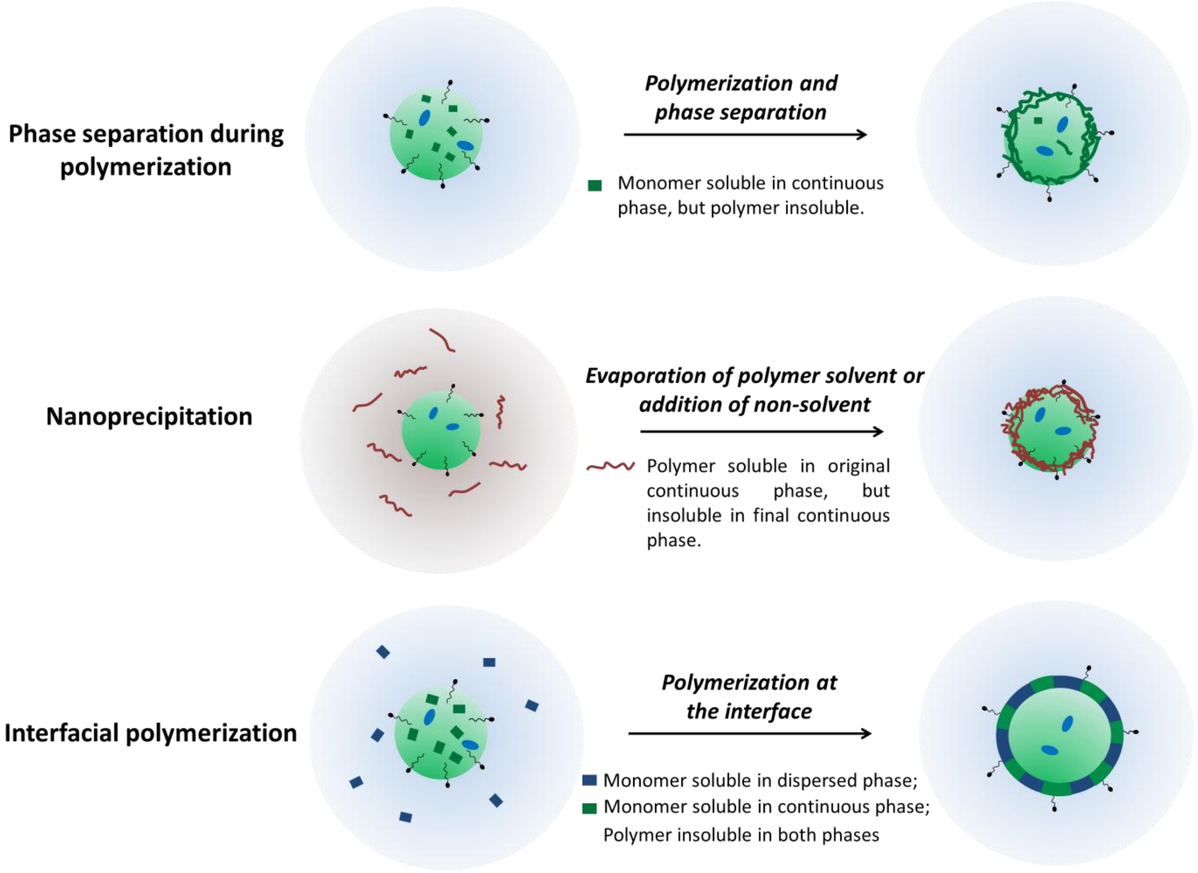
Phase separation during polymerization
Polymerization and phase separation
🟩 Monomer soluble in continuous phase, but polymer insoluble.
Nanoprecipitation
Evaporation of polymer solvent or addition of non-solvent
Polymer soluble in original continuous phase, but insoluble in final continuous phase.
Interfacial polymerization
Polymerization at the interface
🟦 Monomer soluble in dispersed phase;
🟩 Monomer soluble in continuous phase;
Polymer insoluble in both phases

Figure 12 : Schematic summary of the different possibilities to prepare nanocapsules through the miniemulsion process

Independently of the strategy used to prepare the nanocapsules, their formation is explained by both thermodynamic and kinetic factors. For a thermodynamic approach, the work of Torza and Mason proposes a model to predict the different morphologies obtained from two immiscible hydrophobic liquids (oil 1 and oil 2) in water as dispersed phase.[157] The morphologies predicted by the authors are based on the combination of the spreading coefficients from this tertiary system (i, j, k). Spreading coefficients S_i are defined as:

$$S_i = \gamma_{j/k} - (\gamma_{i/j} + \gamma_{i/k})$$

Equation (4)

$\gamma_{i/j}$ is the interfacial tension between phase i and j, etc. Assuming that $\gamma_{o1/w} > \gamma_{o2/w}$ (oil 1 is more hydrophobic as oil 2), morphologies can be predicted from the combination of the spreading coefficients as shown in **Figure 13**.

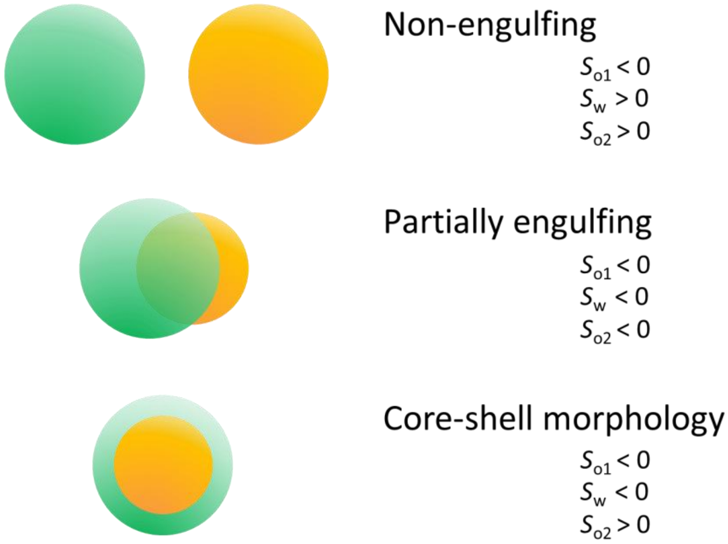

Figure 13: Equilibrium morphologies in a three liquid phase system. Oil 1 is in green, Oil 2 in orange and water is the continuous phase, with $\gamma_{o1/w} > \gamma_{o2/w}$.

This model provides a general idea for the formation of the resulting thermodynamically stable morphology. This can be attributed to the fact that the model does not take kinetic parameters into account. Kinetic parameters as the anchoring effects, corresponding to the interactions between entering radical and surfactant, and leading to polymerization located as the interface, are neglected in the model. In addition the model considers three immiscible liquids, while one component is a polymer with a high viscosity. The presence of the surfactant is also not considered, and it was shown that the nature of the surfactant also plays a role in the morphology of the capsules. Therefore, the polymerization of butyl acrylate in the presence of hexadecane as performed in miniemulsion leads to kinetically controlled structures.[158]

As a result, the necessary requirement for phase separation and subsequent capsule formation is the loss of solubility of the polymer formed in the dispersed phase. However, thermodynamics is not sufficient to explain the structures observed and kinetic parameters (e.g. viscosity of the polymer), also play and determining role.

Capsules formation by phase separation

The dispersed phase consists of a monomer dissolved in an organic liquid, which is a non-solvent for the polymer formed. Under optimized conditions with an adjusted hydrophilicity of the polymer and a suitable oil with long hydrocarbon chain like hexadecane or triglyceride, phase separation occurs and the oil is eventually encapsulated by the polymeric shell formed. The nature of the polymer is important: the ratio of capsules to particles increases with the hydrophilicity of the polymer. This can be observed with homopolymer (e.g. PMMA versus PS) but also by increasing incorporation of more hydrophilic comonomer, like methyl methacrylate or acrylic acid in polystyrene.[159] The size and the thickness of the capsules can be adjusted by varying the ratio of monomer to encapsulated oil. The concentration and nature of the surfactant also had an influence on the morphology, as well as the nature of the initiator: in the case of MMA/hexadecane droplets, capsules where obtained using AIBN as oil-soluble initiator, while the water-soluble initiator potassium persulfate (KPS) yielded nanoparticles. The nature of the initiator can also very important, in the case where the locus of polymerization is kept close to the droplet/water interface. Indeed, capsules were obtained in miniemulsion by polymerization from interfacially active initiators by Van Zyl, firstly by radical polymerization of butylacrylate in hexadecane[158] and later by RAFT polymerization. In the second case, pure polystyrene capsules were obtained, when a suitable RAFT agent, i.e. with no rate retardation and corresponding sufficiently rapid increase in the chain length, was used in the presence of a water-soluble initiator.[160] Rapid polymerization leaded in this case to a rapid increase of viscosity and to a lower chain mobility. These last examples are sometimes also considered as interfacial polymerization, as the polymer is formed from this interface. Finally, cross-linked polystyrene nanocapsules with an isooctane core were also obtained via microemulsion polymerization (complete coverage of the droplets with surfactant), using KPS as initiator.[161]

Nanoprecipitation

The nanoprecipitation technique is based on the precipitation of solvated polymer chains on the interface of stabilized nanodroplets. The addition of a non-solvent to, or the evaporation of a solvent from the continuous phase causes the precipitation of the polymer. Working with preformed available polymers presents some advantages. It avoids the presence of possible residues of monomer or oligomers in the final product. This method is also valuable for polymers, which cannot be synthesized in heterophase, e.g. because of the use of catalysts. Nanoprecipitation is also very suitable for encapsulation, as it removes any risk of cross reaction between the polymerizing monomer(s) and the encapsulated content. For example, indomethacin-loaded poly(D-L-lactide) were successfully prepared.[162] More recently, the encapsulation of hydrophilic antibiotic agent inside poly(methylmetacrylate) (PMMA), poly(caprolactone) (PCL) and poly(methylacrylate) (PMA) capsules was achieved via controlled water-in-oil nanoprecipitation.[163] For this, stabilized water droplets containing the antibiotic were dispersed by ultrasonication in a cyclohexane/dichloromethane (non-solvent/solvent) mixture containing the polymer. The evaporation of dichloromethane (more volatile) led to the precipitation of the polymer at the interface of the droplets and successful encapsulation of the antibiotic inside the consequently formed nanocapsules. For PMMA, the encapsulation efficiency was increased significantly with the overall polymer weight concentration, independently of the molar mass of the polymer (71 000, 335 000 and 996 000 $g \cdot mol^{-1}$). The capsules obtained with the longest PMMA chains remained impermeable after redispersion in water, whereas the ones prepared from the lower molecular weight PMMA lost some of their payload.

Interfacial polymerization

Interfacial polymerization designates the cases, where the polymerization reaction is located at the interface of the two phases. It can proceed in homopolymerization of a monomer, as described previously, or by the reaction between different comonomers, of which one is soluble in the continuous and the other in the dispersed phase. The polymerization has to proceed at the interface then, and very frequently, the polymer formed is soluble neither in the dispersed nor in the continuous phase and precipitates at the interface, where it can grow further.

Interfacial polycondensation reaction in emulsion was firstly reported in the 1950s with the preparation of polyamides.[164, 165] Among others, the synthesis of Nylon by interfacial polycondensation in emulsion in 1964 is regarded as a decisive achievement, as microcapsules with liquid cores were obtained for the first time.[166] Further work on interfacial polycondensation was reviewed by Arshady in 1989, and at this time it was already clearly stated that interfacial polymerization could lead to different morphologies.[167] If the resulting polycondensate is soluble in the droplet phase, particulate microspheres or monolithic microcapsules are formed. If the polymer is insoluble in the droplets, a membrane is formed around the droplets, which are individually encapsulated. As a result, the first encapsulation of proteins in polyamide microcapsules prepared by interfacial polycondensation was reported.[168]

Polyaddition, in contrary to polycondensation, does not lead to the formation of small molecules as side products. Polyaddition in direct miniemulsion was first reported using epoxy-monomers reacting with diamines, dithiols or bisphenols, leading to particles in the nanometer range.[169] An interesting work was carried out with this method by Taira, as they used the two amino groups of lysine for a successful polyaddition reaction with a diepoxy comonomer.[170] The reaction was carried out in inverse miniemulsion, and the particles were used afterwards for pH-induced adsorption and release of single-stranded DNA, via electrostatic interactions with the carboxylic group and free amino residues of the lysine. The interfacial polyaddition of a polyepoxy-amine polymer was achieved both in direct (oil-in-water) and inverse (water-in-oil) emulsion, yielding capsules at the micrometer scale.[171]

Polyaddition was also achieved with other monomers: polyurethane nanocapsules with an oil core were prepared via the interfacial polyaddition of diisocyanate (dissolved in the oil phase) with a diol (dissolved in continuous aqueous phase). The presence of urea bonds was reported, certainly due to the reaction of isocyanate with water during the ultrasonication process.[172] Further studies of synthetic parameters, such as the nature of the surfactant, the variation of pH and the ionic strength in the aqueous phase, and their influence on the stability and size of the capsules were carried out, oriented toward the encapsulation efficiency of the oil inside the polyurethane capsules.[173] An impressive example illustrating the efficiency of this approach was the preparation of core-shell particles: styrene as monomer was successfully encapsulated in a polyurethane shell resulting from interfacial polyaddition. Afterwards, the styrene was polymerized inside the capsules via radical polymerization, leading to polystyrene-core-polyurethane-shell particles.[174]

The same reaction was achieved in inverse miniemulsion by Crespy et al., allowing the preparation of polyurethane and polyurea nanocapsules with a hydrophilic core. The capsules size and shell thickness can be adjusted via the monomer and surfactant concentration.[152, 175] This method opened possibilities for the encapsulation of a water-soluble payload[153] and the use of polysaccharides as polyol was also successful to prepare capsules based on biomacromolecules.[176]

Moreover, interfacial polymerization was also reported using radical polymerization. One can here distinguish two strategies. The first approach is based on the use of two monomers, which both do not homopolymerize but polymerize only in an alternating fashion. One monomer is dissolved in the oil phase (maleate ester), the other in the continuous water phase (polyhydroxy vinyl ether) and alternating polymerization proceeds at the interface, yielding monodispersed nanocapsules.[177] This very elegant interfacial free-radical alternating polymerization was used later to prepare aqueous core cross-linked nanoparticles and study the diffusion release of an encapsulated dye.[178] Another method is based on controlled radical polymerization, more exactly atom transfer radical polymerization (ATRP): it was found that the living chain growth of MMA inside the oils droplets also incorporated up to 24% of poly(ethylene glycol) monomethacrylate monomer present in the water phase. By the addition of a cross-linker (diethylene glycol dimethacrylate), nanocapsules were obtained by interfacial controlled radical polymerization.[179] Similarly, poly(butyl cyanoacrylate) nanocapsules were prepared in inverse miniemulsion thanks to the rapid anionic polymerization of butyl cyanoacrylate at the interface of the water droplets.[180, 181]

II.6 Polyaddition

Addition polymers are polymers obtained by reaction of monomers bound together via an addition reaction, without the formation of any side-product or loss of molecule. This is in contrast to condensation reactions, where small molecules are liberated. A typical example is the preparation of polyurethanes from the polyaddition reaction between a diol and a diisocyanate (see **Figure 14**). Polyurethanes are widely used in the industry for numerous applications, like insulation foams, sealants, coatings, adhesives, or elastomers, depending on their density and stiffness.

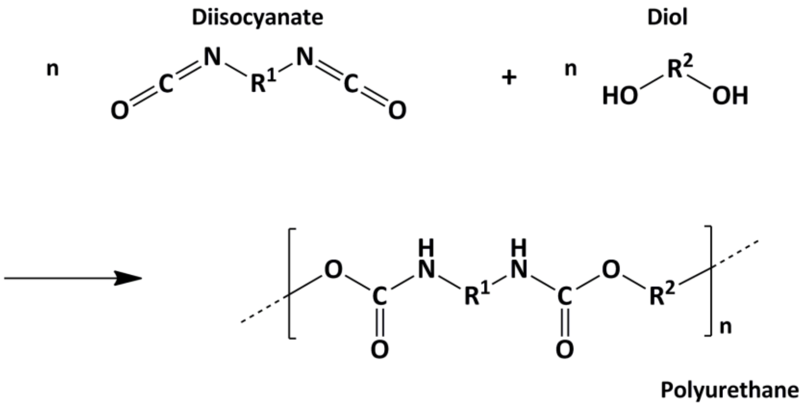

Figure 14 : Polyaddition of diisocyanate and diol to polyurethane

II.6.1 Characteristics of polyaddition

Polyaddition takes place following a step-growth polymerization. It consists on the formation of dimers, trimers, and oligomers, which eventually transform in long polymer chains at high conversion rates (**Figure 15**). In principle, it means that stoichiometric proportions have to be respected precisely and high purity is required to obtain high molecular weights in the case of linear polymers.

In the case of linear polymers, obtained from an A-B functionalized monomer or in the case of perfect stoichiometry between two monomers A-A and B-B, the number average value of the degree of polymerization DP can be obtained from the Carothers equation:

$$DP = \frac{1}{1-p}$$

Equation (5)

With p the conversion rate of monomer at time, defined by:

$$p = \frac{N_0 - N_t}{N_0}$$

Equation (6)

N_0 is the initial number of monomer molecules and N_t is the number of monomer molecules which are still present at the time t during the reaction. The Carothers equation explains the hyperbolic form of the curve representing the degree of polymerization against monomer conversion for a step-growth polymerization (see **Figure 15**).

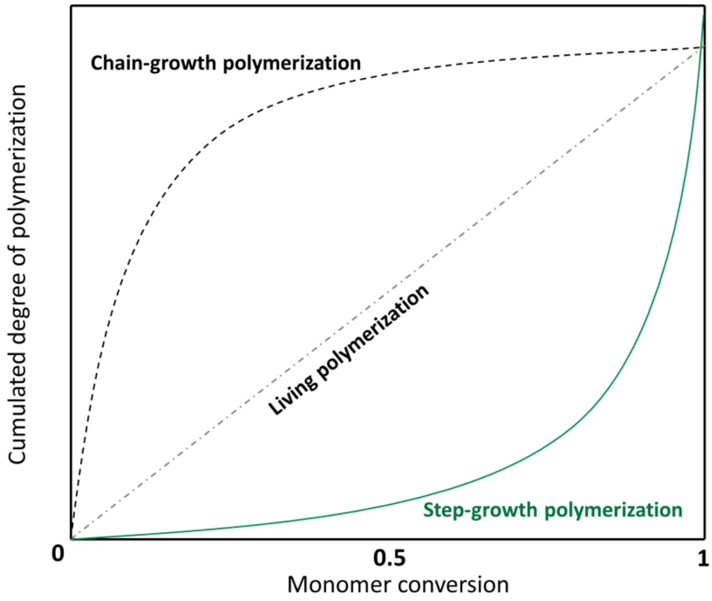

Figure 15: **Evolution of the degree of polymerization with the monomer conversion in a step-growth polymerization. The chain-growth polymerization and living polymerization curves have been traced for comparison.**

If the two difunctional monomers (A-A) and (B-B) are not introduced in equal proportions, one defines the ratio r as $N_{A-A}\ \ N_{B-B}$, with $r < 1$ (where B-B is the monomer in excess). This can be the case in the preparation of functionalized prepolymer. Then, *DP* can be calculated as:

$$DP = \frac{1 + r}{1 + r - 2rp}$$

Equation (7)

For high conversion rates, the average value of the degree of polymerization DP is then limited by:

$$DP_{max} = \frac{1 + r}{1 - r}$$

Equation (8)

Models have also been developed from this equation for branched polymers obtained from monomers with a functionality higher than 2, without taking in account the possibility of cross-linking and network formation.

II.6.2 Reactivity of the isocyanate group

The isocyanate group is an unstable and highly reactive function, which can react with amine and hydroxyl groups, and needs to be blocked when the reactants are stored for several months. The high reactivity of the isocyanate function is illustrated through the mesomeric contributing structures shown in **Figure 16**. The central carbon atom is electrophilic and constitutes the main reactive center of the isocyanate function.

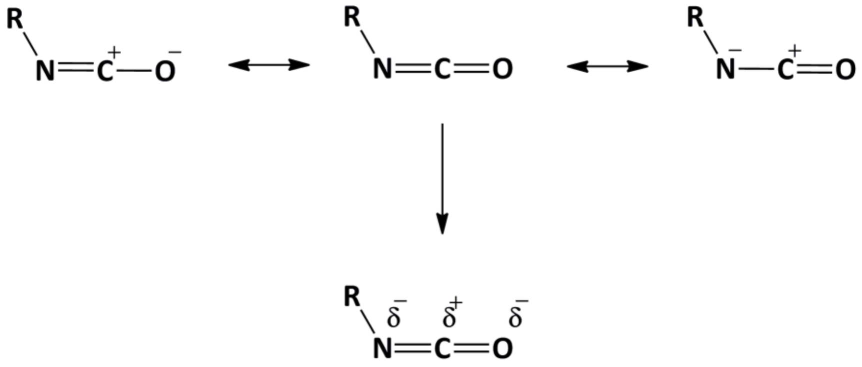

Figure 16: Reactivity of the isocyanate group visualized through its mesomeric contributing structures.

The intended reactions involving isocyanate are mainly the formation of urethane or urea, the mechanism of which is displayed on **Figure 17**.

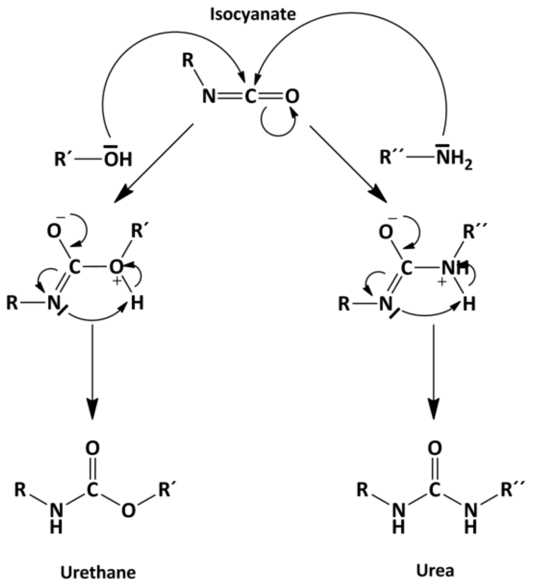

Figure 17: Polyaddition mechanism of the formation of urethane and urea.

Methylene diphenyl diisocyanate (MDI), toluene diisocyanate (TDI), hexamethylene diisocyanate (HDI) and isophorone diisocyanate (IPDI) (see **Figure 18**) are in this order the most frequently used diisocyanate compounds in the industry for the synthesis of polyurethane (by reaction with diol or polyol) and polyurea (by reaction with diamine or polyamine). The reactivity is usually ranked in this order: aromatic isocyanates are more reactive than alicyclic isocyanates, and the latter are more reactive than aliphatic isocyanates. In the case of symmetric diisocyanate, the reactivity of the second isocyanate group is less than the reactivity of the first reacting group.

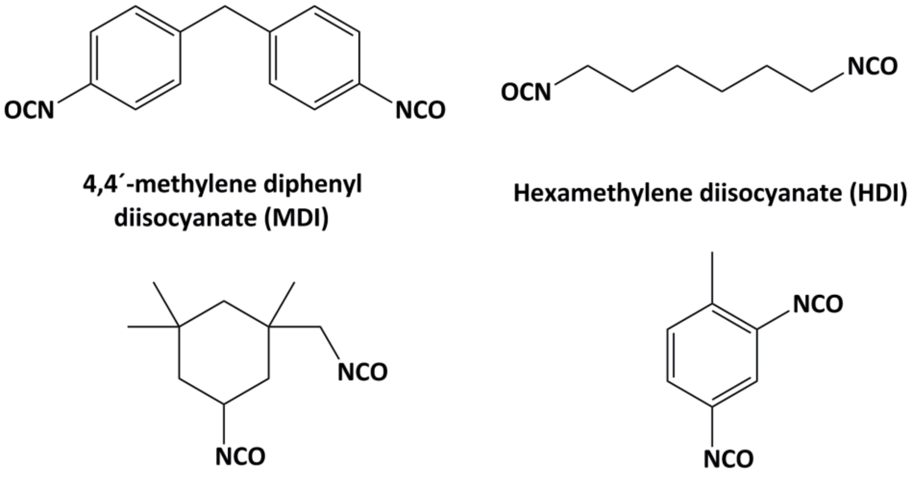
4,4´-methylene diphenyl diisocyanate (MDI)

Hexamethylene diisocyanate (HDI)

Isophorone diisocyanate (IPDI)

Toluene-2,4-diisocyanate (TDI)

Figure 18: Structures of the diisocyanate monomers frequently used in industry for the preparation of polyurethane and polyurea.

As mentioned previously, isocyanates are very reactive species that can have several side reactions when introduced in excess or confronted to other functional groups. Some important side reactions regarding our system are displayed in **Figure 19**.

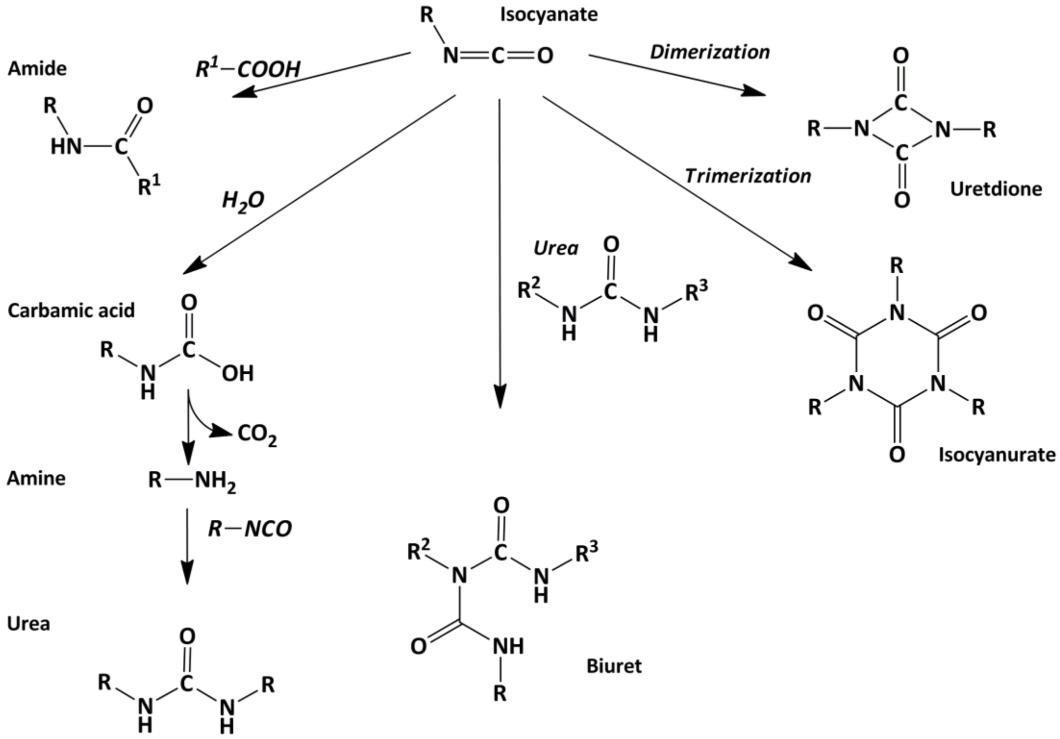

Figure 19: Side reactions likely to occur with the isocyanate group.

It has to be underlined that isocyanate groups can react with water, leading to a primary amine after departure of a carbon dioxide molecule. This primary amine is then liable to react rapidly with another diisocyanate molecule. Even if the reaction rate of isocyanate is much slower with water than with a primary amine, this explains the need of isocyanate excess to obtain capsules in the case of interfacial reaction when the diamine or diol are dissolved in water, as this was the case in inverse emulsion.[50, 153, 175, 182]

The others side reactions possible are the dimerization of the diisocyanate in uretdione and its trimerization in isocyanurate, both catalyzed by bases. Finally, the fact that isocyanate can still react with a urea bond (already a possible product of previous reaction involving isocyanate) to form a biuret-product underlines again the high reactivity of the isocyanate group. A similar reaction with urethane leads to allophanates.

In this thesis, lysine amino acids were introduced in the peptides sequences to allow the formation of urea bonds by an addition reaction of the ε-amine groups of the lysine with the diisocyanate. Thus, peptide-based polymers where prepared via interfacial polyaddition. The same strategy could have been used with serine residues (bearing primary alcohol groups) but lysine was preferred for two reasons: the presence of the amino-group on the *N*-terminus of the peptide, and the fact that addition reaction is faster with primary amine, which for example is an additional factor of security concerning the side-reaction with water.

III. Relevant methods for characterization

III.1 MALDI-TOF mass spectrometry

Matrix-assisted laser desorption/ionization (MALDI) is one the softest ionization technique used in mass-spectrometry. It suits the analysis of large and relatively fragile molecules such as polymers and biopolymers, which are more liable to splitting during the ionization process. The molecule of interest is incorporated in a matrix (crystallized molecule present in large excess), which will act as an energy and charge transfer species between the ionization trigger (UV-laser) and the analyzed molecule. Therefore, a good matrix (e.g. sinapinic acid or 2,5-dihydroxybenzoic acid) possesses the following properties: a good absorption in the range of the laser wavelength to protect efficiently the analyte from disruptive or destructive laser radiations, the relatively low molecular weight for a facile vaporization, and having an acidic group to behave as proton source to facilitate ionization of the molecules.

The type of mass spectrometer widely used after MALDI ionization is the time of flight (or TOF) mass spectrometer. The principle is based on the conversion of the potential energy of a charged molecule in an electric field into kinetic energy, which is proportional to the mass of the molecules. After having gone through the field-free time-of-flight tube with constant speed, the accelerated molecule reaches the detector. The heavier the molecule is, the later it reaches the detector. The time of detection t is precisely related to the molecular weight M of the molecule, following Equation (9):

$$\boldsymbol{t = \frac{d}{\sqrt{2U}}\sqrt{\frac{M}{z}}}$$

Equation (9)

with d the ion path length (m)
U the potential difference (V)
z the charge of the molecule (C)

As only the impact time changes with the weight of the molecule, a TOF spectrometer is suitable for the detection of large molecules. The use of a reflectron, an ion mirror to reverse the direction of travel of the ions entering it, improves the resolution of a spectrum compared to a linear flight tube.

In this thesis, MALDI-TOF MS was used as characterization method for the peptides prepared by SPPS. Moreover, it revealed to be a very useful tool to observe the formation and the enzymatic degradation of peptide-polymer linear conjugates.

III.2 Size-exclusion chromatography[183]

Size-exclusion chromatography is one of the most frequently used techniques to characterize polymers and determine their molecular weight and molecular weight distribution. The analyzed samples are generally injected in a column packed with porous polymer beads. The molecules are separated by their size, defined by the hydrodynamic volume ($V_{H,}$ Equation (11)). Inside the beads filling the column, smaller molecules have access to a larger pore volume than the bigger molecules. As a result, they have a longer pathway and they elute later. To be more exact, the pores inside or between the beads are creating different flow paths, with parabolic flow profile. The bigger molecules, which are excluded from the slower path along the wall, elute earlier. SEC is based on the assumption that interactions of polymer molecules, especially between molecules and stationary phase, have no significant influence on the separation. The goal is that only the size parameter matters for separation and that all chains of a given size elute at the same time regardless of the nature or structure of the polymer. This is the universal calibration principle.[184, 185] The detection of the molecules after the column can be done with two types of detectors; with concentration-sensitive detectors (differential refractometer, UV-detector) or with molecular weight sensitive detectors (differential viscometer, light scattering detector). In concentration-sensitive detectors, it can be assumed that the signal is not influenced by the molecular weight of the polymer chain. For example in the case of differential refractometer, the area of the elution peak can be calculated by:

$$A = k\,\frac{dn}{dc}c$$

Equation (10)

where A is the area of the elution peak on the chromatogram
k is a constant depending from detector and eluent
$\frac{dn}{dc}$ is the refractive index increment (e.g. in $L \cdot g^{-1}$)
c is the weight concentration of the polymer (e.g. in $g \cdot L^{-1}$)

However, when only a concentration detector is used, in order to relate the elution volume of a molecule with its molecular weight, it is necessary to plot a calibration curve (with narrow standards of suitable linear polymers). This is called the conventional calibration, where the calibration curve plotted $\log\ M\ = f(V_{el})$ is fitted with a polynomial function. This method is fully relevant for the analysis of linear polymers with appropriate standards.

To obtain further data on the analyzed samples, it is useful to combine a concentration detector with a detector whose response is a function of the size of the chains. For example, a differential viscometer gives access to the intrinsic viscosity $[\eta]$, which represents the contribution to the viscosity of a single polymer molecule for a given solvent. By definition, the separation is done by a volume proportional to $\eta\ M$ (Equation (11)), called hydrodynamic volume V_H. It is the volume of the equivalent hard sphere increasing the viscosity as much as the polymer chain:

$$V_H = \frac{\eta\ M}{2.5\ N_A}$$

Equation (11)

From a concentration detector and a viscometer, the calibration curve $\log\ \eta\ M\ = f(V_{el})$ takes the hydrodynamic volume as criterion of separation. This is the universal calibration curve of the system: different polymers draw the same calibration curve.[185] A light scattering detector (LALS or MALS) gives direct access to the absolute molecular weight M_w. Triple detection SEC, based on a concentration detector, a viscometer and a light-scattering detector, is the current most advanced method to analyze a polymer sample and to obtain information on its molecular weight, size, branching, and concentration.[183]

In this thesis, SEC was used principally to confirm the polymerization of the peptide at the interface of nanodroplets. As stated previously, SEC data from concentration detectors have to be considered carefully in the absence of relevant standards to convert the elution volume in molecular weight. Moreover, not only linear but also branched polymer were prepared, which would have introduced a further imprecision in the conversion of elution volume to molecular weight. Therefore, elugrams were regularly preferred over molecular weight distribution in the graphic representations of the SEC results.

III.3 DOSY-NMR spectroscopy

Nuclear magnetic resonance (NMR) spectroscopy, beyond its application in medical imaging (MRI, magnetic resonance imaging), is one of the most frequently used characterization technique in chemistry, especially organic chemistry. The principle of nuclear magnetic resonance is defined as such: the nuclei of some isotopes of certain elements have a spin quantum number different from zero, i.e an intrinsic magnetic moment and angular momentum. In a magnetic field (typically applied in the form of pulses), these isotopes absorb and re-emit electromagnetic radiations (relaxation). This energy is at a specific resonance frequency, which depends on the strength of the magnetic field and the magnetic properties of the isotope of the atoms, i.e. the environment of the atoms. The most frequently used atoms are the isotopes of hydrogen ^{1}H and carbon ^{13}C, to plot spectra of these elements but also the interactions and correlations between the atoms, e.g. ^{1}H-^{1}H or ^{1}H-^{13}C via two-dimensional NMR spectroscopy (COSY).

Another type of two-dimensional NMR spectroscopy was used in this thesis: the diffusion ordered spectroscopy (DOSY). This method relates each signal detected in conventional NMR with the diffusion constant *D* of the molecule to which this peaks is belonging (see **Figure 20**). Therefore, DOSY also sorts the molecule by their size, related to the diffusion constant by the Stokes-Einstein equation (see Equation (13)). This method can be particularly useful when a mixture of several molecules is analyzed by NMR spectroscopy (**Figure 20**), or to prove the success of a coupling reaction, e.g. in the case where as small molecule is attached to a big one.

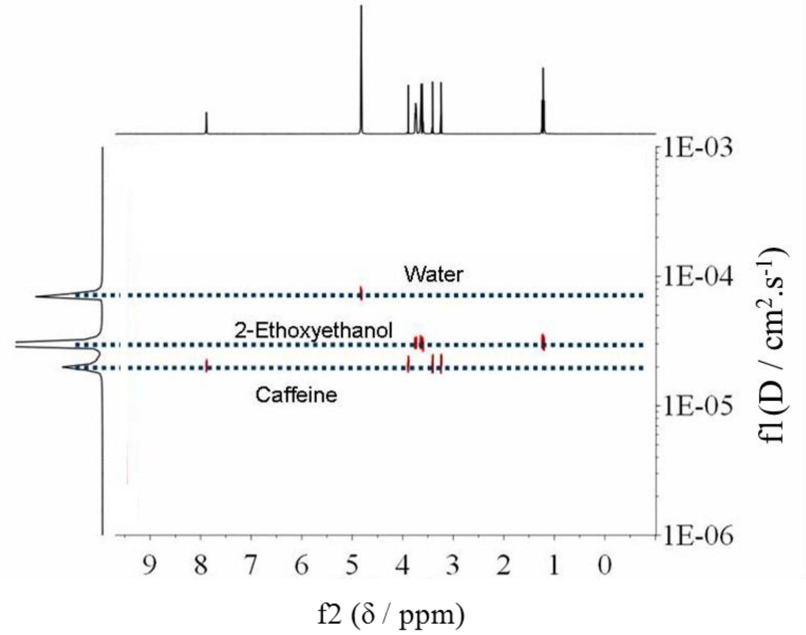

Figure 20: **Example of DOSY-NMR spectrum. The case of a mixture of water (D = 7×10^{-4} cm^2·s^{-1}), 2-ethoxyethanol (D = 3×10^{-4} cm^2·s^{-1}) and caffeine (D = 2×10^{-4} cm^2·s^{-1}).**
Source: http://nmr-analysis.blogspot.com

In this thesis, DOSY-NMR spectroscopy was used to study the coupling reaction of peptide to ω-functionalized polymer on solid phase and in solution.

III.4 Electron microscopy

To overcome the limits of optical microscopy imposed by the diffraction of light, electron microscopy techniques with electron beams of much shorter wavelengths (around 100 000 times) than the photons of visible light were developed. It provides the possibility to observe structures in the nanometer range and thus, electron microscopy allows the characterization of samples with much higher resolution than optical microscopy. Scanning and transmission electron microscopy have become techniques extensively used by material scientists and biologists.

Scanning electron microscopy (SEM)

Electron emission and detection techniques require working under high vacuum. The electron beam is thermionically emitted from an electron gun fitted with tungsten filament cathode or lanthanum hexaboride (LaB_6) cathode and accelerated to the anode. Field emission guns can also be used as electron source. The electron beam, whose energy ranges from 0.5 to 40 keV, is focused by magnetic lenses and passes then through pairs of scanning coils or deflector plates to obtain scanning of the sample surface over a rectangular are (**Figure 21**, left).

In scanning electron microscopy, two types of electrons are mostly used to generate the contrast in the images after interaction with the sample: the backscattered electrons resulting from the elastic scattering and the secondary electrons, coming from inelastic scattering. The secondary electrons originate from the surface and in consequence contain more information on the topology of the samples. Due to their low energy, they can be trapped in the Faraday cage of an Everhart-Thornley detector. The high-energy backscattered electrons are detected with scintillators or semiconductors positioned in doughnut form above the sample holder. As they originate from deeper in the sample, they contain information on the composition of the sample: heavier elements backscatter more electrons and therefore appear brighter (**Figure 21**, right).

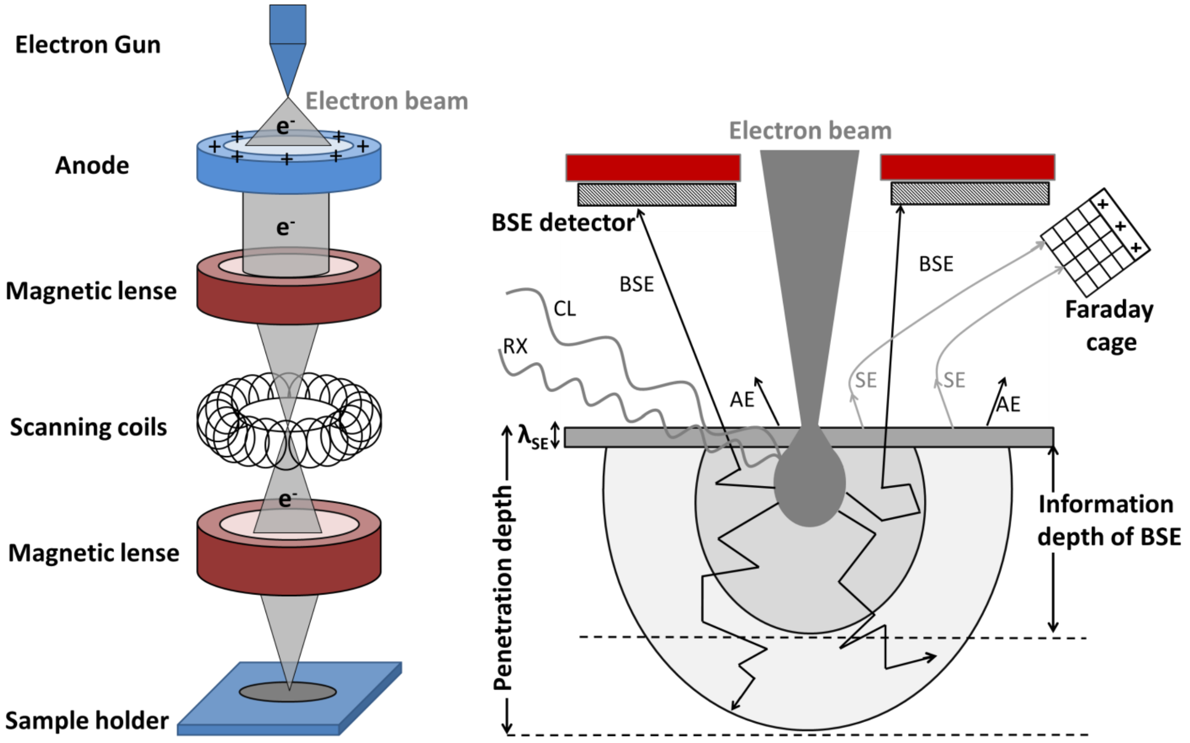
Electron Gun
Electron beam
e-
Anode
e-
Magnetic lense
Scanning coils
e-
Magnetic lense
Sample holder
Electron beam
BSE detector
BSE
BSE
CL
RX
AE
SE
SE
AE
Faraday cage
λSE
Penetration depth
Information depth of BSE

Figure 21: **Operating principle of a scanning electron microscope (*left*) and summary of the interactions of the electron beam with the sample (*right*). Secondary electrons (SE), backscattered electrons (BSE) and Auger electrons (AE – surface information) are generated. Cathodoluminescence (CL – electrical information) and X-rays (RX – composition information) are also generated. λ_{SE} represents the thin layer probed by SE.**

Transmission electron microscopy (TEM)

In transmission electron microscopy (TEM), the difference is that the contrast of the image is mainly obtained from the elastic and inelastic scattering of the electrons in the beam transmitted through a thin sample. Darker areas of the image are observed when fewer electrons are transmitted, corresponding to a denser or thicker regions. In particular, the distinction between particles and capsules for examples is easy, as electrons are transmitted better through the core of the capsules than through their wall.

In this thesis, SEM and TEM were mainly used to observe the nanostructures prepared, and to distinguish if capsules or particles were obtained. The samples were very sensitive to the electron beam and damaged sometimes, although a very low voltage was used in SEM: from 0.2 to 0.3 keV. It was also a confirmation of some size measured with DLS.

III.5 Light scattering

Colloidal systems and polymer molecules in solution interact with visible light by scattering it in all directions, as their size is comparable to or smaller than the wavelength(s) of the incident beam. Scattering occurs mainly under elastic Rayleigh scattering: the wavelength is the same for incident light and scattered light. Using a laser as light source (coherent and monochromatic), the treatment and analysis of the scattered light intensity gives information on size-related parameters of the system (**Figure 22**).

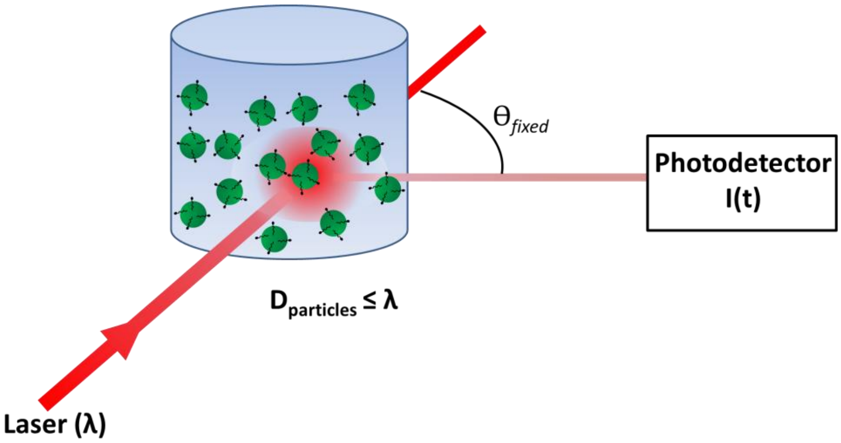

Figure 22: Schematic operating principle of a dynamic light scattering measurement

Dynamic light scattering (DLS, or photon correlation spectroscopy PCS) studies the variation of scattered light intensity in function of time. It leads to information about the size distribution of the sample, as described hereinafter. The particles are in perpetual movement due to Brownian motion and smaller particles diffuse more rapidly. The signal intensity detected fluctuates with time, because of the interferences within the scattered light, mainly due to the Brownian motion of the scattering particles. The mathematic treatment of the intensity $I(t)$ with an autocorrelation function gives in first approximation an exponential decrease, with a characteristic time (or relaxation time) τ. This relaxation time is inversely proportional to the diffusion coefficient D of the particle or polymer chain (Equation (12)), where q is the norm of the scattering vector.

$$\frac{1}{\tau} = Dq^2$$

Equation (12)

The hydrodynamic radius R_H is obtained from the Stokes-Einstein equation:

$$R_H = \frac{k_B T}{6\pi\eta_S D}$$

Equation (13)

with k_B as the Boltzmann constant ($J\cdot K^{-1}$), T as the temperature (K) and η_S ($N\cdot s\cdot m^{-2}$) as the viscosity of the liquid. Dynamic light scattering provides information by measuring single scattering events. However, its relevance is limited by often-encountered multiple scattering events, where the photons are scattered multiples times by the samples before detection. This explains the relevance of a cross-correlation approach (PCCS) in DLS, where the singly scattered light is isolated and the contribution of multiple scattering is mathematically removed.

In comparison to dynamic light scattering, static light scattering deals with the angular variation of scattered intensity, and leads to the molecular weight M_w and gyration radius R_g via the constitution of a Zimm plot.

In this thesis, photon cross correlation spectroscopy (PCCS) was principally used in this work to obtain an idea of the size and size distribution of the nanocapsules prepared. Even if size was not a determining criterion in the project, the capsules had to be in the good size range (between 20 and 1000 nm) and as far as possible monodispersed, in order to enable further use for biomedical application.[7] PCCS also provided valuable information about aggregation and size evolution after redispersion in another continuous phase.

III.6 Absorption and fluorescence[186, 187]

III.6.1 Absorption and UV-Vis spectroscopy

Absorption in physics represents a process where the energy of a photon is taken up by matter. Typically, at the molecular scale, this energy corresponds to the electronic transition from a ground state to an excited state, more precisely from the HOMO to the LUMO. The luminous energy absorbed is generally restituted as vibrational energy at the molecular scale, seen has molecular agitation, i.e. heat at the mesoscopic scale. As the electronic transition from HOMO to LUMO requires a defined amount of energy, depending on the molecule, the light absorption occurs at specific wavelengths.

UV-Vis absorption spectrometry is based on this process and allows the determination of concentrations of molecules in solution in diluted and homogenously distributed samples. The sample is placed into a light beam with tunable wavelength. One defines as transmittance the ratio I/I_0 between the intensity of the beam passed through the sample I, and the intensity of the incident light I_0. The absorbance is then defined as:

$$A = \log \frac{I_0}{I}$$

Equation (14)

The Beer-Lambert law, actually discovered by the French Bouguer in 1729, states an experimental relation between the absorbance of a solution and the concentration c of absorbing species:

$$A = \varepsilon \cdot l \cdot c$$

Equation (15)

In this equation, ε is the molar extinction coefficient of the species, a constant at a given temperature and wavelength, and l is the length of the path through the samples. The absorbance in solution is directly proportional to the concentration, as long as the other parameters are kept constant, and as far as the dispersion of the absorbing substance is homogenous, no scattering from the incident light occurs, the absorbing species are independent, and the excitation radiation is narrow compared to the absorption width.

In this work, UV-Vis spectroscopy was used to detect and quantify molecular species, like peptides or (non-)encapsulated dye. This work was done in solution or in nanocapsules dispersion.

III.6.2 Fluorescence

Fluorescence principle

In certain molecules called fluorophores, the photon energy absorbed is not dissipated by vibrations, but another photon is reemitted, with less energy and thus a greater wavelength. This emission of light is called fluorescence. The process is described in a Jablonski diagram (**Figure 23**). A photon with the energy $h\upsilon_{exc}$ is absorbed. This corresponds to the excitation from the electronic ground state (S_0) to an excited vibrational level (S_1^*) of the electronic excited state (S_1).

As a result, the excited molecule is subjected to conformational changes until the energy level reaches the vibrational ground state of the excited state (S_1). Then, fluorescence occurs: the electron returns to the ground state (S_0), or one of its vibrational level (S_0^*), with emission of a photon of energy $h\upsilon_{em}$. This energy is necessarily lower than the absorbed energy $h\upsilon_{exc}$, because of the vibrational energy loss between (S_1^*) and (S_1). This loss of energy is observable by the greater wavelength of the emitted fluorescence, which corresponds to the Stokes shift $\Delta\lambda$:

$$\Delta\lambda = \lambda_{em} - \lambda_{exc} = \frac{h}{\Delta\upsilon} = \frac{h \cdot c}{\Delta E}$$

Equation (16)

In Equation (16) and in the previous paragraph, υ is the frequency and λ the wavelength of the electromagnetic radiation of speed constant equal to c (299 792 458 $m \cdot s^{-1}$). Subsequently, the larger the Stokes shift is, the easier it is to distinguish experimentally the fluorescent light from the incident exciting laser beam.

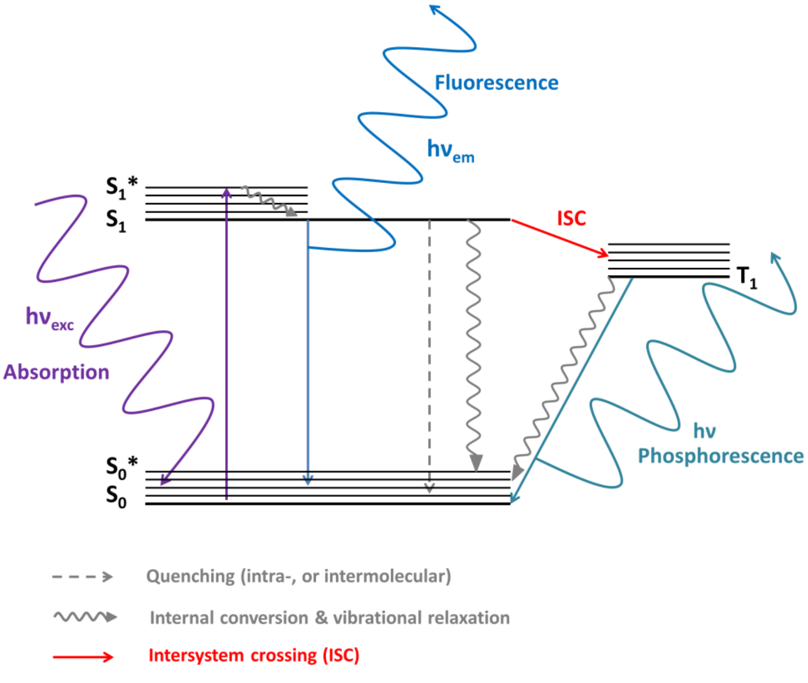
Fluorescence
hν_em
S1*
S1
ISC
T1
hν_exc
Absorption
S0*
S0
hν
Phosphorescence
Quenching (intra-, or intermolecular)
Internal conversion & vibrational relaxation
Intersystem crossing (ISC)

Figure 23: **Simplified Jablonski diagram summarizing the fluorescence process.**

However, all the excited electrons do not return to the ground state upon fluorescence: several non-radiative mechanisms exist, intra- or intermolecular. For example, internal conversion (IC) designates the vibrational energy transfer from an excited vibrational state (S_1^*) to the ground state (S_0). Inter-system crossing (ISC) represents the transmission to a less energetic state, with a different spin multiplicity (e.g. triplet state). Inter-system crossing can be followed by another type of radiative process with return to the original spin multiplicity (singulet); the phosphorescence. Two possibilities for intermolecular mechanisms are the collisional quenching (CQ) and the Förster resonance energy transfer (or fluorescence resonance energy transfer, FRET).

All these mechanisms contribute to depopulate the (S_1) level and decrease the amount of photons emitted by the fluorophore. To quantify the efficiency of light emission, the quantum yield Φ has been defined as the ratio between the number of photons emitted and the number of photons absorbed. After calculation, it is shown that the quantum yield can be expressed by the rate constant k of the mechanisms described previously:

$$\Phi = \frac{k_F}{k_F + k_{IC} + k_{ISC} + k_{FRET} + k_{CQ}} = \frac{k_F}{k_F + k_D}$$

Equation (17)

k_D represents the depopulation rate constant. In summary, the quantum yield is high, as long as the non-fluorescing deactivation processes remains negligible, i.e. kinetically much slower than the photoemission.

Quenching and Förster-resonance energy transfer

One describes as quenching of fluorescence any process that leads to energy transfer from the excited fluorophore to another molecule and induces a diminution of the quantum yield. Several mechanisms can lead to quenching of fluorophore. For example, the energy can be transferred to the quencher by collision. The Stern-Vollmer equation describes the collisional energy transfer in this case:

$$\frac{I_0}{I} = 1 + k_{CQ}[Q]\tau$$

Equation (18)

With I_0 representing the fluorescence intensity observed in the absence of quencher, Q is the quencher concentration, k_{CQ} the rate of collisional quenching and τ the lifetime of the excited state of the fluorophores. As a result, the higher the quencher concentration is, the lower is the fluorescence yield. Equation (18) is also relevant to consider in the case of fluorophore quenching their own fluorescence ("self-quenching").[188] In this case, from a certain fluorophore concentration, a further addition of fluorescent dye does not increase the fluorescence signal and rather tend to decrease it.

A similar equation describes the quenching occurring in case of formation of a static ground-state complex (k_C is the formation constant of the complex):

$$\frac{I_0}{I} = 1 + k_C[Q]$$

Equation (19)

In this case, donor and acceptor bind together to form a dimer with its own properties: no fluorescence and a unique absorption spectrum. This model suits well the aggregation or stacking of hydrophobic dyes in water.

A third mechanism of quenching is particularly interesting: the Förster resonance energy transfer (or FRET) mechanism. The FRET mechanism consists of non-radiative energy transfer to another molecule, which is either a quencher or another fluorophore quenching the fluorescence of the excited dye and reemitting fluorescence with its own emission wavelength (**Figure 24**). Several conditions have to be fulfilled so that FRET takes place:

- The absorption spectrum of the quencher overlaps the emission spectrum of the dye.
- The distance between the fluorophore and the quencher is low (typically less than 10 nm).
- The relative orientation of the donor and acceptor transition dipole moments is not spatially restrained.

Under those conditions, the quenching efficiency of the FRET system Φ_{FRET} depends on the intermolecular distance r between the fluorophore and the quencher, given by:

$$\Phi_{FRET} = \frac{1}{1 + \frac{r}{R_0}^{6}}$$

Equation (20)

R_0 is the Förster radius for one pair donor/acceptor, defined by the distance at which the energy transfer efficiency is 50%.

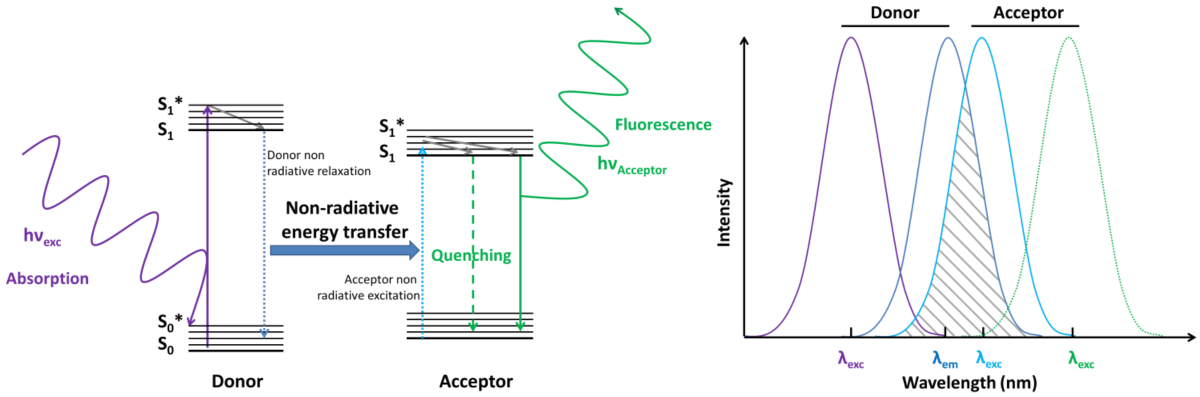
S_1*
S_1
Donor non radiative relaxation
Non-radiative energy transfer
hv_{exc}
Absorption
Acceptor non radiative excitation
S_0*
S_0
Donor
S_1*
S_1
Quenching
Fluorescence
$hv_{Acceptor}$
Acceptor
Donor
Acceptor
Intensity
λ_{exc}
λ_{em}
λ_{exc}
λ_{exc}
Wavelength (nm)

Figure 24: **Simplified Jablonski diagram of a FRET pair with fluorescence emission or quenching (left) and importance of the overlapping between donor emission spectrum and acceptor excitation spectrum for efficient energy transfer (right).**

Please not that very frequently, especially in biophysics and biochemistry, the FRET system is used to transfer fluorescence from one dye to another. The recording of the two fluorescence signals allows one to study of the interactions between two biomolecules labeled one by the fluorescing donor, one by the fluorescing acceptor, e.g. with the study of protein-protein interaction, protein-DNA interactions. It is also relevant to study intramolecular interactions, like the detection of protein conformational changes.[189]

In this thesis, FRET is also used to name internally-quenched fluorescence system, i.e. systems where the fluorescence is quenched by the proximity of a non-emissive quencher. These systems are commonly used to monitor the enzymatic cleavage of peptide.[190, 191] On the intact peptide, a fluorophore/quencher pair surrounds the recognition site. Once the recognition sequence has been cleaved, the distance between the fluorophore and its quencher becomes too large for the quenching to take place and fluorescence recovery is observed. In this thesis, the expression FRET will always refer to the use of internally-quenched fluorescence system, with only one fluorophore.

In this thesis, fluorescence measurements were also carried out to determine some concentration of fluorescent dyes in solution. Indeed, fluorescence measurement is a very sensitive method and after calibration, it allows measurements of concentrations under one part per billion.

Fluorescence microscopy

Fluorescence is also used in optical microscopy. In principle, the sample is illuminated with a light of a specific wavelength, absorbed by the fluorophores of the sample, which reemit light at their emission wavelength. This light is then detected through the microscope objective. The use of two filters is highly important with this technique: a first filter (*excitation filter*) ensures that the excitation beam is at the correct wavelength and almost monochromatic, for specific excitation of the dye. The second filter (*emission filter*) before the objective lenses ensures that none of the excitation light, much more intense that the emitted light, reaches the detector (**Figure 25**).

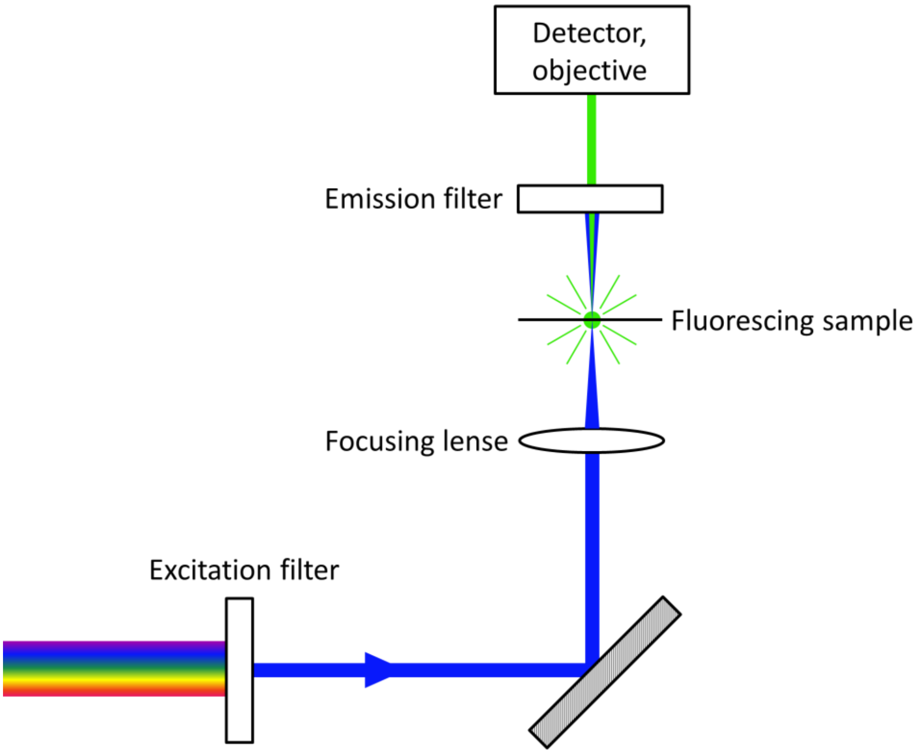

Figure 25: Simplified operating principle of a fluorescence microscope.

Another characteristic of fluorescence has to be considered during fluorescence microscopy, the photobleaching. Photobleaching is the photochemical destruction of a fluorophore or at least the loss of its fluorescent properties. At the excited state, the fluorophore can encounter a photochemical reaction that will prevent the molecule to return to the ground state. Frequently, the generation of free oxygen radicals is involved in the loss of the light emitting properties of the fluorophore. From a statistical point of view, a fluorophore can undergo a finite number of excitation-relaxation cycles prior to photochemical destruction. For this reason, reduction of the irradiation intensity or irradiation time when observing the samples under fluorescence microscopy can be useful. The addition of radical scavengers to the sample is also possible.

Like every classic optical microscope, fluorescence microscopy is limited by light diffraction. Its resolution, or minimal resolving power, the minimum distance between distinguishable objects is around 200 nm (in the range of the half wavelength of the incident light used). Some techniques have been developed to increase the optical resolution: confocal microscopy uses only point illumination and a pinhole is placed in front of the detector to eliminate the out-of-focus signal. Resolution is improved, especially along the depth axis, as only the fluorescence emitted very close to the focal plan is detected. More recently, the concept of “point by point” excitation and “point by point” detection of fluorescence appeared, via the use of two opposing objectives lenses focused, from each side of the sample, on the same point so that the optical pathway through each of the lenses is minimal. Thus, excitation of the molecules in the common focal area, as well as collection from the emitted or reflected light, is made coherently. This technique, called 4Pi-Microscopy, reduces considerably the volume of the focal point observed.[192, 193] The first technique which truly overcomes the diffraction limit is the stimulated emission depletion (STED) microscopy. The idea was proposed in 1994 and achieved in 1999 by Hell.[194, 195] Recently with STED microscopy, the highest resolution was increased up to a few nanometers.[196]

IV. Results and discussion

Strategy

It was shown that the interest for the enzyme responsive materials has been growing within the last twenty years and that the preparation of such materials very frequently requires the synthesis of peptide-polymer conjugates or hybrid species. In particular, the introduction of enzymatically cleavable peptide sequences has been attracting increasing attention, but until now their study has mainly been restricted to conjugates in solution or macroscopic materials like hydrogels.[112, 114, 115, 117] With the recent exception of inorganic conjugates based on gold and silica nanoparticles,[120, 122] the use of such hybrid materials in the form of nanocapsules or nanoparticles has not thoroughly been investigated.[127, 128] Yet, it is an exciting challenge, as nanocapsules and particles pass vasculature without obstruction. Using the cleavability of the peptide for triggered release *in situ* would be an achievement in the field of drug delivery.

On the other hand, the miniemulsion technique is a very efficient tool for the preparation of diverse nanomaterials. The principle of miniemulsion itself, based on stabilized nanodroplets acting as independent reactors, allows the efficient encapsulation of a payload. In particular, several routes (nanoprecipitation, phase separation, interfacial polymerization) can be employed to form nanocapsules with hydrophilic content, as is the case in inverse miniemulsion. For all these reasons, the miniemulsion technique appears as a highly suitable method for the preparation of hybrid peptide nanocapsules, with payload release properties upon enzymatic degradation.

In the "Optimap" project, hepsin was identified as an enzyme of interest. Indeed, hepsin - a cell surface endopeptidase - is reported to be over-expressed in more than 90% of human prostate tumors.[4, 6] Hepsin expression correlates with tumor progression, making it a significant marker and target for prostate cancer.[5] A good peptide substrate sequence for recognition by hepsin was identified to be RQLRVVGG.[197] The objective was to prepare both hepsin-cleavable nanoparticles, for the encapsulation of hydrophobic compounds,[10] and nanocapsules for the encapsulation of hydrophilic content. More precisely, the content should be a hydrophilic dye, self-quenched when encapsulated and which should recover its fluorescence when delivered, as schemed in **Figure 26**. Thus, the desired optical signal will be emitted in the presence of cancerous cells. In addition to this, it was possible to insert a FRET system (more exactly, an internally-quenched fluorescent system) in the peptide sequence, to monitor the cleavage of the peptide sequences constituting the capsules.

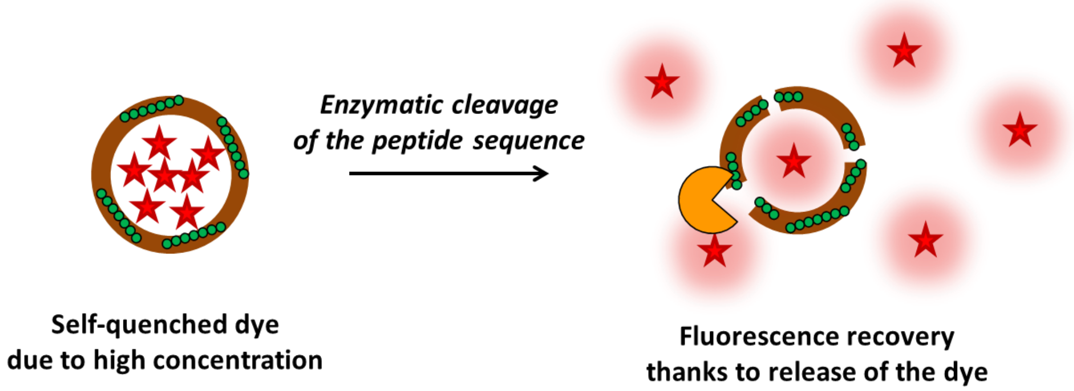

Figure 26: Description of the principle of self-quenching of a dye and fluorescence recovery by dilution.

For the synthesis of the nanocapsules and regarding the different possibilities described previously in miniemulsion, two synthetic strategies are conceivable: the nanoprecipitation of preformed peptide-polymer conjugates with hydrophobic polymeric chains, and the interfacial polymerization of the peptide. While both processes have shown their efficiency for the encapsulation of hydrophilic dyes,[163, 175, 198] the second was already successfully used for temperature- and light-triggered release.[50] However, to study the viability of this process, a simpler peptide sequence (GFF), cleaved by chymotrypsin[199] was initially used. Indeed, this initial system has several convenient properties: the peptide sequence is short, does not carry side-chain reactive groups and chymotrypsin can be used in solution without cell culture experiments.

The first part of this chapter deals with the preparation of peptide-polymer conjugates, with respect to the desired functionalities: the use of a hydrophobic polymer and a significant decrease of molecular weight after cleavage of the peptide recognition site. In a second approach, the preparation of peptide-based hybrid nanocapsules via interfacial polyaddition is presented.

IV.1 Synthesis, characterization and cleavage of linear peptide-polymer conjugates

A significant decrease in molecular weight of the conjugate should be observed by cleavage of the recognition peptide sequence, to insure efficient degradation of the capsules. Therefore, triblock conjugates, with the cleavable peptide sequence located in the middle of the conjugates, are aimed to be synthesized, as the mass of the conjugate would be divided by approximately a factor two upon enzymatic cleavage. The synthesis of multiblock conjugates to fraction a longer chain in several small segments would be even better. The use of a polymer with narrow molecular weight distribution would lead to a significant loss of mass, as for triblock copolymers, the peptide would be located in the middle of the chain. Therefore, carboxy-functionalized polystyrene was prepared by anionic polymerization (see paragraph VI.1.2, M_w = 1260 g·mol^{-1}, PDI = 1.12) and used for the preparation of model triblock polymer-peptide-polymer conjugates via a typical peptide-coupling reaction in solution and on solid phase. The choice of polystyrene is justified by several criteria. For the preparation of our model linear peptide-polymer conjugate, we need a hydrophobic polymer. Polystyrene was chosen as standard hydrophobic polymer and also used in the frame of the diploma thesis of M. Maier.[200] It also presents the advantage to be soluble in DMF as the peptides, which facilitates the coupling reaction between the two different components of the conjugate. Later, the preparation of multiblock peptide-polymer conjugates would be possible in solution by coupling the peptides with homotelechelic polymers, which is possible via anionic polymerization and ATRP, thanks to telechelic initiator.[201, 202]

IV.1.1. Peptide-polymer conjugates via coupling in solution

A first approach to prepare linear peptide-polymer conjugates is the coupling of the two components in solution. DMF, for example, is a common solvent of both the end-functionalized polystyrene and the peptide.

Synthesis of peptide-polymer conjugates in solution

The parameters for the coupling of polymer with peptide were kept as close as possible to the standard parameters used for the peptide synthesis and are described in paragraph VI.3.1. The peptide GFFKG, designated as [-/2 NH_2] and containing no additional feature, was used for these experiments. It contains two primary amine groups surrounding the peptide sequence, making the synthesis of a triblock conjugate (polymer-peptide-polymer) possible. The coupling reaction is represented in **Figure 27**.

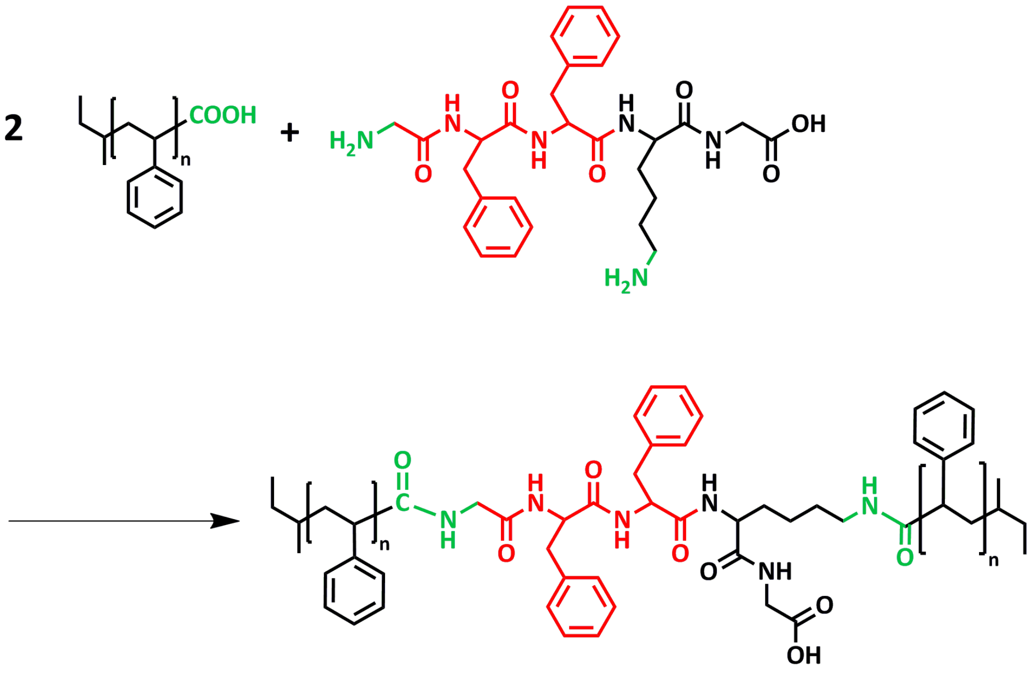

Figure 27: **Scheme for the preparation of triblock peptide-polymer conjugate via solution coupling from peptide [-/2NH$_2$]. The recognition sequence of the peptide is colored in red and the reactive groups in green.**

The workup of the product was challenging, as it is difficult to separate unreacted polymer from the product: washing with acid solution and then methanol removes activator products and possible uncoupled peptide. Polystyrene is not soluble in methanol, but some polystyrene traces were found in the filtrate methanol fraction. After drying, the product was a white powder that should be constituted of polymer and peptide-polymer conjugate.

Characterization of peptide-polymer conjugates in solution

The analysis by ^{1}H NMR spectroscopy shows some traces of peptide in addition to intense polymer peaks. This is a positive indication but it does not prove the coupling of both species. Moreover, the low intensity of the peptide peaks indicates a non-quantitative coupling reaction and is an indication that the product contains pure polymer.

The diffusion-ordered spectroscopy (DOSY) NMR is here of great interest and perfectly suited to the encountered problem concerning the proof of coupling of the peptide with the polymer.

Indeed, if the peptide is covalently bound to the polymer, its characteristic peak in a DOSY spectrum should appear with the same diffusion constant as the polystyrene peaks, which is lower than the reference peptide. This behavior can be observed in **Figure 28** where three DOSY spectra are presented: the peptide [-/2NH$_2$] (green), the carboxyl polystyrene it was coupled with (blue), and the conjugate formed after coupling in solution and workup (red).

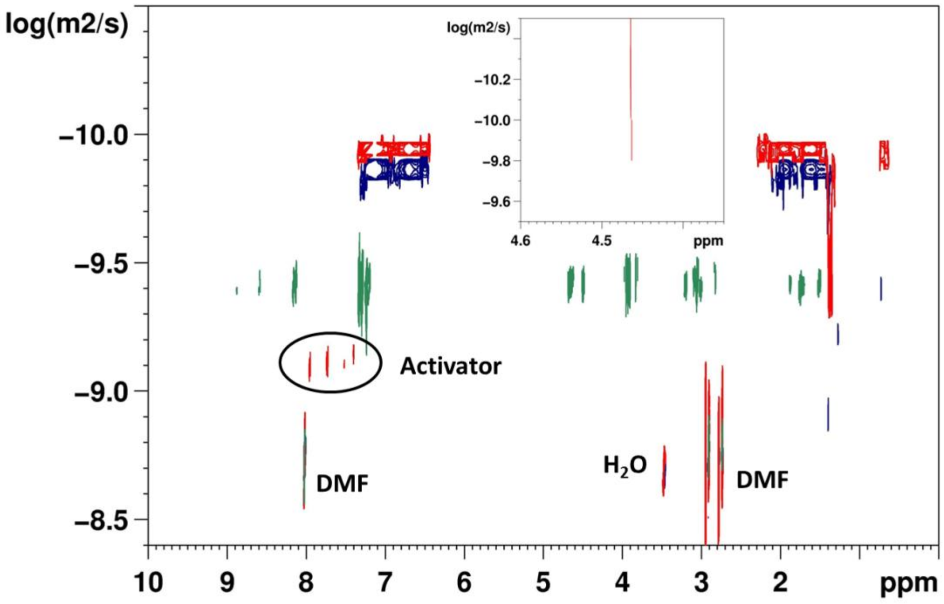

Figure 28: **Overlay of three DOSY spectra showing the coupling of the peptide (green, D = $10^{-9.4}$ $m^2 \cdot s^{-1}$) with the polymer (blue, D =$10^{-9.85}$ $m^2 \cdot s^{-1}$, M_w= 6200 g·mol^{-1}) to a conjugate (red, D = $10^{-9.95}$ $m^2 \cdot s^{-1}$). The insert shows the presence of peptide signal in the conjugate by increasing the intensity of the spectra. All spectra contain DMF (8.0, 2.9 and 2.7 ppm) and water (at 3.5 ppm) peaks (D =$10^{-8.7}$ $m^2 \cdot s^{-1}$).**

The peptide, smaller than the polymer, diffuses faster and has thus a bigger diffusion constant: $D_{\text{peptide}} = 10^{-9.4}$ m^2·s^{-1} while $D_{\text{polymer}} = 10^{-9.85}$ m^2·s^{-1}. Each reactant spectrum is present at one unique ordinate value, with the exception of signals from water and DMF, diffusing much faster. The spectrum of the product also contains DMF and water, but one recognizes directly that the product is mainly constituted of polystyrene. However, this signals (red) correspond to molecules, which have a lower diffusion constant than the polymer. Consequently, they have a larger size. By increasing the intensity of the conjugate signal, a signal appears at 4.5 ppm with $D = 10^{-9.85}$ m^2·s^{-1}. It corresponds to the asymmetric carbons of the main peptide chain and belongs to a molecule diffusing as slowly as the product: the product indeed contains peptide sequences covalently bound to polymer. The absence of free peptide signals is worth being noticed: it was removed during workup. The small molecules $D_{\text{peptide}} = 10^{-9.1}$ $m^2.s^{-1}$ with aromatic NMR signal present in the conjugate were attributed to activators not completely removed during workup.

Another possibility to characterize the product is SEC, as the molecular weight of the peptide is more than doubled in case of success ($2\times M_{\text{PS}} + M_{\text{peptide}} \approx 3\,000$ g·mol^{-1}). But before analyzing the product of the coupling reaction with SEC, some preliminary remarks on the polymer are necessary. The carboxy-functionalized polymer tends to form a dimer in solution as displayed on **Figure 29**.

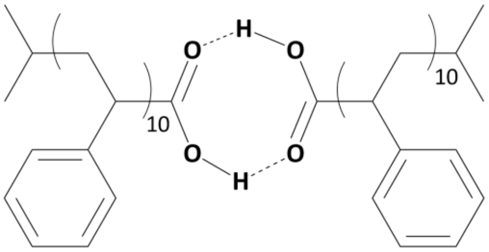

Figure 29: Physical dimer formed by ω-carboxy-functionalized polymer in solution.

This can be observed in the SEC chromatograms: **Figure 30** presents an overlay of the SEC chromatograms from PS-COOLi and PS-COOH. One can clearly see a second peak in the chromatogram of PS-COOH. The second peak is due to the formation of the physical dimer, which is confirmed by the analysis of the molecular weight distribution: the mass are approximately doubled in the second peak present in sample PS-COOH.

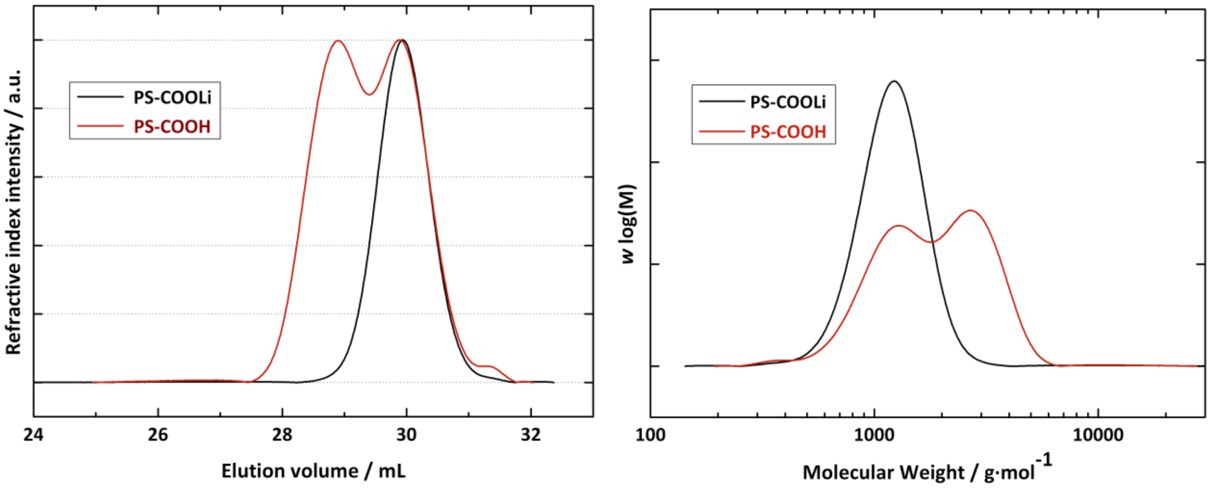

Figure 30: Formation of physical "polymer-dimer" through comparison of SEC elugrams (left) and molecular weight distribution (right) of the end-product (PS-COOH) with an intermediary product (PS-COOLi, M_w=1250 g·mol^{-1}) of the same size.

Subsequent measurements with MALDI-TOF mass spectroscopy of the polymer (**Figure 36**) confirm the monomodal mass distribution centered at around 1000 g·mol^{-1}. Therefore, the molecular weight distribution obtained from the SEC chromatograms of PS-COOLi was used in the whole thesis for calculations involving the weight of the polymer, e.g. stoichiometric proportions.

Coming back to the characterization of the product obtained by coupling reactions of the peptide [-/2NH$_2$] with PS-COOH, the SEC chromatograms of functionalized polystyrene and of the coupling reaction product are superimposed in **Figure 31** (left).

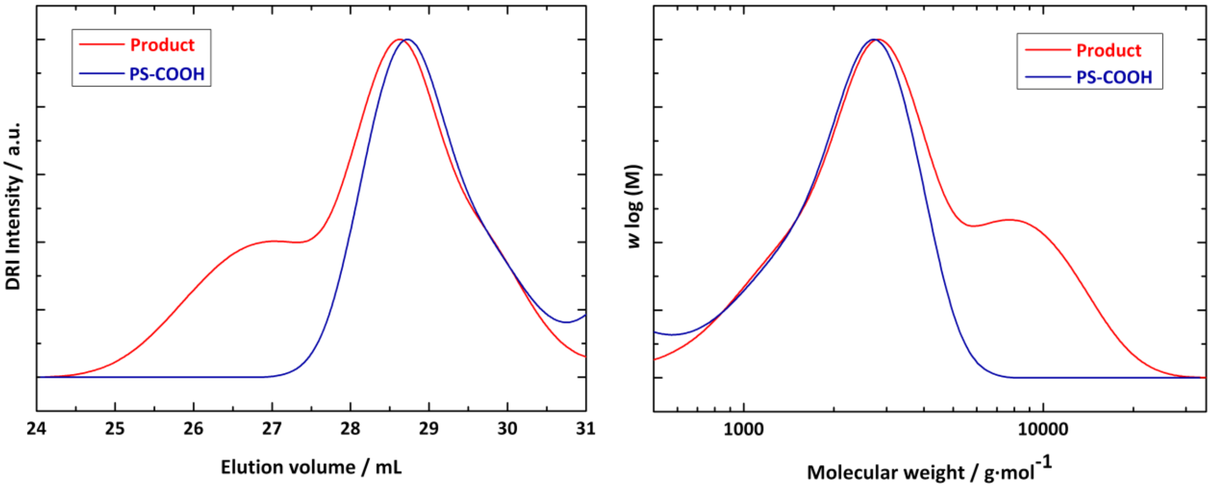

Figure 31: **SEC elugrams (left) and molecular weight distribution (right, calibration polystyrene) of carboxy end-functionalized polystyrene and peptide-polymer conjugated product.**

In the SEC chromatogram of the product, one observes the presence of a shoulder in the region of lower elution volume, which is not present in the chromatogram of the polymer. Molecules larger than the original polymers are generated during the reaction. The size difference between the macromolecules constituting the two peaks is all the more important, that the polymer peak corresponds to a physical dimer of polymer, with chains twice longer as a single polymer chain, as explicated above. However, the majority of the product has the same shape as the polymer: the coupling reaction in solution is far from being quantitative. Assuming that all conjugates are triblock polymer-peptide-polymer, ^{1}H-NMR analyses gives a product made of 2.2 polymer chains for 1 conjugate (under the assumption that the conjugates are all peptide-polymer diblock, one finds 3.2 polymer chains per conjugate). Considering the consequent shift of the elution volume of the shoulder and the corresponding molecular weight increase with PS calibration (**Figure 31**, right), one explanation could be that branching reactions occur by coupling of an amine group of the peptide with the C-terminus of another peptide. Yet, only the carboxylic groups of the polymers were activated before mixing the reactants, to lower the probability of this side reaction, but it might still take place. Overall, the main problem remains, that a minor amount of peptide-conjugates are formed: the yield of the coupling reaction in solution is not high enough.

Conclusion

The coupling reaction between ω-carboxy-functionalized polystyrene and amino functionalized peptide in solution in DMF shows promising results. A size increase of the product after coupling has been detected with SEC and in DOSY-NMR, and the proof of covalent coupling between peptide and polymer is shown. However, the use of a polymer, which has a size distribution, complicates the work with stoichiometric proportions of reactants. The reaction is far from being quantitative, although the remaining peptide can be removed from the product. More problematic is the majority of unreacted polystyrene, which cannot be simply separated from the conjugate. Such technical difficulties do not speak in favor of the coupling in solution, which will be compared in the next paragraph to the coupling on solid phase.

IV.1.2 Triblock peptide-polymer conjugates via coupling on solid phase

In the case of peptide-polymer coupling, it is possible to take all advantages of solid-phase coupling like in SPPS, such as the use of excess reactant, followed by the washing of the polymer which has not reacted with the peptide, which means that there is no problem of stoichiometry anymore but foremost no mixture of polymer and conjugate in the product. One issue could be the steric hindrance: it could be difficult for the polymer to access and react with the peptide inside the mesh of the cross-linked resin. Therefore, low-loaded resin (the amount of peptide is 0.33 $\mathrm{mol \cdot g^{-1}}$ of resin vs. 0.61 $\mathrm{mol \cdot g^{-1}}$ for a standard resin) was used. It should favor the coupling reaction, at least by limiting the steric obstructions between peptides next to each other. However, it is reminded that the use of a short polystyrene chain length (M_w = 1250 $\mathrm{g \cdot mol^{-1}}$, PDI = 1.12) as model system should also minimize this negative effect.

Synthesis of conjugates via coupling on solid phase

The coupling reaction was performed in a microwave oven, with parameters similar to the conventional peptide coupling. Only the reaction time was increased (three times 30 minutes compared to than 5 min), as the reaction between the polymer and the peptide is expected to be slower than with an amino acid (due to diffusion of the polymer inside the resin and the steric hindrance). The reaction is outlined in **Figure 32**. Concerning the structure of the peptide prepared, the lysine residue was used as branching point to obtain two terminal amine groups ready to react with the functional polymer and form a triblock peptide-polymer conjugate. A consequence is that the recognition sequence is present twice, which should make the peptide easier to cleave. Because of the unusual configuration of the peptide [Y-shape/2NH_2] or [“Y”/2NH_2], it was also synthesized and characterized alone, separately from solid-phase coupling experiments (see paragraph VI.2.2) The product was selectively precipitated in methanol and dried after coupling reaction to the peptide and a usual cleavage in TFA/TIS/H_2O solution. Considering that the reaction was quantitative and that $M_{\text{polymer}} = M_w = 1250$ g·mol^{-1}, the yield of the reaction after purification was 11%.

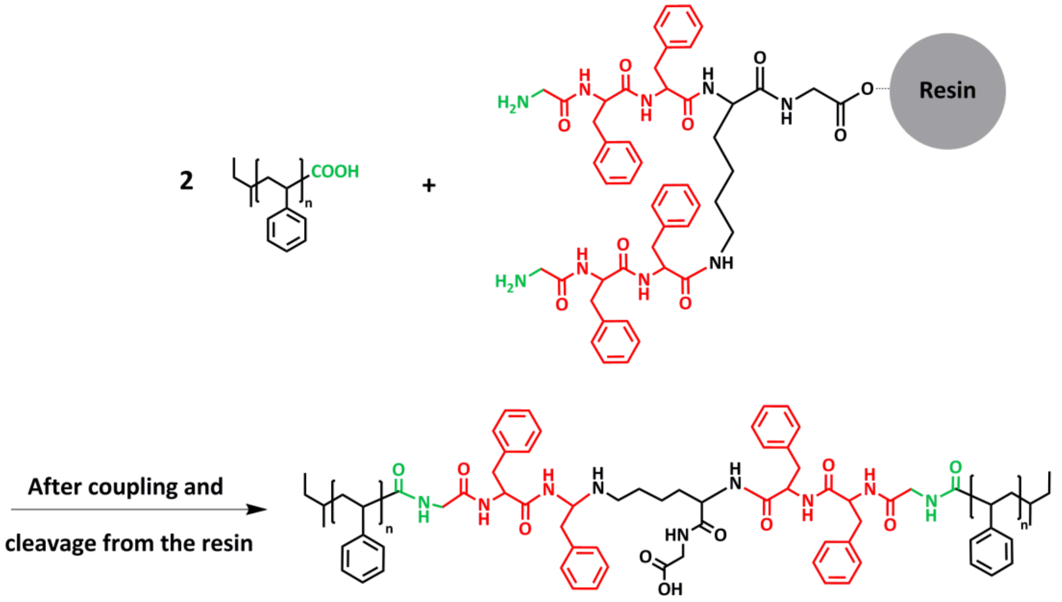

Figure 32: Scheme of the coupling reaction on solid phase between peptide [“Y”/2NH_2] and shorter PS-COOH chains. The recognition sequence of the peptide is colored in red and the reactive groups in green.

Characterization of the triblock conjugate

The dried product was investigated by ^{1}H-NMR (**Figure 33**) and DOSY-NMR (**Figure 34**), SEC (**Figure 35**), and MALDI-TOF MS (**Figure 36**). It is reminded that regarding the method employed, the presence of polystyrene would already guarantee a successful coupling, as the uncoupled polystyrene is washed away during the solid-phase coupling process. This is exactly what is detected in the ^{1}H-NMR spectrum (**Figure 33**): one can clearly observe the presence of aromatic protons of polystyrene in the product, as well as some characteristic peaks from the peptide (asymmetric carbon atoms around 4.5 ppm). Moreover, the primary amine peak of the peptide at 7.85 ppm is not to be seen any more in the conjugate. By integrating these peaks as references, one can estimate that there are 22 styrene units per conjugate, which is in good agreement with the ratio theoretically expected (23) for triblock linear conjugate with the polystyrene used for this experiment (M_w = 1250 g·mol^{-1} corresponds to a *DP* of 11.5 for PS-COOH).

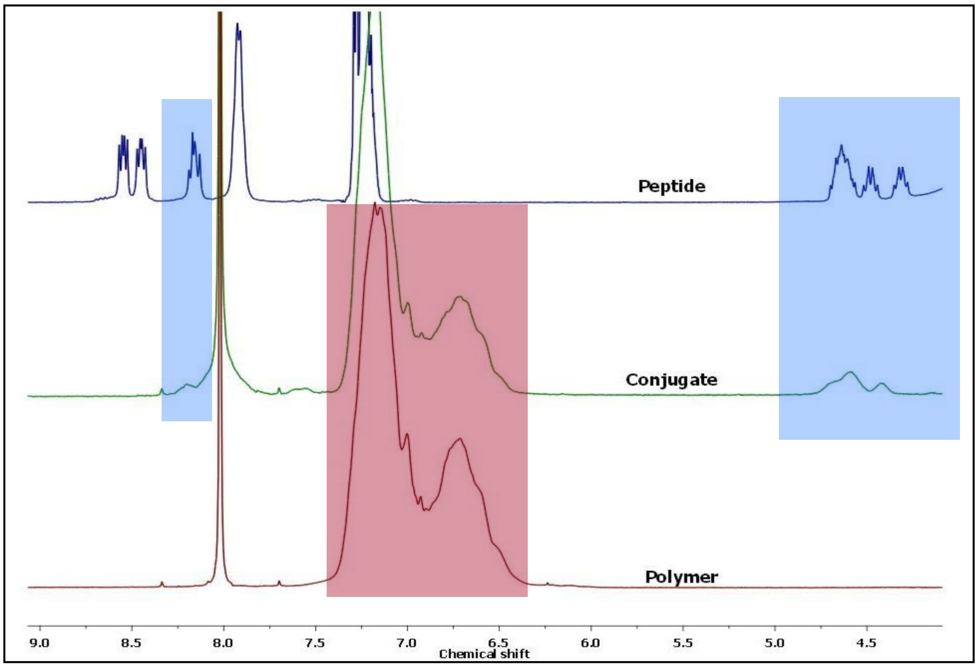

Figure 33: **Superposition of part of the ^{1}H-NMR spectra of peptide, polymer and conjugate product showing the presence of characteristic peaks of the peptide and polymer in the conjugate.**

Moreover, the product was also characterized with DOSY-NMR spectroscopy, as confirmation. The results are superimposed in **Figure 34**: the peptide signal (green), the polymer (blue) and the conjugate product (red). Thanks to the trace of the NMR spectrum of the conjugate, one can clearly see that the characteristic peaks of the peptide belong to a molecule which does not diffuse as quickly as the peptide and additionally is much bigger than the polymer ($D_{polymer} = 10^{-9.55}$ $m^2 \cdot s^{-1}$ while $D_{conjugate} = 10^{-9.68}$ $m^2 \cdot s^{-1}$). The peptide-polymer linear conjugate has been prepared successfully. No free peptide is detected, which confirms the efficiency of the workup.

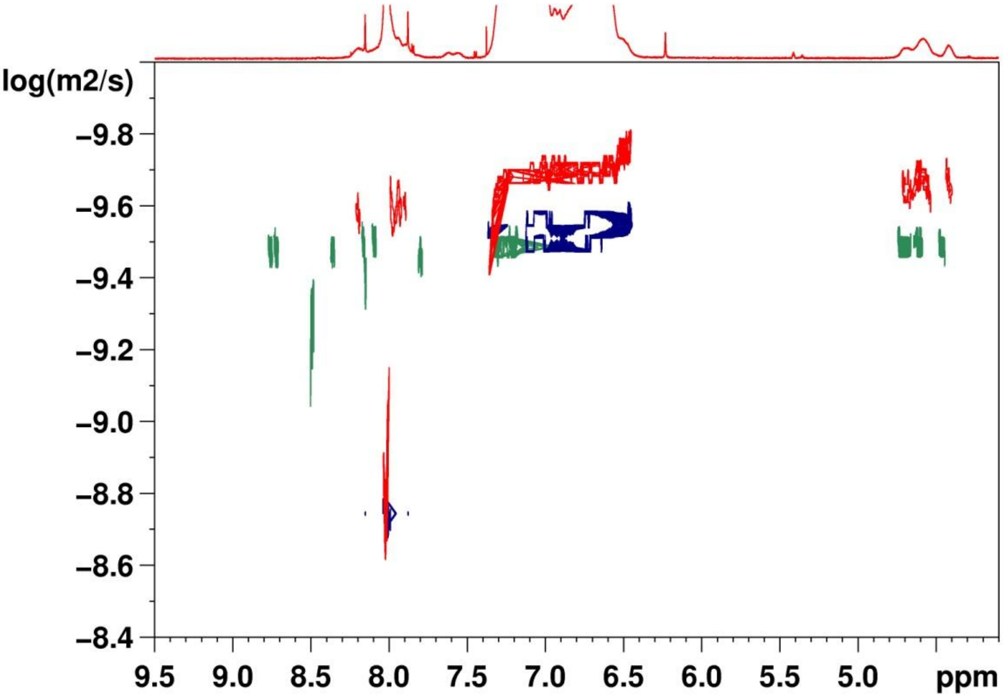

Figure 34: **Overlay of three DOSY-NMR spectra showing the solid-phase coupling of the peptide (green, log $D = 10^{-9.47}$ $m^2 \cdot s^{-1}$) with the polymer (blue, log $D = 10^{-9.55}$ $m^2 \cdot s^{-1}$, M_w= 1250 g·mol^{-1}) to the conjugate (red, log $D = 10^{-9.68}$ $m^2 \cdot s^{-1}$). The ^{1}H-NMR spectra of the conjugate is traced above, with characteristic peaks of the peptide and of the polymer.**

The SEC-chromatograms sketched in **Figure 35** confirm undoubtedly a significant increase of the size of the molecules, especially since we know that the end-functionalized polystyrene is mainly present in “dimer” form (see paragraph IV.1.1). More important, here no shoulder is detected as in solution coupling, but a shift of the complete peak towards lower elution volumes takes place. It seems surprising to observe a narrower size distribution for the conjugate than for the polymer. There are several explanations: the signal of the polymer is broad because of the presence of polymer and polymer “dimer”: one can actually see the shoulder in the tail of the peak. The conjugate also has less or no more amine peaks available and is less liable to present an adsorption tail from the interaction with the column. The peak of the conjugate is also narrower because of the workup of the product. Indeed, only the conjugates with the longest polystyrene chains have precipitated when methanol was added. The washing methanol fraction still contains some conjugates (detected in NMR and observed in MALDI-TOF – see **Figure 36**), which have not precipitated because they are made from shorter polystyrene chains. This contributes to the higher narrowness of the peak of the purified product compared to the polymer in the SEC chromatograms. Finally, on the solid phase, the conjugate has a smaller size compared to the first chains detected in case of coupling in solution (V_{el} = 27.7 mL in SEC for conjugates prepared on solid phase against V_{el} = 26.9 mL for the product of solution coupling). It supports the hypothesis of the formation from branching points in the conjugates during solution coupling, as mentioned previously.

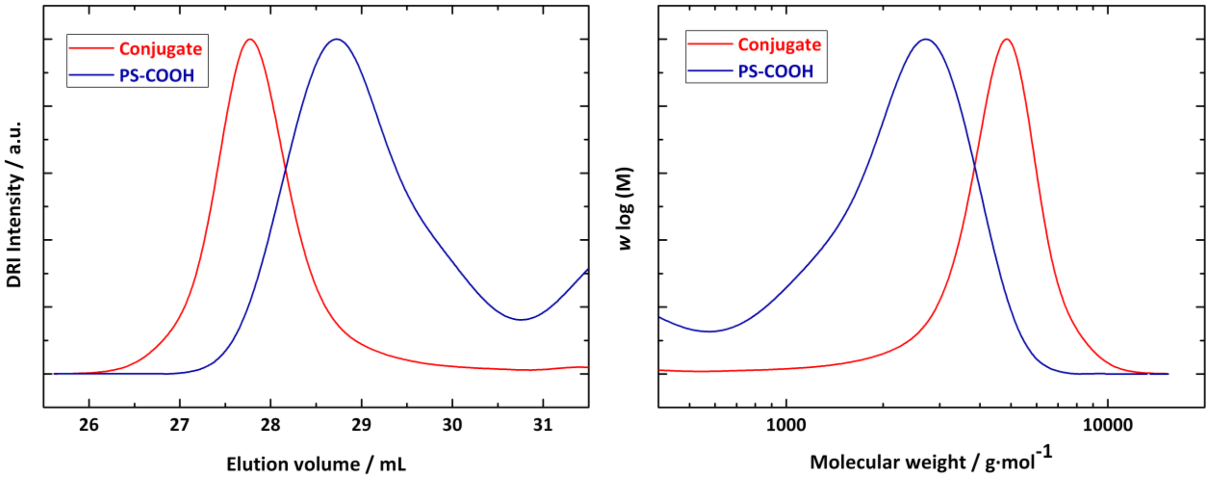

Figure 35: **Overlay of SEC chromatograms (left) and molecular weight distribution (right, calibration polystyrene) from reference polystyrene and from solid-phase coupling conjugated product.**

At this point, it can be asserted that the solid-phase coupling leads to the successful synthesis of the desired peptide-polymer conjugate. From here, the nature of this conjugate (di- or triblock) will be investigated, mainly with MALDI-TOF mass spectroscopy.

Figure 36 presents two MALDI-TOF mass spectra of the polymer and of the conjugate product. While the mass spectra of the polymer shows good agreement with the SEC data, the spectra of the peptide-polymer conjugate shows a significant mass increase. As in the case of the polymer, the series of peaks is separated by exactly M_{styrene}= 104 g·mol^{-1}, which confirms the presence of polystyrene in the products. The analysis of the molecular weight measured also gives information on the nature of the product (diblock or triblock). Indeed, the molecular weight of the polymer distribution (blue) is centered on 1250 g·mol^{-1} and the longest polymer chains have a molecular weight of approximately 2000 g·mol^{-1}. As M_{peptide} = 906 g·mol^{-1}, one would expect for diblock conjugates a distribution centered at 2150 g·mol^{-1} with a maximum molecular weight around 2900 g·mol^{-1}, and centered at 3400 g·mol^{-1} with peaks up to 4900 g·mol^{-1} in the case of triblock conjugates. The mass distribution of the purified conjugate product (red) is centered at 3200 g·mol^{-1} with the presence of peaks over 4200 g·mol^{-1}. This distribution fits with the molecular weights expected in the case of triblock copolymer. The analysis of the molecular weight values speaks in favor of the preparation of triblock rather than diblock conjugates.

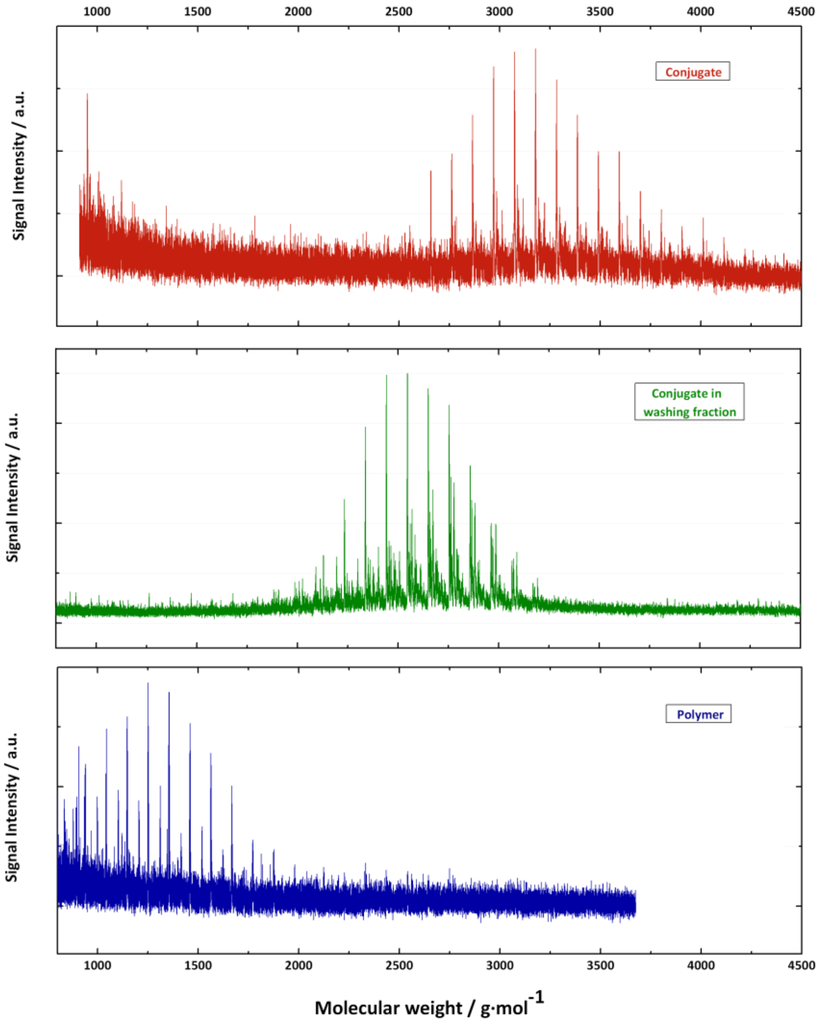

Figure 36: **MALDI-TOF MS of the reference polymer (bottom, blue), of the conjugate product after solid-state coupling (up, red) and of the conjugate contained in the washing fraction (middle, green). Mass difference between the peaks correspond to a styrene unit (104 g·mol^{-1}).**

However, the attempts to precisely attribute each peak to a conjugate with a defined number of styrene units remained unsuccessful. This would have been particularly interesting, as in case of success, a qualitative distinction between di- and triblock conjugate would have been possible, the diblock and triblock peptide-polymer conjugates belonging theoretically to two distinct series of peaks. This would be due to the presence of one butyl-residue (from initiator sec-butyl lithium in anionic polymerization) in the diblock or two butyl-residues in the triblock. The non-precipitated conjugates present in the washing fraction (green) have a lower molecular weight than these in the purified product: the shortest conjugates are soluble in methanol because of the peptide sequence and the too short polystyrene chains. The mass distributions of the purified and the non-precipitated conjugates have main peaks with the exact molecular mass. This speaks in favor of the formation of triblock conjugates, also for the non-purified conjugates.

Finally, a ninhydrin test for the detection of primary amines was processed on the product and turned out to be negative, as expected for a triblock conjugate, whereas a diblock conjugate still has a free amine group. At the end, all indications observed speak in favor of the formation of triblock "polymer-peptide-polymer" conjugate. This is a satisfying result, as a possible enzymatic degradation would be easier to observe, and above all because this is the structure needed for the preparation of nanocapsules. One can be surprised that with such low yields (11%), only triblock conjugates and no diblock are obtained. The only reasonable explanation is that diblock conjugates do not precipitate in methanol, like the shortest triblock conjugates.

IV.1.3 Enzymatic cleavage of triblock peptide-polymer conjugates

As shown above, linear triblock peptide-polymer conjugates were synthesized on solid phase using peptide-coupling chemistry. It is now of primary interest to see whether enzymes can cleave such hydrophobic conjugates in heterophase. Microparticles of conjugates were prepared by ultrasonication of a dispersion of the conjugate in water and solution of trypsin preparation was added. The description of the experimental protocol used for an enzymatic cleavage is available in paragraph VI.5.1. The MALDI-TOF MS analyses of the dried product are plotted in **Figure 37**.

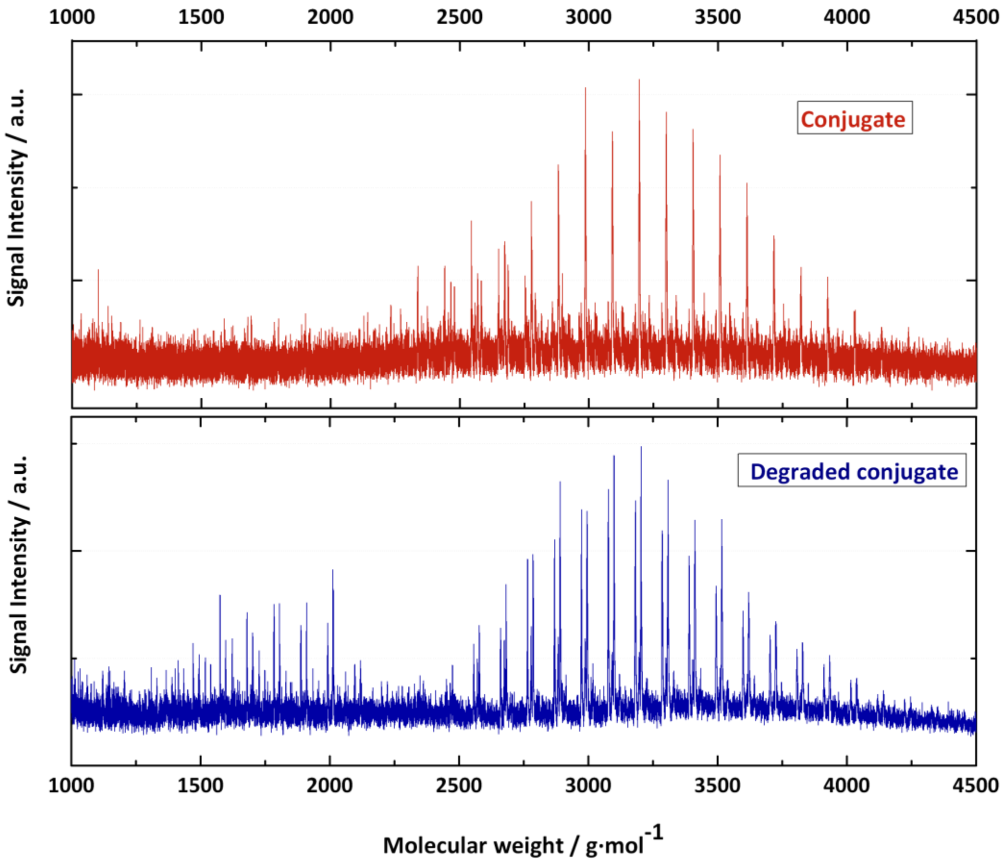

Figure 37: **MALDI-TOF MS of triblock conjugates before (top) and after (bottom) enzymatic cleavage. The series of the conjugate correspond to ionization with cation K^+, whereas the degraded product contains product with cations Na^+ and K^+.**

In the mass spectrum of the sample treated with the enzyme, the original peaks of the conjugates are still present, but a new series of peaks are visible after the experiment. The new peaks show lower masses than the intact conjugates (around 1 500 g·mol^{-1} less) and their peaks are all separated by an interval of 104 g·mol^{-1}. The peaks could not be assigned to a polystyrene chain containing a defined number of styrene units with a pending GF residue, as it would have been theoretically expected after cleavage of the GFF recognition sequence by chymotrypsin.[199] However, the presence of such a regular peaks series should not be due to destruction of the conjugates during the ultrasonication process, which would have surely lead to more varied degradation products. As a result, it can be stated that a partial enzymatic degradation of triblock linear conjugates in heterophase was successfully achieved in this experiment.

Conclusion

In this first part, two routes to prepare linear peptide-polymer conjugates via a direct coupling method were investigated. The reaction in solution led to the successful synthesis of conjugates, but the reaction was not quantitative and it was very difficult to separate the conjugate from the remaining polymer. In solid phase, the washing of excess reactant polymer during the synthetic process gives a product which is much easier to purify afterwards. Yet, the yields obtained were relatively low. The conjugates were thoroughly characterized and at the end, partial enzymatic degradation in heterophase was achieved. Although these results are very interesting and still let place for further experiments, and even more exhaustive characterization, the approach of coupling step between (short) hydrophobic polymers and a simple peptide has shown its limits. The above-mentioned difficulties would certainly increase with the molecular weight of the polymer, and longer chains are required for nanoprecipitation.[163] Another method was investigated, with higher peptide content and more efficient coupling.

For all these reasons, the second method presented in the next part can be considered as a more straightforward approach. The goal is to achieve the preparation of nanocapsules by interfacial polyaddition of the peptide dissolved in dispersed phase with another monomer dissolved in the continuous phase. Therefore, it was decided to use the amine group of lysine to react with isocyanate group and form urea bonds to prepare the desired hybrid polymer.

IV.2 Development of a method to prepare peptide-based hybrids nanocapsules

The protocol developed is inspired by the work published by other members of the group,[152, 153, 175] with the preparation of polyurethane and polyurea nanocapsules by interfacial polyaddition in inverse miniemulsion. Nevertheless, they were mainly working with various systems, based on small molecules (1,6-diaminohexane, 1,6-hexanediol, diethylenetriamine) with a high density of reactive groups reacting with TDI or other diisocyanate molecules. Crespy reported successful experiments using dextran or starch as polyalcohol, and TDI as cross-linker.[152] The use of macromolecules is possible but in these cases as well, the density of reactive group was very high with three hydroxyl groups per sugar unit. It was then necessary to adapt their protocols, by taking in consideration the specificities of a peptide-based system.

- While the work of Rosenbauer[175] was carried out with water as dispersed phase, the peptides used in this thesis are not water soluble (enough). It is thus necessary to tailor this system to another solvent for the disperse phase. DMF and DMSO are good candidates, as they dissolved the peptides well. Crespy had already successfully performed experiments with DMSO and formamide as dispersed phase.[152]

- The change of solvent may lead to the utilization of other surfactants to stabilize the nanodroplets. In addition to this, the surfactant used – typically a nonionic surfactant in the case of inverse miniemulsion – should not bear functions liable to react with isocyanate group, e.g. amine or alcohol.

- The use of significantly big (from 1000 to 2000 g·mol^{-1}) and expensive oligopeptides as diamine or polyamine will certainly restrain the experiments to small amounts of peptides for each assay, especially during the establishment of the method. However, by reason of molecular weight difference between peptide (around 1000 g·mol^{-1}) and TDI (174 g·mol^{1}), the concentration of peptide in the dispersed phase has to be high so that the amount of equivalent TDI remains significant, and also to achieve a sufficient solid content.

IV.2.1 Choice of the surfactant

The use of Lubrizol U (polyisobutylene-succinimide pentamine), used as a surfmer by Rosenbauer and al.,[50, 175] was avoided since it would have reacted with TDI.

The first tries were carried out with three different surfactants: polyglycerol polyricinolate (PGPR), Fortegra 100 (epoxy toughener from Dow Chemicals) and poly(butylene-*co*-ethylene)-*b*-poly(ethylene oxide) (P(B/E-*b*-EO), in DMF and DMSO. Strictly speaking, PGPR, Fortegra 100 and P(B/E-*b*-EO) are all likely to react with TDI as these large surfactants carry one or few alcohol group(s). Although several different concentrations of surfactant were used, only the miniemulsions prepared with the surfactant P(B/E-*b*-EO) were stable. From this point, all the miniemulsions were stabilized with this linear nonionic block copolymer.

IV.2.2 Optimization of synthetic parameters

As system leading to stable nanodroplets: cyclohexane was chosen as continuous phase with DMSO or DMF as dispersed phase stabilized with P(B/E-*b*-EO). The following parameters were investigated during a series of experiment:

- Possible use of lithium bromide as osmotic pressure agent: indeed, in addition to its osmotic agent role, the salt could also help dissolving a large amount of peptide in the dispersed phase.
- Concentration of surfactant P(B/E-*b*-EO): on the one hand, an increasing concentration of surfactant should ensure the formation of smaller droplets and therefore smaller capsules. On the other hand, due to the low amount of reactant, as less surfactant as possible is be preferable.
- Variation of TDI equivalents: as diisocyanate, TDI can react with a variety of different nucleophilic groups as described in paragraph II.6.2. In our case, with the exception of the amino groups of the peptide, the most probable are water molecules (DMF and DMSO were not dried), and hydroxyl end-groups of the P(B/E-*b*-EO) surfactant, but also reactions with the carboxylic end-group of the peptide or with the amide or urea are possible. However, please note that the reactivity of TDI with amino groups is much larger than for hydroxyl groups.[203] As a result, it may be necessary to vary the amount of TDI to obtain the nanocapsules, but also to adjust the thickness of their shell.[153, 175]

Each sample corresponding to a different combination of those parameters was prepared. For every sample prepared, a stable suspension was obtained. The sizes measurements with PCCS of all the samples prepared are listed in **Table 1** and summarized graphically in **Figure 38**.

Table 1: Summary of size and size distribution measurements obtained with PCCS for the study of synthetic parameters.

			Dispersed phase DMF									Dispersed phase DMSO								
			Surfactant concentration[a] / wt%									*Surfactant concentration*[a] / wt%								
			0.3			0.5			1			0.3			0.5			1		
			Size (nm)									Size (nm)								
			x_{10}	x_{50}	x_{90}	x_{10}	x_{50}	x_{90}	x_{10}	x_{50}	x_{90}	x_{10}	x_{50}	x_{90}	x_{10}	x_{50}	x_{90}	x_{10}	x_{50}	x_{90}
No LiBr	**TDI equivalent[b]**	**0.5**	433	515	590	489	522	628	495	561	647	344	466	544	239	274	316	175	203	235
		1.0	437	518	595	443	522	599	380	499	569	319	395	519	276	317	366	183	215	252
		1.5	402	502	569	534	620	806	502	568	649	299	362	509	290	338	439	175	203	235
		2	459	524	596	500	567	653	488	560	656	320	387	507	279	325	389	183	211	242
LiBr	**TDI equivalent[b]**	**0.5**	281	338	485	268	313	382	228	268	314	/[c]	/[c]	/[c]	292	353	504	227	263	304
		1.0	259	297	340	290	338	439	234	275	321	430	512	585	300	344	440	227	266	310
		1.5	280	331	443	314	379	492	279	325	389	402	502	569	300	350	470	222	259	310
		2	282	327	386	298	355	489	279	325	389	356	471	543	303	364	508	217	253	295

(a) Related to the continuous phase. Related to dispersed phase, the concentration equal respectively to 3.0, 4.5 and 9.0 wt%
(b) Related to the amount of amine groups on peptide [“Y”-NH_2]
(c) Sample lost by accident

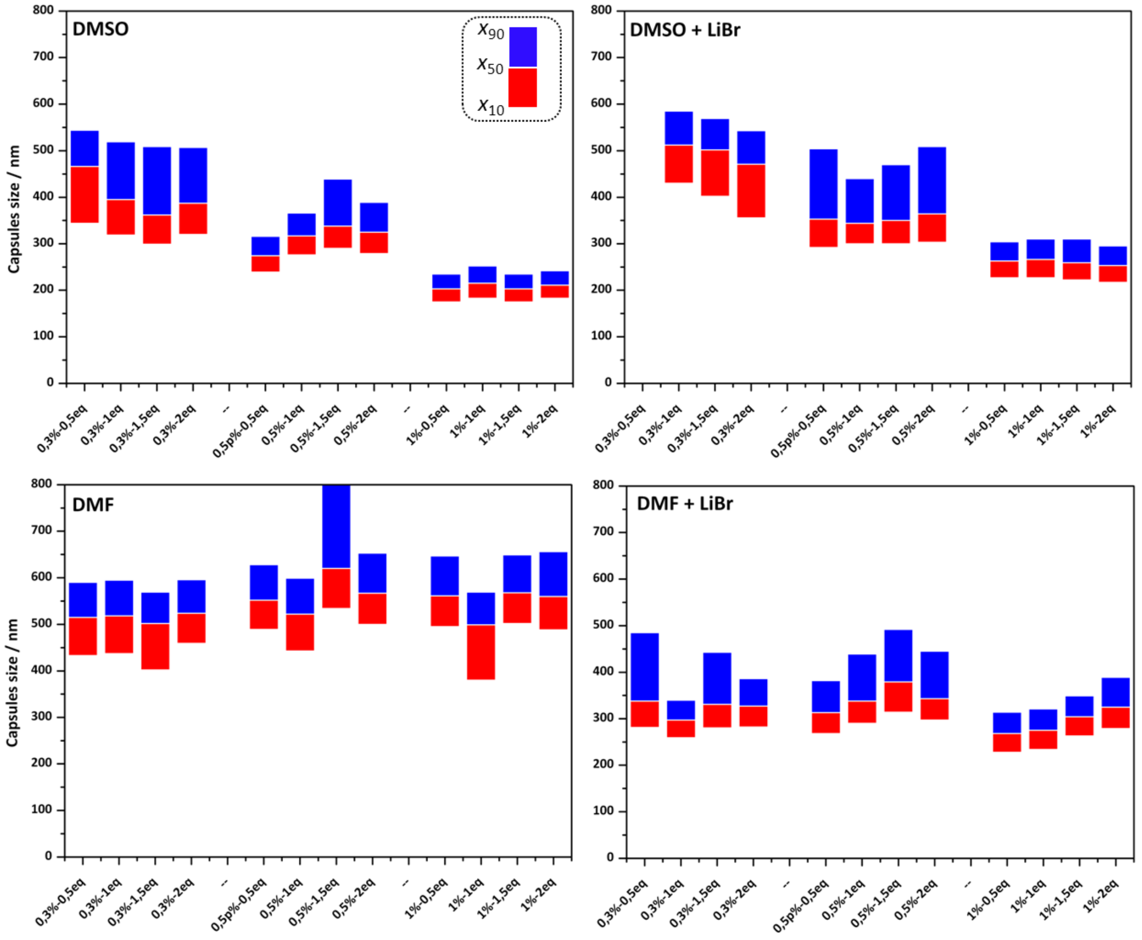

Figure 38: **Summary of the size distribution measured during a series of experiments to optimize the following parameters: nature of the dispersed phas,e amounts of TDI equivalents and concentration of surfactant. For example, 0.3%-1.5 eq. means 0.3 wt.% surfactant related to continuous phase and 1.5 equivalents TDI per amine group on the peptide. x_n is the value for which n% of the particles are smaller than this value.**

In this paragraph, the main results and trends to be noticed, concerning the stability and the particles size of this series of experiments are reported. It is remarkable that all the samples prepared result in stable dispersions, independently of the dispersed phase or of surfactant ratio. Indeed, ten randomly chosen samples show negligible size variations one month later. The size of the particles is in the range of a few hundreds nanometers (from 200 to 500 nm approximately). Nanoparticles are obtained, however they are relatively big, especially in the perspective of cellular uptake. It actually seems that the general system employed, provides a stable basis for the production of peptide-based capsules. The influence of the synthetic parameters studied can be summarized as following.

In pure DMSO, the size distribution of the capsules follows the expected results in miniemulsion: the size of the capsules decreases when the concentration of surfactant increases: from 420 nm in average with 0.3 wt.% surfactant to the continuous phase, to 210 nm with 1 wt.% surfactant. Besides, an increasing amount of surfactant leads to a narrower size distribution, which confirms that the surfactant efficiently stabilizes the droplets. In pure DMF, capsules of relatively big sizes ($x_{50\text{-average}}$ ≈ 550 nm) and with broad size distribution are obtained. Furthermore, the increase of the surfactant concentration does not lead to a smaller size of the droplets: probably, Ostwald ripening occurs more easily with DMF, less polar than DMSO and more likely to diffuse through cyclohexane. It is highlighted here that TDI was added to the miniemulsion only a few minutes after ultrasonication.

Moreover, DMSO (ρ = 1.1 $kg \cdot L^{-1}$ at room temperature) is a more dense solvent than DMF (ρ = 0.95 $kg \cdot L^{-1}$). For this reason, as the same weight of solvent was added, it is expected to obtain smaller droplets (and afterwards capsules) with DMSO as dispersed phase than with DMF.

The addition of LiBr in the DMF-based dispersed phase has a strong influence on the size distribution of the capsules. Overall, they are significantly smaller (330 nm in average with LiBr against 550 nm without). The increase of the surfactant concentration slightly decreases the size of the capsules: from 360 nm with 0.3 wt.% surfactant to 290 nm with 1 wt.% over 345 nm for 0.5%. In conclusion, LiBr plays fully the role of an osmotic agent in DMF, as it limits Ostwald ripening and contributes to the stabilization of smaller droplets.

The addition of LiBr in DMSO almost does affect neither the size of the capsules, nor the broadness of their distribution. This can be explained by the higher polarity of DMSO, which limits its diffusion through the continuous cyclohexane phase. The effect of LiBr as osmotic pressure agent is thus not predominant in DMSO.

Generally, the amount of TDI equivalents added does not have a significant influence on the size of the particles. This confirms the results reported previously with a polyaddition system in miniemulsion, where the size of the capsules was unchanged by increasing amounts of TDI, whereas the thickness of the capsules was slightly increasing.[153]

IV.2.3 Characterization of the peptide-based hybrid by electron microscopy

The structure of the capsules obtained from these dispersions was observed by scanning electron microscopy (SEM) and transmission electron microscopy (TEM). In addition to the confirmation of a proceeded polyaddition, the micrographs also give structural information on the nano-objects synthesized.

Scanning electron (SE) micrographs observed from some samples presented on **Table 1** are displayed in **Figure 39**.

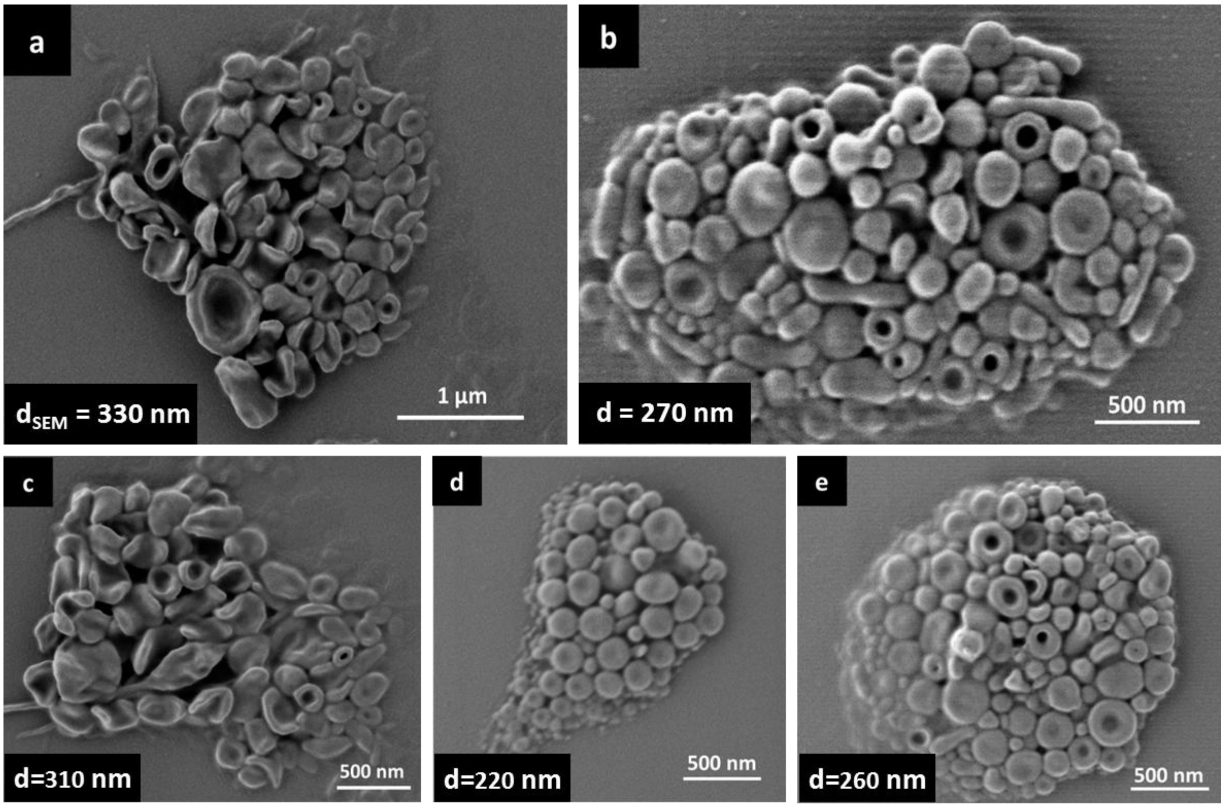

Figure 39: **Collection of scanning electron (SE) micrographs, all obtained from DMF with 5 g·L^{-1} LiBr as dispersed phase if not stated otherwise a) 1% surfactant with 1 equivalent TDI, in pure DMF b) 1% surfactant and 1.5 equivalents TDI – c) 1% surfactant and 1 equivalent TDI – d) 0.3% surfactant and 1.5 equivalents TDI – e) 0.3% surfactant and 1 equivalent TDI.**

All pictures presented in **Figure 39** show nanostructures with sizes comparable to those observed with PCCS. Moreover, capsule structures (collapsed due to the vacuum) are observed in each sample. Both characteristics indicate that the interfacial polyaddition reaction proceeds successfully forming the desired capsules structure. The few non-collapsed structures can be interpreted as non-collapsed capsules or particles. In these cases, transmission electron microscopy can help differentiating them. Overall, scanning electron microscopy confirms the results obtained until here and displays some very nice capsules structures. Transmission electron (TE) micrographs of other samples issued from **Table 1** are displayed in **Figure 40**.

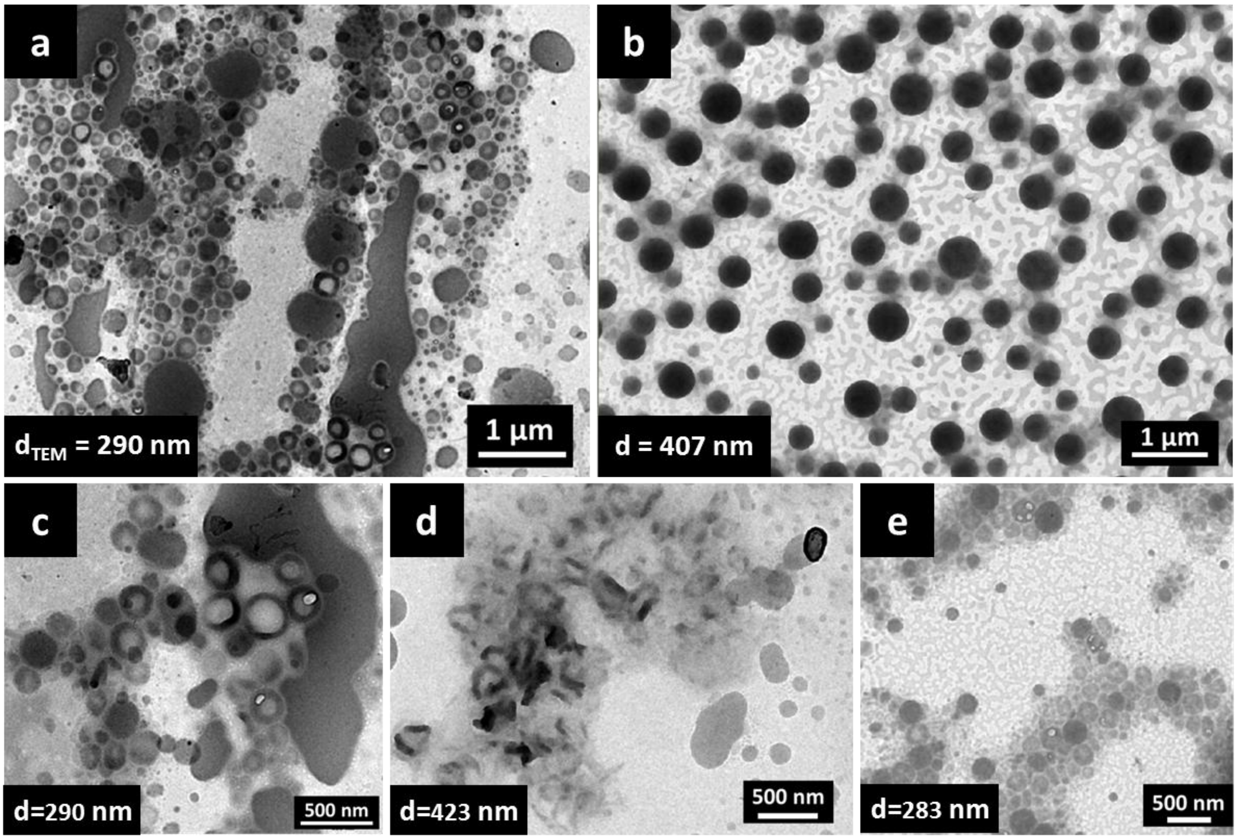

Figure 40: **Collection of transmission electron (TE) micrographs on samples using DMF with 5g·L^{-1} LiBr as dispersed phase if not stated otherwise, with the following parameters: a) 0.3% surfactant and 1 equivalent TDI, c) is an enlarged part of a) – b) 0.5% surfactant and 1 equivalent TDI – d) 0.5% surfactant and 2 equivalents TDI in pure DMF – e) 0.5% surfactant and 1.5 equivalent TDI.**

The micrographs confirm the presence of capsules in the samples. For example, micrographs from **Figure 39e** and **Figure 40a** correspond to the same sample and demonstrates that some collapsed particles observed with SEM correspond to capsules in TEM. Some samples (**Figure 40d**) present rather "angular" capsules while more round structures are observed on (**Figure 40c**). Even more interesting is the graduation of structures from capsules (**Figure 40a**) to a sample with particles (**Figure 40b**) over sample presenting mix of both (**Figure 40e**). To sum up, the TEM analyses confirm the presence of solid nanocapsules in many samples.

No correlation between the size of the particles and the amount of TDI equivalents was determined, as seen from the PCCS results (**Figure 38**). Similarly, no obvious relation between the amount of equivalent TDI and the thickness of the capsules was observed. It has to be mentioned that all the pictures displayed previously in SEM and TEM were prepared with DMF as dispersed phase. The samples prepared with DMSO presented a film or undefined melted structures on the surface. Possibly the degree of polymerization is lower in DMSO and the structures are not rigid enough for observation under electron microscopy. This was not investigated further and does not prove that the interfacial addition reaction is not occurring, but this observation definitely played a role in the choice of DMF for dispersed phase for the following experiments. Finally, capsules structures were observed for each surfactant concentration. The surfactant concentration cannot be considered as a critical parameter for the structure of the peptide-based nanoparticles.

Conclusion

As a result, it was decided to carry on the next experiments with the following investigated parameters:

- Keeping the concentration of peptide in dispersed phase (50 mg peptide in 0.75 g).
- DMF with 5 $g \cdot L^{-1}$ lithium bromide as solvent for the dispersed phase.
- P(B/E-*b*-EO) surfactant in the proportions of 0.5 wt.% to continuous phase.
- A TDI equivalent amount of 1.5 related to the number of amine groups on the peptide.

The choice of DMF with lithium bromide was principally motivated by the guaranty of peptide dissolution, as the peptides used subsequently are liable to be more hydrophobic because of the presence of the FRET system. The importance of the lithium bromide addition was confirmed by the experiments, especially to decrease the size of the components of the dispersions in DMF. The choice of the surfactant ratio was the result of a compromise between a lower size of the capsules and a contribution of the surfactant to the solid content maintained as low as possible, because it is already important. Finally, choosing 1.5 equivalent of TDI was done principally on the experience that an excess of isocyanate was an effective rule, because of side reaction with water or alcohol group of the surfactant[152, 175] but this parameter is liable to be changed in the next experiments depending on the nature of the peptide.

Here are a few remarks concerning the developed system. In cyclohexane, the solid content of the miniemulsion is approximately 1.5 wt.% (depending on TDI equivalent and presence or absence of encapsulated dye). The peptide represents around 60% weight of this solid content.

IV.3 Synthesis, characterization, and cleavage of peptide based hybrid nanocapsules

IV.3.1 Peptides used for capsules preparation

Description of the peptides

In this part, 4 different peptides used for preparing the nanocapsules are introduced. The structures of these peptides are displayed and the characteristics of each of them are briefly presented.

Peptide [Mant/2NH$_2$] - K(Mant)GFFY(NO$_2$)G

The peptide K(Mant)GFFY(NO$_2$)G, designated as [Mant/2NH$_2$] (see **Figure 41**) contains a FRET system surrounding the recognition sequence GFF. The FRET system – consisting of a fluorophore/quencher pair – is introduced for optical detection of the peptide cleavage of the peptide sequence, via an increase of fluorescence. Here the fluorophore is the *N*-methylanthraniloyl- (Mant) group (λ_{ex} = 315 nm and λ_{em} = 425 nm) and 3-nitrotyrosine (Tyr(NO$_2$)) the suitable quencher.[204] The addition reaction is possible at both extremities of the peptide through the amine group in *N*-terminus and the lysine in penultimate position. To sum up, if one neglects the much slower[203] possible reaction of TDI with the C-terminus carboxylic group, this peptide is designed for the preparation of linear peptide base polymer.

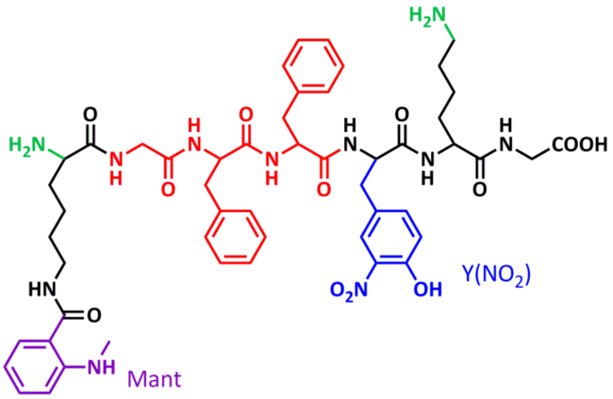

Figure 41: **Structure of peptide [Mant/2NH$_2$]. The recognition sequence is traced in red, the fluorophore group in violet, the quencher in blue and the reactive groups for polyaddition in green.**

Peptide [Mant/3NH$_2$] - K(Mant)KGFFY(NO$_2$)G

The peptide K(Mant)KGFFY(NO$_2$)G, designated as [Mant/3NH$_2$] (see **Figure 42**) is the same than the previous one, with the exception that the additional lysine in second position brings a third amine group (two lysine amino acids and the *N*-terminus). Therefore, this peptide should potentially lead to longer chains, probably branched or even cross-linked. It is legitimate to wonder why the lysine is introduced in second position, after the dye, rather than before. This is due to the Mant-lysine amino acid, from which it is not possible to synthesize further linearly. Indeed, the secondary amine on the Mant group can react with an amino acid during further coupling reactions. Other protective groups were considered.[10] Unfortunately, complete methylation of the amino group is not relevant as the product N,N´-dimethylanthranil acid does not exhibit fluorescence.[205] As a result, the sequence between the fluorescent dye and the quencher is not exactly the same as in peptide [Mant/2NH$_2$] presented above. In this sequence [Mant/3NH$_2$], the additional connecting lysine had to be introduced inside the FRET pair.

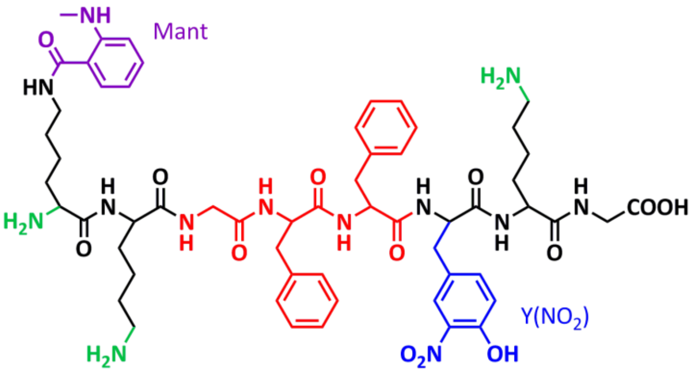

Figure 42: Structure of peptide [Mant/3NH$_2$].

Peptide [Mca/3NH$_2$] - KK(Mca)GFFK(Dnp)G

The peptide KK(Mca)GFFK(Dnp)G, designated as [Mca/3NH$_2$] (see **Figure 43**), is the replica of the previous one with two differences: the fluorophore/quencher pair has now been changed to (7-Methoxycoumarin-4-yl)-acetyl- (Mca, λ_{ex} = 340 nm and λ_{em} = 405 nm) / dinitrophenyl (Dnp).[190] The second lysine was placed here in *N*-terminus position, to have the FRET pair framing only the recognition sequence.

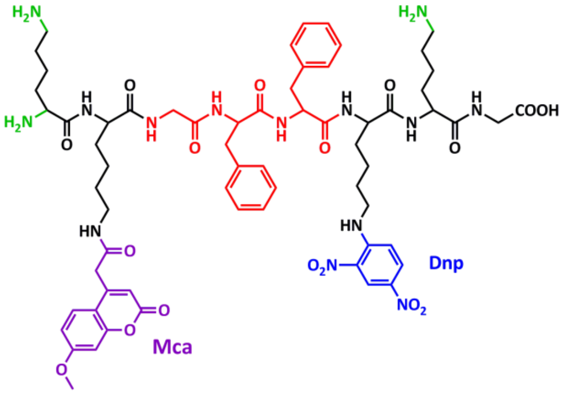

Figure 43: Structure of peptide [Mca/3NH$_2$].

Peptide [Mca/7NH$_2$] - KKKK(Mca)GFFK(Dnp)-KKKG

The peptide KKKK(Mca)GFFK(Dnp)KKKG, designated as [Mant/7NH$_2$] (**Figure 44**), is similar to the previous one: it has the same recognition sequence, and the same FRET system. It differs only in the number of lysine amino acids: three at the beginning and three at the end of the sequence, which gives a total of seven amino acids. This peptide is multi-functionalized to increase the probability of formation of branched polymers. It is expected to generate longer peptide-based polymeric chains as well as a better entrapment of encapsulated molecules.

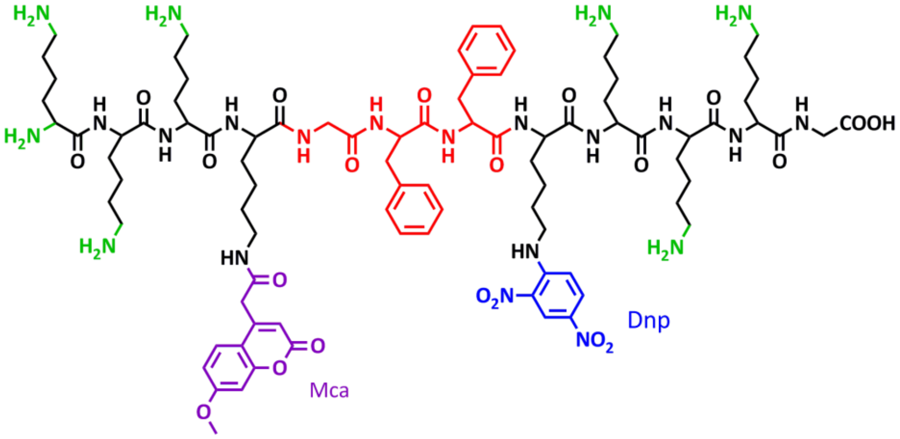

Figure 44: Structure of peptide [Mca/7NH$_2$].

Cleavage of free peptides in solution

As all the peptides carry a FRET system surrounding the recognition site, the cleavage in solution of those peptides can be monitored by fluorescence measurements. The cleavage of each peptide by trypsin preparation is represented in **Figure 45**.

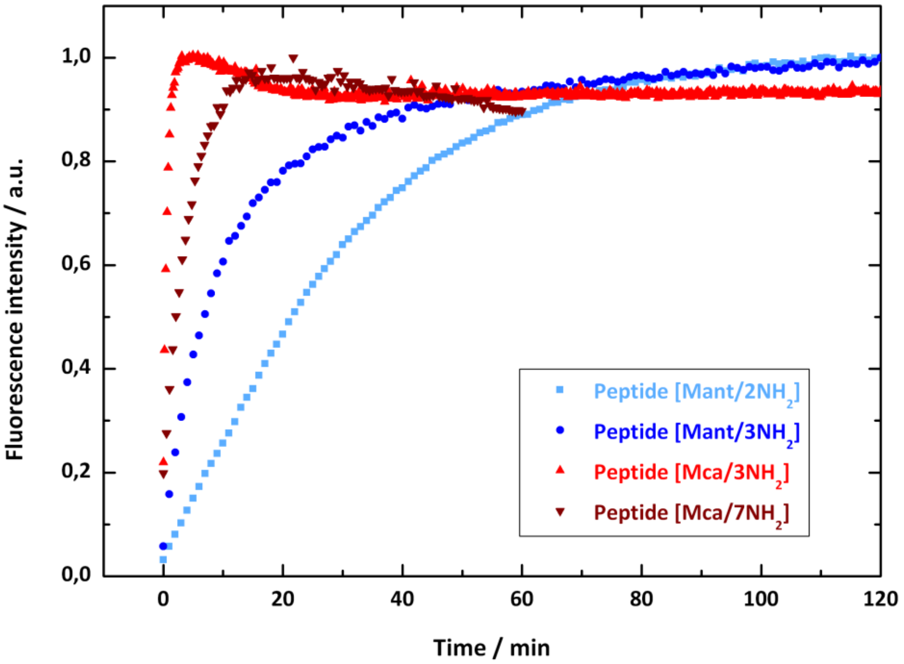

Figure 45: **Enzymatic cleavage against time of the peptides used to prepare the nanocapsules. All curves were normalized with maximum point equal to the unity. Concentrations of peptide are 10^{-5} M. *Measurements done by N. Kotman.***

An increase of fluorescence is observed for each peptide: all of them are cleaved by the commercial trypsin preparation, in a time scale ranging from a few minutes to one hour. As the graphs are normalized and the peptides do not contain the same FRET pair, no remark is done here concerning the efficiency of the quenching or the relative amount of peptide actually cleaved. Comments on the kinetics can still be done with a pairwise comparison of peptides differing from only one parameter. Peptide [Mca/3NH$_2$] is cleaved much faster than peptide [Mant/3NH$_2$], although both peptides have three surrounding amine groups. More than the nature of the FRET pair, this difference is attributed to the fact that the Mca/Dnp FRET pair is attached to the peptide with a lysine as flexible linker, whereas in peptide [Mant/3NH$_2$], the Y(NO$_2$) group is closer to the peptide backbone and can hamper the recognition of the sequence by the active site of the enzyme. Furthermore, the addition of surrounding lysine residues (variation of hydrophilicity) has an influence on the enzymatic cleavage, but only to certain extend. Indeed, while the comparison between peptide [Mant/2NH$_2$] and [Mant/3NH$_2$] shows that the addition of a lysine accelerates the cleavage, results obtained with peptide [Mca/3NH$_2$] and [Mca/7NH$_2$] tend to demonstrate that a too big number of lysine brings probably more steric hindrance than benefic hydrophilicity. Another explanation could be the following: trypsin is known to cleave in the C-terminus of a lysine. It is possible, that the increasing amount of lysine favors this other cleavage reaction, which does not lead to fluorescence recovery, as the lysine residues are located outside the FRET pair. As a result, this competitive cleavage reaction could slow down the degradation of the recognition site by chymotrypsin, especially in the presence of numerous lysine residues, as in the case of peptide [Mca/7NH_2].

The influence of surfactant P(B/E-*b*-EO) and SDS on the enzymatic cleavage was also tested in relevant concentrations regarding the future miniemulsions (0.25 wt.% for P(B/E-*b*-EO) and 0.3 wt.% for SDS corresponding to their maximal concentration possible without dialysis). The fluorescence increase and its speed were similar for peptide [Mant/2NH_2] and [Mant/3NH_2] with the presence of surfactant. No significant difference in the cleavage of the dissolved peptide sequences were observed in water or in PBS buffer in the presence of surfactant.

IV.3.2 Preparation and characterization of hybrid nanocapsules with FRET pair Mant/Y(NO_2)

The nanocapsules were prepared with the standard protocol described in the experimental part, which is summarized in **Figure 46**. The parameters are described in **Table 2**. The samples were characterized thoroughly with the methods described in the following paragraphs before redispersion in water.

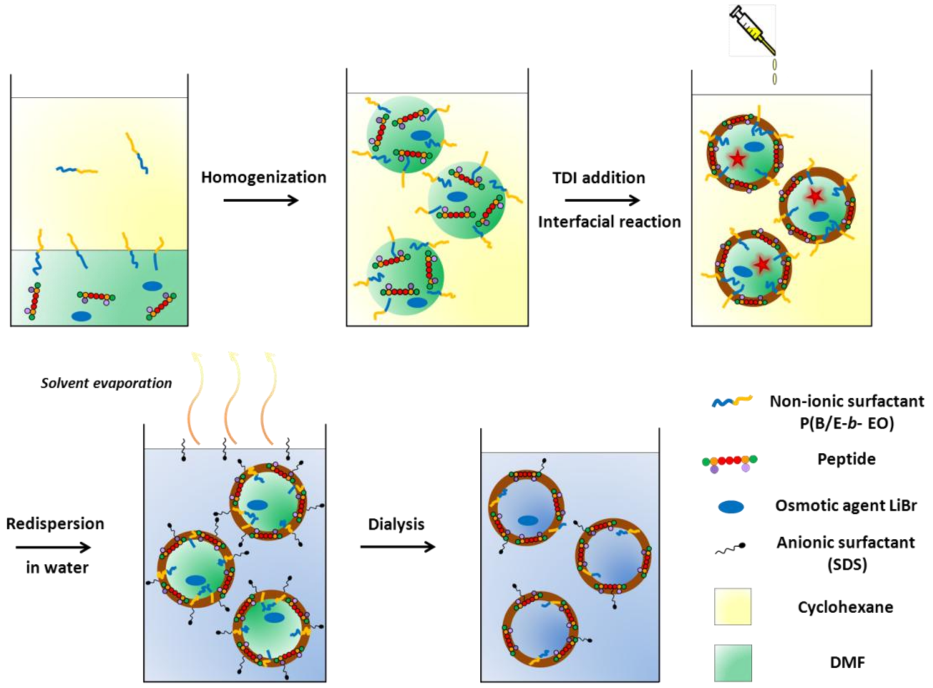
Homogenization
TDI addition
Interfacial reaction
Solvent evaporation
Redispersion in water
Dialysis
Non-ionic surfactant P(B/E-b- EO)
Peptide
Osmotic agent LiBr
Anionic surfactant (SDS)
Cyclohexane
DMF

Figure 46: **Schematic representation of standard protocol for the preparation of peptide-based nanocapsules.**

Table 2: Dispersions prepared from peptide containing the FRET pair Mant/Y(NO_2).

Sample	Peptide used	Dispersed phase	TDI equivalents	x_{50} in cyclohexane (nm)
JA46	[Mant/2NH_2]	DMF + 5 g·L^{-1} LiBr	1.5	232⒜
JA47	[Mant/3NH_2]	DMF + 5 g·L^{-1} LiBr	1.5	208⒜

Verified polymerization via SEC

In order to verify the successful addition reaction of these new peptides bearing FRET systems, one method to characterize the capsules, not used until now, is the size exclusion chromatography. The SEC chromatograms were measured at 270 nm, which allows a selective detection of the products made of peptide and TDI (absorbance of the aromatic groups: phenylalanine residues, FRET pair and of TDI), as the surfactant P(B/E-*b*-EO) is not absorbing at this wavelength. Mainly, the objective of such an analysis is to observe the formation of macromolecules after the polyaddition step. It will also be relevant to compare the size of the polymer chains obtained from the two different kinds of peptide: from peptide [Mant/2NH_2] (linear) or from [Mant/3NH_2] (possibility of branching). The SEC chromatograms of the peptides and of the corresponding freeze-dried suspension after polyaddition are displayed in **Figure 47.**

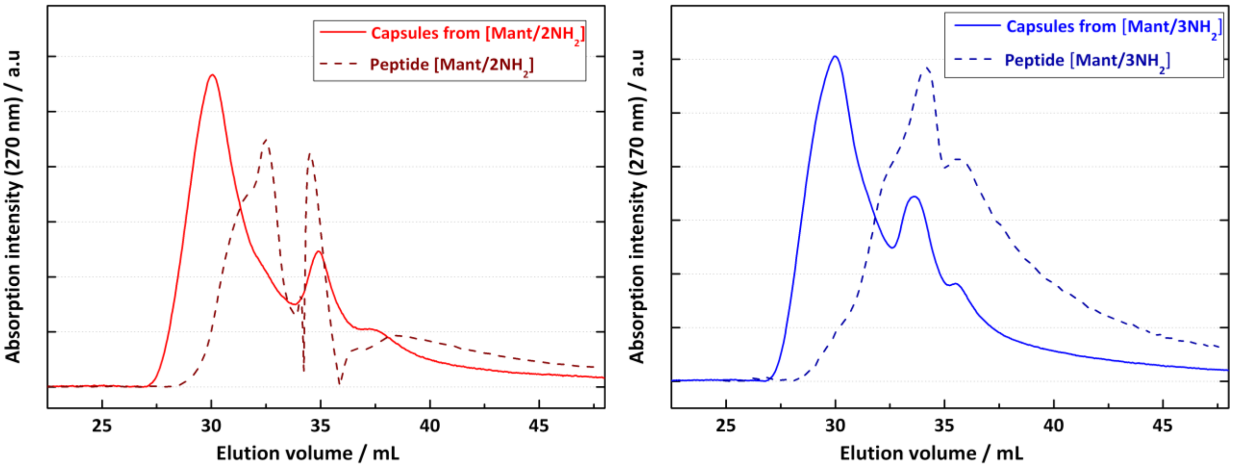

Figure 47: Overlay of SEC chromatograms from peptide and polymers. Left: Peptide [Mant/2NH_2] and its polymer (red) generated via interfacial polyaddition. Right: Peptide [Mant/3NH_2] and its polymer (blue).

The first remark to be done concerning those SEC chromatograms are the signs of adsorption of both peptides on the column. One can see it clearly from the asymmetric form of the peaks, with the presence of a tail. It means, that the strict conditions for SEC are not fulfilled, as the mobile phase interacts with the stationary phase. However, the main result is that there is a clear shift toward lower elution volumes – i.e. towards higher molecular weights – showing that polyaddition took place in both cases. No molecular weight distributions are displayed, as there was no relevant standard available to plot a calibration curve. Moreover, the usual standards are linear, whereas here a most likely polymer with branching points was prepared from [Mant/3NH$_2$]. However, one could expect a more significant shift of the elution volume towards higher molecular weight, especially in the case of the polymers formed from [Mant/3NH$_2$]. This can be explained principally by two reasons: polyaddition does not yield a high degree of polymerization for not too high conversion (see paragraph II.6.1). Additionally, it is published that branched polymers have lower hydrodynamic radii than linear polymers of equal molecular weight, as they form a denser structure in solution.[184] Formulated in another way, a branched polymer with higher molecular weight will elute at the same time that a linear polymer with lower molecular weight but the same hydrodynamic volume in solution. According to **Figure 47**, there is no significant difference of the hydrodynamic volume between the polymers formed in polyaddition from peptide [Mant/2NH$_2$] and the polymers formed from [Mant/3NH$_2$]. The formation of macromolecules during the polyaddition stage is a good sign but one should not formulate any other conclusion yet.

Confirmed consumption of peptide monomer via HPLC

Another possibility to determine quantitatively how well the addition polymerization proceeded is HPLC. Using this method, an estimation of the monomer conversion can be achieved. The samples were dissolved in a THF/0.1 wt.% TFA in H$_2$O solution. This mixture did not fully dissolve all the components of the freeze-dried miniemulsion but at least, it is sure that the free peptide remaining is fully extracted, as it is completely soluble in DMF. **Figure 48** presents the HPLC elugrams of the peptide and the dissolved part of the freeze-dried inverse dispersions.

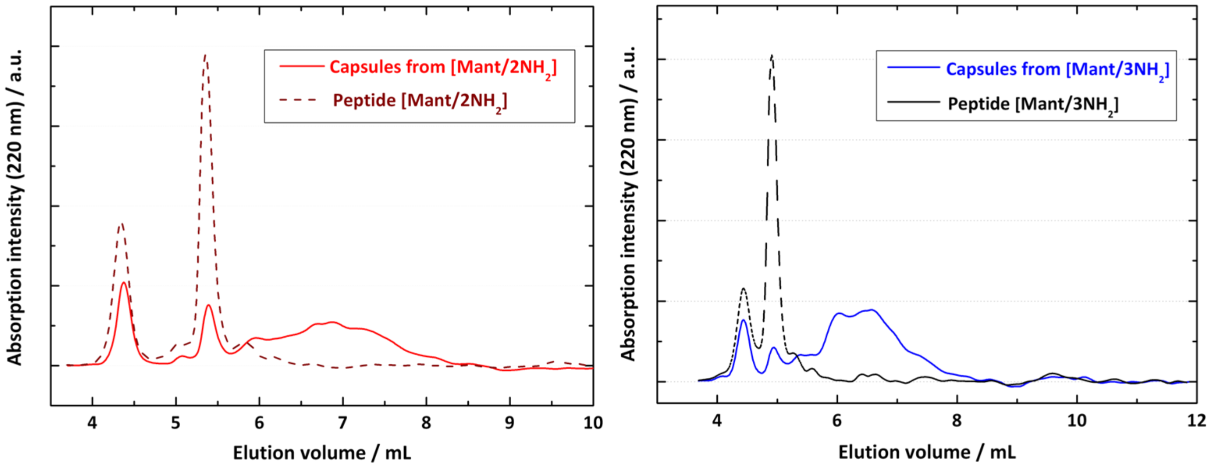

Figure 48: **Overlay of 2 HPLC chromatograms of peptide and polymers. On the left (red), peptide [Mant/2NH$_2$] with its polymer formed by interfacial polyaddition and on the right (blue), peptide [Mant/3NH$_2$] with its polymer. In each curve, the overall peptide amount (as free peptide or polymer) injected is the same.**

Both elugram overlays clearly show that the amount of free peptide is less in the extracted sample after the interfacial reaction. Polyaddition proceeded, with only a small amount of unreacted monomer peptide left. A higher conversion of peptide is obtained with the cross-linker peptide. This confirms the importance of a multifunctional peptide in the preparation of the capsules: an increasing conversion would be synonym of longer chains and probably of better encapsulation of the payload.

Limited additional information of infrared spectroscopy

Infrared (IR) spectroscopy is useful to follow the reaction of the isocyanate group.[175] It was even used to estimate the ratio of urethane and urea bonds when nanocapsules were prepared from 1,6-hexanediol and TDI, with water as dispersed phase. Consequently, IR spectroscopy brings relevant information on the peptide-based capsules. **Figure 49** presents the overlay of the IR spectra from peptide [Mant/3NH$_2$] and of the freeze dried capsules obtained by interfacial polyaddition.

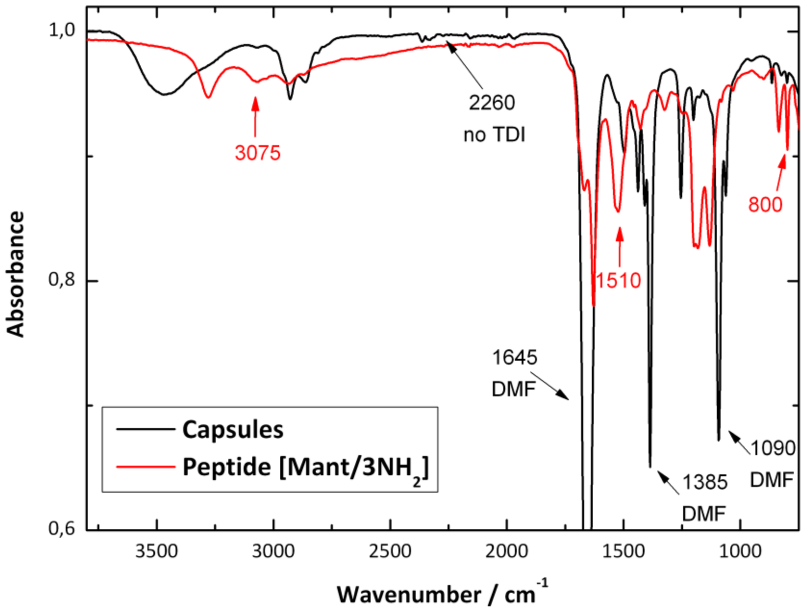

Figure 49: **Overlay of IR spectra from peptide [Mant/3NH$_2$] and from capsules formed by interfacial polyaddition of this peptide with TDI in inverse miniemulsion.**

The spectrum of peptide [Mant/3NH$_2$] presents a maximum absorption peak at 1630 cm^{-1}. It corresponds to the C=O bonds of the peptides, presents in the numerous amide bounds and the carboxylic acid in C-terminus. One observes also broad peaks at 3285, 3075 and 2940 cm^{-1}, which correspond to the NH bonds of the amino and amide groups of the peptide. The other peaks are not easy to attribute, but the spectrum still constitutes a fingerprint of the peptide. The spectrum of the freeze-dried capsules presents three intense absorption bands at 1645, 1385 and 1090 cm^{-1}. They belong to DMF, the solvent of the dispersed phase, which has not been completely removed during the freeze-drying process. This is also the case for the peaks at 2930 and 2860 cm^{-1}. The broad peak at 3480 cm^{-1} is attributed to the surfactant, which also contribute to DMF peak at 2930 cm^{-1}. However, in the spectra of the capsules, one can clearly identify some peaks of the peptides, with a reduced intensity e.g. at 3075, 1510 and 800 cm^{-1}. One notices also the absence of the intense absorption band due to isocyanate in TDI at 2260 cm^{-1}: TDI has fully reacted.

In conclusion, the IR spectroscopy does not bring decisive information on the characterization of the nanocapsules. This is due to the presence of remaining DMF after freeze-drying in the capsules samples, and also to the presence of several carbonyl groups in the original peptide. However, the reaction of the isocyanate groups of TDI was observed.

For these reasons, IR spectroscopy was not used as routine method to characterize the preparation of the nanocapsules and SEC was preferred to control the success of the polyaddition reactions.

Size and size distribution of the capsules via PCCS

PCCS measurements (see **Table 3**) show a narrow size distribution for both samples, which are centered at 232 nm from capsules obtained from [Mant/2NH$_2$] and 208 nm from [Mant/3NH$_2$], respectively. Interesting is the comparison of these values with those of the sample prepared with exactly the same parameters with only a different peptide [“Y”/2NH$_2$]. The size measured for this sample was 379 nm (see **Figure 38**, sample DMF + LiBr, 0.5 wt.% surfactant, 1.5 TDI equivalents), while the molecular weight of the peptide is comparable: 1024 g·mol^{-1} and 7 amino acids for peptide [Mant/2NH$_2$], 1152 g·mol^{-1} and 8 amino acids for [Mant/3NH$_2$], 906 g·mol^{-1} and 8 amino acids for peptide [“Y”/2NH$_2$]. A significant reduction of the size of the particles is observed for the peptides containing the FRET system Mant/Y(NO$_2$). This could be explained by the nature of the FRET system, bearing polar groups both on the fluorophore and on the quencher. The presence of these polar groups combined with the hydrophobic moieties of the phenylalanine residues could make the peptides surface active, or more surface active than it was without the FRET pair. Thus, the peptide could take a more important role in the stabilization of the droplets and this could explain the smaller size measured for the capsules prepared with FRET pair. This explanation is supported by the fact that the capsules obtained with three polar amine groups (peptide [Mant/3NH$_2$], 208 nm) are slightly smaller than those obtained with [Mant/2NH$_2$] (232 nm), even if the difference is not very significant.

Investigation of the capsules in electron microscopy

The nanocapsules prepared with this generation of peptides containing a FRET system were investigated with scanning and transmission electronic microscopy.

The micrographs presented in **Figure 50** are representative for the samples obtained from peptide [Mant/2NH$_2$] and [Mant/3NH$_2$] (JA46 and JA47). In **Figure 50** (left), within a film-like structure, collapsed capsules can be observed, circled in orange. The formation of the film can be attributed to too short peptide-based polymers (insufficient polymerization or branching). Melting of the capsules because of it thermal properties or the behavior of residual DMF as softener are also conceivable. Observation of these samples under transmission electron microscope was challenging as well. Though the high beam sensitivity, capsules-like structures were observed (**Figure 50**, right). The size of the capsules observed on the micrographs corresponds to the sizes measured in PCCS, with here 306 nm measured on SE micrographs against 208 nm in PCCS. In conclusion, the observations via electron microscopy confirm the formation of capsules like structure also for samples prepared with FRET-containing peptides.

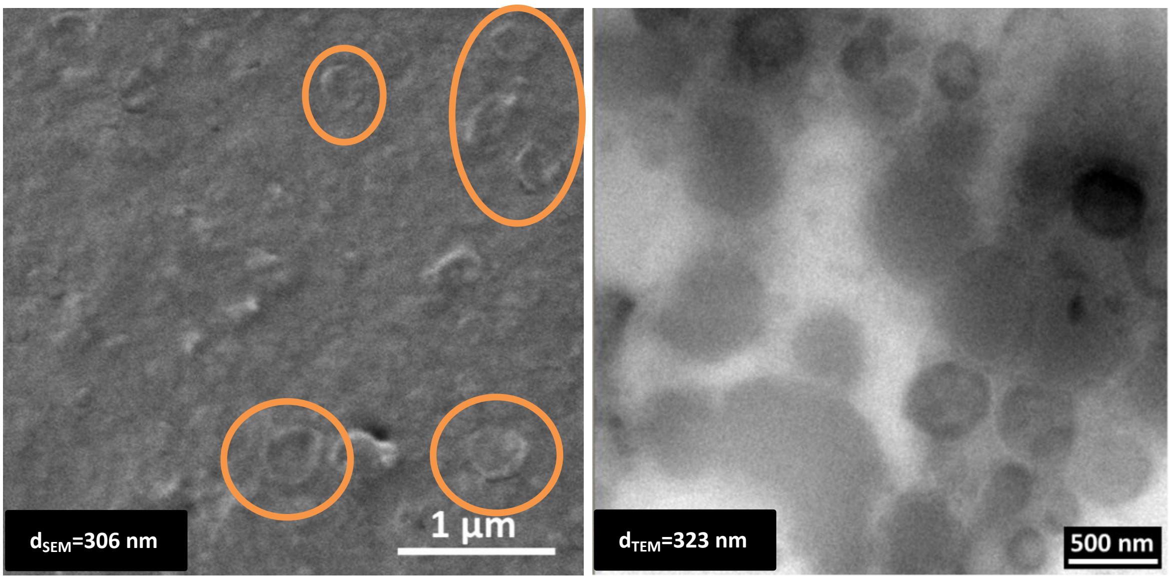

Figure 50: **SE and TE micrographs of nanocapsules prepared with standard parameters (DMF+LiBr, 0.5 wt.% surfactant) from peptide [Mant/3NH$_2$] with 1.5 equivalents of TDI (JA47).**

IV.3.3 Redispersion in water and enzymatic cleavage experiments

Since the process of redispersion was improved, a brief description of the redispersion process is given for each series of different samples. During redispersion in water, the solid content drops from 1.5% to around 1% (dilution by a factor two but addition of SDS surfactant).

Redispersion in water

The original miniemulsions in cyclohexane were redispersed in a double amount (weight) of water containing 0.3 wt.% SDS. Cyclohexane was evaporated overnight at 40 °C under strong agitation. The redispersed systems were then put a few minutes in an ultrasonication bath and stirred before PCCS measurements. The samples were then dialyzed with membranes (M.W.C.O 14 kDa) to reduce the amount of surfactant (SDS and P(B/E-*b*-EO)), eliminate the DMF and remove the free peptide molecules or peptide oligomers not covalently bound to the capsules. After dialysis, the size of the nanocapsules was measured. The enzymatic cleavage was then proceeded as soon as possible to lower the risk of contamination. The ultrasonication bath was used to limit particle aggregation after dialysis. Mild ultrasonication was preferred instead of using a tip, which could degrade the nanocapsules.

Table 3: PCCS size measurements at different stage of redispersion process.

Sample	Peptide used	x_{50} in cyclohexane (nm)	*Comments*	x_{50} in water before dialysis (nm)	*Comments*	x_{50} in water after dialysis (nm)	*Comments*
JA46	[Mant/2NH$_2$]	232$^{(a)}$	Narrow, monomodal	683	Bimodal	497	Bimodal
JA47	[Mant/3NH$_2$]	208$^{(a)}$	Narrow, monomodal	488	Broad, trimodal	489	Broad, bimodal

$^{(a)}$For comparison, with the same synthetic parameters (DMF+LiBr, 0.5 wt% surfactant, 1.5 TDI equivalents) and from peptide ["Y"/2NH$_2$], x_{50} = 379 nm was measured in cyclohexane (**Table 1**).

One can see clearly in **Table 3** that the size of the particles strongly increases after redispersion. A first explanation for this size increase is the swelling of the peptide-based capsules after transfer from cyclohexane into water. However, the measurements with PCCS do not only show a significant size increase, the size distribution becomes broader and multimodal after redispersion into water: there is also a formation of aggregates during the redispersion process. The dialysis of the samples does not seem to generate additional aggregates: the dispersions are stable in water, at least a few days.

Enzymatic cleavage experiments

After, the capsules were redispersed successfully into water. The samples were ready to be treated with enzyme, here with trypsin. The principle of the experiment is shown on **Figure 51**.

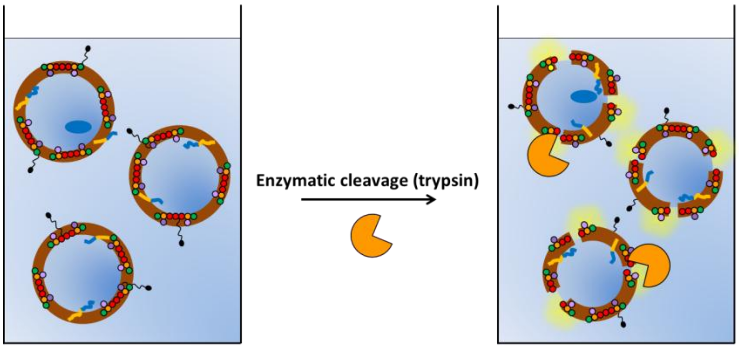

Figure 51: **Schematic representation of the enzymatic cleavage of the peptide-based nanocapsules with fluorescence recovery of the FRET system.**

The cleavage of the peptides sequences of the capsules is monitored through the recovery of fluorescence of the Mant group in the FRET system (λ_{em} = 425 nm). The results of the fluorescence measurements are displayed in **Figure 52**.

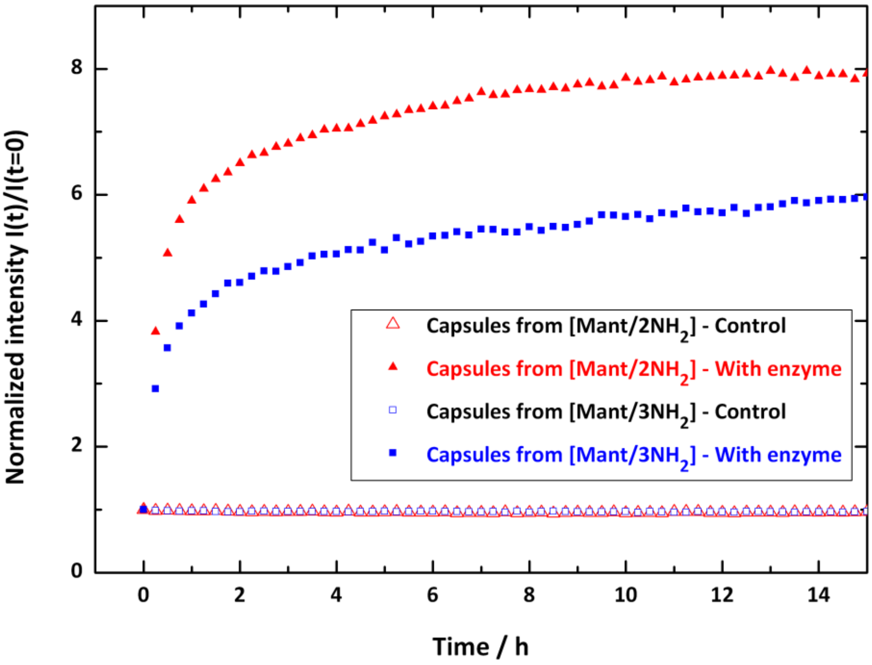

Figure 52: Enzymatic cleavage of peptide-based nanocapsules with time. The theoretical concentrations of peptides incorporated in the capsules were 3.3×10^{-4} M for [Mant/2NH$_2$] and 2.9×10^{-4} M for [Mant/3NH$_2$]. ***Measurements done by N. Kotman.***

One clearly observes that the fluorescence increases strongly, compared to its initial value for the capsules based on both peptides, while it remains unchanged when no enzyme is added to the dispersions. Moreover, the remaining free peptide molecules were removed by dialysis, so no fluorescence increase is due to the cleavage of free peptide in solution in water. This clearly demonstrates that some peptide sequences belonging to the capsules are cleaved, separating fluorescing dye and quencher away from each other and leading to a significant fluorescence increase. The concentrations of the peptides in **Figure 52** were calculated from their apparent molecular weight, taking into account the dilution during redispersion and considering that 10% of the overall peptide had been removed during dialysis (see **Table 6**). It also seems that the speed of the process is changed, as the fluorescence increase last for many hours and is not completely over after 12 h. This is confirmed in **Figure 53**, comparing the fluorescence increases for peptide [Mant/2NH$_2$] and the capsules made of this peptide (JA46). A clear difference of the recovery speed is observed, as the free peptide is degraded much quicker than the peptide-based polymer of the capsules. Two reasons can explain this difference. For steric and conformational reasons, it is easy to assume that the peptide sequences are not cleaved as easily in heterophase as in solution. In addition to this, it is very likely that the progressive degradation of the peptides at the surface of the nanocapsules makes new peptide sequences available for degradation. This could explain the shape of the curves from capsules' degradation: after a first part with an exponential-like increase, the fluorescence increase continues and does not reach a stable maximal value within 14 h.

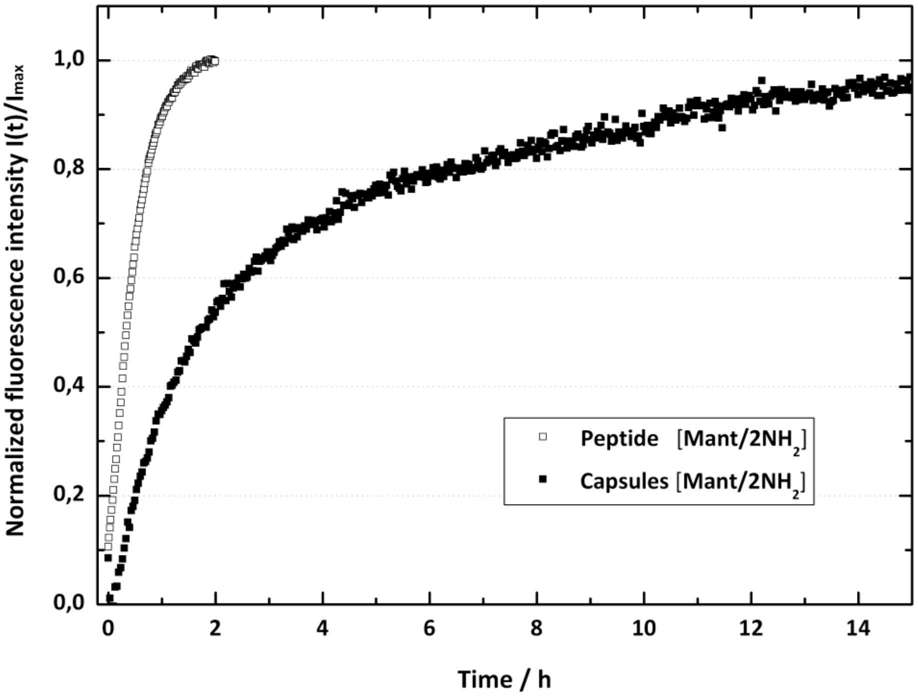

Figure 53: **Comparison of enzymatic cleavage of peptide [Mant/$2NH_2$] in solution and as building block of nanocapsules showing the differences in the cleavage of the peptide over time, between homo- and heterophase.**

V.3.4 Change to a FRET pair Mca/Dnp

The dye/quencher pair lysine(Mant)/3-nitro-tyrosine worked properly and allowed observing and monitoring the cleavage of the peptide sequence in solution and also from the nanocapsules. However, it presents some drawbacks: the secondary amine on the Mant group is liable to react with other molecules[10]. First of all, during SPPS, it can react with the activated amino acid added afterwards, creating a branching point and leading to undesired products. The Mant amino acid should thus be placed in the *N*-terminus. This is not satisfying for the introduction of other amino acids during SPPS between the *N*-terminus and the FRET pair. For example, it forces the addition of a lysine residue inside the FRET pair in the case of [Mant/$3NH_2$]. One consequence is that a strict quantitative comparison of the cleavage experiments between peptides [Mant/2NH$_2$] and [Mant/3NH$_2$] is not possible. Moreover, during the interfacial polyaddition reaction in miniemulsion, the secondary amine of the Mant group can also react with TDI. In addition to the change of the chemical structure, these reactions may degrade the fluorescing properties of the dye and interfere with the fluorescence measurements during the enzymatic cleavage. These drawbacks are the reasons responsible of the change to the Mca fluorophore.

As a result, a new dye/quencher pair was chosen: 7-methoxy-coumarin (Mca) and the corresponding quencher 2,4-dinitrophenyl (Dnp), both attached to the side-chain of lysine. This pair is a common and well-established FRET system[190], commercially available, but more expensive than the previous one. Besides, Mca group has a slightly higher absorption maximum (340 nm) than Mant (315 nm), making it easier to detect (e.g. less noise in UV detection). Nonetheless, the emitting wavelength remains at the border between UV and visible light (405 nm), even lower than for Mant (425 nm), which does not open more possibilities for optical microscopy characterization, as the confocal or STED microscope available are usually not equipped with UV lasers.

It was decided to go further with branching or cross-linking of the polymer, as the ultimate goal is the encapsulation of small molecules, which are more prone to diffuse out of the capsules if the walls are less dense. The two peptides prepared carry here three – in the case of peptide [Mca/3NH$_2$] – and seven – in the case of peptide [Mca/7NH$_2$] – amine functions, as displayed in their structure respectively on **Figure 43** and **Figure 44**. This should increase the branching of the polymer, which could have an effect on the encapsulation of a dye and its release.

Size and size distribution via PCCS

The dispersions prepared from [Mca/3NH$_2$] and [Mca/7NH$_2$] were characterized by PCCS; the results can be found in **Table 4**. After the reaction with TDI and before redispersion, monodispersed suspensions with narrow size distributions were obtained in all cases. One observes a further size reduction of the particles compared to those mentioned previously in **Table 3**: for two comparable experiments with the same parameters and peptides differing only from the nature of the FRET system, x_{50} decreases from 208 nm with Mant/Tyr(NO$_2$) as FRET pair to 154 nm with Mca/Dnp. It seems that the peptide prepared with the new FRET pair (Mca/Dnp) is more interfacially active and play a further role of stabilizer of the droplets. This is due to the structure of the new FRET pair, e.g. with the presence of two polar nitroxy group on the quencher.

Verified polymerization via SEC

The freeze dried dispersions were analyzed by SEC, (detection at $\lambda = 325$ nm), which allows an exclusive detection of the peptide-based products (exclusive absorption of the Mca/Dnp FRET pair) and ensures that no signal due to surfactant or solvent superimposes. A standard sample of each peptide with 2 equivalents of TDI was analyzed. The overlay of the elugrams of both polymers with their respective peptide references are plotted in **Figure 54**.

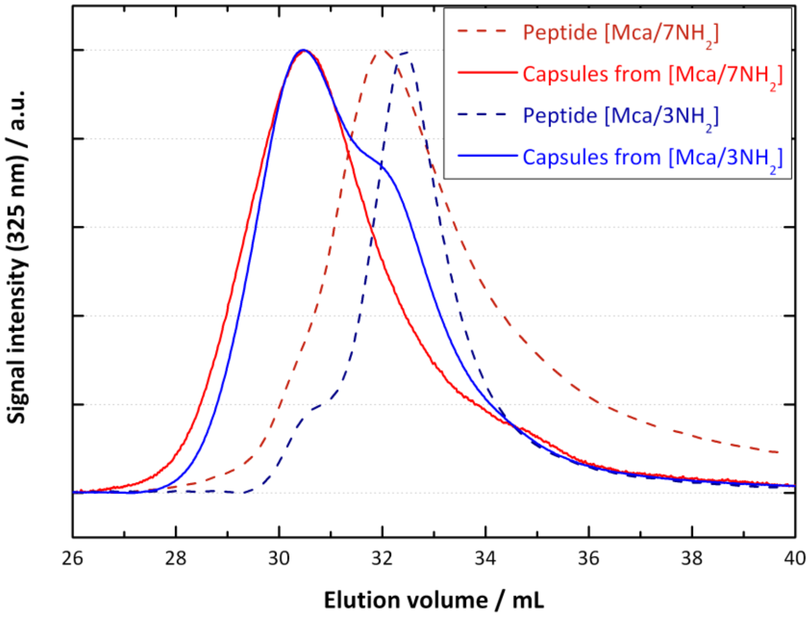

Figure 54: **SEC chromatograms overlay of peptide [Mca/3NH$_2$], [Mca/7NH$_2$] and their respective polymer after miniemulsion polyaddition with 2 equivalents of TDI.**

Several features can be seen in this diagram. First of all, a long adsorption tail is following the peak, especially in the case of peptide [Mca/7NH$_2$], which can be attributed to the presence of amine group favoring adsorption of the peptide on the stationary phase. Despite this drawback, the analysis shows that the peptide with more lysine residues (larger size) elutes slightly faster. This is in accordance with the SEC theory. A second result observed on this graph is that a significant shift toward higher molecular weights is visible between the peptide and the molecules extracted from the dispersions. Thus, the polyaddition proceeded with peptide [Mca/3NH$_2$] and peptide [Mca/7NH$_2$], but a shoulder of probably unreacted peptide can still be observed in the chromatogram of the sample with less amine groups. Surprisingly, the macromolecules obtained from peptide [Mca/7NH$_2$] are not significantly larger than those obtained from [Mca/3NH$_2$], at least according to their hydrodynamic radius. It is still possible that polymer with a denser branching have been prepared in the case of peptide [Mca/7NH$_2$]. To sum-up, even if SEC shows its limitation in the characterization of peptide based polymer, it clearly shows the success of peptide polyaddition reaction in miniemulsion.

Influence of TDI equivalents amount

The influence of the amount of TDI equivalents on the size of the peptide based polymer chain was studied with peptide [Mca/7NH$_2$]. The results are presented in **Figure 55**.

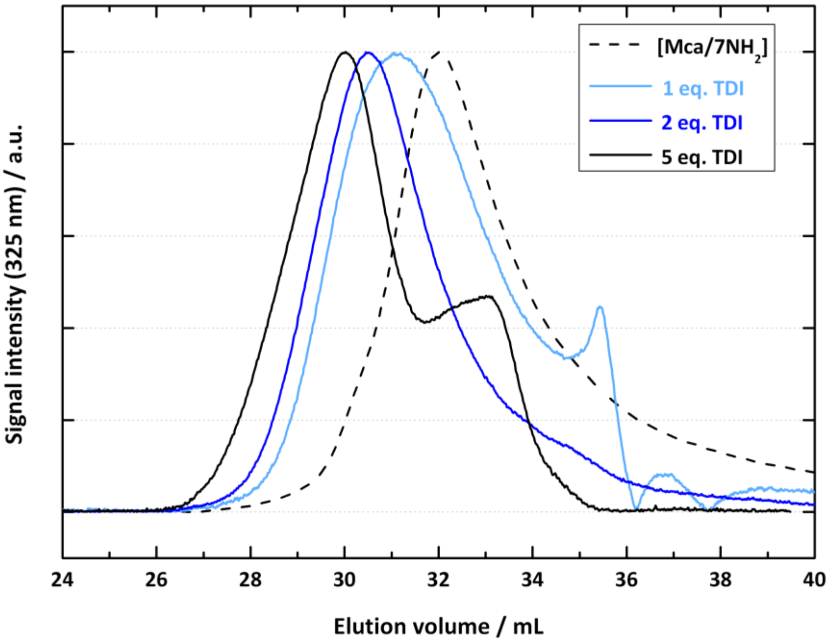

Figure 55: **Overlay of the SEC chromatograms of [Mca/7NH$_2$] and of the polymer obtained by interfacial polyaddition in miniemulsion with various amounts of TDI.**

One can clearly observes a progressive decrease of the elution volume, i.e. an increase of molecular weight with increasing TDI equivalents amount. Even if this result is expected, it demonstrates that an excess of TDI is necessary to reach higher molecular weights for the peptide-based polymer formed by interfacial polyaddition in miniemulsion. TDI probably reacts with other molecules like traces of water in DMF (see paragraph II.6.2) in addition to the reaction with the low amount of hydroxyl group from the surfactant. It also shows that the amount of TDI equivalents is a key parameter determining the length of polymer chains and could therefore be an important parameter for the encapsulation efficiency or payload release.

The amounts of TDI equivalents can not only have an influence on the sizes of the polymer chains, but also on the size of the particles. The sizes of the capsules measured with PCCS for different amounts of TDI are summarized in **Table 4**.

Table 4: Influence of peptide functionality and TDI equivalent number on the size of the nanoparticles obtained after interfacial polyaddition.

Sample name	Peptide	TDI equivalent	x_{50} in cyclohexane (nm)
JA60	[Mca/3NH$_2$]	1.5	153*
JA79	[Mca/7NH$_2$]	2	155*
JA86	[Mca/7NH$_2$]	1	162*
JA84	[Mca/7NH$_2$]	5	288*

*All samples had a monomodal and narrow size distribution

The results presented in **Table 4** show that neither the amount of amine groups on the peptide nor the amount of TDI equivalents have a significant influence on the size of the nanocapsules prepared by interfacial polyaddition in miniemulsion. All dispersions measured by PCCS exhibit small particle sizes (additional stabilizing effect of the peptide) and narrow size distributions. However, a large excess of TDI (5 equivalents) leads to significantly larger capsules (288 nm). It can be assumed that in this case, a too large amount of amino groups react first with TDI and some addition reactions between different capsules start proceeding, causing aggregations.

Investigation of the structure by electron microscopy

These samples were also characterized with SEM (**Figure 56)** and TEM (**Figure 57**). A clear difference with the former samples is observed. On the micrographs, the nano-objects generated with peptide [Mca/3NH$_2$] and [Mca/7NH$_2$] are looking much more like particles rather than capsules. They also have a smaller size than those measured by PCCS (see **Table 4**).

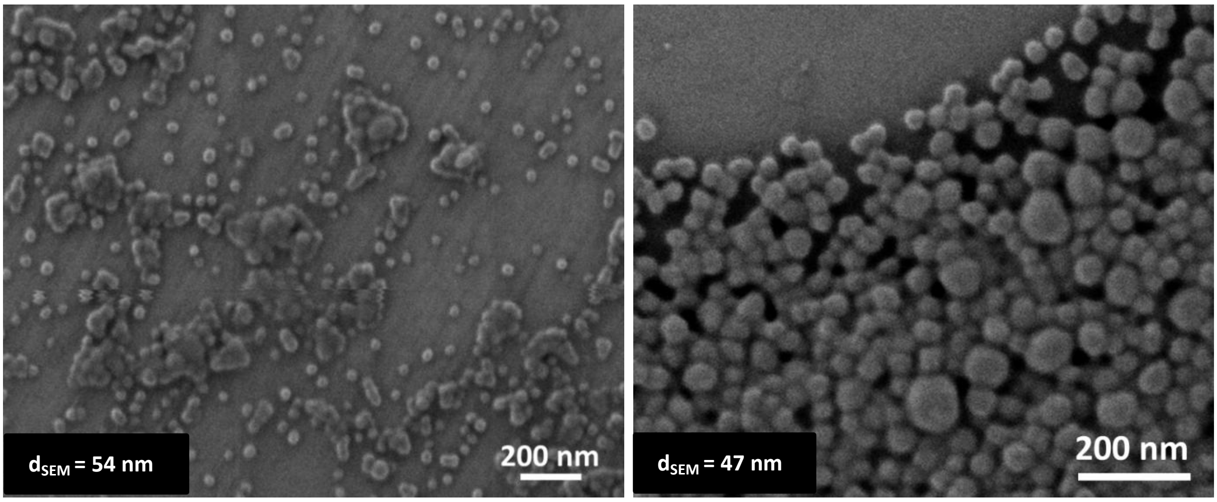

Figure 56: **SE micrographs of nanoparticles prepared with standard parameters (DMF+LiBr, 0.5 wt.% surfactant) from peptide [Mca/7NH$_2$] with 2 equivalents TDI (left, JA79) and 5 equivalents TDI (right, JA84).**

PCCS measurements in cyclohexane revealed that these particles made of [Mca/7NH$_2$] have a comparable size as the ones produced from peptide [Mant/2NH$_2$] and [Mant/3NH$_2$] (155 nm against 232 and 208 nm). However, they appear significantly smaller on the electron micrographs. While the size measured on the micrographs with the peptides containing Mant/Y(NO$_2$) group was similar to those measured with PCCS, the size of the particles measured on the micrograph (around 50 nm) is much smaller than those measured by PCCS. The differences observed can be explained as following: the change of the fluorophore/quencher pair leads to a more polar peptide. The hybrid polymer formed at the interface remains soluble in DMF, and can diffuse inside the droplets. As a result, swollen particles (with around 10% polymer solid content) are obtained. In this case with PCCS, the measurement is done with swollen particles. The size measured is actually the size of the droplets containing the peptide-base polymer. The particles observed on the micrographs correspond to the dry state of these particles, with low solid content. The evaporation of the DMF results in the shrinkage of the particles. The observations stated with SEM are confirmed by the size of particles measured on TE micrographs (**Figure 57**, average size 46 nm).

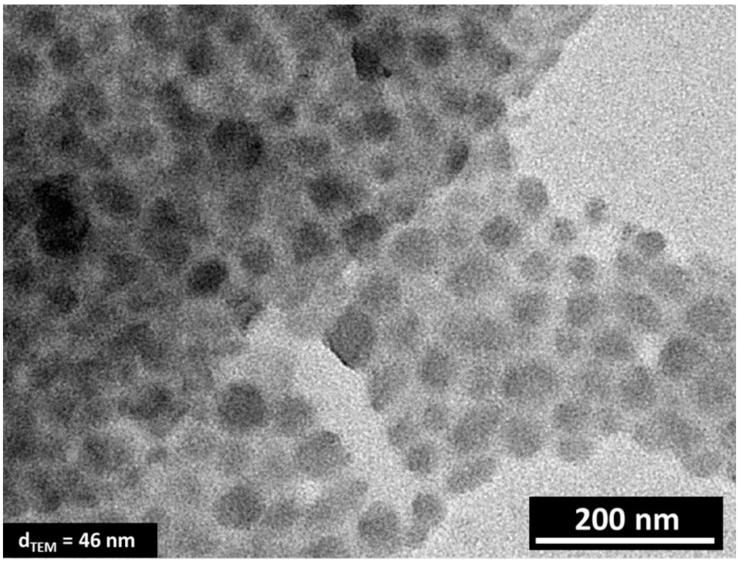

Figure 57: **TE micrograph of nanoparticles prepared with standard parameters (DMF+LiBr, 0.5 wt.% surfactant), and 1.5 equivalents of TDI from peptide [Mca/3NH$_2$] (sample JA60).**

IV.3.5. Redispersion in water and enzymatic cleavage experiments

Redispersion in water – Quantification of free peptide

In the following paragraph, the expression "free peptide" represents a peptide molecule or oligomers not covalently bound to a polymeric chain constituting the particles.

The redispersion in water was processed as described before. It appears that the determination of the peptide amount is challenging: in UV absorption analysis, the values recorded are affected by scattering of the capsules. It is not a satisfying method to quantify some species like the peptide in this case, especially at such a low wavelength of 325 nm, which is close to the size of the particles. This time, during dialysis, the dialysate is kept and analyzed with fluorescence spectroscopy (the concentration is too low for UV absorption). Indeed, even if the fluorescence is quenched, there is still a fluorescent signal detected, proportional to the peptide concentration. For the standard sample from peptide [Mca/3NH_2] and 2 TDI equivalents, the concentration of "free peptide" was found to be 10% of the total amount of peptide in the first dialysis water (see **Table 6**). This method clearly presents some drawbacks: one has to assume that no cleavage of the peptide occurred, which would consequently increase the fluorescence and overestimate the concentration of "free peptide". On the other hand, this method allows the detection of "free oligomers", not covalently bound to the capsules, which are removed during the dialysis.

Fluorescence microscopy

Another method to characterize the nanocapsules after dialysis is fluorescence microscopy. As the capsules are made of a peptide containing a FRET system, they already contain a fluorescing group (Mca, λ_{em} = 405 nm). Indeed, the quenching of the fluorophore in the FRET group lowers the intensity of fluorescence, but it remains detectable, as shown in **Figure 58**. Important is the fact that the fluorescing peptide sequences are localized at some precise defined locations and are not homogeneously distributed: they are gathered in nanostructures. This confirms that the degradation detected later is due to the cleavage of peptide sequences belonging to the nanocapsules. The use of fluorescence microscopy does not allow a precise size interpretation of the structures, but the presence of fluorescing dots with various sizes is obvious. It confirms the size increase detected with PCCS after redispersion in water, presumably due to the formation of aggregates.

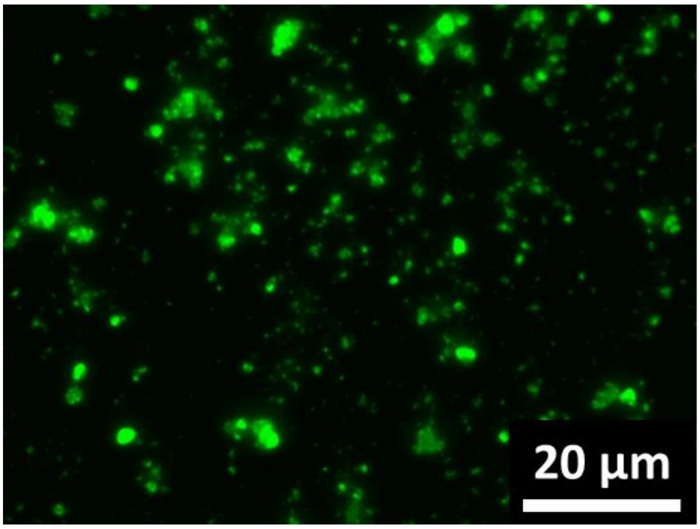

Figure 58: Fluorescence micrograph of dialyzed nanocapsules prepared with standard parameters (DMF+LiBr, 0.5 wt.% surfactant) and 2 equivalents TDI from peptide [Mca/7NH$_2$].

Enzymatic cleavage of nanocapsules made from peptides with the Mca/Dnp FRET pair

The nanocapsules prepared from peptides with the Mca-based FRET system were treated with trypsin for enzymatic cleavage. The results are displayed in **Figure 59**, for both peptides [Mca/3NH$_2$] and [Mca/7NH$_2$].

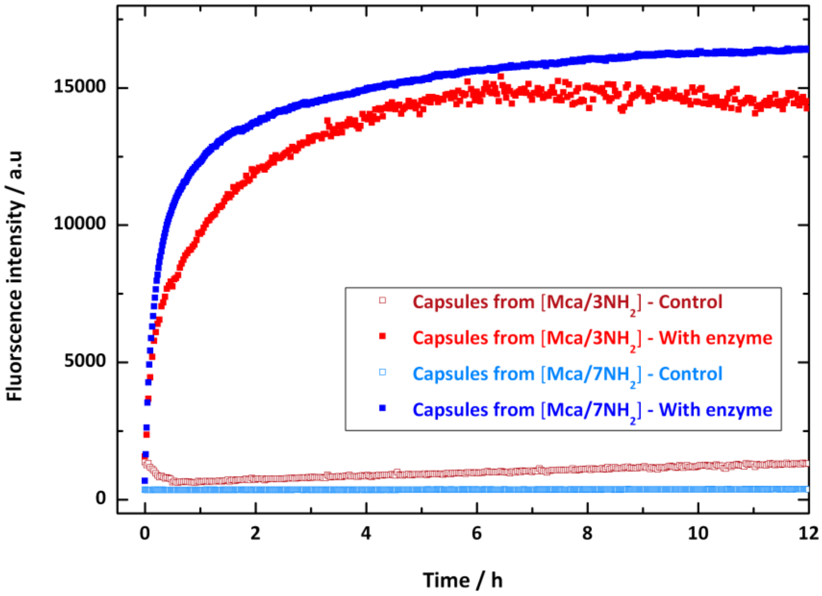

Figure 59: Enzymatic degradation with time of nanocapsules made from peptide [Mca/3NH$_2$] and [Mca/7NH$_2$]. ***Measurements done by N. Kotman.***

The increase of the Mca fluorescence intensity is indisputable and in the same time and amplitude range for both peptides. Although the comparison in terms of amplitude is not strictly possible, it is stressed out that the expected fluorescence increase is not the same as the concentrations of peptide are different (same solid content during preparation but the peptides have different molecular weights). It is interesting to observe that the sample with more branching amine groups in the peptide takes more time to reach its maximum value. Even if it not a decisive parameter, the branching of the peptides in the polymer plays a role in the degradation speed of the capsules by the enzyme.

IV.3.6 On the solubility of the polymer and phase separation

The morphology of the structures prepared with peptides bearing a FRET pair was described as particle-like. This could be due to the increasing solubility of the polymer formed at the DMF/cyclohexane interface in DMF, a consequence of the more polar peptide used, due to the presence of additional lysine residues and possibly of the new FRET system. The peptide is more polar, but still not soluble in H_2O at the concentrations used for the dispersed phase. It would mean that by increasing the polarity of the dispersed phase, one could cause the interfacial precipitation of the peptide based polymer and obtain capsules with a liquid core. Some experiments were done with DMSO and water as more polar solvents. It appears that the use of a dispersed phase constituted of 50% H_2O and 50% DMSO w/w yields a stable miniemulsion. After the addition of 2 equivalents of TDI, a dispersion stable for a few days was obtained and the particles size was measured as x_{50} = 1050 nm (monomodal and narrow distribution). The analyses of these dispersions via SEM and TEM (in **Figure 60** and **Figure 61** respectively) show structures completely different than the particles obtained before.

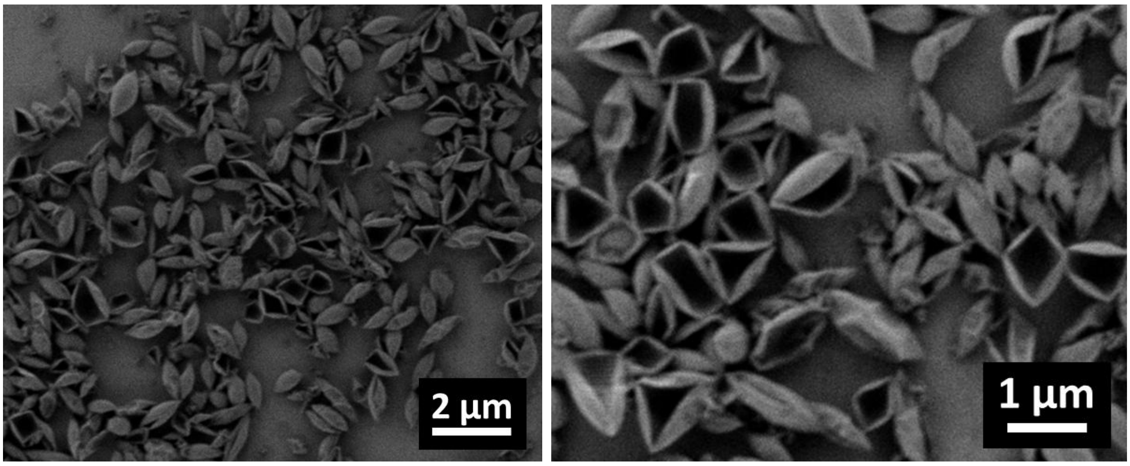

Figure 60: **SE micrographs of nanocapsules prepared from peptide [Mca/7NH$_2$] with 5 g·L^{-1} LiBr DMF/H_2O 50/50 w/w as dispersed phase and 2 equivalents TDI (JA90).**

A closer look at the micrographs confirms the observation of collapsed, wrapped, and/or opened solid capsules with a distinct rigid shell remaining after evaporation of the core. Particularly in TEM, the shell is distinguished and no doubt is left that the samples are peptide-based hybrid shells with liquid core.

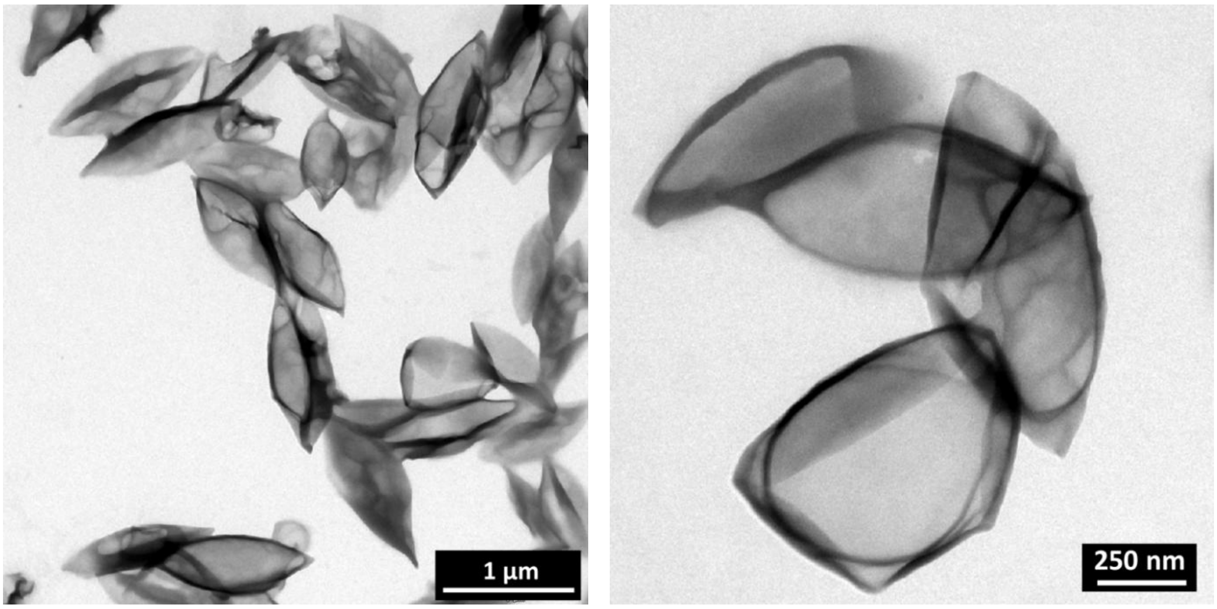

Figure 61: TE micrographs of nanocapsules prepared from peptide [Mca/7NH$_2$] with 5g·L^{-1} LiBr DMF/H$_2$O 50/50 w/w as dispersed phase and 2 equivalents TDI (JA90).

The possible role played by water reacting with TDI was not investigated here. This sample was not stable enough to be redispersed into water and submitted to enzymatic cleavage. Other samples were prepared with pure DMSO (JA69), pure water (JA70) and their mix together (JA82) as solvent for the dispersed phase. When no synthetic problems, like peptide solubility or gelification of the dispersed phase, were encountered, the emulsions were not stable. However, it has been demonstrated here that tuning the nature of the dispersed phase can greatly influence the morphology, to be obtained in a desired manner.

IV.4 Synthesis, characterization, and cleavage of peptide based hybrid nanocapsules loaded with fluorescing polymer

After hybrid nanocapsules have successfully been prepared and cleaved, the next step is the encapsulation of a fluorescent dye in such structures, as the aim of the project is the enzymatically triggered release of encapsulated substances. However, to be certain that an encapsulation without leaks was achieved, despite the large mesh-size of the polymer network in the capsules (corresponding to the length of the peptide), the first encapsulation experiments were conducted with a fluorescent water-soluble polymer. The synthesis via radical polymerization of poly(vinylpyrrolidone-*co*-Bodipy) is described in paragraph VI.1.3. It is reminded that polyvinylpyrrolidone was chosen as water-soluble polymer by reason of its chemical inertness to TDI. The fluorescence of the polymer (M_n = 18800 g·mol^{-1}, PDI = 6.5) is ensured by the presence of 0.5 wt.% Bodipy-methacrylate monomer in the polymer chain (see structure in **Figure 86**).

IV.4.1 Synthesis of the capsules and possible influence of encapsulated polymer on the capsules

The experimental protocol to prepare the capsules was exactly the same as previously, with the only exception that the fluorescing polymer was dissolved in the dispersed phase with the peptide. The list of the samples can be found in **Table 5**.

Influence of entrapped polymer on the interfacial polyaddition

The fluorescing polymer has been chosen in such a manner, that it does not react with TDI. However, the polymer could have an effect on the polyaddition reaction at the interface, e.g. its presence should increase the viscosity of the dispersed phase, lower the diffusion of the peptide to the interface and thus slow down the interfacial reaction. For this reason, it is sensible to compare the SEC chromatograms of dissolved capsules with and without polymer. Two overlays are presented in **Figure 62**, presenting the chromatograms of the polymers obtained from peptide [Mca/3NH$_2$] and [Mca/7NH$_2$], with and without the presence of fluorescent polymer in the dispersed phase.

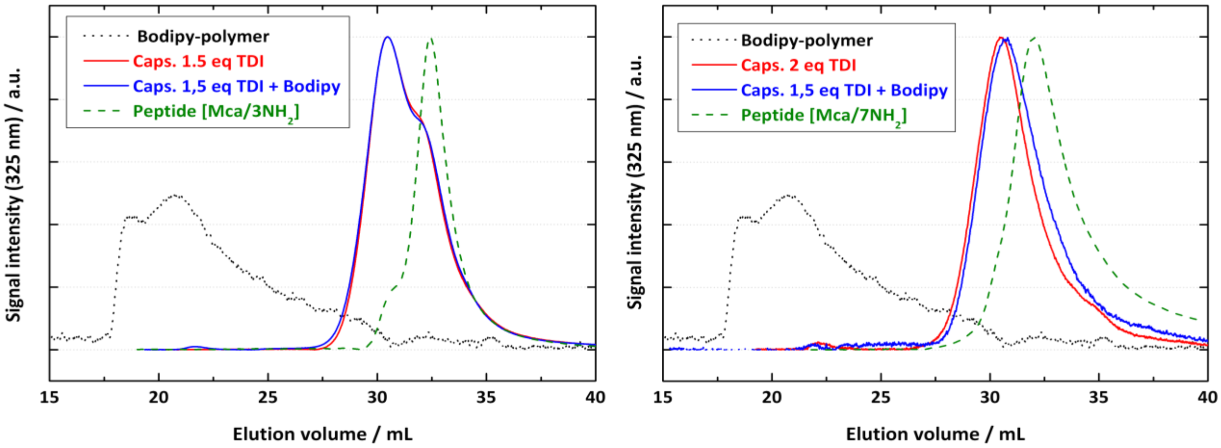

Figure 62: **SEC chromatograms overlay of peptide-based polymers obtained from peptide [Mca/3NH$_2$] (left) and [Mca/7NH$_2$] (right) with and without encapsulation from P(VP-*co*-Bodipy).**

In the two diagrams, the elugram of the peptide is traced as reference. One observes that for both peptides, the polyaddition reaction proceeded well in the presence of polymer. The chromatograms of the samples with and without entrapped polymer are very similar: they overlap almost exactly for both polymers obtained from peptides [Mca/3NH$_2$] and [Mca/7NH$_2$]. One recognizes the shoulder corresponding to the unreacted peptide in the case of peptide [Mca/3NH$_2$]. The elugrams of the encapsulated polymer is also displayed, to demonstrate that the polymer does not contribute to the peaks analyzed as peptide signals. It also shows that the fluorescing polymer (or more exactly its Bodipy units) is too low concentrated in the capsules, to be detected by UV-absorbance at 325 nm.

Influence of entrapped polymer on the size of the capsules

The sizes of the samples prepared with the same parameters with the exception of the presence/absence of poly(*N*-vinylpyrrolidone-*co*-Bodipy-methacrylate) abbreviated P(VP-*co*-Bodipy) are presented in **Table 5**.

Table 5: Influence of the encapsulation of P(VP-*co*-Bodipy) on the size of the nanocapsules for several synthetic parameters.

Sample names	Peptide (NH2)	TDI equivalents	x_{50} in cyclohexane *without* P(VP-*co*-Bodipy) (nm)	x_{50} in cyclohexane *with* P(VP-*co*-Bodipy) (nm)
JA60-61	[Mca/3NH$_2$]	1,5	153	230
JA86-87	[Mca/3NH$_2$]	1	162	386
JA79-68	[Mca/3NH$_2$]	2-1,5	155	214
JA84-83	[Mca/3NH$_2$]	5	288	230

One can observe, that in almost every case, the presence of P(VP-*co*-Bodipy) increases the size of the capsules or particles. It was shown in the previous paragraph, that the presence of the fluorescent polymer had not effect on the polyaddition reaction with the peptide. However, the addition of polymer in the dispersed phase certainly increases its viscosity in addition to the solid content. With a similar shear-stress applied during ultrasonication, it is expected that the size of the droplets slightly increases for a more viscous dispersed phase. Consequently, bigger capsules are obtained after polyaddition.

IV.4.2 Investigation with electron microscopy

Series of samples from peptide [Mca/3NH$_2$] and [Mca/7NH$_2$] with entrapped polymers was also investigated with electron microscopy. Some representative micrographs are presented in **Figure 63** (SEM) and **Figure 64** (TEM).

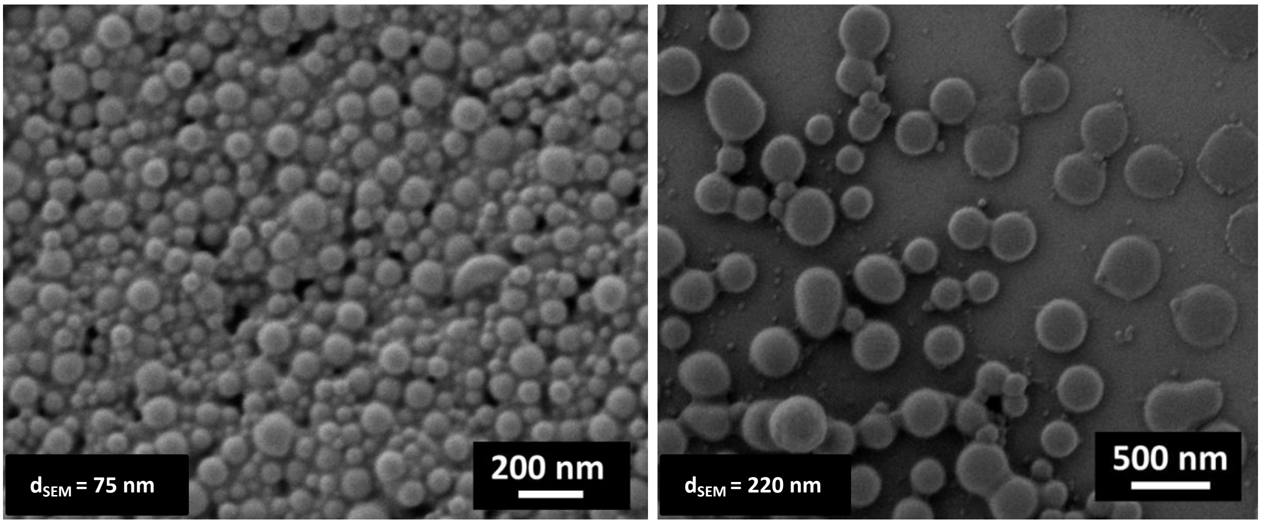

Figure 63: SE micrographs of nanocapsules prepared with standard parameters (DMF+LiBr, 0.5 wt.% surfactant) from peptide [Mca/7NH$_2$] with respectively 1.5 (left) and 5 (right) TDI equivalents.

The structures observed are actually comparable to the ones obtained without any encapsulated material. Obviously, homogeneous particles are present rather than core-shell capsules, attesting that the addition of polymer did not lead to phase separation. This is not surprising, as the P(VP-co-Bodipy) is very soluble in DMF, the solvent of the dispersed phase. On the micrographs, the particles also appear bigger than those obtained without polymer payload, which supports the explanation proposed in the previous paragraph: the particles actually have a higher solids content, due to the presence in significant quantities of the entrapped polymer (20 mg for 50 mg peptide) and are bigger after evaporation of the solvent.

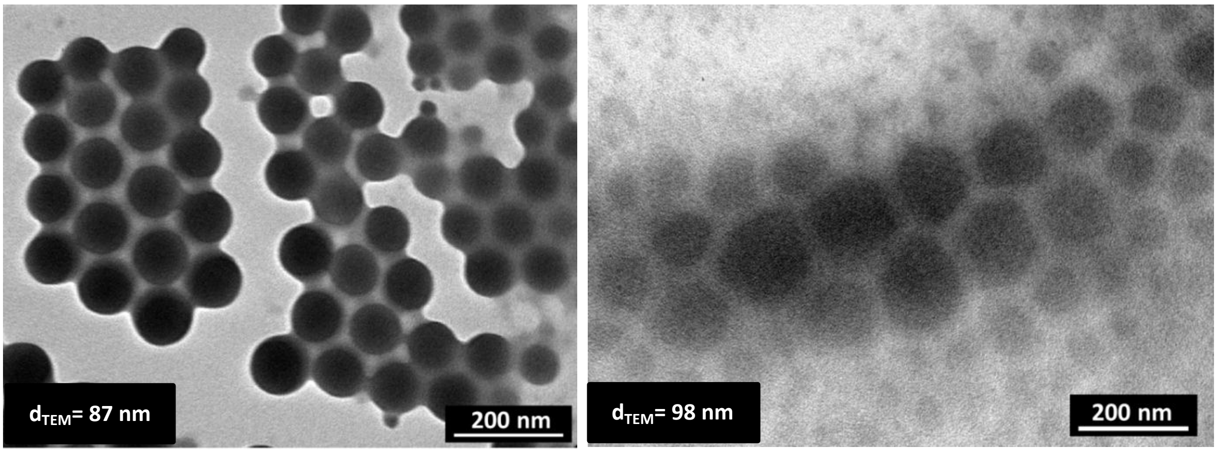

Figure 64: **TE micrographs of nanocapsules prepared from [Mca/7NH$_2$] with 1.5 TDI equivalents (left, JA68) and [Mca/3NH$_2$] with 2 TDI equivalents (right, JA75).**

IV.4.3. Redispersion into water and preconditioning

Quantification of free peptide

All the redispersed samples were prepared as described previously, but the dialysis was carried out differently for some samples (**Table 6**). Some of them were divided in two equal parts after redispersion, and dialyzed with membranes of different pore sizes: the standard cut-off of 14 kDa and another membrane with a cut-off of 100 kDa. This experiment aims to determine, if some long peptide-based polymer chains are too big to be washed during dialysis with standard membranes. In this case, they would be cleaved afterward in solution even if they do not belong to the capsules, which would be misleading.

Table 6: Amount of free peptide* dialyzed out depending on molecular weight cut-off of the membrane.

Sample names	Peptide	Diisocyanate equivalent	Free peptide dialyzed 14kDa (%)	Free peptide dialyzed 100 kDa (%)
JA68	[Mca/3NH$_2$]	1.5	11	15
JA72	[Mca/3NH$_2$]	2	8	6

* The concentration of free peptide was determined by fluorescence measurement in the dialysate with a calibration curve of free quenched peptide, assuming that no peptide was degraded prior to fluorescence measurements.

One observes that the incorporation efficiency, more exactly the amount of peptide dialyzed, is not drastically changed by the cut-off of the membrane. It means that there is no significant amount of very long free peptide chain likely to be cleaved outside of the capsules. This experiment rather highlights the imprecision of such an analytical process: for sample JA72, it is not clear why find less peptide dialyzed out with a 100 kDa M.W.C.O membrane than with a 14 kDa membrane.

Determination of polymer encapsulation efficiency

A selective detection of the P(VP-*co*-Bodipy) is also possible in the dialysate via fluorescence measurements at 530 nm. However, due to the low dye content of the polymer and the small amount of polymer entrapped per sample, the calibration curve shows that, without further concentration of the dialysate, it would only be possible to detect up to 3% of released polymer. Interestingly, no significant signal was detected at the emitting wavelength of Bodipy. This means that the encapsulation efficiency of the fluorescing water soluble polymer is higher than 97%.

Fluorescence microscopy of hybrid capsules with encapsulated polymer

To confirm the encapsulation of the polymer inside the capsules, the miniemulsions were investigated with fluorescence microscopy after redispersion with the two excitation wavelengths corresponding to the Mca (405 nm, belonging to peptides chains, constituting the capsules) and Bodipy (530 nm, encapsulated polymer) fluorescences.

In **Figure 65**, the micrographs show that the Mca groups and the Bodipy are both well localized inside the nanoparticles and not free in solution. The superposition of the two micrographs shows a perfect overlapping, proving that the fluorescing polymer is located only in the capsules.

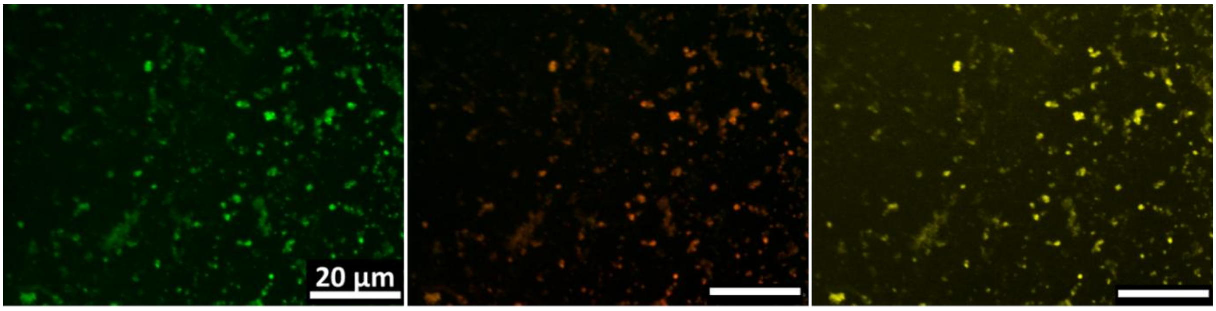

Figure 65: **Micrographs obtained by fluorescence microscopy of peptide-based nanocapsules with encapsulated P(VP-*co*-Bodipy). Peptide fluorescence (Mca, λ = 405 nm) is colored in green (left), Bodipy fluorescence in orange (center, λ = 530 nm) and superimposition of both pictures (right).**

IV.4.4. Cleavage of nanocapsules with encapsulated fluorescent polymer

The enzymatic degradation was investigated with the peptide-based nanocapsules with a fluorescing payload (see **Figure 66**). The fluorescence increase is clearly observed. One observes almost no differences in the shape of the curves, when comparing the capsules with or without a payload (see **Figure 59**): the presence of the entrapped fluorescent polymer has no influence on the degradation of the peptide-based capsules. Both curves have the shape already described previously: they start with an exponential increase and continue with a slightly positive slope without reaching a plateau within 12 h, as if some new peptide sequence were progressively accessible.

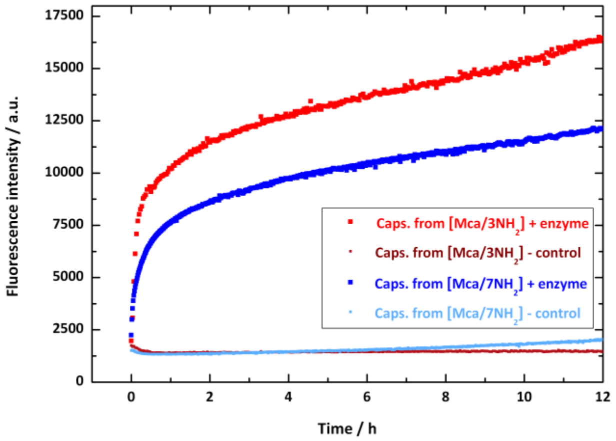

Figure 66: **Enzymatic degradation with time of peptide-based nanocapsules with a fluorescing polymer payload P(VP-*co*-Bodipy).** ***Measurements done by N. Kotman.***

No variation of the signal intensity was observed at the wavelength corresponding to the fluorescence of Bodipy. As the concentration of Bodipy is relatively low, we do not expect self-quenching effects due to high concentration. After the enzymatic degradation and centrifugation, one clearly observes a precipitate, corresponding to the nanocapsules which are not solubilized upon enzymatic cleavage. An explanation for this could be the formation of hydrogen bonds between the lactam units of the poly(vinylpyrrolidone) and the peptides. Besides, the capsules are not fully degraded and the precipitate still contains almost the entire amount of the dye-polymer, as no fluorescence of Bodipy was detected in the supernatant after centrifugation. This supports the idea that the particles are not fully degraded within the first hours: the suspension observed at the end of cleavage experiment still contains particles, as no water-soluble polymer is released.

Conclusion

In this part, it was shown that the preparation of enzymatically cleavable peptide-based nanoparticles allows the encapsulation of dye-labeled polymer in a very efficient way. This macro-dye is not released upon cleavage of the peptide sequence, but this will be the goal of the next part. Here, the encapsulation of such a polymeric dye can be of interest in many cases. It can serve as an internal reference for the determination of the capsule concentration in system where dilution occurs e.g. *in vivo*, to normalize the evolving signal of the FRET system. Secondly, in the case where the cleavage of the peptide is certain and therefore the FRET detection not necessary, it can be used as practical fluorescent marker.

IV.5 Synthesis, characterization, and cleavage of peptide based hybrid nanocapsules with release of fluorophore

IV.5.1 Synthesis of the capsules – Size and morphology

This part deals with the encapsulation of small fluorescing molecules, the sulforhodamine 101 (SR-101, M = 606 g·mol^{-1}), into the peptide-based nanocapsules. The light emission of the dye is not pH sensitive and has very convenient wavelengths for a specific detection in the nanocapsules system (λ_{ex} = 580 nm, λ_{em} = 605 nm). This dye was encapsulated in nanostructures based on peptide [Mca/3NH$_2$] and [Mca/7NH$_2$]. The SR-101 was simply dissolved in the dispersed phase containing the peptide prior to agitation.

A series of capsules with encapsulated sulforhodamine was prepared. The list of the samples is given in **Table 7**, as well as the size of the capsules measured by PCCS.

Table 7: Summary of size distribution of samples prepared with encapsulated SR-101.

Sample names	Peptide (NH$_2$)	TDI (equivalents)	x_{50} in cyclohexane (nm)
JA80	[Mca/7NH$_2$]	2	158
JA93	[Mca/3NH$_2$]	1	140
JA94	[Mca/7NH$_2$]	2	155
JA95	[Mca/7NH$_2$]	1	164
JA96	[Mca/7NH$_2$]	5	145

A comparison with **Table 5** shows that the encapsulation of SR-101 does not influence the size of the capsules compared to the samples without any payload. The data also demonstrate that neither the amount of TDI nor the number of reactive amino groups have a significant influence on the size of the capsules. This confirms the results reported previously. Micrographs obtained with SEM and TEM are presented in **Figure 67** and **Figure 68** respectively.

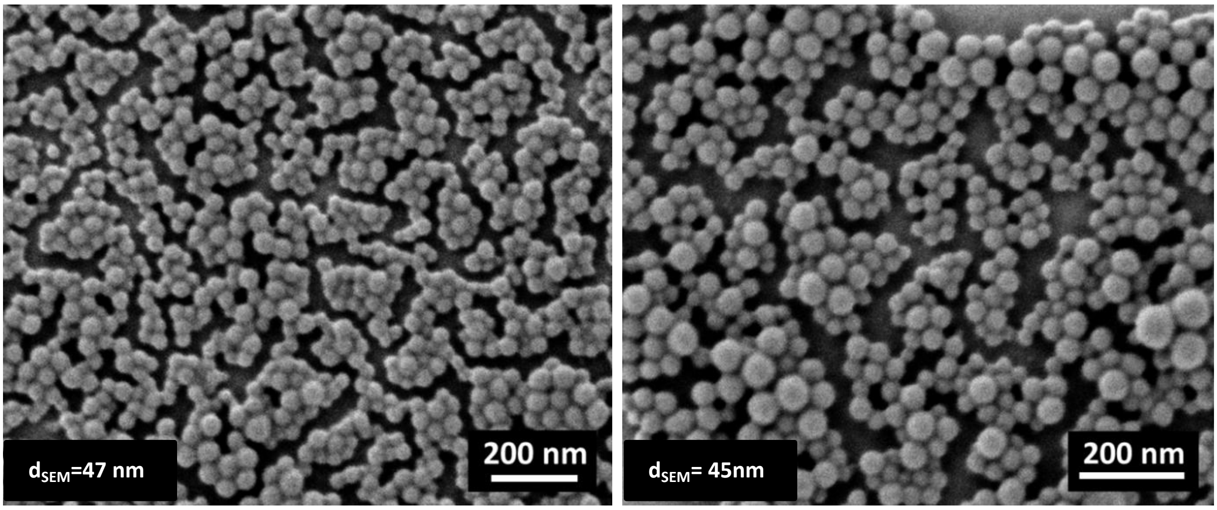

Figure 67: **SE micrographs of nanocapsules with encapsulated sulforhodamineSR-101 prepared with standards parameters (DMF+LiBr, 0.5 wt.% surfactant) from peptide [Mca/7NH$_2$] with respectively 2 (left, JA94) and 5 (right, JA96) TDI equivalents.**

In the case of dispersions prepared from the Mca-based FRET pair with encapsulated dye SR-101, particle-like structures are observed in scanning electron microscopy. This was already the case for the capsules prepared from the same peptide without payload (**Figure 56**). Average sizes in the range of 50 nm are obtained by measuring the particles on the electrons micrographs. This is comparable to the size measured without encapsulated sulforhodamine and confirms that the dispersions prepared with the peptide bearing the Mca/Dnp FRET pair correspond to swollen nanoparticles and not to nanocapsules containing a polymeric shell with a liquid core. This analysis of the structure and the size is confirmed by the transmission electron micrographs (**Figure 68**).

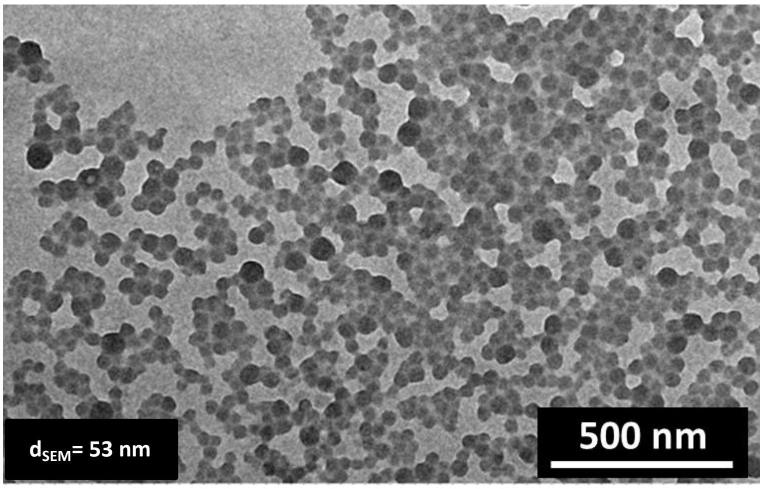

Figure 68: TE micrographs of nanocapsules with encapsulated sulforhodamine prepared with standards parameters (DMF+LiBr, 0.5 wt.% surfactant) from peptide [Mca/7NH_2] with 5 TDI equivalents (sample JA96).

IV.5.2 Improved redispersion into water with mild ultrasonication

One problem remains during the redispersion stage: aggregates are formed and they are not disassembled by mechanical agitation or ultrasound bath, as shown by PCCS measurements. Redispersion in a larger volume of water did not lead to better results as well. This problem was described for the first hybrid capsules prepared in miniemulsion (see **Table 3**) and remained present for all samples mentioned until this point. Another possibility to separate the capsules forming the aggregates is the use of an ultrasonication tip. In the previous samples, this option not chosen, in order to avoid breaking the peptide sequence building the capsules. However, because of the not-well redispersed sample obtained using only stirring and ultrasonication bath, the use and influence of ultrasonication tip was tested. Sample JA79 (capsules made from peptide [Mca-7NH_2], 2 TDI equivalents and no payload) was mildly ultrasonicated in different ways after redispersion in water and the evaporation of cyclohexane. This sample was divided in three parts, as summarized in **Table 8**. The first part was kept as reference, the second briefly ultrasonicated (1 min, low amplitude of 30%) and the third longer (3 min, 30% amplitude).

Table 8: Summary of size evolution by redispersion of the nanocapsules with the help of ultrasonication tip.

Sample names	US-tip process (time, intensity)	x_{50} in water before dialysis (nm)	x_{50} in water after dialysis (nm)
JA79-a	/	1195 (broad-mono)	960 (precip)
JA79-b	1 min, 30%	313 (mono)	334
JA79-c	1 min + 2 min, 30%	212 (mono)	208

The results of this experiment were fully satisfying. As stated in **Table 8**, the ultrasonication tip separates the aggregates progressively: after one minute the size decreased considerably and after three minutes it reached a size comparable with the one measured before redispersion (x_{50} = 153 nm). Additionally, the sizes measured after dialysis were similar for the ultrasonicated samples: they are stable, whereas minor precipitation was observed for the reference sample. It surely comes from the biggest aggregates, as the size measured was slightly smaller after dialysis. The samples were investigated with fluorescence microscope. **Figure 69** presents the different pictures of samples before redispersion in cyclohexane and after redispersion and dialysis in water with and without prior ultrasonication.

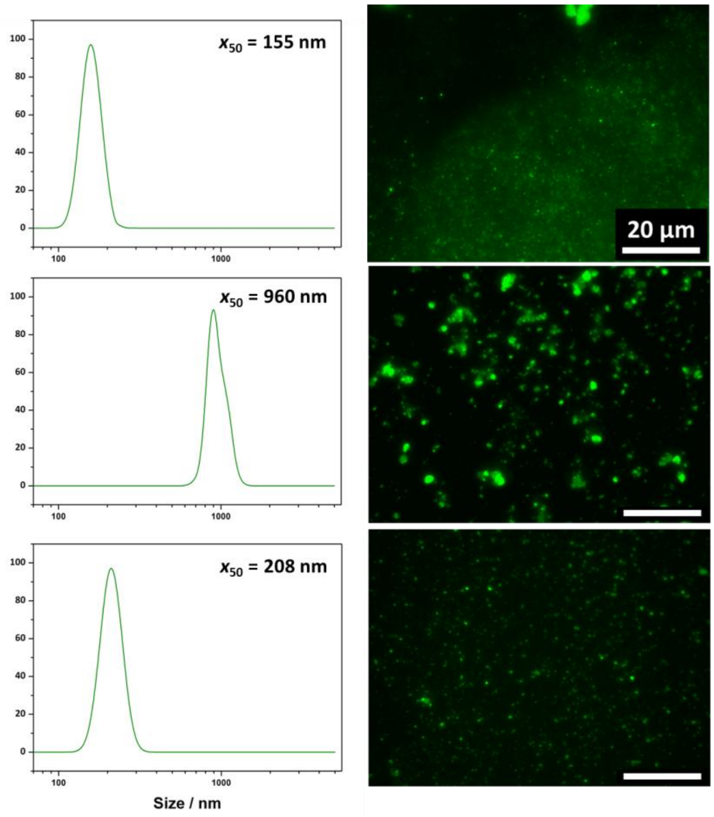

Figure 69: **Fluorescence micrographs of [Mca/7NH$_2$]-based nanocapsules with 2 equivalents TDI, in cyclohexane before redispersion (JA79, *top*, x_{50} = 155 nm), after redispersion and dialysis without (JA79-a, *middle,* x_{50} = 960 nm) or with (JA79-c, *bottom,* x_{50} = 208 nm) ultrasonication for redispersion.**

The pictures confirm the information obtained via PCCS measurements in **Table 8**. The use of the ultrasonication tip under mild conditions reduces the size of the structures. It separates the aggregates and the particle observed after ultrasonication have a size comparable to the original capsules before redispersion. Even if such an experiment does not prove that the ultrasonication treatment disaggregates the capsules and let them intact, it demonstrates at least that after dialysis, the peptide sequences still belong to nanostructures and have to be cleaved in heterophase.

Even more interesting is the enzymatic cleavage of these three samples, presented in **Figure 70**. The control samples, without enzyme, all have a stable and similar value, meaning that no peptide cleavage occurred (a higher value would have been interpreted as a destruction of the peptide sequence, a lower as a dismantling of the capsules with liberation of polymer chains removed during dialysis). In presence of trypsin, the fluorescence of the Mca group increases until a similar end value, indicating successful cleavage of similar amounts of peptides. The non-ultrasonicated sample exhibits a slightly lower end value, probably due to aggregation and partial precipitation as mentioned before. The most relevant observation is that the smaller the capsules (or their aggregates) are, the faster the cleavage is. This can be explained by the larger surface area readily available for the enzyme. One notices also, that the fluorescence increase is lower for the capsules redispersed without ultrasonication, which is also attributed to the presence of aggregates. Some peptide sequences are not accessible to the enzyme, because of aggregate precipitation or due to the lack of place for an enzyme to cleave a peptide located between aggregated capsules.

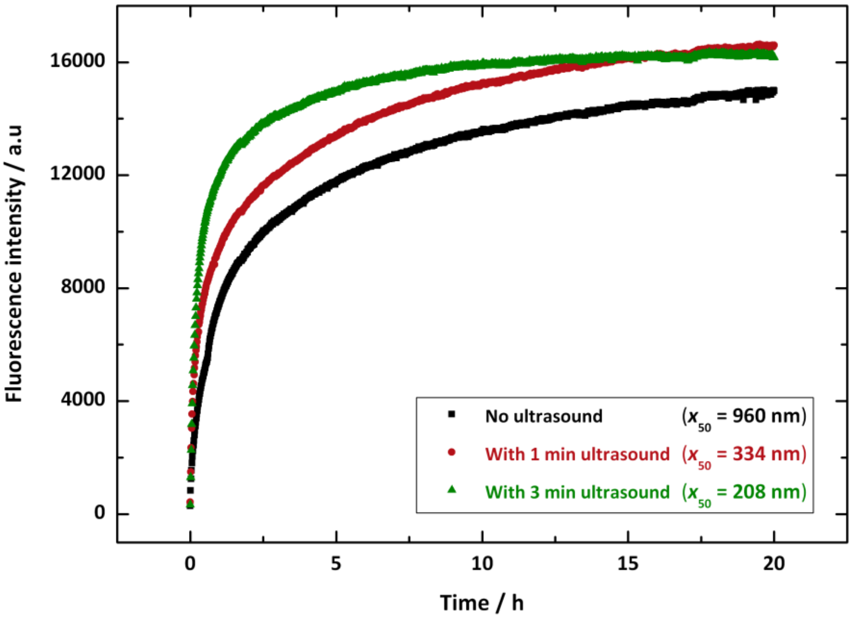

Figure 70: **Influence of ultrasonication after redispersion of the sample JA79 on the degradation of the nanocapsules. All samples were dialyzed afterward. Fluorescence signal are raw data corrected by the intensity of control sample without enzyme.**

It was demonstrated that the use of an ultrasonication tip under mild conditions does not only preserve the peptide based nanocapsules and improves their redispersion in water, but that it also results in more stable dispersions and a faster cleavage of the peptide sequences. Additionally the effect of redispersion via ultrasonication on the encapsulated dye was also investigated. A fraction of the first sample prepared with encapsulated sulforhodamine (capsules from peptide [Mca/7NH$_2$], 2 TDI equivalents and SR-101), was submitted to a second mild ultrasonication tip treatment after dialysis. The fluorescence intensity was compared with the one of the fraction ultrasonicated only prior dialysis and no significant difference was observed. It means that no quenched encapsulated dye was released during the second ultrasonication process. The applied redispersion process does not induce a significant release of encapsulated sulforhodamine, which will be washed away during dialysis in the next samples. Taking into account all the advantages that the improved redispersion process offers, it was applied to all the samples prepared afterwards (samples JA79 to JA 99 in **Table 13** - appendix).

IV.5.3 Influence of TDI equivalent and functionality of the peptide after the encapsulation of sulforhodamine

Characterization of the capsules

A series of nanocapsules was prepared to investigate the influence of two synthetic parameters after the encapsulation of the small water-soluble dye SR-101. As previously, the number of TDI equivalents, as well as the number of reactive groups on the peptide were studied. The size of the macromolecules was analyzed after polyaddition. The samples were all redispersed in water, sonicated with ultrasound-tip and dialyzed. The fluorescence (λ_{em} = 605 nm, corresponding to SR-101) of the two first dialysates was quantified to determine the amount of free SR-101 contained inside. All the data are summarized in **Table 9**.

Table 9: Summary of size of the capsules and encapsulation efficiency of SR-101 by varying chemical synthetic parameters.

Sample	Peptide	TDI eq. to amino groups	x_{50} measured by PCCS (nm)			SR-101 Encapsulation Efficiency (%)		
			Before redispersion	After redispersion and US	After dialysis	Free in dialysate #1	Free in dialysate #2	Encaps. Efficiency
JA93	**[Mca/3NH$_2$]**	**2**	140	348	**308**	24,7	0,3	**75**
JA95	**[Mca/7NH$_2$]**	**1**	167	216	**211**	9,0	0,5	**91**
JA94	**[Mca/7NH$_2$]**	**2**	155	332	**318**	6,7	0,3	**93**
JA96	**[Mca/7NH$_2$]**	**5**	146	780	/	1,7	0,3	**98**

The SEC elugrams of the samples for studying the influence of the amount of TDI equivalents are presented in **Figure 71**. The chromatogram of SR-101 was also plotted, as SR-101 is absorbing at 325 nm and brings an additional peak. On the other side, as the amount of SR-101 is the same for all these samples, the peak of SR-101 provides a nice internal standard, even if it contains a small contribution from the remaining free peptide.

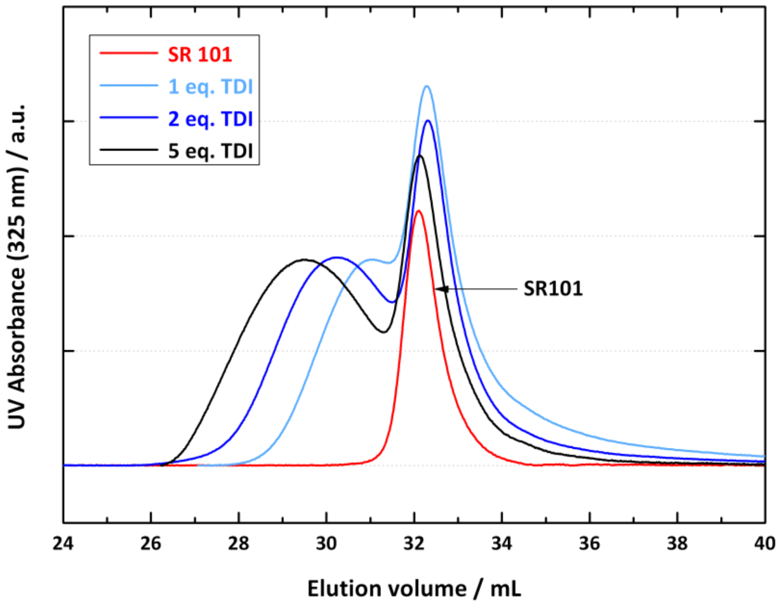

Figure 71: **Influence of the amount of TDI equivalent on the size of polymer prepared from peptide [Mca/7NH$_2$] with encapsulated sulforhodamine. The elugrams of the polymers are normalized to the same total area.**

One observes in **Figure 71** that an increasing amount of TDI equivalent, from 1:1 stoichiometry to large excess (1:5), results in capsules made of larger peptide-based polymer. This confirms the observations reported with the same peptide without payload (see **Figure 55**). In the case of sulforhodamine encapsulation as well, there are no major differences in the size of the polymer chain obtained, even if a slightly broader distribution toward higher molecular weight is observed in the case of the peptide with more amine groups.

Redispersion and encapsulation efficiency

As stated in **Table 9** the redispersion process was successful (size, stability) for all the samples. The only exception is the sample with a large excess of TDI (5 equivalents), which was not optimally redispersed and partially flocculated during dialysis. This is not surprising as larger sizes had already been reported for the samples with a large excess of TDI (see **Table 5**). Here, the size after polyaddition in cyclohexane was comparable to the other samples, but it is possible that inter-capsules polyaddition reactions with reactive isocyanate group remaining at the surface occurred during redispersion in water (see paragraph II.6.2).

The precise analysis of the encapsulation efficiency reveals several interesting results. Firstly, the encapsulation is successful: in all samples, a large majority of dye is encapsulated (> 75%). Secondly, both parameters studied have a predicable influence on the encapsulation efficiency: an increase of the TDI equivalent (larger chains and denser network) leads to a slightly better encapsulation with the peptide containing seven amine groups. For this peptide, the encapsulation efficiency is very high for all samples (> 90%), whatever the number of TDI equivalent. More reactive groups on the peptide increase consequently the encapsulation efficiency (3 to 7 reactive groups lead from 75 to 93%). This parameter plays a decisive role in the encapsulation efficiency.

Considering both the encapsulation efficiency results and the SEC measurements, it appears that, if the use of a multibranching peptide and a large excess of TDI does not lead to an infinitely long peptide-based polymer, it strongly enhances the branching density of the capsules, which turns out to be a determining criterion for a high encapsulation efficiency.

Fluorescence microscopy of the capsules with entrapped dye

The peptide-based hybrid nanocapsules with encapsulated sulforhodamine SR-101 were investigated with fluorescence microscopy, at two different excitations wavelengths, stimulating either the fluorescence of Mca (dye of the FRET system on the peptide), or the fluorescence of encapsulated sulforhodamine. It is reminded that fluorescence of the Mca group in the FRET system is quenched but remains high enough for the detection with a fluorescence microscope. This is also the case for SR-101, the fluorescence of which is still easily detectable in fluorescence microscopy despite its self-quenching. The micrographs are displayed in **Figure 72**.

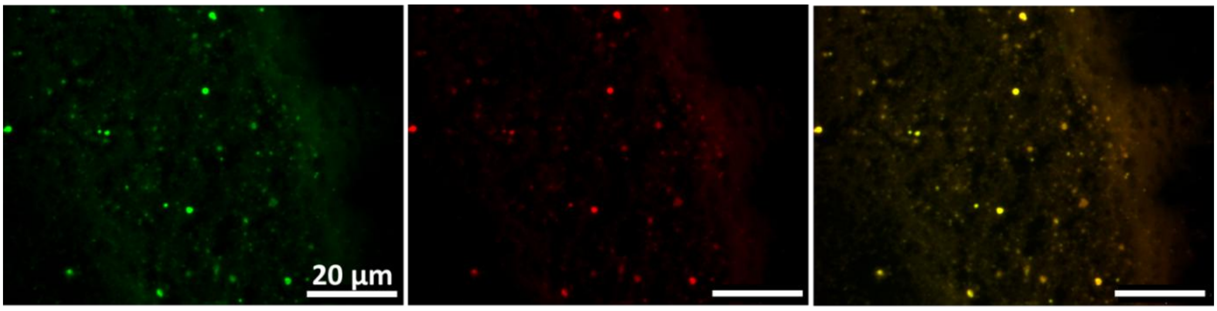

Figure 72: **Fluorescence micrographs of [Mca/7NH$_2$]-based nanocapsules with 2 TDI equivalents and encapsulated dye. The fluorescence of the peptide (Mca, green, *left*) of the encapsulated dye (SR-101, red, *middle*) and superimposition of the two first pictures (*right*).**

The repartition of fluorescence of the Mca group is identical compared with the one displayed in **Figure 65**. This confirms that the ultrasonication process for redispersion has no destructive effect on the capsules. The fluorescence of sulforhodamine is also clearly localized in defined structures, proving its successful encapsulation. Finally, the two micrographs overlap perfectly, showing that the sulforhodamine is homogenously encapsulated in all the peptide-based capsules, and is only present in the peptide-based capsules. The fluorescence microscopy analyses confirm that the encapsulation of the water-soluble sulforhodamine dye is very efficient. The next step is the study of the dye release upon enzymatic cleavage, but before the necessary conditions for a live monitoring of this release has to be fulfilled.

Self-quenching of the encapsulated sulforhodamine inside the capsules

The strategy to observe the release of the dye is based on its high concentration inside the capsules leading to intermolecular self-quenching of the fluorescence. Therefore, for preparing the miniemulsion, SR-101 was dissolved at the concentration of 11×10^{-3} M, much larger than the concentration of 3.2×10^{-6} M where self-quenching was reported to start in water.[153] The release of diluted fluorophore outside of the capsules should lead to a fluorescence increase. However, it has to be demonstrated first that an efficient quenching is taking place when SR-101 is encapsulated. Therefore, time-correlated single photon counting (TCSPC) measurements were carried out by Dr. A. Turshatov. Two different samples were investigated: a dispersion of nanocapsules (after redispersion and dialysis) and a SR-101 solution with a comparable absorption value at 580 nm. Thus, the concentration of SR-101 in both samples was in the same range. The results of TCSPC analysis are displayed in **Figure 73,** after normalization upon absorption values at 580nm. One observes that the fluorescence decay is far more intense in the sample where SR-101 is in solution than if is encapsulated. Additionally, for a similar overall concentration of a SR-101, the steady-state intensity is 42 times higher in solution than in the capsules. A very strong quenching of SR-101 is taking place inside the capsules.

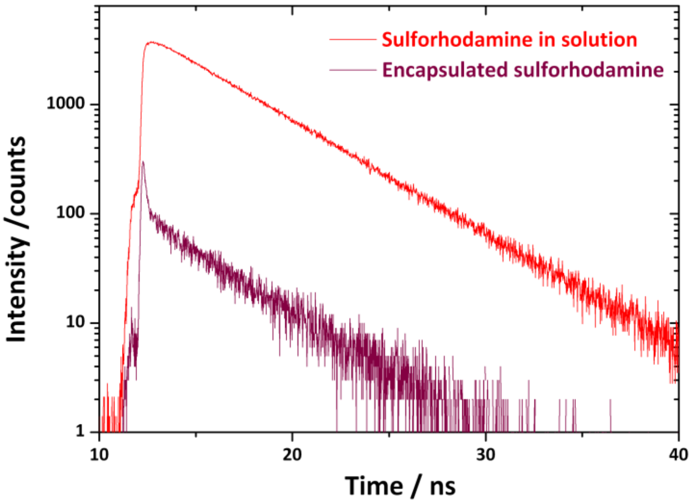

Figure 73: Temporal decays of fluorescence (λ_{ex} = 580 nm, λ_{em} = 605 nm) of dye SR-101 encapsulated in nanocapsules (brown, steady state intensity = 910 counts·s^{-1}, sample JA94a) and in solution in water solution (red, steady state intensity = 39 200 counts·s^{-1}), for a same absorption at λ = 580 nm. *Measured by A. Turshatov.*

IV.5.4 Release of payload via enzymatic cleavage of peptide based nanocapsules

After the preparation of enzymatically cleavable peptide-based hybrid nanocapsules and their successful degradation, it was shown that a small water soluble fluorescent dye is efficiently encapsulated and quenched in our system. Now, in addition to enzymatic degradation monitored via the fluorescence signal of the FRET system, the fluorescence recovery of the self-quenched dye is expected, as schemed in **Figure 74**.

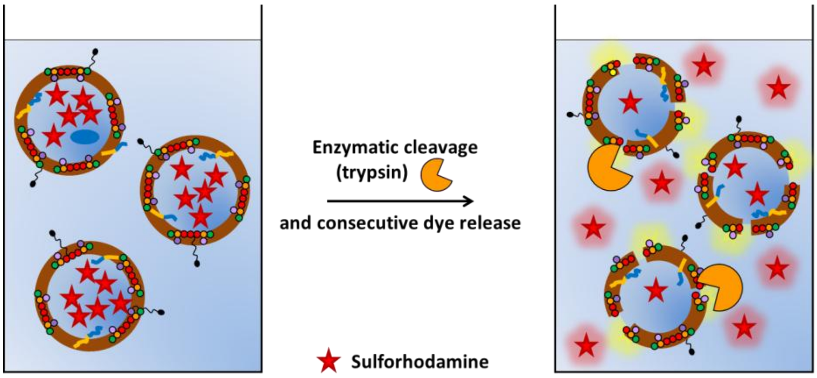

Figure 74: Schematic representation of the enzymatic cleavage of the peptide-based nanocapsules with fluorescence recovery of the FRET system and of the self-quenched encapsulated dye.

The results of the enzymatic degradation are presented and analyzed in **Figure 75**.

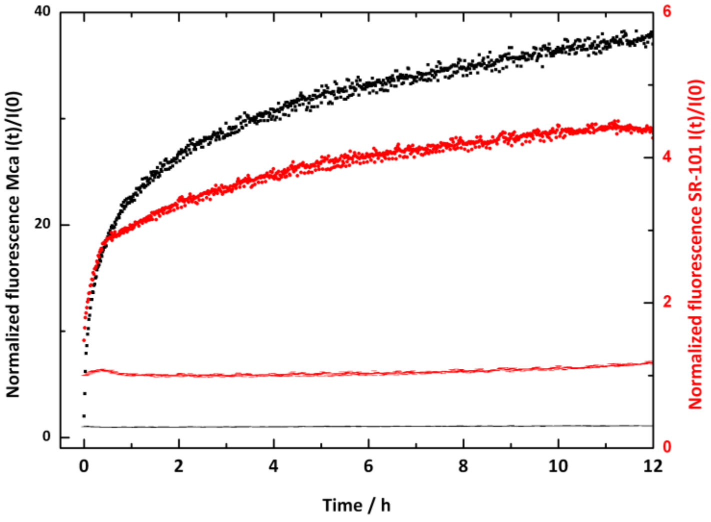

Figure 75: **Enzymatic cleavage of peptide-based nanocapsules with release of encapsulated SR-101. The fluorescence signals are from Mca (λ = 405 nm, capsules wall, black) and sulforhodamine SR-101 (λ = 605 nm encapsulated dye, red) in capsules from [Mca/7NH_2] with 2 TDI equivalents.** ***Measurements done by N. Kotman.***

The signal of both Mca and SR-101 are increasing within a few hours. The curve of the FRET system is very similar to those observed previously without payload or with encapsulated polymer. The fluorescence signal of sulforhodamine also increases as expected, namely the recovery of fluorescence due to the liberation of molecules entrapped in the capsules previously. Indeed self-quenching due to high concentration no longer occurs for the molecules released in solution. Even more interesting is that both curves have very similar shapes. It supports the assumption, that the increase of SR-101 fluorescence intensity is due to the release of the dye, triggered by the cleavage of the enzymatic sequence. It is also worth comparing the behavior of nanocapsules prepared with different parameters (functionality of the peptide, numbers of TDI equivalent) upon enzymatic degradation. The comparison of the Mca and SR-101 signals are presented in **Figure 76** and **Figure 77**, respectively.

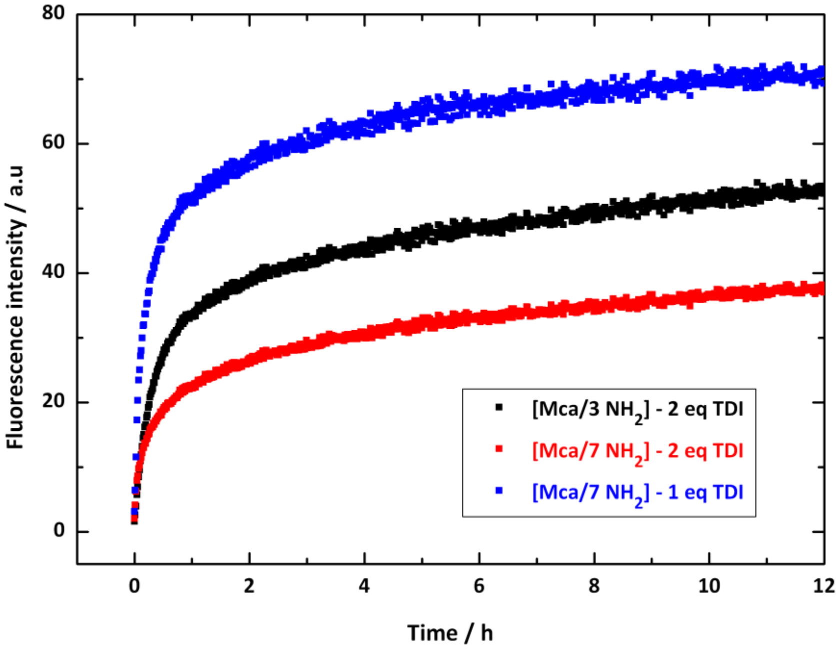

Figure 76: **Enzymatic cleavage of peptide-based nanocapsules. Fluorescence signal from Mca (λ_{em} = 405 nm) are displayed for samples with encapsulated SR-101 and with different synthetic parameters.** ***Measurements done by N. Kotman.***

The diagrams in **Figure 76** show that independently of the synthetic parameters, all three samples present a similar response to the enzymatic cleavage. It was already explained, why the comparison of samples with two different peptides cannot be done exactly (different amounts of peptide used) but it is expected that the sample with the larger amount of peptides (due to lower molecular weight, here capsules from [Mca/3NH$_2$] in black) shows a higher increase of fluorescence (compared with [Mca/7NH$_2$], in red). Nevertheless, the comparison for capsules prepared with the same peptide but different equivalents of TDI comonomer shows that the peptide degradation is higher in the case of shorter and probably less branched polymer chain. The analysis of the corresponding sulforhodamine fluorescence evolution is not as straightforward as in the case of the fluorescence of Mca, as shown in **Figure 77**.

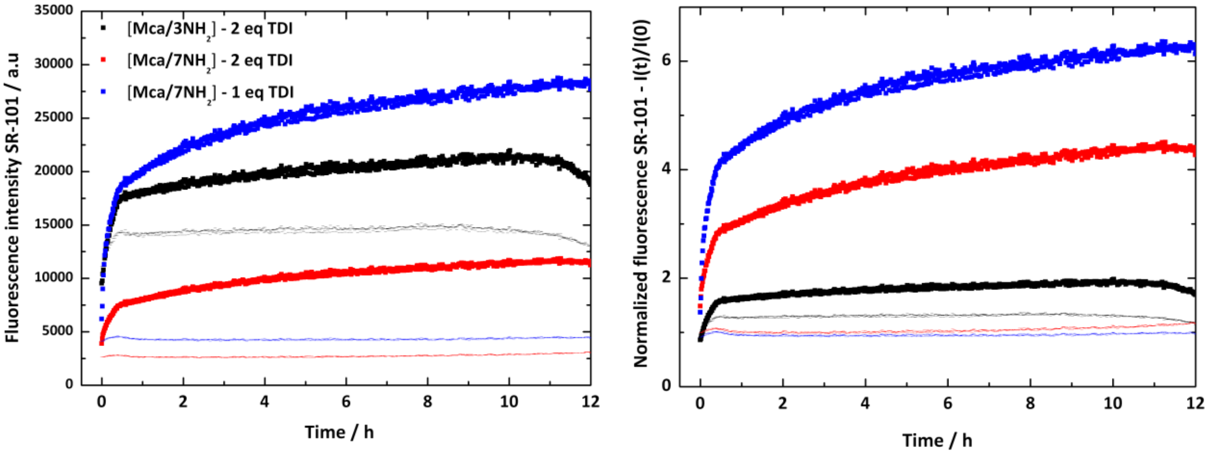

Figure 77: **Release of encapsulated SR-101 (λ_{em} = 605 nm) upon enzymatic cleavage for samples with different synthetic parameters. Absolute intensity values are displayed on the left, while normalized intensities are plotted on the right. The control experiments without addition of enzyme are traced with a thinner line. *Measurements done by N. Kotman.***

The fluorescence signals are plotted here with both absolute and normalized values. This shows how an "apparently" low relative fluorescent increase can correspond to a significant increase in the absolute value, like here in the case of the capsules prepared from [Mca/3NH$_2$] (black in **Figure 77)**. This is due to the higher value of the SR-101 fluorescence in the control sample. It is also relevant to notice, that the fluorescence background is more intense, when the functionality of the peptide decreases (14000 a.u. for [Mca/3NH$_2$] against 2500 a.u. for [Mca/7NH$_2$] with 2 TDI equivalents). Similarly, the samples with capsules made of polymers formed with less TDI (i.e. shorter chains) have a higher baseline value (4500 a.u. for [Mca/7NH$_2$] with 1 TDI equivalent). To sum up, the fluorescence background increases when the encapsulation efficiency decreases. This trend confirms the quenching of the dye entrapped into the particles.

The comparison of fluorescence intensity for the capsules made of peptide [Mca/7NH$_2$] with 2 TDI (red) or only 1 TDI (blue) equivalent(s) shows, that the fluorescence increase is stronger with less equivalents of TDI. More SR-101 is released when the chains of the capsules are shorter. In this perspective, the sample named [Mca/7NH$_2$] - 1 eq (see **Table 9**, entry JA91) TDI seems very suitable, as it combines very good encapsulation efficiency (91%), with a stronger response to the enzymatic cleavage and consequently a better release of the encapsulated dye.

V.5.5 Quantitative approach of cleavage and release

The enzymatic cleavage of peptide-based nanocapsules was demonstrated. Moreover, the triggered release of encapsulated dye was also observed. However, it would be interesting to obtain quantitative information on the proportion of the peptide sequences which are cleaved. Similarly, the proportion of the released SR-101 should also be determined.

Quantifying the cleavage of peptide

It was stated previously, that the determination of the peptide amount present inside the capsules is not straightforward. The measurement of the (quenched) fluorescence intensity was not satisfying, as scattering takes place at this wavelength (405 nm) considering the size of the capsules. Moreover, the polymerization of the peptide may induce some rigidity in the chain and the quenching efficiency could be lowered, compared to peptide in solution.[186, 206] An indirect method was preferred, therefore the peptide dialyzed out was quantified via fluorescence measurements (see paragraph V.3.5). To quantify the amount of peptide cleaved in the nanocapsules, the best approximation is obtained by comparing the overall fluorescence increase in capsule suspensions with the increase of fluorescence observed with different concentrations of the peptide, using exactly the same parameters for the fluorescence measurements. This work was processed with peptide [Mca/7NH$_2$] at various peptide concentrations.

Table 10: Increase of fluorescence during enzymatic cleavage in dependence of the peptide concentration.

Peptide concentration (mol·L^{-1})	10^{-6}	2×10^{-6}	5×10^{-6}	10^{-5}	2×10^{-5}
Absolute fluorescence increase (a.u.)	1 200	3 600	6 400	12 650	22 700

For all dispersions and cleavage experiments prepared from peptide [Mca/7NH$_2$], the fluorescence increase was located between 15000 and 20000 a.u within 12 h; the calculations were then done assuming that the amount of peptide cleaved on the nanocapsules was comprised between the amounts of peptide cleaved in a 10^{-5} M solution and in a 2×10^{-5} M solution, assuming quantitative cleavage. Taking into account the amount of peptide dialyzed out (around 15%) and dilution factors, it means that between 4.8% and 9.5% of the peptide present in the nanocapsules is degraded within the first 12 h.

This is the best approximation that can be obtained. However, this approximation is under-estimated because of the scattering due to the capsules. These values show that a consequent amount of the peptide is degraded and confirm that the capsules are not fully degraded within a few hours, which was observed visually on all samples.

Quantifying the release of encapsulated dye

Another challenge is the determination of the quantity of the released payload. A first approach is possible using TCSPC: this method was used to observe the efficient cleavage of encapsulated sulforhodamine. It can also be used to observe the fluorescence recovery. **Figure 78** displays TCSPC measurements of the same sample at different stages: before and after overnight cleavage, and after an intensive ultrasonication treatment (3 min, 70% amplitude).

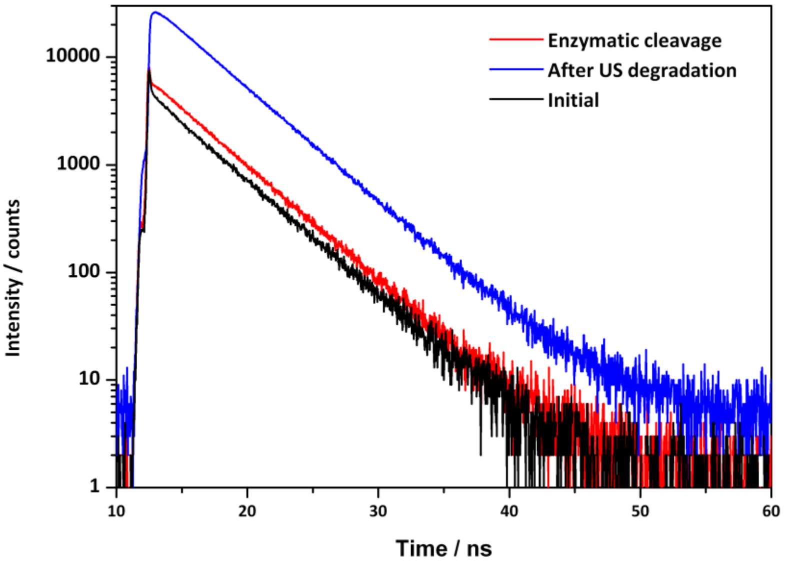

Figure 78: **Fluorescence decays of sulforhodamine SR-101 originally encapsulated inside the capsules. Steady-state intensity was also measured separately: initial state before enzymatic cleavage: 10 500 counts·s^{-1}, after enzymatic cleavage (16 h): 14 000 counts·s^{-1}, after ultrasonication 67 000 counts·s^{-1}.**

The analysis of fluorescence with the TCSPC technique (**Figure 78**) shows that the fluorescence intensity and the life-time of the sulforhodamine excited state both increased during the enzymatic cleavage, which confirms the results obtained with fluorescence measurements for the previous samples. Moreover, the steady-state intensity increased by 33%: there is recovery of fluorescence of quenched sulforhodamine. The ultrasonication of the sample afterwards also brings some information: the increase of fluorescence is more significant, as visualized in **Figure 78**, with a higher intensity and a consequently increased lifetime of the fluorescence. This is also confirmed by the steady-state intensity (+540% increase). Even if the nanocapsules are not fully degraded, it shows that only a little amount of encapsulated dye is released within the first 16 h.

Another strategy to study the release of sulforhodamine is the centrifugation of the samples after enzymatic cleavage. Assuming that all - and only - the released sulforhodamine molecules are present in solution after centrifugation, it is possible to calculate the proportion of sulforhodamine released.

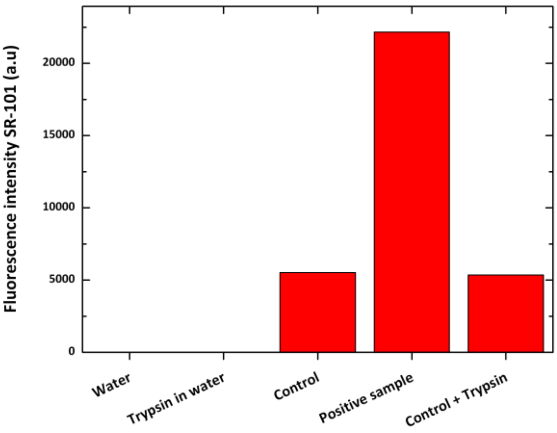

Figure 79: **Fluorescence intensity of the supernatant collected after centrifugation of the nanocapsules (from [Mca/7NH$_2$], supernatant diluted 5x). *Positive sample*: addition of trypsin, let overnight at 37 °C and centrifugation. *Control*: same protocol as previously without trypsin preparation. *Control + trypsin*: addition of trypsin preparation to *control* and measurement of fluorescence after 24 h.**

The results of these experiments are summarized in **Figure 79**. One observes that no fluorescence is emitted in water, or due to the presence of enzyme. The fluorescence intensity in the supernatant is much higher when enzyme was added: sulforhodamine is released, due to enzymatic cleavage. However, fluorescence is also observed in the supernatant without addition of enzyme. Either it comes from degradation of the capsules during centrifugation or from the presence of small capsules in the supernatant. The addition of enzyme to the supernatant after centrifugation yields no increase of the fluorescence: no additional SR-101 was released, which tends to demonstrate that the sulforhodamine present in the control samples is in solution. Then, converting the fluorescence value to the original concentration in the supernatant, one obtains that 3.7% of the encapsulated SR-101 are released in solution (2.8% if the SR-101 present in the control is withdrawn). This value seems to be relatively low, but thanks to the efficient quenching of the encapsulated sulforhodamine, this is sufficient to detect easily variations of fluorescence.

In conclusion, the release of sulforhodamine triggered by the addition of enzyme was confirmed by various analyses, such as the TCSPC technique or centrifugation experiments. Even though this release concerns a minor amount of the encapsulated dye, it is largely sufficient to observe the release properly.

IV.6 Hepsin-cleavable nanocapsules

IV.6.1 Identification of hepsin-cleavable sequence

The main goal of the project was to synthesize hepsin-cleavable nanocapsules with cargo-release properties. The proof of principle has been successfully demonstrated with a model peptide sequence cleaved by a non-specific protease. The next step of this project is the adaptation of this system to a more specific enzyme, namely hepsin. Hepsin is a transmembrane protease, which is strongly overexpressed by prostate cancerous cells. The peptide sequence RQLR-VVGG was reported as a good substrate for hepsin.[197] As a result, the peptide sequence displayed in **Figure 80** was prepared by SPPS with the same features as the previous sequence. The recognition site is surrounded by the Mca/Dnp FRET pair and lysine amino acids are added at both extremities for an interfacial polyaddition reaction with diisocyanate. This peptide will be referred to as peptide [heps/Mca/7NH$_2$].

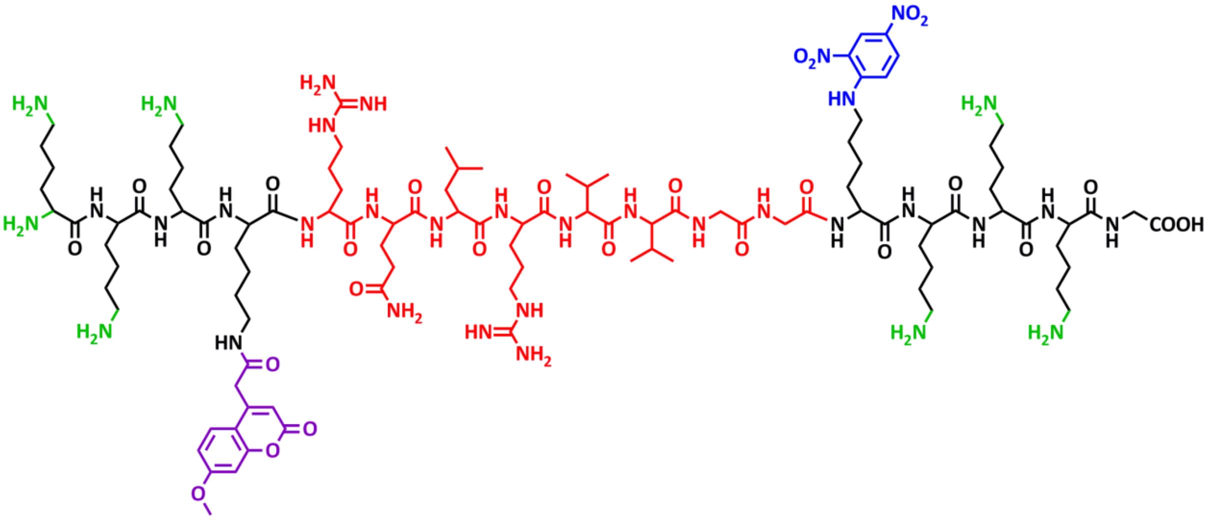

Figure 80: **Formula of the peptide [heps/Mca/7NH$_2$] synthesized for the preparation of hepsin-cleavable nanocapsules via interfacial polyaddition.**

It is important to notice that the recognition sequence of hepsin contains amino acids with side-groups, which can react with TDI, such as arginine (R) and glutamine (Q). Six lysine residues (i.e. 7 NH_2 groups for the peptide overall) were introduced in the peptide sequence, as this type of peptide gave the best results in terms or encapsulation with the GFF peptide sequence. Moreover here, the preeminence of lysine residues should statistically let some recognition sequence unreacted, so that they can be cleaved by hepsin.

To test the cleavability of the peptide, a 10^{-5} mol·L^{-1} peptide solution was obtained by adding a solution of peptide [heps/Mca/7NH_2] to samples containing hepsin-positive cell lines from prostate cancer and other control samples. The evolution of Mca fluorescence is displayed in **Figure 81**.

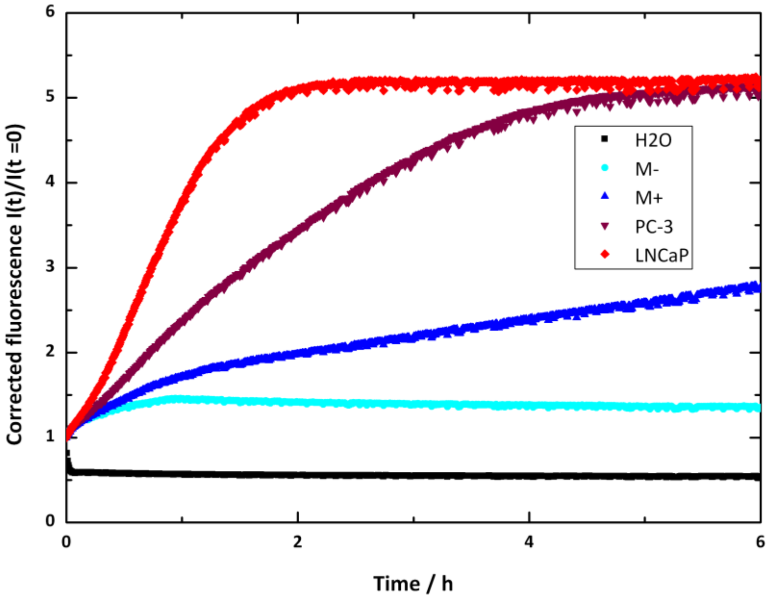

Figure 81: **Cleavage of peptide [heps/Mca/7NH_2] over time in various biological media. M- and M+ represents the cell culture medium respectively without/with FCS (fetal calf serum). PC-3 (hepsin negative) and LNCaP (hepsin positive) are both cell lines from prostate cancer, cultivated in M+. *Measurements done by N. Kotman.***

The observation of the fluorescence evolution contains diverse information. In water and in cell culture medium without FCS, the fluorescence level remains stable, which means that the peptide is not cleaved. The addition of FCS, which contains a variety of proteins and proteolytic agents, leads to a continuous and progressive increase of fluorescence. There are in this serum proteases which are able to cleave the peptide somewhere between the components of the FRET pair. In the samples prepared with the cell cultures, the fluorescence increases to reach a maximum value within a few hours. The peptide is degraded by both types of cells, hepsin-positive or negative. However, a significant difference is observed between the two types of cells. The degradation of the peptide by the hepsin-positive cells (2h) is much faster than by the hepsin-negative cells (around 6h). These results of peptide degradation correspond to the results described in the literature, the peptide sequence RGLRVVGG clearly degraded by hepsin. However, the hespin-negative cells have proteolytic biomolecules capable to degrade the recognition sequence, as the cleavage of the substrate is faster with these cells than in the cell culture medium with serum.

V.6.2 Preparation of the capsules

The nanocapsules were prepared similarly as previously, with the exception of the dispersed phase. A strong gelification was observed when the peptide was dissolved in DMF containing 5 $g \cdot L^{-1}$ LiBr (sample JA98). As a result, 0.9 g DMSO with 5 $g \cdot L^{-1}$ LiBr was used as dispersed phase instead of 0.75 g DMF, which correspond to the same volume of dispersed phase. The capsules size was measured by PCCS to be 412 nm. This larger size cannot be attributed to the increased volume of the dispersed phase, only multiplied by a factor 1.05 with respect to density of DMF and DMSO. It is possible that the hepsin-cleavable peptide sequence is less surface active than the peptides used previously in the precedent parts. However, this size distribution centered at 412 nm is comparable with the size obtained with peptide [“Y”/$2NH_2$] with similar synthetic parameters, which was measured at 364 nm (See **Figure 38**, sample DMSO + LiBr, 0.5 wt.% surfactant, 2 TDI equivalents).

Similarly to what was observed for previous samples, the use of DMSO as solvent for the dispersed phase made the EM investigation challenging: films were observed in SEM and particle-like structures were observed with TEM (**Figure 82**). The capsules were then redispersed into water and mildly ultrasonicated before dialysis. After dialysis, the size of the capsules was 450 nm and the encapsulation efficiency of SR-101 was calculated to be 94% after analysis of the three first dialysates.

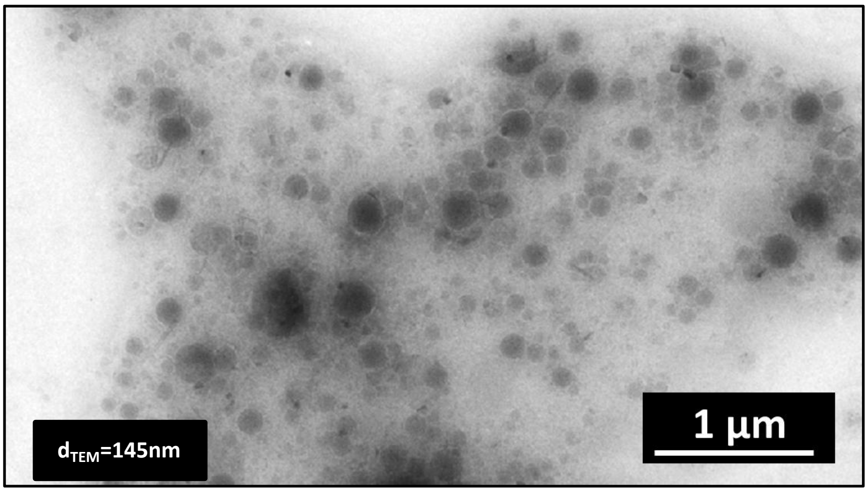

Figure 82: TE micrographs of nanocapsules obtained from peptide [heps/Mca/$7NH_2$] via interfacial polyaddition (JA99).

V.6.3 Cleavage of the capsules in cell culture

The dispersion of nanocapsules was given to LNCaP cell cultures, as well as to the suitable controls. The evolution of the fluorescence against the time was recorded as soon as the dispersions were added. The results are summarized in **Figure 83**.

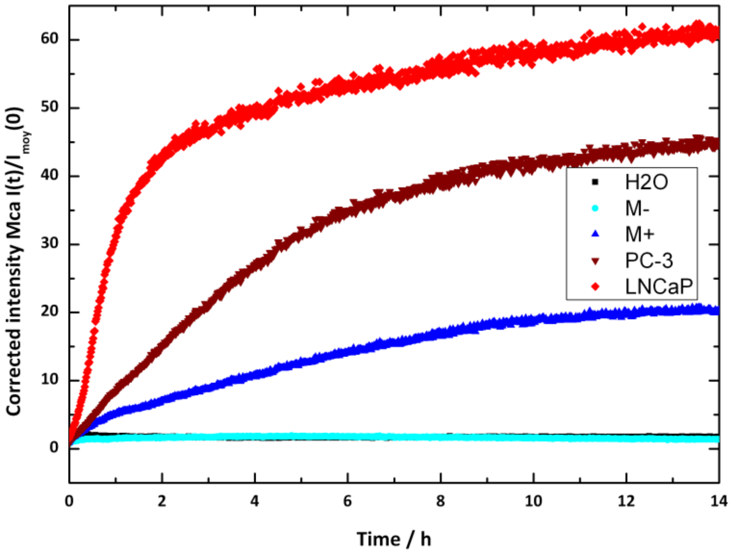

Figure 83: Cleavage of nanocapsules prepared from peptide [heps/Mca/$7NH_2$] over time in various biological media. M- and M+ represent the cell culture medium respectively without/with FCS (fetal calf serum). PC-3 (hepsin negative) and LNCaP (hepsin positive) are both cell lines from prostatic cancer, cultivated in M+. ***Measurements done by N. Kotman.***

To a certain extent, the results with the nanocapsules are comparable with those obtained with the free peptide. Qualitatively, fluorescence increase is observed neither in water nor in the cell culture medium without serum. A slight fluorescence increase is recorded in the cell culture medium with FCS: slower cleavage of the recognition site from the proteolytic enzyme contained in the serum also occurs in heterophase. Most of all, a strong and rapid fluorescence increase is recorded in the case of the hepsin-positive cells. It is also interesting to notice that the shape of the curve is not the same as for the free peptide: after 14 hours, no maximum has been reached and a fluorescence increase still takes place, which signifies that further cleavable sites become accessible to the enzymes. In the case of the hepsin-negative cells, a fluorescence increase is also observed, but it is clearly slower than for hepsin-positive cells, as well as less intense.

In conclusion, the preparation of peptide-based nanocapsules prepared via interfacial miniemulsion was transferred successfully to a hepsin-cleavable peptide sequence. Not only the capsules were degradable in cell culture, but it was found that the degradation is faster and more significant for the cells expressing hepsin transmembrane protease.

V. Conclusion and perspectives

Conclusion and perspectives

Within this thesis, new approaches for the concepts of peptide-polymer conjugates and peptide-based hybrid nanomaterials have been investigated. In the first part, the synthesis of a triblock polymer-peptide-polymer was carried out following a typical peptide coupling reaction, both in solution and on solid phase. The peptide sequence was chosen, so that it is cleaved by an enzyme preparation of trypsin. End-functionalized polystyrene was used as a model hydrophobic polymer and coupled to the peptide. The results show successful coupling reactions in both methods, while the solid-phase method produced a more defined product. Suspensions consisting of peptide-polymer conjugates particles were prepared in water by ultrasonication. In contact with the enzyme, the peptide constituting the conjugates was cleaved, as determined by mass spectroscopy. This demonstrates the enzymatic cleavage in heterophase of enzymatic sequence bond to hydrophobic polymers, and is of great interest for the encapsulation and delivery of hydrophobic molecules.

A second approach was the preparation of peptide-based hybrid nanocapsules. This was achieved by interfacial polyaddition in inverse miniemulsion with the peptide sequence functionalized with additional amino acids. A method suitable to the use of a peptide sequence for interfacial polyaddition was developed. It was shown that the polarity of the dispersed phase influences the structures prepared, from particle-like to polymeric shell with a liquid core.

The peptide sequence was equipped with a FRET pair (more exactly, an internally-quenched fluorescent system) which allowed the real-time monitoring of the enzymatic cleavage of the recognition site. This system showed the successful cleavage of the peptide-based nanocapsules when trypsin preparation was added to the suspensions. Additionally, a water-soluble fluorescent polymer was efficiently entrapped and its possible use as marker for the capsules was highlighted. Furthermore, a small water-soluble fluorescent dye (SR-101) was successfully encapsulated and the encapsulation efficiency as a function of the functionality of the peptide and the amount of comonomer equivalent (toluene diisocyanate) was studied. The fluorescent dye was encapsulated at such a high concentration, that self-quenching occurred. Thus, the release of the encapsulated dye triggered by the enzymatic cleavage of the peptide resulted in a fluorescence recovery of the dye. The fluorescence recovery of the FRET pair in the peptide and of the encapsulated dye correlated well.

Finally, nanocapsules based on a hepsin-cleavable peptide sequence were prepared. Hepsin is an enzyme, which is highly upregulated in prostate cancer cells. The cleavage of the nanocapsules was investigated with healthy and "cancerous" (hepsin-expressing) cell cultures. The degradation, followed via fluorescence recovery of the FRET system, was faster for the suspensions introduced in the hepsin expressing cell cultures.

In summary, this work tackles the domain of responsive nanomaterials for drug delivery from a new perspective. It presents the adaptation of the miniemulsion process for hybrid peptide-based materials, and their successful use in preparing specific enzyme-responsive nanoparticles with hydrophilic payload release properties.

Further developments in this area are conceivable. Whereas the main part of the work is carried out with a model peptide sequence, the last section deals with a much more specific enzyme/recognition site pair. The use of such nanomaterials responding exclusively to specific enzymes is one of the next challenges of this project. However, the use of reactive diisocyanate as a comonomer for polyaddition is not suitable to the functionality of certain amino acids (e.g. serine, arginine, glutamine…). Therefore, it would be relevant to use another, more specific reaction, for the interfacial coupling. As this reaction should be specific, obtains high yields under mild conditions, reactions classified as "click-chemistry", such as thiol-ene reaction or azide-alkyne Huisgen cycloaddition, present good alternative candidates.

Other further developments deal with the features of the nanocapsules, such as the encapsulation, or the use of a FRET pair based on a near infrared dye for studying the excitation and fluorescence propagation in prostatic tissue. The encapsulation of therapeutic agents, like anticancer drugs, and their efficiency after enzymatically-triggered release would also be interesting and necessary studies. The peptide-based nanocapsules prepared by miniemulsion are only at their beginnings when considering the potential applications, especially for use in biological systems like specifically-triggered drug release.

VI. Experimental part

VI.1 Materials

VI.1.1 Chemicals

All chemicals were used as received, if not especially mentioned in the experimental part.

Amino acids

With the exception of Fmoc-Lys(Mant), prepared by M. Maier[10], Fmoc-Lys(Mca)-OH, Fmoc-Lys-(Dnp) and Fmoc-Tyr(3-NO_2)-OH (from Bachem), all (L)-Fmoc-protected amino acids and preloaded resin (Fmoc-Gly-Wang resin, 100-200 mesh, loaded 0.79 $mmol \cdot g^{-1}$ or 0.30 $mmol \cdot g^{-1}$) for SPPS were purchased by Novabiochem (Merck). The purity of the commercial amino acids was ≥ 98%.

Other chemicals

1-Hydroxybenzotriazole hydrate (HOBt, H_2O, Fluka, ≥98%), *N*-[(1H-benzotriazol-1-yl)(dimethylamino)methylene]-*N*-methyl-methanaminium hexafluoro-phosphate *N*-oxide (HBTU), ethyl cyano-glyoxylate-2-oxime (Oxyma Pure, Merck, ≥98%) and *N,N*-diisopropyethylamine (Fluka, ≥98%) were used for peptide coupling reaction. Trifluoroacetic acid (TFA, Acros, 99%), triisopropylsilane (TIS, Alfa Aesar, 99%) and were used for the cleavage of the peptide from the resin.

The monomer styrene (Aldrich, ≥99.5%) and *N*-vinylpyrrolidone (VP, Aldrich, 99%) were purified at described in the polymerization parts. Toluene-2,4-diisocyanate (TDI, Sigma-Aldrich, ≥98%) and (HDI, Sigma-Aldrich, ≥98%) were used for the interfacial polyaddition. Salt lithium bromide (≥ 99%, anhydrous, Alfa Aesar) and sec-butyl lithium (Alfa Aesar) were used.

Sulforhodamine 101 (SR-101, Sigma-Aldrich) and boron-dipyrromethene-phenylmethacrylate furnished and synthesized by Andrey Turshatov, were used for their fluorescing properties.

The surfactants tested and used were sodium dodecyl sulfate (SDS, Merck, 99%), Fortegra 100 (Dow) and polyglycerol polyricinoleate (PGPR, Danisco). The block copolymer emulsifier poly(butylene-*co*-ethylene)-*block*-poly(ethylene oxide) P(B/E-*b*-EO) consisting of a poly(butylene-*co*-ethylene) block (M_w = 3700 $g \cdot mol^{-1}$) and a poly(ethylene oxide) block (M_w = 7300 $g \cdot mol^{-1}$) was synthesized starting from Kraton liquid (Shell), which was dissolved in toluene, by adding ethylene oxide under typical conditions of anionic polymerization.[207]

Solvents

The solvents used were acetonitrile (99.99%, Fisher), cyclohexane (p.a, VWR), diethyl ether (Sigma Aldrich, ≥99.5%), *N*, *N*-dimethylformamide (DMF, p.a., Sigma Aldrich) and d^8-dimethylformamide (Sigma Aldrich, 99.9%), dimethylsulfoxyde and d^6-dimethylsulfoxyde (DMSO, Sigma Aldrich, 99.9%), dichloromethane (DCM, 99.99%, Fisher), 1,4-dioxane (Sigma-Aldrich, stabilized, ≥99.5%), ethyl acetate (Fisher, ≥99.9%), *N*-methylpyrrolidone (Sigma Aldrich, 99%), methanol (Fisher, ≥99.9%), and tetrahydrofuran (THF, Sigma Aldrich, ≥99.9%). Milli-Q water was used as water constituent of the dispersed phase miniemulsion.

VI.1.2 Synthesis of carboxylic acid end-functionalized polystyrene by anionic polymerization

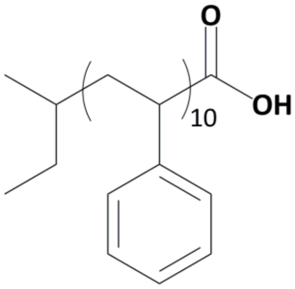

Figure 84: Structure of ω-carboxy-functionalized polystyrene prepared by anionic copolymerization.

The preparation of carboxylic acid end-functionalized polystyrene (PS-COOH, **Figure 84**) was carried out by T. Wagner with anionic polymerization, adapted from a protocol described in the literature.[208] THF was distilled and purified with diphenylethyl lithium and styrene was distilled after purification via fluorenyl lithium. Sec-butyl lithium was used as initiator to polymerize styrene with a targeted degree of polymerization $DP = 10$. Then, the solution of polymer is placed under carbon dioxide bubbling. The concentration of polymer was low enough to prevent the formation of “multi-arm” ketone or tertiary alcohol polymer.[209] At this stage, the acid group is still in the form of lithium salt (PS-COOLi) but already suitable and convenient for SEC analysis. The transformation of the lithium salt in carboxylic acid group was done under bubbling of hydrogen chloride, and the end-product PS-COOH was precipitated in methanol. The synthetic process is summarized in **Figure 85**.

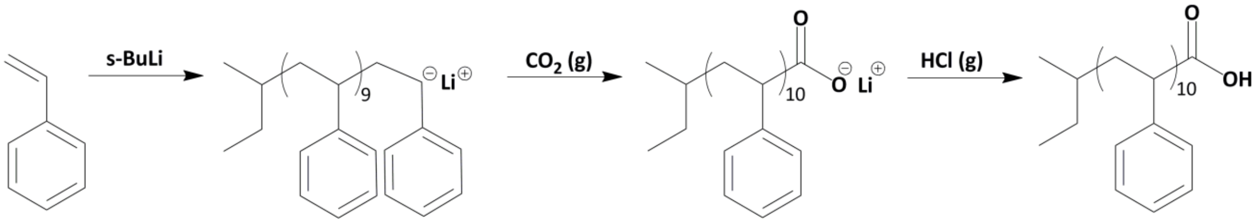

Figure 85: **Summary of the synthetic route to prepare ω-carboxy-functionalized polystyrene via anionic polymerization.**

Two polymers of different molecular weights were prepared. The molecular weight distribution was measured by SEC analysis: Batch#1 PS-COOH (M_n = 1120 g·mol^{-1}, M_w = 1250 g·mol^{-1}, PDI=1.12 in THF, calibration PS) and Batch#2 PS-COOH (M_n = 5900 g·mol^{-1}, M_w = 6200 g·mol^{-1}, PDI = 1.04 in THF). More precisely, the molar mass distributions were obtained from elugrams of PS-COOLi, and not from the end product PS-COOH. Indeed, the final product, the carboxy-functionalized polymer tends to form a dimer in solution, as discussed in paragraph IV.1.1.b (see **Figure 30**).

VI.1.3 Radical synthesis of poly(vinylpyrrolidone-*co*-(boron-dipyrromethene-phenylmethacrylate)

The preparation of a water soluble, fluorescent polymer was carried out to encapsulate a water soluble payload which is surely not leaking through the wall of the peptide-based nanocapsules. Among the water soluble polymer, poly(vinylpyrrolidone) was chosen for its non-reactivity with TDI. It was copolymerized in solution with a small amount of a methacrylate monomer functionalized with a fluorescing group, as shown in **Figure 86**.

1.5 g *N*-Vinylpyrrolidone (9.10^{-3} mol, M = 111 g·mol^{-1}), purified twice on an aluminum oxide column, and 5 mg boron-dipyrromethene-phenylmethacrylate (Bodipy monomer, 0.33 wt.%) were dissolved in 3.5 g of 1,4-dioxane (also purified twice on aluminum oxide column, T_B = 102 °C under 1 atm) and degased under argon. Then 16 mg initiator V-59 (2,2'-azobis(2-methylbutyronitrile), 8.3 10^{-5} mol, M = 192 g·mol^{-1}, 10 hours decomposition half-time at 67 °C) were added. The whole solution was degased again and the reaction proceeded for 65 h at 70 °C under argon.

A very viscous mixture was obtained. A ^{1}H-NMR analysis in 1,4-dioxane-d^8 of the raw product shows yields higher than 99.5% (proton attached to the *sp*^{2} carbon atom of *N*-vinylpyrrolidone monomer hardly detectable at $\delta = 6.95$ ppm and $\delta = 4.40$ ppm).

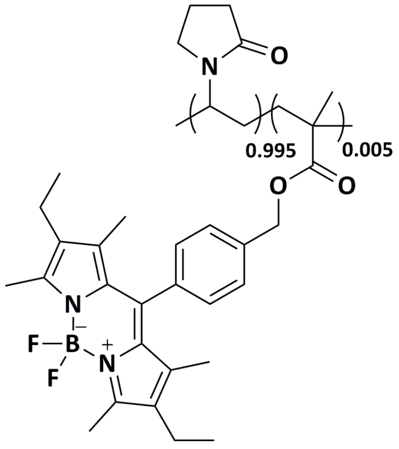

Figure 86: **Statistic composition of fluorescing water soluble polymer for encapsulation.**

Purification was carried out as following: the polymer was completely dissolved in a minimum amount of 1,4-dioxane and precipitated by low boiling petrol ether addition. The liquid fraction was removed and the polymer was dissolved in 1,4-dioxane. After three precipitations, the polymer is washed with petrol ether and dried overnight at 35 °C in a vacuum oven.

A fine orange powder was obtained, confirming the successful copolymerization of the Bodipy-monomer. The polymer is soluble in water and in DMF. SEC analysis was carried out in DMF: UV detection at 440 nm clearly shows that the Bodipy-monomer had copolymerized and that there was no monomer left in the purified product. Refraction index detector gives the following mass distribution: M_n = 18800 g·mol^{-1}, M_w= 122300 g·mol^{-1}, PDI = 6.5 with poly(vinylpyridine) calibration.

VI.2 Synthesis and preparation of peptides

VI.2.1. Solid-Phase Peptide Synthesis (SPPS)

The peptide sequences were prepared using standard solid-phase 9-fluorenyl-methoxycarbonyl (Fmoc) chemistry with a microwave assisted automated peptide-synthesizer (Liberty, CEM). The parameters used for coupling and deprotection steps are mentioned below.

- **Coupling**: 300 s under microwave heating, with a temperature reaching and stabilized at 75 °C after around 90 s, with HBTU and HOBt or Oxyma Pure as activators, DIEA as base, following the amounts indicated in **Table 11**.

Table 11: Equivalents amounts of reactants used in SPPS depending on the amount synthesized.

Peptide amount synthesized (mmol)	Activator equivalent (HBTU & HOBt or Oxyma Pure)	Activator base (DIEA) equivalent	Amino acid equivalent
0.1	5	10	5
0.5	5	10	4

- **Deprotection**: a first deprotection stage of 30 s (temperature reaching around 50 °C at the end) followed by a second one during 180 s (temperature 75 °C) with a 20 wt.% solution of piperazine in DMF.

- **Washing:** the resin was washed 3 to 5 times between each coupling or deprotection step.

- **Cleavage:** Cleavage of peptide from the resin was performed using a mixture of TFA/TIS/H_2O (95%/2.5%/2.5%) for 15 h at ambient temperature. After filtration, the peptides were precipitated and centrifuged three times in in cold diethyl ether, and dried over vacuum.

VI.2.2 Peptides

In this paragraph, all the peptides mentioned later for the preparation of linear peptide-polymer conjugates or peptide based hybrid nanocapsules are listed, schemed and characterized, mainly through ^{1}H-NMR spectroscopy and MALDI-TOF MS. The use of these two methods in addition to HPLC for the purity allows an exhaustive characterization of the peptide.

Peptide GFFKG – [-/2NH$_2$]

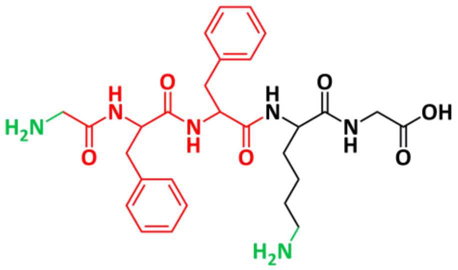

Figure 87: Structure of peptide [-/2NH$_2$].

^{1}H-NMR (DMF-d$_7$, 300 MHz): δ [ppm] 13.2 (br. s, 1H), 8.86 (d, $^2J_{HH}$ = 8.4 Hz, 1H), 8.60 (d, $^2J_{HH}$ = 8.3 Hz, 1H), 8.43 (br. s, 6H), 8.17 (m, 2H), 7.15-7.35 (m, 10H), 4.67 (m, 2H), 4.51 (m, 1H), 3.86 (m, 4H), 3.07 (m, 4H), 2.83 (m, 2H), 1.40-1,90 (m, 6H).

MALDI-TOF MS: Mass calculated M = 554.29 – found: Batch#1: 555 [M+H]$^+$, 577 [M+Na]$^+$, 593 [M+K]$^+$, Batch#2: 555 [M+H]$^+$, 577 [M+Na]$^+$, 593 [M+K]$^+$

Yield (gross) Batch#1: 64% (0.5 mmol), Batch#2: 91% (0.5)

HPLC: Gradient methanol/0.1% TFA in H$_2$O from 20/80 to 100/0 in 10 min; 1 mL·min^{-1}, UV 220 nm, Batch#1 t_R: 5.6 min (98%), 6.8 min (2%), Batch#2 t_R: 5.6 min (97%), 6.9 min (3%).

Peptide (GFF)$_2$KG – [“Y”/2NH$_2$]

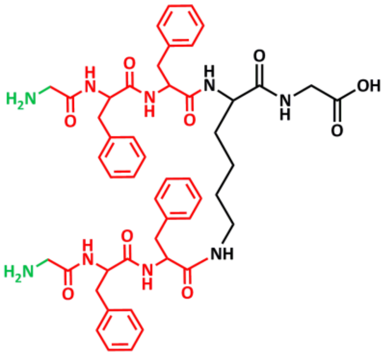

Figure 88: **Structure of peptide [“Y”/2NH$_2$]. Due to the ramification, the coupling step was repeated twice for each amino acid following the branching point (lysine).**

^{1}H-NMR (DMF-d$_7$, 300 MHz): δ [ppm] 13.0 (br. s, 1H), 8.75 (d, $^2J_{HH}$ = 8.7 Hz, 1H), 8.71(d, $^2J_{HH}$ = 8.7 Hz 1H), 8.45-8,60 (br. s, 6H), 8.49 (d, $^2J_{HH}$ = 8.1 Hz, 1H), 8.36 (d, $^2J_{HH}$ = 8.2 Hz, 1H), 8.16 (t, $^2J_{HH}$ = 5.9 Hz, 1H), 8.09 (d,1H), 7.80 (t, $^2J_{HH}$ = 3.4 Hz, 1H) 7.15-7.35 (m, 20H), 4.72 (m, 3H), 4.61 (m, 1H), 4.46 (m, 1H), 3.92 (m, 6H), 3.12 (m, 8H), 2.92 (m, 2H), 1.30-1.55 (br. m, 6H).

MALDI-TOF MS: Mass calculated M = 905.44 – found: Batch#1: 928 [M+Na]$^+$, 944 [M+K]$^+$, Batch#2: 906 [M+H]$^+$, 912 [M+Li]$^+$, 928 [M+Na]$^+$, 944 [M+K]$^+$, Batch#3: 906 [M+H]$^+$, 928 [M+Na]$^+$, 946 [M+K]$^+$, Batch#4: 906 [M+H]$^+$, 928 [M+Na]$^+$, 945 [M+K]$^+$, Batch#1 907 [M+H]$^+$, 929 [M+Na]$^+$, 945 [M+K]$^+$.

Yield (gross) Batch#1: 64% (0.1 mmol), Batch#2: 64% (0.1), Batch#3: 72% (0.5), Batch#4: 59% (0.5), Batch#5: 55% (0.5).

HPLC: Gradient methanol/0.1% TFA in H_2O from 20/80 to 100/0 in 10 min; 1 mL·min^{-1}, UV 220 nm, Batch#1 t_R: 7.6 min (92%), 8.3 min (3%), 8.6 min (5%), Batch#2 t_R: 7.6 min (91%), 7.8 min (5%), 8,3 (4%), Batch#3 t_R: 7.6 min (90%), 8,3 min (6%), Batch#4 t_R: 7.7 min (92%), 8,7 min (7%), Batch#5 t_R: 7.6 min (91%), 8,3 min (5%), 8.6 min (4%)

Peptide K(Mant)GFFY(NO$_2$)KG – [Mant/2NH$_2$]

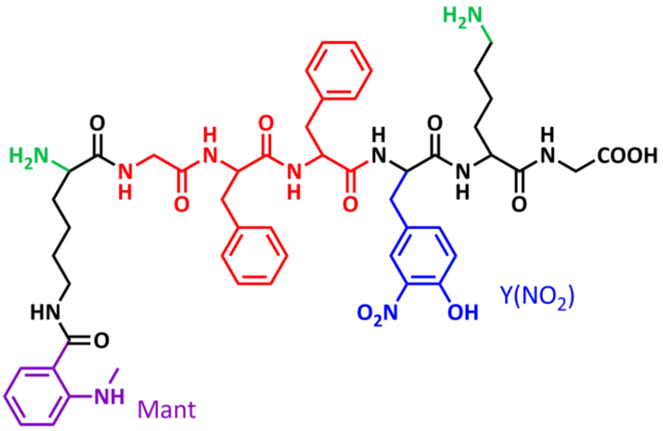

Figure 89: Structure of peptide [Mant/2NH$_2$].

^{1}H-NMR (DMSO-d$_6$, 300 MHz): δ [ppm] 12.60 (br. s, 1H), 10.78 (s, 1H), 8.51 (m, 1H), 8.32 (t, $^2J_{HH}$ = 8.4 Hz 1H), 8.0-8,29 (m, 5H), 7.65 (br., 6H), 7.48 (dd, $^2J_{HH}$ = 8.6 Hz, $^3J_{HH}$ = 2.5 Hz, 1H), 7.43 (dd, $^2J_{HH}$ = 8.5 Hz, $^3J_{HH}$ = 2.4 Hz, 1H), 7.15-7.29 (m, 11H), 7.01 (d, $^2J_{HH}$ = 8.5 Hz, 1H) 6.60 (d, $^2J_{HH}$ = 8.7 Hz, 1H), 6,53 (t, $^2J_{HH}$ = 8.2 Hz 1H), 4.50 (m, 3H), 4.30 (m, 2H), 3.8 (m, 4H), 3.17 (m, 4H), 2.6-3.0 (m, 6H), 2.73 (s, 3H) 1.52 (br. m, 12H).

MALDI-TOF MS: Mass calculated M = 1023.48 - Found 1025 $[M+H]^+$, 1047 $[M+Na]^+$, 1063 $[M+K]^+$

Yield (gross) 72% (0.5 mmol).

HPLC: Gradient methanol/0.1% TFA in H_2O from 20/80 to 100/0 in 10 min; 1 $mL\cdot min^{-1}$, UV 220 nm, t_R: 4.4 min (17%), 5.3 min (83%).

Peptide K(Mant)KGFFY(NO_2)KG – [Mant/3NH_2]

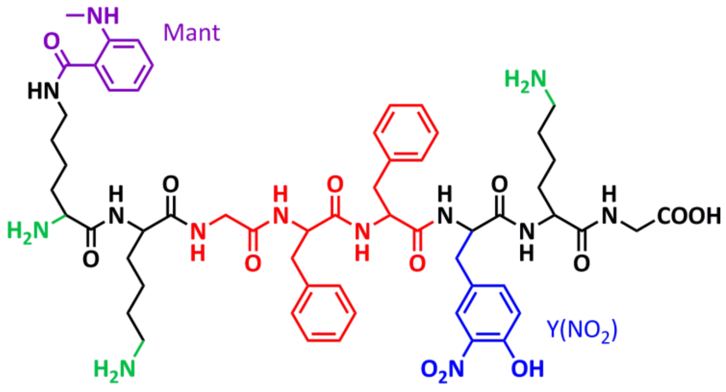

Figure 90: Structure of peptide [Mant/3NH_2]

^{1}H-NMR (DMSO-d_6, 300 MHz): δ [ppm] 12.6 (br. s, 1H), 10.79 (s, 1H), 8.54 (d, $^{2}J_{HH}$ = 8.4 Hz, 1H), 8.07-8,29 (m, 4H), 7.99 (d, $^{2}J_{HH}$ = 8.3 Hz, 1H), 7.81 (d, $^{2}J_{HH}$ =2.4 Hz 1H), 7.65 (br., 10H), 7.48 (dd, $^{2}J_{HH}$ = 8.6 Hz, $^{3}J_{HH}$ = 2.6 Hz 1H), 7.43 (dd, $^{2}J_{HH}$ = 8.5 Hz, $^{3}J_{HH}$ = 2,4 Hz 1H), 7,29 (m,1H), 7.15-7.27 (m, 10H), 7.02 (d, $^{2}J_{HH}$ = 8.5 Hz, 1H) 6.60 (d, $^{2}J_{HH}$ = 8.3 Hz, 1H), 6,53 (t, $^{2}J_{HH}$ = 8.4 Hz, 1H), 4.40-4,65 (m, 4H), 4.31 (m, 2H), 3.8 (m, 4H), 3.17 (m, 4H), 2.62-3.04 (m, 8H), 2.73 (s, 3H) 1.52 (br. m, 18H).

MALDI-TOF MS: Mass calculated for M = 1151.48 - found 1152 $[M+H]^+$, 1174 $[M+Na]^+$, 1190 $[M+K]^+$

Yield (gross) 68% (0.5 mmol).

HPLC: Gradient Methanol/0.1% TFA in H_2O from 20/80 to 100/0 in 10 min; 1 $mL\cdot min^{-1}$, UV 220 nm, t_R: 4.4 min (9%), 4.9 min (91%).

Peptide KK(Mca)GFFK(Dnp)KG – [Mca/3NH$_2$]

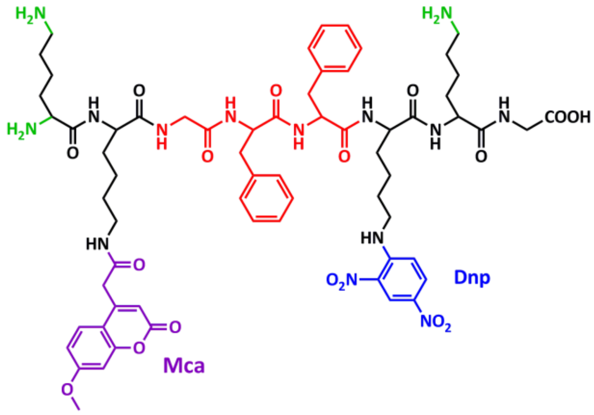
H$_2$N
H$_2$N
H$_2$N
HN
HN
O$_2$N
NO$_2$
COOH
Dnp
Mca

Figure 91: Structure of peptide [Mca/3NH$_2$].

^{1}H-NMR (DMSO-d$_6$, 300 MHz): δ [ppm] 12.55 (br. s, 1H), 8.88 (d, $^{2}J_{\mathrm{HH}}$ = 2.7 Hz, 1H), 8.82 (d, $^{2}J_{\mathrm{HH}}$ = 2.9 Hz 1H), 8.48 (d, $^{2}J_{\mathrm{HH}}$ = 7.7 Hz, 1H), 8.32 (d, 1H), 8.05-8,25 (m, 4H), 7.98 (d, $^{2}J_{\mathrm{HH}}$ = 7.2 Hz, 1H), 7.69-7,46 (br. m, 10H), 7,25 (d,1H), 7.10-7.20 (m, 10H), 7.02 (d, $^{2}J_{\mathrm{HH}}$ = 4.2 Hz, 1H), 6.98 (dd, $^{2}J_{\mathrm{HH}}$ = 8.8 Hz, $^{3}J_{\mathrm{HH}}$ = 4.1 Hz, 1H), 6.23 (s, 1H), 4.55 (m, 2H), 4.30 (m, 4H), 3.85 (s, 3H), 3,79 (d, $^{2}J_{\mathrm{HH}}$ = 4.4 Hz 1H), 3.76 (d, $^{2}J_{\mathrm{HH}}$ = 4.8 Hz, 1H), 3.66 (s, 2H), 3.5 (s, 2H), 3.04 (m, 4H), 2.61-2.82 (m, 4H), 1,44-1.68 (br. m, 24H).

MALDI-TOF MS: Mass calculated M = 1320.61 - found 1321 $[M+H]^+$, 1343 $[M+Na]^+$, 1359 $[M+K]^+$

Yield (gross) 75% (0.5 mmol).

HPLC: Gradient acetonitrile/0.1% TFA in H$_2$O from 30/70 to 100/0 in 20 min; 1 mL·min^{-1}, UV 340 nm, t_R: 3.4 min (12%), 3.6 min (80%), 3.8 min (8%).

Peptide KKKK(Mca)GFFK(Dnp)KKKG – [Mca/7NH$_2$]

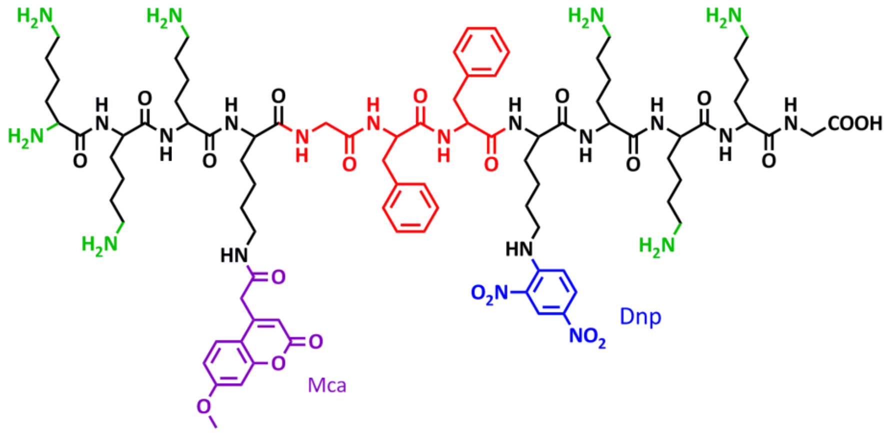
H$_2$N
H$_2$N
H$_2$N
H$_2$N
H$_2$N
H$_2$N
H$_2$N
HN
HN
O$_2$N
NO$_2$
COOH
Dnp
Mca

Figure 92: Structure of peptide [Mca/7NH$_2$].

^{1}H-NMR (DMSO-d$_6$, 300 MHz): δ [ppm] 12.65 (br. s, 1H), 8.88 (d, $^2J_{\mathrm{HH}}$ = 2.7 Hz, 1H), 8.82 (d, $^2J_{\mathrm{HH}}$ = 2,7 Hz 1H), 8.57 (d, $^2J_{\mathrm{HH}}$ = 7.7 Hz, 1H), 8.32 (d, $^2J_{\mathrm{HH}}$ = 3.7 Hz, 1H), 8.05-8,25 (m, 11H), 7.70-7,85 (br., 21H), 7.68 (d, $^2J_{\mathrm{HH}}$ = 8.8 Hz, 1H), 7,25 (s,1H), 7.06-7.23 (m, 10H), 7.0 (d, 1H, $^2J_{\mathrm{HH}}$ = 4.2 Hz), 6.96 (dd, $^2J_{\mathrm{HH}}$ = 8.8 Hz, $^3J_{\mathrm{HH}}$ = 2.4 Hz, 1H), 6.23 (s, 1H), 4.55 (m, 3H), 4.30 (m, 7H), 3.85 (s, 3H), 3,79 (m, 1H), 3.72 (m, 1H), 3.67 (s, 2H), 3.6 (s, 2H), 2.94-3.02 (m, 4H), 2.61-2.81 (m, 12H), 1.41-1,72 (br. m, 48H).

MALDI-TOF MS: Mass calculated M = 1834.00 – found: 1837 [M+H]$^+$, 1844 [M+Li]$^+$, 1859 [M+Na]$^+$, 1876 [M+K]$^+$

Yield (gross) 92% (0.5 mmol).

HPLC: Gradient Acetonitrile/0.1% TFA in H_2O from 10/90 to 80/20 in 20 min; 1 mL·min^{-1}, UV 340 nm, t_R: 7.9 min (89%), 8.3 min (11%).

Peptide KKKK(Mca)RQLRVVGGK(Dnp)KKKG – [heps/Mca/7NH$_2$]

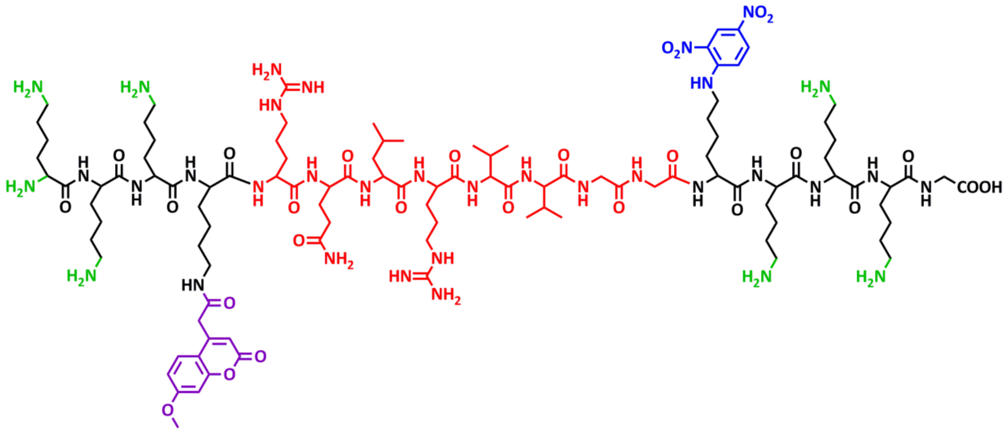

Figure 93: Structure of peptide [heps/Mca/7NH$_2$]

^{1}H-NMR (DMSO-d$_6$, 300 MHz): δ [ppm] 11.68 (br. s, 1H), 8.88 (m, 2H), 8.42 (m, 1H), 8.24 (d, $^2J_{\mathrm{HH}}$ = 3.8 Hz, 1H), 8.08-8.20 (m,5H), 7.80-8,05 (m, 20H), 7.22 (d, $^2J_{\mathrm{HH}}$ = 8.8 Hz, 1H) in 7.1-7.5 (m,12H), 7.0 (d, 1H, $^2J_{\mathrm{HH}}$ = 4.1 Hz), 6.96 (dd, $^2J_{\mathrm{HH}}$ = 8.7 Hz, $^3J_{\mathrm{HH}}$ = 2.4 Hz, 1H), 6.23 (s, 1H), 4.23 (m, 14H), 3.86 (s, 3H), 3.72-3.78 (m, 7H), 3.0-3,17 (m, 4H), 2.94-3.0 (m, 2H), 2.75 (m, 12H), 1.91-2.03 (m, 6H), 1.41-1,72 (br. m, 59H), 0.79-0.86 (m, 18H).

MALDI-TOF MS: Mass calculated M = 2348.36 – found: 2350 [M+H]$^+$, 2224 [M-Lys+H]$^+$, 2094 [M-2·Lys+H]$^+$, [M-3·Lys+H]$^+$

Yield (gross) 56% (0.1 mmol).

HPLC: Gradient acetonitrile/0.1% TFA in H_2O from 10/90 to 20/80 in 20 min; 1 mL·min^{-1}, UV 340 nm, t_R: 6.8 min (6%) 7.1 min (78%), 7.4 min (16%).

A few precisions still have to be added. When the synthesis was successful, the peptides were used as such for the preparation of conjugates or nanocapsules. Regarding the process of cleavage, the peptides obtained do not strictly correspond to the formula drawn above: all the amine groups (in our case the lysine residues and the *N*-terminus) are actually in the form of the trifluoroacetate salt. This could have an influence on the reaction in organic solvent. Therefore, a process from the literature[210] was tried to eliminate the counter ion. It consists in the precipitation of the peptide under basic pH by sodium hydroxide addition. In our case, we observed the gelification of the peptide, very unpractical to dry and compromising the further steps.

However, this salt is still present on the peptide and this has consequences: each peptide has a "true" molecular weight (corresponding to the structures displayed, observed in MALDI-TOF MS) and an "apparent" molecular weight (linking the mass obtained and the quantity of peptide synthesized, to calculate the yield for example). All characteristics of the peptides are summarized in **Table 12**.

Table 12: Summary of "apparent" and "true" molecular weight of the peptide prepared.

Peptide	FRET System	Amine functionality	Molecular weight (g·mol^{-1})	"Apparent" molecular weight (g·mol^{-1})
[-/2NH$_2$]	/	2	555	783
["Y"/2NH$_2$]	/	2	906	1134
[Mant/2NH$_2$]	Mant/Y(NO$_2$)	2	1024	1252
[Mant/3NH$_2$]	Mant/Y(NO$_2$)	3	1150	1492
[Mca/3NH$_2$]	Mca/Dnp	3	1320	1662
[Mca/7NH$_2$]	Mca/Dnp	7	1834	2632
[heps/Mca/7NH$_2$]	Mca/Dnp	7	2348	3146

Later, the peptides listed above were used as such for the preparation of linear peptide-polymer conjugates or peptide-based hybrid nanocapsules.

VI.3 Peptide-polymer coupling reactions

All the peptide-polymer coupling reactions presented in this thesis are based on the same reaction used for peptide synthesis: the synthesis of an amide bound between a carboxylic acid group and an amine. One can actually see the carboxylic acid ω-functionalized polymer as a large terminal amino acid, especially in case of solid-phase coupling. Therefore, the same standard coupling method as in SPPS was used (see above, paragraph VI.2).

VI.3.1 Peptide-polymer coupling in solution

Polymer and peptide [-/2NH_2] were – as far as possible, because of polymer distribution – under stoichiometric proportions to form a triblock conjugate: two polymers for one peptide. Activators were introduced in the same proportions as for standard peptide coupling, and were premixed to the polymer to favor its activation rather than the C-terminus of the peptide. The reaction in solution was processed at 75 °C in microwave oven during 150 min, to balance the dilution effect (factor 1.5) but principally to overcome possible steric inhibition due to presence of the polymer under the form of physical dimer.
After the reaction DMF was evaporated under vacuum. The solid remaining was washed 3 times on Frit N°4 with 1 wt.% sulfuric acid solution, then 3 times with methanol and dried.

VI.3.2 Peptide-polymer coupling on solid phase

The coupling reaction was processed on peptide [“Y”-2NH_2] deprotected but still attached to the resin, as represented in **Figure 94**. In this case, the polystyrene was considered as a normal amino acid added at the end of the peptide sequence, as it was soluble at the usual concentration in DMF (0.2 M). 90 min (three times 30 min with introduction of new polymer reactant) were left to the polymer to react instead of 5 min usually for the amino acids. Then, the product was cleaved in TFA solution, following the normal protocol, and was precipitated and washed three times with methanol (instead diethyl ether) to get rid of the TFA but also of some possible peptide not conjugated to a polymer chains. Once dried in vacuum, the product of solid-phase coupling was characterized and submitted to enzymatic cleavage.

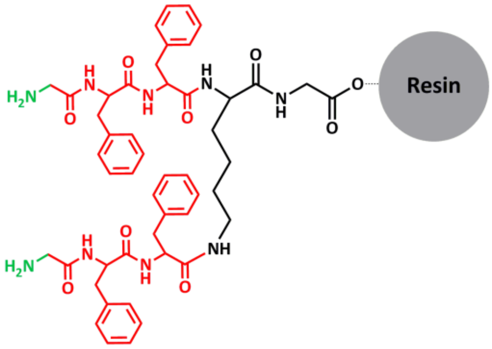

Figure 94: **Structure of peptide [“Y”/2NH_2] still attached to the resin for solution coupling.**

VI.4 Preparation of peptide-based nanocapsules in miniemulsion

Each miniemulsion was prepared following the same experimental protocol, described herein.

Preparation of miniemulsion

50 mg of peptide (apparent molecular weight) were dissolved in 0.75 g polar solvent for dispersed phase (usually DMF containing 5 $g \cdot L^{-1}$ lithium bromide). Dyes like P(VP-*co*-Bodipy) or SR-101 were also dissolved in the dispersed phase at that stage. Then, 6.75 g cyclohexane containing 0.5 wt.% surfactant poly(butylene-*co*-ethylene)-*b*-poly(ethylene oxide) P(B/E-*b*-EO) were added and the mixture was stirred for one hour at 1000 rpm. Then, ultrasonication (3 min total, applied in pulses of 10 s with 10 s pause, 70% intensity) was applied to the sample with a ¼´´ tip under ice cooling. A toluene diisocyanate (TDI) solution in cyclohexane was prepared, so that around 0.5 g contains precisely the desired stoichiometric amount of the TDI to be added. The solution was freshly prepared and added directly after ultrasonication of the sample. The solution was added drop wisely to the stirred miniemulsion with a syringe and left under agitation for 15 h.

In the case of dye encapsulation, the amounts were the following: 5 mg of SR-101, or 21 mg of P(VP-*co*-Bodipy).

Redispersion in water

The cyclohexane based miniemulsion was dispersed in twice its weight of distilled water with 0.3 wt.% SDS. Later, the sample was stirred at maximum 45 °C until complete cyclohexane evaporation. This was followed by weighing the sample. To ensure complete evaporation, the weight was brought under its expected value and adjusted with distilled water at least two times. From samples JA79, the samples were ultrasonicated afterward under mild conditions (3 min total, applied in pulses of 10 s with 10 s pause, 70% intensity) to break up aggregates.

Dialysis

Before enzymatic cleavage, the samples were all dialyzed in ≈ 2 L water at least during one week, with daily water change each working day. Dialysis was done with 14 kDa (exceptionally 100 kDa as indicated in results & discussion part) molecular weight cut-off membrane: to remove free peptide, not encapsulated dye (especially for samples sonicated after redispersion) and to reduce surfactant concentration. The amount of dialyzed peptide and not encapsulated dye were determined by fluorescence measurements of the dialysate water.

General remarks

To summarize the previous paragraphs, here are a few parameters of our system.

In cyclohexane, the solid content of the miniemulsion is approximately 1.5% (depending on TDI equivalent and presence/absence of encapsulated dye).

The peptide represents around 60% weight of this solid content.

The surfactant P(B/E-*b*-EO) concentration of 0.5 wt.% in cyclohexane corresponds to 4.5 wt.% of dispersed phase.

After redispersion in water, the solid content drops to around 1% (dilution by a factor two but addition of SDS surfactant).

If there is no free peptide removed during dialysis, the "concentration" of peptide sequences in the final miniemulsion is in the range of 10^{-3} mol·L^{-1} depending on the molecular weight of the peptide.

Concerning the encapsulated fluorescing polymer: 21 mg of P(VP-co-Bodipy) were added to the dispersed phase. It corresponds to 0.1 wt.% of Bodipy dye related to solid content in the capsules, a sufficient and standard concentration in miniemulsion to observe fluorescence.

About the encapsulation of SR-101, 5 mg were introduced into the dispersed phase. This represents a concentration of 10.5 mM, much higher than the 3.2 10^{-6} M where self-concentration quenching starts occuring[153] and should ensure an efficient quenching of fluorescence in the capsules synthesized.

VI.5 Appendix

VI.5.1 Methods

^{1}H-NMR spectroscopy

^{1}H-NMR spectra were recorded on Bruker DRX spectrometers (300, 400, 700 MHz) at 298.7 K.

DOSY-NMR spectroscopy

Diffusion ordered spectroscopy NMR (DOSY-NMR) experiments were conducted on a Bruker Avance-III 700 MHz NMR Spectrometer employing a 5 mm BBI ^{1}H/X *z*-gradient probe with a gradient strength of 5.35 [G·mm^{-1}]. The gradient strength was properly calibrated by analysis of a sample of $^2H_2O/^1H_2O$ at a defined temperature and comparison with the theoretical diffusion coefficient of $^2H_2O/^1H_2O$. The temperature was kept constant at 298.3 K using the Bruker Topspin 2.1 software monitoring a standard ^{1}H methanol NMR sample. The gradient strength was varied in 32 or 64 steps from 2% to 100%. The diffusion time was 350 ms, while the gradient pulse length was 1.1 ms. For the diffusion measurements a 2D sequence (Bruker program: dstebpgp3s) was employed using double stimulated echo for convection compensation. For estimation of the error in the determination of diffusion constants the standard deviation of decay curves for selected proton peaks, was fitted using the Bruker SimFit package and appropriate diffusion fit functions. Relative S.D.s were of the order of $1 \cdot 10^{-3}$. As an internal frequency lock, deuterons of DMSO-d$_6$ were used.

Centrifugation

Centrifugation of the nanocapsules to analyze the supernatant of enzymatic cleavage was carried out on a Sigma 3-30k centrifuge. The samples were centrifuged at 20 000 rpm during 20 min and supernatant was deducted carefully.

Dialysis

The samples were dialyzed against 2 L deionized water (dialysis tube, cut-off generally 14 kDa, also 100 kDa when influence of the cut-off was studied) for at least one week (water changed at least every day) to remove surfactants, non-encapsulated dye and possible unreacted peptide.

High-performance liquid chromatography (HPLC)

HPLC was performed in different gradients of THF/0.1 % TFA in H_2O or Acetonitrile/0.1 % TFA in H_2O employing a reversed phase HD C_8 column (Macherey-Nagel) using a series 1100 pump (Hewlett Packard) and an auto 1200 series sampler (Agilent Technologies). Substances were detected by a UV-Vis detector S-3702 (Soma) at 220 nm. Flow was 1 $mL\cdot min^{-1}$ and the concentration of the sample 1 $mg\cdot mL^{-1}$.

Size-exclusion chromatography (SEC)

SEC measurements were carried out in DMF or THF, with samples of the concentration of 1 $g\cdot L^{-1}$. Sample injection was performed by a 717plus auto sampler (Waters) at 60 °C (DMF) and 30°C (THF). Flow was 1 $mL\cdot min^{-1}$. In DMF, three GRAM columns (PSS), 300 x 80 mm, 10 µm particle size with respective pore sizes of 10^6, 10^4 und 10^3 Å were employed. In THF, three SDV columns (PSS) with the dimensions 300 × 80 mm, 10 µm particle size and pore sizes of 10^6, 10^4 und 500 Å were employed. Detection was accomplished with DRI Shodex RI-101 detector (ERC) and UV-Vis S-3702 detector (Soma).

Fluorescence microscopy

Digital fluorescence micrographs were acquired with an inverted wide field microscope system from Olympus (IX70, CellF software) equipped with a 100× objective (1.3 NA), a mercury lamp, a 12 bit CCD camera (F-View II) and appropriate filter sets for Mca (ex. 360/10 nm, beamsplitter 400 nm, em. 420 nm), Bodipy (ex. 510/20 nm, beamsplitter 520 nm, em. 542-570 nm) and SR-101 (ex. 530/20 nm, beamsplitter 550 nm, em. 570 nm).

Fluorescence measurements

Fluorescence spectroscopy was carried out on a Tecan M1000 micro plate reader, for enzymatic cleavage experiment (see below) as well as for concentration determination in solution or dispersion. The wavelengths used for the fluorescent dyes were the following: SR-101 (λ_{ex} = 580nm, λ_{em} =605 nm), Bodipy (520 nm, 530 nm), Mca (340 nm, 405 nm) and Mant (315 nm, 425 nm), 5 nm bandwidth for both excitation and emission for all dyes.

MALDI-TOF MS

MALDI-TOF MS analyses were obtained on a Bruker-Daltonics Reflex-TOF, in reflex (peptide) or linear (polymer) mode. The acceleration voltage was 20 kV in both cases. The samples (solid state) were incorporated in 2,5-dihydroxy benzoic acid (DHB) matrix and desorbed with a nitrogen laser (λ = 337 nm).

Photon cross correlation spectroscopy (PCCS)

Particle size was determined by photon cross correlation spectroscopy (PCCS) from a Nanophox device (Sympatec GmbH). Measurements were done with 100 µL of dispersion diluted in 2.5 mL cyclohexane or water, with the detectors set to 90° from the incident beam.

Scanning electron microscopy (SEM)

Scanning electron micrographs (SEM) were taken on a Gemini 1530 (Carl Zeiss AG) with an InLens detector and acceleration voltage of 0.2-0.3 kV. Samples were prepared by drop-casting of 5 µL of diluted dispersions in cyclohexane on a silicon wafer.

Transmission electron microscopy (TEM)

Transmission electron micrographs (TEM) were obtained with a FEI Tecnai F20 microscope, acceleration voltage of 200 kV. The samples were prepared with 5 µL of diluted dispersions placed on a 300 mesh carbon-coated copper grid.

Time-correlated single photon counting (TCSPC)

The fluorescence decays were recorded by TCSPC technique with Fluo Time 200 (Picoquant GmbH) spectrometer. Supercontinuum laser SC450-PP (10 MHz, pulse duration ~10 ps) (Fianium, Inc.) was used as excitation source. Laser beam λ = 580 nm with spectral bandwidth 5 nm was selected by a custom designed monochromator [D. Wildanger, E. Rittweger, L Kastrup and S. W. Hell, *Optics Express* 2008, *16*, 9614] and coupled into a multimode optical fiber (Thorlabs, Inc.). The value of estimated instrument response function (IRF) of the setup equals 260 ps. Additional longpass filter (λ_{cut} = 593 nm, Semrock, Inc.) was placed in front of detection path for complete diminishing scattered light, that is extremely important when highly scattered objects are investigated.

UV-VIS measurements

UV-Vis spectroscopy was carried out on a Lambda25 spectrometer (Perkin Elmer) or on a Tecan M1000 micro plate reader. For quantitative detection of certain characteristic groups, the followings absorption wavelengths were used: SR-101 (580 nm), Bodipy (525 nm), Mca (340 nm) and Mant (315 nm).

Ultrasonication

Ultrasonication steps were carried out on a Branson 450D sonifier (1/8”, 1/4” or 1/2” diameter tip, depending on the volume of the sample), for miniemulsion formation (3 min total, applied in pulses of 10s with 10s pause, 70% intensity) and some redispersion (3 min total, applied in pulses of 10 s with 10 s pause, 30% intensity). During ultrasonication, the sample was cooled with an ice bath to prevent solvent evaporation.

Enzymatic cleavage experiments

A trypsin preparation was used for the cleavage of the peptide with GFF recognition site. The trypsin preparation (*Invitrogen*) actually consists of trypsin, chymotrypsin and traces of pancreatin, according to the answer of the producer to our inquiry. The cleavage experiments of the nanocapsules were carried out by diluting the dispersion 5 times in water and adding trypsin preparation to a final enzyme concentration of 2.5 $g \cdot L^{-1}$. Fluorescence intensities (Mca, $\lambda_{em} = 405$ nm, $\lambda_{ex} = 340$ nm and SR-101, $\lambda_{em} = 605$ nm, $\lambda_{ex} = 580$ nm) were monitored using a Tecan M1000 microplate reader at 37 °C. Measurements were conducted every minute and the plate was briefly shaken (5 s) before each of them. Each data point corresponds to the average value of 8 replicates. In the case of preparations of samples for other methods (e.g. TCSPC, centrifugation), the proportions were kept identical.

For the enzymatic degradation of the microparticles prepared from linear triblock peptide-polymer conjugate, it was processed as following: 20 mg of conjugates were introduced in 9 mL PBS buffer and were ultrasonicated (2 min total, applied in pulses of 5 s with 5 s pause, 70% intensity). 1 mL of trypsin solution was added to a final concentration of 2.5 $g \cdot L^{-1}$. The sample was then agitated at 37 °C for 24 h and the water was evaporated. MALDI-TOF MS analyses were performed with the remaining solid mixture conjugate/enzyme/salt.

VI.5.2 Summary of FRET-peptide based hybrid nanocapsules

Table 13 : Summary of peptide-based hybrid nanocapsules prepared from peptides carrying a FRET pair.

Sample	Peptide	Dispersed phase	TDI equivalent	Encapsulation	x_{50} (PCCS) in cyclohexane / nm	Comments
JA46	[Mant/2NH$_2$]	DMF + LiBr	1.5	-	232	/
JA47	[Mant/3NH$_2$]	DMF + LiBr	1.5	-	208	/
JA49	[Mant/2NH$_2$]	DMF + LiBr	1.5	SR-101	226	/
JA50	[Mant/3NH$_2$]	DMF + LiBr	1.5	SR-101	224	/
JA60	[Mca/3NH$_2$]	DMF + LiBr	1.5	-	153	/
JA61	[Mca/3NH$_2$]	DMF + LiBr	1.5	Bodipy-polymer	230	/
JA62	[Mca/3NH$_2$]	DMF	1.5	Bodipy-polymer	281	/
JA63	[Mca/3NH$_2$]	H_2O + LiBr	1.5	SR-101	149	/
JA65	[Mca/3NH$_2$]	DMF + LiBr	1.5	Bodipy-polymer	201	/
JA68	[Mca/7NH$_2$]	DMF + LiBr	1.5	Bodipy-polymer	217	/
JA69	[Mca/7NH$_2$]	DMSO + LiBr	1.5	Bodipy-polymer	406 (bimodal)	/
JA70	[Mca/7NH$_2$]	H_2O + LiBr	1.5	Bodipy-polymer	Not stable	/
JA71	[Mca/3NH$_2$]	DMF + LiBr + DIEA	2	Bodipy-polymer	/	Gelification dispersed phase
JA72	[Mca/3NH$_2$]	DMF + LiBr	2	Bodipy-polymer	226	/
JA73	[Mca/3NH$_2$]	DMF + LiBr + DIEA	2 (HDI)	Bodipy-polymer	/	Gelification dispersed phase
JA74	[Mca/3NH$_2$]	DMF + LiBr	2 (HDI)	Bodipy-polymer	214	/
JA79	[Mca/7NH$_2$]	DMF + LiBr	2	-	155	1st sample with US redispersion
JA80	[Mca/7NH$_2$]	DMF + LiBr	2	SR-101	158	/
JA81	[Mca/7NH$_2$]	DMSO + LiBr	5	-	1155	/
JA82	[Mca/7NH$_2$]	H_2O/DMSO + LiBr	5	-	Not stable	/
JA83	[Mca/7NH$_2$]	DMF + LiBr	5	Bodipy-polymer	230	Not fully dissolved in SEC
JA84	[Mca/7NH$_2$]	DMF + LiBr	5	-	288	/
JA86	[Mca/7NH$_2$]	DMF + LiBr	1	-	162	/
JA87	[Mca/7NH$_2$]	DMF + LiBr	1	Bodipy-polymer	386	/
JA90	[Mca/7NH$_2$]	H_2O/DMF + LiBr	2	-	1058	Core/shell capsules
JA93	[Mca/3NH$_2$]	DMF + LiBr	2	SR-101	140	/
JA94	[Mca/7NH$_2$]	DMF + LiBr	2	SR-101	155	/
JA95	[Mca/7NH$_2$]	DMF + LiBr	1	SR-101	164	/
JA96	[Mca/7NH$_2$]	DMF + LiBr	5	SR-101	145	/
JA98	[heps/Mca/7NH$_2$]	DMF + LiBr	2	SR-101	/	Gelification dispersed phase
JA99	[heps/Mca/7NH$_2$]	DMSO + LiBr	2	SR-101	412	/

Abbreviations

Bodipy	boron-dipyrromethene
DOSY-NMR	Diffusion-Ordered SpectroscopY NMR
DMF	*N,N*-dimethylformamide
DMSO	dimethylsulfoxyde
Dnp	2,4-dinitrophenyl
HBTU	2-(1H-Benzotriazole-1-yl)-1,1,3,3-tetramethyluronium hexafluorophosphate
HOBt	1-hydroxybenzotriazole
HPLC	high-performance liquid chromatography
LiBr	lithium bromide
MALDI-TOF	matrix-assisted laser desorption/ionization – time of flight
Mant	methylanthraniloyl
Mca	(7-Methoxycoumarin-4-yl)-acetyl-
MS	mass spectroscopy
NIPAM	*N*-isopropylacrylamide
NMR	nuclear magnetic resonance
OEGMA	oligo(ethylene glycol) methacrylate
P(B/E-*b*-EO)	poly[(butylene-*co*-ethylene)-*b*-(ethylene oxide)]
PCCS	photon cross correlation spectroscopy
PDI	polydispersity index
PEO	poly(ethylene oxide)
PBS	phosphate buffered saline
PPS	poly(propylene sulfide)
PS	polystyrene
PVP	polyvinylpyrrolidone
SDS	sodium dodecyl sulfate

SEC	size exclusion chromatography
SEM	scanning electron microscopy
SR-101	sulforhodamine 101
TDI	2,4-toluene diisocyanate
TEM	transmission electron microscopy
TCSPC	time-correlated single photon counting
Tyr(NO_2)	3-nitrotyrosine
UV-Vis	ultraviolet-visible

Symbols

δ	chemical shift
d	average diameter of particles determined from the micrographs
D	diffusion constant
DP	degree of polymerization
I	intensity
λ	wavelength
M	molecular weight
M_n	number averaged molecular weight
M_w	mass averaged molecular weight
ρ	density
T_B	boiling point
t_R	retention time
V_{el}	elution volume
x_{50}	average size of the particles in suspension determined by PCCS
wt.%	weight percentage

Bibliographic references

[1] *IARC Worldwide Cancer Incidence Statistics—Prostate*, in *JNCI Cancer Spectrum*, Oxford University Press, **2001**.

[2] *Cancer statistics, 2005* in *CA Cancer J Clin, Vol. 55*, **2005**, pp. 10–30.

[3] American Cancer Society, *Report to the Nation on the Status of Cancer*, **2011**.

[4] S. M. Dhanasekaran, T. R. Barrette, D. Ghosh, R. Shah, S. Varambally, K. Kurachi, K. J. Pienta, M. A. Rubin, A. M. Chinnaiyan, *Nature* **2001**, *412*, 822-826.

[5] K. A. Kelly, S. R. Setlur, R. Ross, R. Anbazhagan, P. Waterman, M. A. Rubin, R. Weissleder, *Cancer Res.* **2008**, *68*, 2286-2291.

[6] M. Tripathi, S. Nandana, H. Yamashita, R. Ganesan, D. Kirchhofer, V. Quaranta, *J. Biol. Chem.* **2008**, *283*, 30576-30584.

[7] F. Zhao, Y. Zhao, Y. Liu, X. Chang, C. Chen, Y. Zhao, *Small* **2011**, *7*, 1322-1337.

[8] J. Shi, A. R. Votruba, O. C. Farokhzad, R. Langer, *Nano Lett.* **2010**, *10*, 3223-3230.

[9] K. Riehemann, S. W. Schneider, T. A. Luger, B. Godin, M. Ferrari, H. Fuchs, *Angew. Chem., Int. Ed. Engl.* **2009**, *48*, 872-897.

[10] M. Maier, PhD thesis, *Synthese von selektiv Protease-spaltbaren Nanopartikeln*, University of Mainz, Germany **2011**.

[11] S. Nayak, L. A. Lyon, *Angew. Chem., Int. Ed. Engl.* **2005**, *44*, 7686-7708.

[12] J. F. Lutz, A. Hoth, *Macromolecules* **2006**, *39*, 893-896.

[13] B. Jeong, S. W. Kim, Y. H. Bae, *Adv. Drug Delivery Rev.* **2002**, *54*, 37-51.

[14] A. Kikuchi, T. Okano, *Adv. Drug Delivery Rev.* **2002**, *54*, 53-77.

[15] J.-F. Lutz, *J. Polym. Sci., Part A: Polym. Chem.* **2008**, *46*, 3459-3470.

[16] J. F. Lutz, *Adv. Mater.* **2011**, *23*, 2237-2243.

[17] S. R. Abulateefeh, A. O. Saeed, J. W. Aylott, W. C. Chan, M. C. Garnett, B. R. Saunders, C. Alexander, *Chem. Commun.* **2009**, 6068-6070.

[18] J. E. Chung, M. Yokoyama, M. Yamato, T. Aoyagi, Y. Sakurai, T. Okano, *J. Controlled Release* **1999**, *62*, 115-127.

[19] F. Kohori, K. Sakai, T. Aoyagi, M. Yokoyama, Y. Sakurai, T. Okano, *J. Controlled Release* **1998**, *55*, 87-98.

[20] J. Park, M. Moon, M. Seo, H. Choi, S. Y. Kim, *Macromolecules* **2010**, *43*, 8304-8313.

[21] J. E. Chung, M. Yokoyama, T. Okano, *J. Controlled Release* **2000**, *65*, 93-103.

[22] K. Kataoka, A. Harada, Y. Nagasaki, *Adv. Drug Delivery Rev.* **2001**, *47*, 113-131.

[23] F. Kohori, K. Sakai, T. Aoyagi, M. Yokoyama, M. Yamato, Y. Sakurai, T. Okano, *Colloid Surf. B-Biointerfaces* **1999**, *16*, 195-205.

[24] L. C. Dong, A. S. Hoffman, *J. Controlled Release* **1990**, *13*, 21-31.

[25] J.-F. Lutz, K. Weichenhan, O. Akdemir, A. Hoth, *Macromolecules* **2007**, *40*, 2503-2508.

[26] T. Okano, Y. H. Bae, H. Jacobs, S. W. Kim, *J. Controlled Release* **1990**, *11*, 255-265.

[27] T. Cai, M. Marquez, Z. Hu, *Langmuir* **2007**, *23*, 8663-8666.

[28] T. Zhou, W. Wu, S. Zhou, *Polymer* **2010**, *51*, 3926-3933.

[29] G. Pasparakis, C. Alexander, *Angew. Chem., Int. Ed. Engl.* **2008**, *47*, 4847-4850.

[30] M. K. M. Leung, G. K. Such, A. P. R. Johnston, D. P. Biswas, Z. Zhu, Y. Yan, J.-F. Lutz, F. Caruso, *Small* **2011**, *7*, 1075-1085.

[31] H. F. Gao, W. L. Yang, K. Min, L. S. Zha, C. C. Wang, S. K. Fu, *Polymer* **2005**, *46*, 1087-1093.

[32] K. Uhlig, E. Wischerhoff, J.-F. Lutz, A. Laschewsky, M. S. Jaeger, A. Lankenau, C. Duschl, *Soft Matter* **2010**, *6*, 4262-4267.

[33] Z. Zarafshani, T. Obata, J.-F. Lutz, *Biomacromolecules* **2010**, *11*, 2130-2135.

[34] T. R. Kyriakides, C. Y. Cheung, N. Murthy, P. Bornstein, P. S. Stayton, A. S. Hoffman, *J. Controlled Release* **2002**, *78*, 295-303.

[35] C. Donini, D. N. Robinson, P. Colombo, F. Giordano, N. A. Peppas, *Int. J. Pharm.* **2002**, *245*, 83-91.

[36] U. Borchert, U. Lipprandt, M. Bilang, A. Kimpfler, A. Rank, R. Peschka-Suss, R. Schubert, P. Lindner, S. Forster, *Langmuir* **2006**, *22*, 5843-5847.

[37] S. Y. Liu, J. V. M. Weaver, Y. Q. Tang, N. C. Billingham, S. P. Armes, K. Tribe, *Macromolecules* **2002**, *35*, 6121-6131.

[38] S. Y. Liu, S. P. Armes, *Angew. Chem., Int. Ed. Engl.* **2002**, *41*, 1413-1416.

[39] R. Kishi, T. Miura, H. Kihara, T. Asano, M. Shibata, R. Yosomiya, *J. Appl. Polym. Sci.* **2003**, *89*, 75-84.

[40] D. Kuckling, A. Richter, K. F. Arndt, *Macromol. Mater. Eng.* **2003**, *288*, 144-151.

[41] V. T. Pinkrah, M. J. Snowden, J. C. Mitchell, J. Seidel, B. Z. Chowdhry, G. R. Fern, *Langmuir* **2003**, *19*, 585-590.

[42] E. Kharlampieva, V. Kozlovskaya, O. Zavgorodnya, G. D. Lilly, N. A. Kotov, V. V. Tsukruk, *Soft Matter* **2010**, *6*, 800-807.

[43] K. E. Broaders, S. J. Pastine, S. Grandhe, J. M. J. Frechet, *Chem. Commun.* **2011**, *47*, 665-667.

[44] G.-C. Kuang, Y. Ji, X.-R. Jia, Y. Li, E.-Q. Chen, Z.-X. Zhang, Y. Wei, *Tetrahedron* **2009**, *65*, 3496-3501.

[45] L. A. Connal, R. Vestberg, C. J. Hawker, G. G. Qiao, *Adv. Funct. Mater.* **2008**, *18*, 3315-3322.

[46] D. J. Shi, M. Matsusaki, T. Kaneko, M. Akashi, *Macromolecules* **2008**, *41*, 8167-8172.

[47] J. Q. Jiang, B. Qi, M. Lepage, Y. Zhao, *Macromolecules* **2007**, *40*, 790-792.

[48] D. Klinger, K. Landfester, *Soft Matter* **2011**, *7*, 1426-1440.

[49] R. Huschka, O. Neumann, A. Barhoumi, N. J. Halas, *Nano Lett.* **2010**, *10*, 4117-4122.

[50] E. M. Rosenbauer, M. Wagner, A. Musyanovych, K. Landfester, *Macromolecules* **2010**, *43*, 5083-5093.

[51] A. Napoli, M. Valentini, N. Tirelli, M. Muller, J. A. Hubbell, *Nat. Mater.* **2004**, *3*, 183-189.

[52] A. Rehor, J. A. Hubbell, N. Tirelli, *Langmuir* **2005**, *21*, 411-417.

[53] Y. Ma, W.-F. Dong, M. A. Hempenius, H. Mohwald, G. J. Vancso, *Nat. Mater.* **2006**, *5*, 724-729.

[54] P. Panizzi, M. Nahrendorf, M. Wildgruber, P. Waterman, J.-L. Figueiredo, E. Aikawa, J. McCarthy, R. Weissleder, S. A. Hilderbrand, *J. Am. Chem. Soc.* **2009**, *131*, 15739-15744.

[55] A. N. Zelikin, J. F. Quinn, F. Caruso, *Biomacromolecules* **2006**, *7*, 27-30.

[56] F. Fischelghodsian, L. Brown, E. Mathiowitz, D. Brandenburg, R. Langer, *Proc. Natl. Acad. Sci. U. S. A.* **1988**, *85*, 2403-2406.

[57] A. N. Koo, H. J. Lee, S. E. Kim, J. H. Chang, C. Park, C. Kim, J. H. Park, S. C. Lee, *Chem. Commun.* **2008**, 6570-6572.

[58] B. L. Allen, J. D. Johnson, J. P. Walker, *ACS Nano* **2011**, *5*, 5263-5272.

[59] E. Campo, J. Munoz, R. Miquel, A. Palacin, A. Cardesa, B. F. Sloane, R. Emmertbuck, *Am. J. Pathol.* **1994**, *145*, 301-309.

[60] H. H. Heidtmann, U. Salge, M. Abrahamson, M. Bencina, L. Kastelic, N. KopitarJerala, V. Turk, T. T. Lah, *Clin. Exp. Metastasis* **1997**, *15*, 368-381.

[61] B. Werle, C. Kraft, T. T. Lah, J. Kos, U. Schanzenbacher, K. Kayser, W. Ebert, E. Spiess, *Cancer* **2000**, *89*, 2282-2291.

[62] E. Liaudet-Coopman, M. Beaujouin, D. Derocq, M. Garcia, M. Glondu-Lassis, V. Laurent-Matha, C. Prebois, H. Rochefort, F. Vignon, *Cancer Lett.* **2006**, *237*, 167-179.

[63] P. Briozzo, M. Morisset, F. Capony, C. Rougeot, H. Rochefort, *Cancer Res.* **1988**, *48*, 3688-3692.

[64] E. I. Deryugina, J. P. Quigley, *Cancer and Metastasis Reviews* **2006**, *25*, 9-34.

[65] J. Hu, P. E. Van den Steen, Q.-X. A. Sang, G. Opdenakker, *Nat. Rev. Drug Discovery* **2007**, *6*, 480-498.

[66] D. Aili, M. M. Stevens, *Chem. Soc. Rev.* **2010**, *39*, 3358-3370.

[67] H. A. Klok, *J. Polym. Sci., Part A: Polym. Chem.* **2005**, *43*, 1-17.
[68] F. E. Alemdaroglu, A. Herrmann, *Org. Biomol. Chem.* **2007**, *5*, 1311-1320.
[69] H. R. Marsden, A. Kros, *Macromol. Biosci.* **2009**, *9*, 939-951.
[70] J. Hentschel, H. G. Borner, *J. Am. Chem. Soc.* **2006**, *128*, 14142-14149.
[71] I. C. Reynhout, D. Lowik, J. C. M. van Hest, J. Cornelissen, R. J. M. Nolte, *Chem. Commun.* **2005**, 602-604.
[72] A. Rosler, H. A. Klok, I. W. Hamley, V. Castelletto, O. O. Mykhaylyk, *Biomacromolecules* **2003**, *4*, 859-863.
[73] Y. G. Takei, M. Matsukata, T. Aoki, K. Sanui, N. Ogata, A. Kikuchi, Y. Sakurai, T. Okano, *Bioconjugate Chem.* **1994**, *5*, 577-582.
[74] M. G. J. ten Cate, N. Severin, H. G. Borner, *Macromolecules* **2006**, *39*, 7831-7838.
[75] J. F. Lutz, *Angew. Chem., Int. Ed. Engl.* **2007**, *46*, 1018-1025.
[76] W. Agut, R. Agnaou, S. Lecommandoux, D. Taton, *Macromol. Rapid Commun.* **2008**, *29*, 1147-1155.
[77] T. B. Yu, J. Z. Bai, Z. B. Guan, *Angew. Chem., Int. Ed. Engl.* **2009**, *48*, 1097-1101.
[78] C. Boyer, J. Liu, V. Bulmus, T. P. Davis, C. Barner-Kowollik, M. H. Stenzel, *Macromolecules* **2008**, *41*, 5641-5650.
[79] M. Li, P. De, S. R. Gondi, B. S. Sumerlin, *Macromol. Rapid Commun.* **2008**, *29*, 1172-1176.
[80] J. F. Lutz, H. G. Borner, K. Weichenhan, *Macromolecules* **2006**, *39*, 6376-6383.
[81] A. J. T. Dirks, S. S. van Berkel, N. S. Hatzakis, J. A. Opsteen, F. L. van Delft, J. Cornelissen, A. E. Rowan, J. C. M. van Hest, F. Rutjes, R. J. M. Nolte, *Chem. Commun.* **2005**, 4172-4174.
[82] J. F. Lutz, H. G. Borner, K. Weichenhan, *Aust. J. Chem.* **2007**, *60*, 410-413.
[83] M. A. Gauthier, H. A. Klok, *Chem. Commun.* **2008**, 2591-2611.
[84] F. Stoica, C. Alexander, N. Tirelli, A. F. Miller, A. Saiani, *Chem. Commun.* **2008**, 4433-4435.
[85] D. J. Adams, I. Young, *J. Polym. Sci., Part A: Polym. Chem.* **2008**, *46*, 6082-6090.
[86] L. Ayres, P. Hans, J. Adams, D. Lowik, J. C. M. van Hest, *J. Polym. Sci., Part A: Polym. Chem.* **2005**, *43*, 6355-6366.
[87] M. L. Becker, J. Q. Liu, K. L. Wooley, *Biomacromolecules* **2005**, *6*, 220-228.
[88] R. M. Broyer, G. M. Quaker, H. D. Maynard, *J. Am. Chem. Soc.* **2008**, *130*, 1041-1047.
[89] J. Couet, M. Biesalski, *Macromolecules* **2006**, *39*, 7258-7268.
[90] S. Loschonsky, J. Couet, M. Biesalski, *Macromol. Rapid Commun.* **2008**, *29*, 309-315.
[91] Y. Mei, K. L. Beers, H. C. M. Byrd, D. L. Vanderhart, N. R. Washburn, *J. Am. Chem. Soc.* **2004**, *126*, 3472-3476.
[92] H. Rettig, E. Krause, H. G. Borner, *Macromol. Rapid Commun.* **2004**, *25*, 1251-1256.
[93] C. Boyer, V. Bulmus, J. Q. Liu, T. P. Davis, M. H. Stenzel, C. Barner-Kowollik, *J. Am. Chem. Soc.* **2007**, *129*, 7145-7154.
[94] P. De, M. Li, S. R. Gondi, B. S. Sumerlin, *J. Am. Chem. Soc.* **2008**, *130*, 11288-+.
[95] J. Hentschel, K. Bleek, O. Ernst, J. F. Lutz, H. G. Borner, *Macromolecules* **2008**, *41*, 1073-1075.
[96] M. G. J. ten Cate, H. G. Borner, *Macromol. Chem. Phys.* **2007**, *208*, 1437-1446.
[97] M. G. J. ten Cate, H. Rettig, K. Bernhardt, H. G. Borner, *Macromolecules* **2005**, *38*, 10643-10649.
[98] R. J. I. Knoop, M. de Geus, G. J. M. Habraken, C. E. Koning, H. Menzel, A. Heise, *Macromolecules* **2010**, *43*, 4126-4132.
[99] J. Rodriguez-Hernandez, F. Checot, Y. Gnanou, S. Lecommandoux, *Prog. Polym. Sci.* **2005**, *30*, 691-724.
[100] F. Checot, A. Brulet, J. Oberdisse, Y. Gnanou, O. Mondain-Monval, S. Lecommandoux, *Langmuir* **2005**, *21*, 4308-4315.
[101] F. Checot, S. Lecommandoux, Y. Gnanou, H. A. Klok, *Angew. Chem., Int. Ed. Engl.* **2002**, *41*, 1339-1343.
[102] H. A. Klok, J. F. Langenwalter, S. Lecommandoux, *Macromolecules* **2000**, *33*, 7819-7826.
[103] H. A. Klok, S. Lecommandoux, *Adv. Mater.* **2001**, *13*, 1217-1229.
[104] H.-A. Klok, S. Lecommandoux, *Peptide Hybrid Polymers* **2006**, *202*, 75-111.

[105] K. Knop, R. Hoogenboom, D. Fischer, U. S. Schubert, *Angew. Chem., Int. Ed. Engl.* **2010**, *49*, 6288-6308.

[106] A. K. H. Hirsch, F. Diederich, M. Antonietti, H. G. Borner, *Soft Matter* **2010**, *6*, 88-91.

[107] R. Duncan, H. C. Cable, J. B. Lloyd, P. Rejmanova, J. Kopecek, *Macromol. Chem. Phys.* **1983**, *184*, 1997-2008.

[108] R. Duncan, J. Kopecek, *Adv. Polym. Sci.* **1984**, *57*, 51-101.

[109] R. Duncan, L. W. Seymour, K. B. Ohare, P. A. Flanagan, S. Wedge, I. C. Hume, K. Ulbrich, J. Strohalm, V. Subr, F. Spreafico, M. Grandi, M. Ripamonti, M. Farao, A. Suarato, *J. Controlled Release* **1992**, *19*, 331-346.

[110] J. Kopecek, P. Rejmanova, V. Chytry, *Macromol. Chem. Phys.* **1981**, *182*, 799-809.

[111] A. Sintov, R. J. Levy, *Int. J. Pharm.* **1997**, *146*, 55-62.

[112] Y. Suzuki, M. Tanihara, Y. Nishimura, K. Suzuki, Y. Kakimaru, Y. Shimizu, *J. Biomed. Mater. Res.* **1998**, *42*, 112-116.

[113] J. R. Tauro, R. A. Gemeinhart, *Bioconjugate Chem.* **2005**, *16*, 1133-1139.

[114] J. L. West, J. A. Hubbell, *Macromolecules* **1999**, *32*, 241-244.

[115] M. P. Lutolf, G. P. Raeber, A. H. Zisch, N. Tirelli, J. A. Hubbell, *Adv. Mater.* **2003**, *15*, 888-+.

[116] M. R. Lutolf, F. E. Weber, H. G. Schmoekel, J. C. Schense, T. Kohler, R. Muller, J. A. Hubbell, *Nat. Biotechnol.* **2003**, *21*, 513-518.

[117] S. G. Levesque, M. S. Shoichet, *Bioconjugate Chem.* **2007**, *18*, 874-885.

[118] S. Kim, K. E. Healy, *Biomacromolecules* **2003**, *4*, 1214-1223.

[119] P. D. Thornton, R. J. Mart, R. V. Ulijn, *Adv. Mater.* **2007**, *19*, 1252-+.

[120] V. See, P. Free, Y. Cesbron, P. Nativo, U. Shaheen, D. J. Rigden, D. G. Spiller, D. G. Fernig, M. R. H. White, I. A. Prior, M. Brust, B. Lounis, R. Levy, *ACS Nano* **2009**, *3*, 2461-2468.

[121] C. Coll, L. Mondragon, R. Martinez-Manez, F. Sancenon, M. D. Marcos, J. Soto, P. Amoros, E. Perez-Paya, *Angew. Chem., Int. Ed. Engl.* **2011**, *50*, 2138-2140.

[122] K. Patel, S. Angelos, W. R. Dichtel, A. Coskun, Y. W. Yang, J. I. Zink, J. F. Stoddart, *J. Am. Chem. Soc.* **2008**, *130*, 2382-2383.

[123] A. Schlossbauer, J. Kecht, T. Bein, *Angew. Chem., Int. Ed. Engl.* **2009**, *48*, 3092-3095.

[124] Z. Gu, M. Yan, B. L. Hu, K. I. Joo, A. Biswas, Y. Huang, Y. F. Lu, P. Wang, Y. Tang, *Nano Lett.* **2009**, *9*, 4533-4538.

[125] G. F. Schneider, V. Subr, K. Ulbrich, G. Decher, *Nano Lett.* **2009**, *9*, 636-642.

[126] M. Maier, N. Kotman, C. Friedrichs, J. Andrieu, M. Wagner, R. Graf, W. S. L. Strauss, V. Mailaender, C. K. Weiss, K. Landfester, *Macromolecules* **2011**, *44*, 6258-6267.

[127] M. T. Basel, T. B. Shrestha, D. L. Troyer, S. H. Bossmann, *ACS Nano* **2011**, *5*, 2162-2175.

[128] L. C. Glangchai, M. Caldorera-Moore, L. Shi, K. Roy, *J. Controlled Release* **2008**, *125*, 263-272.

[129] B. Law, R. Weissleder, C. H. Tung, *Biomacromolecules* **2006**, *7*, 1261-1265.

[130] N. L. Benoiton, *Chemistry of Peptide Synthesis*, Crc Press-Taylor & Francis Group, **2006**.

[131] J. Howl, *Peptide Synthesis and Applications*, Humana Press, Totowa, New Jersey, **2005**.

[132] W. C. W. P. D. Chan, *Fmoc-Solid Phase Peptide Synthesis (A Practical Approach)*, Oxford University Press, Oxford (United Kingdom), **2000**.

[133] R. B. Merrifield, *Science* **1965**, *150*, 178-&.

[134] R. B. Merrifield, *J. Am. Chem. Soc.* **1963**, *85*, 2149-&.

[135] J. K. Chang, M. Shimizu, S. S. Wang, *J. Org. Chem.* **1976**, *41*, 3255-3258.

[136] S. S. Wang, *J. Org. Chem.* **1976**, *41*, 3258-3261.

[137] P. Sieber, *Tetrahedron Lett.* **1987**, *28*, 6147-6150.

[138] C. Montalbetti, V. Falque, *Tetrahedron* **2005**, *61*, 10827-10852.

[139] L. A. Carpino, *J. Am. Chem. Soc.* **1993**, *115*, 4397-4398.

[140] J. H. Jones, G. T. Young, *Chem. Commun.* **1967**, 35-&.

[141] D. Hudson, *J. Org. Chem.* **1988**, *53*, 617-624.

[142] R. Subiros-Funosas, R. Prohens, R. Barbas, A. El-Faham, F. Albericio, *Chemistry-a European Journal* **2009**, *15*, 9394-9403.

[143] L. A. Carpino, D. Ionescu, A. ElFaham, *J. Org. Chem.* **1996**, *61*, 2460-2465.

[144] M. Slebioda, M. A. Stamand, F. M. F. Chen, N. L. Benoiton, *Canadian Journal of Chemistry-Revue Canadienne De Chimie* **1988**, *66*, 2540-2544.

[145] S. A. Palasek, Z. J. Cox, J. M. Collins, *J. Pept. Sci.* **2007**, *13*, 143-148.

[146] K. Landfester, N. Bechthold, S. Forster, M. Antonietti, *Macromol. Rapid Commun.* **1999**, *20*, 81-84.

[147] K. Landfester, *Adv. Mater.* **2001**, *13*, 765-768.

[148] K. Landfester, *Annu. Rev. Mater. Res.* **2006**, *36*, 231-279.

[149] K. Landfester, *Angew. Chem., Int. Ed. Engl.* **2009**, *48*, 4488-4507.

[150] K. Landfester, C. K. Weiss, *Adv. Polym. Sci.* **2010**, *229*, 1-49.

[151] C. K. Weiss, K. Landfester, *Adv. Polym. Sci.* **2010**, *233*, 185-236.

[152] D. Crespy, M. Stark, C. Hoffmann-Richter, U. Ziener, K. Landfester, *Macromolecules* **2007**, *40*, 3122-3135.

[153] U. Paiphansiri, J. Dausend, A. Musyanovych, V. Mailander, K. Landfester, *Macromol. Biosci.* **2009**, *9*, 575-584.

[154] F. Caruso, D. Trau, H. Mohwald, R. Renneberg, *Langmuir* **2000**, *16*, 1485-1488.

[155] Y. Wang, A. S. Angelatos, F. Caruso, *Chem. Mater.* **2008**, *20*, 848-858.

[156] A. N. Zelikin, A. L. Becker, A. P. R. Johnston, K. L. Wark, F. Turatti, F. Caruso, *ACS Nano* **2007**, *1*, 63-69.

[157] S. Torza, S. G. Mason, *J. Colloid Interface Sci.* **1970**, *33*, 67-&.

[158] A. J. P. van Zyl, R. D. Sanderson, D. de Wet-Roos, B. Klumperman, *Macromolecules* **2003**, *36*, 8621-8629.

[159] F. Tiarks, K. Landfester, M. Antonietti, *Langmuir* **2001**, *17*, 908-918.

[160] A. J. P. van Zyl, R. F. P. Bosch, J. B. McLeary, R. D. Sanderson, B. Klumperman, *Polymer* **2005**, *46*, 3607-3615.

[161] J. Jang, K. Lee, *Chem. Commun.* **2002**, 1098-1099.

[162] H. Fessi, F. Puisieux, J. P. Devissaguet, N. Ammoury, S. Benita, *Int. J. Pharm.* **1989**, *55*, R1-R4.

[163] U. Paiphansiri, P. Tangboriboonrat, K. Landfester, *Macromol. Biosci.* **2006**, *6*, 33-40.

[164] P. W. Morgan, S. L. Kwolek, *J. Polym. Sci.* **1959**, *40*, 299-327.

[165] E. L. Wittbecker, P. W. Morgan, *J. Polym. Sci.* **1959**, *40*, 289-297.

[166] T. M. S. Chang, *Science* **1964**, *146*, 524-&.

[167] R. Arshady, *J. Microencapsulation* **1989**, *6*, 13-28.

[168] T. M. S. Chang, Macintos.Fc, S. G. Mason, *Can. J. Physiol. Pharmacol.* **1966**, *44*, 115-&.

[169] K. Landfester, F. Tiarks, H. P. Hentze, M. Antonietti, *Macromol. Chem. Phys.* **2000**, *201*, 1-5.

[170] S. Taira, Y. Z. Du, M. Kodaka, *Biotechnol. Bioeng.* **2006**, *93*, 396-400.

[171] N. Yamazaki, Y. Z. Du, M. Nagai, S. Omi, *Colloid Surf. B-Biointerfaces* **2003**, *29*, 159-169.

[172] L. Torini, J. F. Argillier, N. Zydowicz, *Macromolecules* **2005**, *38*, 3225-3236.

[173] H. Johnsen, R. B. Schmid, *J. Microencapsulation* **2007**, *24*, 731-742.

[174] M. Takasu, H. Kawaguchi, *Colloid Polym. Sci.* **2005**, *283*, 805-811.

[175] E.-M. Rosenbauer, K. Landfester, A. Musyanovych, *Langmuir* **2009**, *25*, 12084-12091.

[176] G. Baier, A. Musyanovych, M. Dass, S. Theisinger, K. Landfester, *Biomacromolecules* **2010**, *11*, 960-968.

[177] C. Scott, D. Wu, C. C. Ho, C. C. Co, *J. Am. Chem. Soc.* **2005**, *127*, 4160-4161.

[178] D. Wu, C. Scott, C. C. Ho, C. C. Co, *Macromolecules* **2006**, *39*, 5848-5853.

[179] M. M. Ali, H. D. H. Stover, *J. Polym. Sci., Part A: Polym. Chem.* **2006**, *44*, 156-171.

[180] A. Musyanovych, K. Landfester, *Prog. Colloid Polym. Sci.* **2008**, *134*, 120-127.

[181] G. Baier, A. Musyanovych, K. Landfester, A. Best, S. Lorenz, V. Mailaender, *Macromol. Biosci.* **2011**, *11*, 1099-1109.

[182] D. Crespy, K. Landfester, *Polymer* **2009**, *50*, 1616-1620.

[183] S. B. H. G. Mori, *Size Exclusion Chromatography*, Springer, **1999**.

[184] M. Gaborieau, J. Nicolas, M. Save, B. Charleux, J.-P. Vairon, R. G. Gilbert, P. Castignolles, *J. Chromatogr. A* **2008**, *1190*, 215-233.

[185] Z. Grubisic, P. Rempp, H. Benoit, *J. Polym. Sci. B Polym. Lett.* **1967**, *5*, 753.

[186] J. R. Lakowicz, *Principles of Fluorescence Spectroscopy, 2nd Ed.*, Kluwer Academic /Plenum Publishers, New York, **1999**.

[187] B. Valeur, *Molecular Fluorescence Principle and Applications*, Wiley-VCH, Weinheim, Germany, **2002**.

[188] R. I. Macdonald, *J. Biol. Chem.* **1990**, *265*, 13533-13539.

[189] J. R. Silvius, I. R. Nabi, *Mol. Membr. Biol.* **2006**, *23*, 5-16.

[190] C. G. Knight, F. Willenbrock, G. Murphy, *FEBS Lett.* **1992**, *296*, 263-266.

[191] A. Yaron, A. Carmel, E. Katchalskikatzir, *Anal. Biochem.* **1979**, *95*, 228-235.

[192] C. Cremer, T. Cremer, *Microscopica Acta* **1978**, *81*, 31-44.

[193] S. W. Hell, E. H. K. Stelzer, S. Lindek, C. Cremer, *Opt. Lett.* **1994**, *19*, 222-224.

[194] S. W. Hell, J. Wichmann, *Opt. Lett.* **1994**, *19*, 780-782.

[195] T. A. Klar, S. W. Hell, *Opt. Lett.* **1999**, *24*, 954-956.

[196] E. Rittweger, K. Y. Han, S. E. Irvine, C. Eggeling, S. W. Hell, *Nat. Photonics* **2009**, *3*, 144-147.

[197] F. Beliveau, A. Desilets, R. Leduc, *FEBS J.* **2009**, *276*, 2213-2226.

[198] U. Paiphansiri, P. Tangboriboonrat, K. Landfester, *Macromol. Symp.* **2007**, *251*, 54-62.

[199] W. Appel, *Clin. Biochem.* **1986**, *19*, 317-322.

[200] M. Maier, Diploma thesis, *Synthese eines enzymatisch spaltbaren Peptid-Polymer-Konjugats für den Einsatz in Heterophase*, University of Ulm **2008**.

[201] K. A. Davis, B. Charleux, K. Matyjaszewski, *J. Polym. Sci., Part A: Polym. Chem.* **2000**, *38*, 2274-2283.

[202] K. A. Davis, K. Matyjaszewski, *Macromolecules* **2000**, *33*, 4039-4047.

[203] J. Dudley, *Polyurea Elastomer Technology: History, Chemistry and Basic Formulating techniques*, **2004**.

[204] L. M. Bech, S. B. Sorensen, K. Breddam, *Biochemistry* **1993**, *32*, 2845-2852.

[205] R. Kuhn, K. Geider, *Chemische Berichte-Recueil* **1968**, *101*, 3587-&.

[206] R. E. Dale, J. Eisinger, W. E. Blumberg, *Biophys. J.* **1979**, *26*, 161-193.

[207] H. Schlaad, H. Kukula, J. Rudloff, I. Below, *Macromolecules* **2001**, *34*, 4302-4304.

[208] R. P. Quirk, W. C. Chen, *Macromol. Chem. Phys.* **1982**, *183*, 2071-2076.

[209] R. P. Quirk, J. Yin, L. J. Fetters, *Macromolecules* **1989**, *22*, 85-90.

[210] S. Roux, E. Zekri, B. Rousseau, M. Paternostre, J. C. Cintrat, N. Fay, *J. Pept. Sci.* **2008**, *14*, 354-359.

Acknowledgments

First of all, I would like to thank my PhD-supervisor, Prof. Landfester for her enthusiasm, for giving me the opportunity to work in her group on such a captivating research project and in such good working conditions. Besides, I will always be grateful for having had her confidence in me before I even started my master thesis in Australia.

I would also like to thank Prof. Holger Frey (University of Mainz), who kindly agreed to be the second reporter of this thesis.

I had an amazing supervisor, especially for an "*Anorganiker*". Thank you for the nice work together: your advice, your ideas, your support and your scientific curiosity along these three years, as well as the correction of this thesis. I wish you the very best in the future.

Vielen Dank auch an my two partners on the Optimap project, for the good collaboration with them. Partner #1, thank you for starting the project in a right direction and your preliminary synthetic work. I may be taller than you, but in the lab, you were my big brother. Partner #2, I will definitely keep good memories of the meetings looking for new experimental protocols, and the excitation before the first cleavage experiments of the capsules.

During these three years, I managed to enter almost every single room of the institute, looking for chemicals, willing to test another characterization method or asking for some further explanations. I would like to thank these colleagues for their help and advices. Among them, my gratitude goes especially to some scientists for the numerous series of SEC samples injected, for the HPLC measurements, NMR measurements, TEM measurements, the fluorescence microscopy experiments, and for the fluorescence life-time measurements.

I am also grateful to my colleagues in the group of our project leader, for scientific discussions, sharing knowledge and ideas, but also nice and lively musical atmosphere in the lab. Generally, I would like to thank many colleagues from the AK Landfester for the advices, the help provided *"dem jungen Franzosen"*, and the nice working atmosphere, without forgetting sports and grills. It was just an amazing and constructive experience to work here, in such an international group.

Many thanks go to three French speaking scientists for giving me the opportunity to discuss about science (or completely other topics) in French, and enjoying each time the pleasure to practice one´s mother tongue and play with "*les subtiles nuances de la langue de Molière*", sometimes also known as "*blagues Carambar*".

For several reasons, the office 1.316 was a window on the world to me. I would like to thank my *"Bürokollegen"* for the nice and essential moments shared in the office. Especially my neighbor on the left side: thanks for your help, your kindness, your friendship and the evening and night sessions in 1.316, the office that almost never sleeps.

Arriving at the end of my PhD-time, I can´t help thinking about two persons... A. B., thanks for everything. I am still wondering if I will first be able, either to *"hablan español"*, or to dance salsa. As long as the *Karambolage* keeps going on...

My warmest thanks to "the Brolloc". Guys, just thanks for your presence despite the distance within the last years. You guys are just … wait for it … awesome! Cheers, to the future!

Je ne saurais finir ces lignes sans une pensée pour mes amis et ma famille. Il est juste impossible de décrire tout ce que vous m´avez apporté, non seulement ces dernières années mais depuis bien plus longtemps. Merci.

Curriculum Vitae

Julien Andrieu

Born the August 9th 1985 (26 year old) in Nantes – France

French nationality

Education

2003	Baccaulérat Série S (Mention Bien) Lycée G. Clemenceau, Nantes – France
2003-2005	Student in classe préparatoire aux Grandes Ecoles (PCSI, PC) Lycée G. Clemenceau, Nantes – France
2005-2008	Student at **Ecole Nationale Supérieure Chimie de Montpellier** (ENSCM) University of Montpellier, Montpellier – France
2007	**Research internship** under the supervision of Dr. J. F. Lutz *Synthesis of biodegradable thermoresponsive polymer* IAP, Fraunhofer Institute, Golm – Germany
2008	**MSc thesis** under the supervision of Dr. P. Castignolles and Prof. R. G. Gilbert *Shear degradation of starch in size-exclusion chromatography* CNAFS, University of Queensland, Brisbane – Australia
2008	**Diplôme d'ingénieur chimiste** (ENSCM, Montpellier – France) & **Master of Science** (MSc, University of Montpellier – France) **in chemistry and physical chemistry of materials**
2008-2011	**PhD thesis** under the supervision of Prof. K. Landfester *Synthesis of enzyme-cleavable peptide-based nanocapsules* Max-Planck Institute for Polymer Research (Mainz, Germany)

Publications and presentations

(In the frame of the PhD-thesis)

Publications

- Maier, M.; Kotman, N.; Friedrichs, C.; Andrieu, J.; Wagner, M.; Graf, R.; Strauss, W. S. L.; Mailänder, V.; Weiss, C. K.; Landfester, K. "Highly site specific, protease cleavable peptide-polymer nanoparticles", *Macromolecules* **2011,** *44*, 6258-6267.
  DOI: 10.1021/ma201149b

- Andrieu, J.; Kotman, N.; Maier, M.; Mailänder, V.; W. S. L. Strauss, Weiss, C. K.; Landfester, K. "Live monitoring of cargo release from peptide-based hybrid nanocapsules induced by enzyme cleavage",*Macromol. Rapid. Commun., accepted.*
  DOI: 10.1002/marc.201100729

Oral presentations

- "Development of enzyme-cleavable nanocapsules"
  Opening Meeting of the E.U. Project "Bacteriosafe" (FP7 Project #245 500)
  September 6-8th 2010, Hirschegg, Austria.

- "Synthesis of peptide-based nanocapsules by interfacial polyaddition in miniemulsion"
  38th JEPO Symposium, September 19-24th2010, La Teste de Buch, France.

- "Specific enzymatic cleavage and payload release from peptide-based hybrid nanocapsules"
  The Chemical Browsers - 100thAnniversary of the ENS Chimie Montpellier,
  November 17th 2011, Montpellier, France.

Posters

- J. Andrieu, E. M. Aschenbrenner, M. Maier, L. Ragupathy, C. K. Weiss, K. Landfester
  "Enzymatic reactions and synthesis of enzyme degradable polymers"
  Frontiers in Polymer Science (1st Symposium), May 7-9th 2009, Mainz, Germany.

- J. Andrieu, N. Kotman, C. K. Weiss, K. Landfester
  "Synthesis of peptide-based hybrid nanocapsules by interfacial polyaddition in miniemulsion"
  UK Colloids 2011, July 4-6th 2011, London, U-K.